SYNTHESIS AND CHARACTERIZATION OF HIGH REFRACTIVE INDEX HYDROPHOBIC POLYACRYLATES

A THESIS SUBMITTED TO THE

UNIVERSITY OF PUNE

FOR THE DEGREE OF

DOCTOR OF PHILOSOPHY

(IN CHEMISTRY)

BY

RAVINDRA VASANT GHORPADE

RESEARCH GUIDE

Dr. S. Ponrathnam

POLYMER SCIENCE AND ENGINEERING DIVISION

NATIONAL CHEMICAL LABORATORY

PUNE 411 008, INDIA

September 2012

राष्ट्रीय रासायनिक प्रयोगशाला
(वैज्ञानिक तथा औद्योगिक अनुसंधान परिषद)
डॉ. होमी भाभा मार्ग, पुणे - 411 008. भारत
NATIONAL CHEMICAL LABORATORY
(Council of Scientific & Industrial Research)
Dr. Homi Bhabha Road, Pune - 411 008. India.

1950-2010 Celebrating Sixty Years of Science
हीरक जयन्ती वर्ष 2009-10

CERTIFICATE

Certified that the work incorporated in the thesis entitled **"Synthesis and Characterization of High Refractive Index Hydrophobic Polyacrylates"** submitted by **Ravindra V. Ghorpade** was carried out by the candidate at National Chemical Laboratory, Pune – 411008, under my supervision. Such material as obtained from other sources has been duly acknowledged in this thesis.

September 2012

Pune

Dr. S. Ponrathnam

(Research guide)

Dr. N. N. Chavan

(Co-Guide)

Communication Channels

☎
NCL Level DID : 2590
NCL Board No. : +91-20-25902000
EPABX : +91-20-25893300
+91-20-25893400

FAX
Director's Office : +91-20-25902601
COA's Office : +91-20-25902660
COS&P's Office : +91-20-25902664

WEBSITE
www.ncl-india.org

DECLARATION

I hereby declare that the thesis entitled **"Synthesis and Characterization of High Refractive Index Hydrophobic Polyacrylates"** submitted for Ph.D. degree to the University of Pune has been carried out at National Chemical Laboratory, Pune, India, under the supervision of **Dr. S. Ponrathnam,** Division of Polymer Science and Engineering, National Chemical Laboratory, Pune - 411008. The work is original and has not been submitted in part or full by me for any degree or diploma to this or any other University.

September 2012 (**Ravindra V. Ghorpade)**

Pune

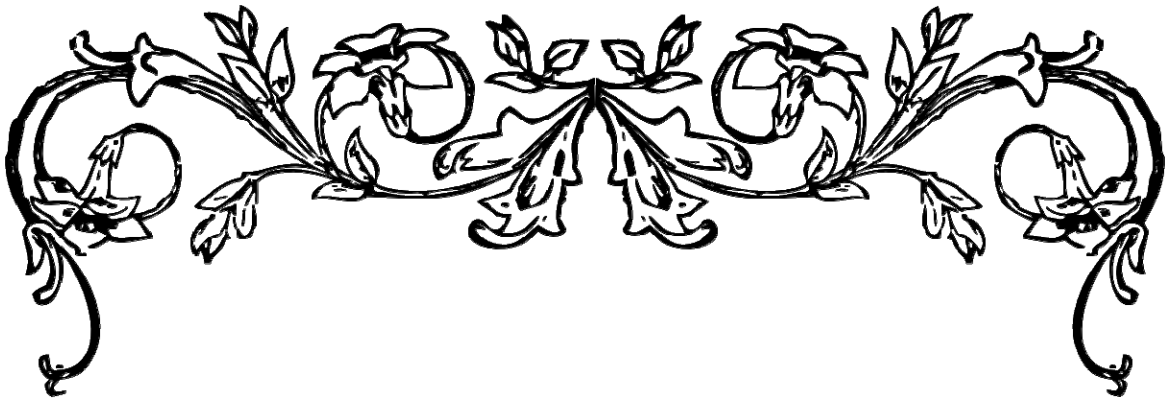

Dedicated to My

Beloved Parents

Aai & Dada

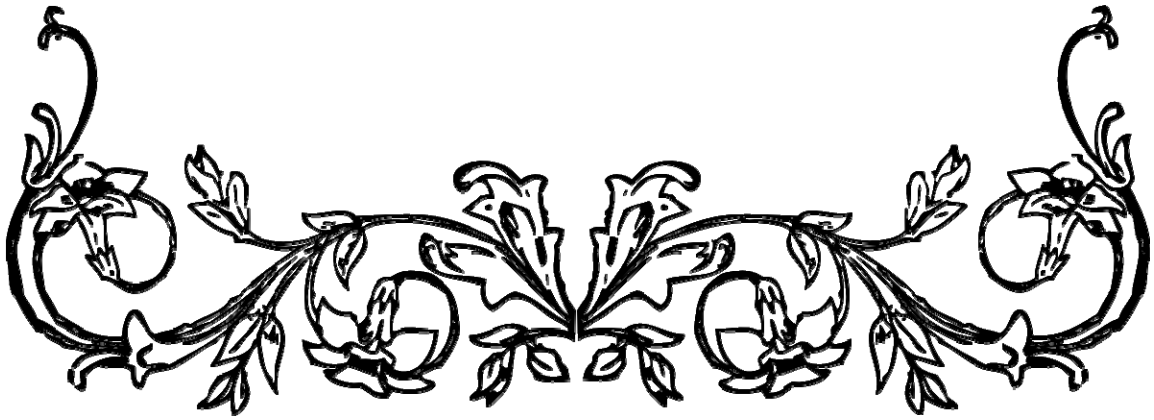

ACKNOWLEDGEMENT

In the voyage of my life, many people with or without knowing, have contributed significantly to help me to reach this level through their constant support and encouragement. Thus, without acknowledging their effort, this thesis may not be complete.

I reserve the first and best part of it to my research guide ***Dr. S. Ponrathnam****, whose noble principles and whole hearted dedication to science has gained my unassailable respect. He has been thoroughly supportive during my stay here and his fatherly care can never find an equal match. I absolutely admire his desire to do high quality science and instilling the thirst for science in not only his students but in all whom he comes across and I wish I could imbibe some of those qualities and exercise them for the rest of my life. I learned a lot about chemistry under his constant guidance. My deepest regards and reverence are always due for his wonderful personality.*

It gives me immense pleasure to express my sincere and heartfelt gratitude to my research co-guide ***Dr. N. N. Chavan****, who guided me through scientific skills, and provided constant support that made this part of my journey completed a lot easier than it would have otherwise been.*

My special thanks go to ***Dr. C. R. Rajan****, His scientific intuition as well as management skills inspire and enrich my growth as a student, a researcher. It is very rare to find some person, who always inspires to strive and excel in life and I am fortunate that I have found Dr. Rajan.*

Most importantly I would like to thank my family: my ***father, mother*** *and* ***grandfather.*** *They instilled in me the qualities that have made me what I am today. Without them I could not have succeeded, I would have been no one and nowhere. No words would be sufficient in describing the affection and support of my* ***sisters*** *throughout my life in all aspects. Moreover, I am grateful more than I can express for their constant help throughout from my academic life. They were essential to making the man I am today.*

I am very thankful to ***Dr. Smita Mule*** *and* ***Sunil Bhongle*** *for their help in HPLC/GC analysis. I thank* ***Polymer Characterisation, NMR and CMC groups*** *for their help in obtaining the analytical data. The invaluable help I received from*

Dr. Mrs. Puranik *for crystallography,* ***Dr. Ayesha Khan*** *(IBB, UoP) for cytotoxicity is also appreciated. I am sincerely thankful to* ***Dr. Ramesh Ghadge, Dr. Qureshi, Dr. Tambe****,* ***Dr. Saini and Dr. Tayal*** *for their fruitful scientific discussions. I sincerely acknowledge* ***Dr. R. Mao*** *(Indium Corp. USA) for providing computer programs.*

I can never forget the help from my seniors ***Dr. Harikrishna, Dr. Sarika*** *and* ***Dr. Ganesh,*** *I am thankful for their constant support. An individual thanks to my senior and friend* ***Abdul Wasif Shaikh*** *who have helped me in all possible ways during the tenure of my work at NCL.*

I would like to thank my past labmates and moreover I should say friends ***Mohasin, Khudbuddin, Kalpana*** *and* ***John*** *for their helpful hand and cheerful attitude that had made my working very easy and enjoyable.*

I wish to thank my friendly and cooperative labmates ***Sonali, Archana, Kishor, Punith, Sachin, Sumedh*** *and* ***Siona*** *for providing a cheerful atmosphere in the lab.*

I am fortunate to have good supportive staff. Specifically, I am thankful to ***Mr. S. Sathe*** *and* ***L. Giri*** *for their technical help.*

Apart from my lab, there are friends who are well-wishers, always encouraged and supported me. I would like to thank ***Shridhar, Rupesh, Manoj, Satish, Chinmay, Nagesh, Anil, Mohanraj, Rupesh B., Alkesh, Anurag, Niraj, Abhijit and Manzoor*** *for cheerful attitude during my stay at NCL.*

I am grateful to Council of Scientific and Industrial Research (CSIR), India for the research fellowship. I am thankful to ***Dr. Sourav Pal****, Director, NCL for allowing me to carry out research work and extending me all the possible infrastructural facilities during my research stay in NCL. The entire* ***library staffs*** *for providing excellent facilities are gratefully acknowledged.*

I wish to thank great scientific community whose achievements are constant source of inspiration for me.

Ravindra V. Ghorpade

TABLE OF CONTENTS

CHAPTER I

INTRODUCTION

CHAPTER II

AIMS AND OBJECTIVES

CHAPTER III

MONOMER SYNTHESIS AND HOMOPOLYMERISATION

CHAPTER IV

COPOLYMERISATION STUDIES

CHAPTER V

BULK POLYMER NETWORKS

CHAPTER VI

BULK POLYMERISATION KINETICS

CHAPTER VII

SUMMARY AND CONCLUSIONS

LIST OF FIGURES

Chapter I: INTRODUCTION

Chapter III: MONOMER SYNTHESIS AND HOMOPOLYMERISATION

Chapter IV: COPOLYMERISATION STUDIES

Chapter V: BULK POLYMER NETWORKS

Chapter VII: SUMMARY AND CONCLUSION

LIST OF TABLES

Chapter I: INTRODUCTION

Chapter III: MONOMER SYNTHESIS AND HOMOPOLYMERISATION

Chapter IV: COPOLYMERISATION STUDIES

Chapter VI: BULK POLYMERISATION KINETICS

Chapter VII: SUMMARY AND CONCLUSIONS

TABLE NO.	CAPTION	PAGE NO.
7.1	Structures of new monomers	275
7.2	Reactivity ratios of new monomer combinations	277

LIST OF SCHEMES

Chapter III: MONOMER SYNTHESIS AND HOMOPOLYMERISATION

Chapter IV: COPOLYMERISATION STUDIES

Chapter V: BULK POLYMER NETWORKS

LIST OF ABBREVIATIONS

AIBN	2,2'-Azoisobutyronitrile
BSS	Balanced Salt Solution
CA	Contact Angle
DAR -TPO	Duracure-TPO
DCM	Dichloromethane
DEPT	Distortionless Enhancement by Polarization Transfer
DSC	Differential Scanning Calorimetry
EGDMA	Ethylene Glycol Dimethacrylate
EMK	Ethyl Methyl Ketone
EWC	Equilibrium Water Content
Ex KT	Extended Kelen-Tudos
FDA	Food and Drugs Administration
FR	Fineman-Ross
GPC	Gel Permeable Chromatography
HDDMA	1,6-Hexanediol dimethacrylate
IOL	Intraocular Lens
IR	Infra Red
IRG -659	Irgacure-659
KT	Kelen-Tudos
MH	Mao-Huglin
MTT	3-(4,5-Dimethylthiazol-2-yl)-2,5-diphenyltetrazolium bromide
NMR	Nuclear Magnetic Resonance
PCO	Phacoemulsification
PDI	Polydispersity Index
PEA	2-Phenylethyl acrylate
PEMA	2-Phenylethyl methacrylate
PI	Photoinitiator
PMMA	Poly(methyl methacrylate)
PPEA	2-Phenoxy-2-phenylethyl acrylate
PPEM	2-Phenoxy-2-phenylethyl methacrylate
PTEA	2-Phenyl-2-(phenylthio)ethyl acrylate
PTEM	2-Phenyl-2-(phenylthio)ethyl acrylate
RI	Refractive Index
TGA	Thermogravimetric Analysis
TLC	Thin Layer Chromatography
TMS	Tetramethylsilane
UV	Ultraviolet-visible

Synthesis and Characterization of High Refractive Index Hydrophobic Polyacrylates

Abstract

The thesis has been divided into seven chapters which comprise of introduction to high refractive index polymers and intraocular lenses (IOLs), aims and objectives, monomer synthesis and homopolymerisation, copolymerisation studies of new monomer combinations and characterisation of copolymers, synthesis of bulk polymer networks and their evaluation, bulk polymerisation kinetics of 2-phenylethyl (meth)acrylate monomers using photo and thermal initiators and summary and conclusions.

The refractive index of materials can be increased by increasing the polarisability of substituent groups. By incorporating aromatic rings, atoms like oxygen and sulphur into polymers, high refractive index polymers have been obtained. By reacting phenol and thiophenol with styrene oxide, aromatic and sulphur containing aromatic alcohols were synthesised. The reaction of intermediate alcohols with acryloyl chloride and methacryloyl chloride yielded acrylates and methacrylates, respectively. Synthesised alcohols and monomers were characterised by different spectroscopic techniques to confirm structures. Homopolymerisation of newer monomers was carried out by free radical solution polymerisation. Optical and thermal properties of homopolymers were determined.

The properties of copolymers depend strongly on their composition; therefore in order to tailor some for specific applications, it is necessary to control their synthesis, and, in particular, to know the reactivity ratios of their constituent monomers. Free radical copolymerisation of 2-phenylethyl (meth)acrylate with newer monomers, in ethyl

methyl ketone using, AIBN as initiator, at 70 °C, were investigated. Monomer reactivity ratios were determined using the Fineman-Ross (FR), Kelen-Tudos (KT), extended Kelen-Tudos (Ex-KT) and Mao-Huglin (MH) graphical methods. Structural parameters of the copolymers were obtained by calculating the dyad monomer sequence fractions and the mean sequence length. Thermal and optical properties of copolymers are reported.

There is a need for flexible polymers with higher refractive index for better performing intraocular lenses (IOLs). Synthesis of new acrylic cross-linked copolymer networks suited to use as the foldable IOLs and studies concerning IOL polymer properties are all reported. New copolymers were synthesised from phenylated acrylates with new aromatic and sulphur containing aromatic (meth)acrylates using bulk free-radical polymerisation. Copolymers had low T_g, high refractive index, and were flexible. We report the optical, thermomechanical, and surface properties, as well as cytotoxicity of this series of novel (meth)acrylate copolymer networks.

Kinetic parameters of bulk photopolymerisation of 2-phenylethyl (meth)acrylate monomers using acetophenone type as well as phosphine oxide type photoinitiators were investigated at different temperatures and photoinitiator concentrations. Free radical bulk polymerisation of 2-phenylethyl (meth)acrylate was studied with AIBN as initiator by differential scanning calorimetry in the non-isothermal mode to determine activation energies (E_a) and rates of polymerisation.

Chapter I

Introduction

1.1 Introduction

In recent years, there has been an ever growing research interest in transparent, high refractive index polymers. Researchers have been making dedicated efforts in the last two decades to synthesise newer amorphous polymers that may possess potentials for optical applications. Since plastics (polymeric materials) are derived from active monomers, it is of utmost importance that suitable new monomers are developed. Thus, synthesised molecular entities necessary for polymerisation as well as desired optical properties in the eventual plastic needs to be incorporated. Optical plastics have been a priority area for material researchers worldwide, mainly, to find alternative materials to glass, a conceptual optical material in use over the years.

Use of optical plastic materials with high refractive index has increased many folds in present times. The higher the refractive index attained, greater the light refracted through the lens, thereby increasing the focusing power. These optical materials dramatically reduce optics profile and make lens lighter and thinner.[1,2] Optical polymeric thin films contribute to reducing the volume occupied by lenses in optical assemblies, which can advantageously make an optical apparatus lightweight and small.[3] High refractive index, very high optical transparency and low birefringence are the most important factors in optical applications. There are numerous advantages of using plastics for optical, particularly ophthalmic end uses.

Transparent composite materials are becoming increasingly important in applications ranging from protective coatings to optical communications. Optical materials are useful to control the flow and intensity of light. Examples of useful optical products include optical light fibres, light tubes, optical films including totally internal

reflecting films, retroreflective sheeting and ophthalmic lenses.[4-10] Newer high refractive index monomers can be used in compositions to make light management films. Thus liquid crystal displays, adhesives, magnifying lenses, binoculars and telescopes require monomers with high refractive index.[11-13] High refractive index polymers are of importance in dentistry, optical eyewear, holography and microelectronics.[14]

1.2 Comparison of Glass vs. Plastic Optical Materials

Glass and plastics each have their own unique advantages. Glass is harder, heavier but more durable than plastic. The very wide range of glass allows the designer to choose materials with desirable optical properties such as refractive index and dispersion to achieve better optical performance. This kind of freedom is limited with plastic materials. However, plastic optics offers other design freedoms that are not achievable or economical with glass optics. Glass lenses are made by grinding and polishing where as precision plastic lens are made by injection molding and casting. The difference in manufacturing process provides plastic optics some unique advantages such as high volume production capability and low manufacturing cost, design sophistication, unique design possibility and consistent quality. Plastic materials are more sensitive to environment changes such as temperature and humidity. In addition, the material flow pattern and shrinkage during molding also limit the surface accuracy that is achievable with plastic optics. The index distribution within a mould component may be inhomogeneous and of varying polarisation. The properties of high refractive index optical plastic materials can also be enhanced by optical top coating.[15]

Some advantages of optical plastics are as follows: (i) Low density; (ii) Low raw material cost; (iii) Good impact resistance; (iv) Excellent configuration flexibility; (v)

High transmittance of incident light; (vi) Safety involved in their use because when optical polymers break, the fragments tend to be large and obtuse and hence pose less danger and (vii) Ease of application of surface coating (which is used to disperse light or create a contrasting appearance)

1.3 Types of optical plastics

The capability of modern polymer molding technology to produce good surface quality has made it possible to manufacture different optical components for a wide variety of applications such as spectacle lenses, contact lenses, intraocular lenses, consumer products, instrumentation etc. The major types of polymers suitable for the optical applications are poly(meth)acrylates, polycarbonates, polyurethanes, polystyrenes and polysulphones.

1.4 Essential Properties for Optical Applications

Selection of a material for optical applications is done on the basis of (a) Physico-chemical properties and (b) Performance criteria of the product for a given application for which the material is to be selected.

The material selected is such that its physical properties are compatible with the environment in which it is to operate, having optical properties consistent with the desired level of performance.[16] The physical properties to be considered for optical applications include density, hardness, rigidity, stability at service temperature, thermal expansion, electrical and thermal conductivity, affinity to absorb and retain water, additives and radiation resistance.[17,18] Optical properties to be considered are spectral transmission, refractive index, purity, homogeneity, surface finish and strain.[18-21]

The performance criteria based on the material selected include mainly the weathering studies under different environmental conditions, machinability, biocompatibility, bio-degradability etc.

In this chapter we will focus on refractive index, one of the important properties for optical plastics.

1.5 Refractive Index

The refractive index (n) of a material is defined as the ratio of the speed of light in vacuum (c) to its speed in the material (v). Because of this definition the refractive index has no units. When an incident ray of light passes from vacuum into another medium, its velocity is reduced and the ray is bent or refracted towards the normal to the medium's surface. The angle between the incident ray and the normal is the angle of incidence (α); the angle between the refracted ray and the normal is the angle of refraction (β). For a given medium the ratio of the sines of the angles of incidence and refraction is constant.[22]

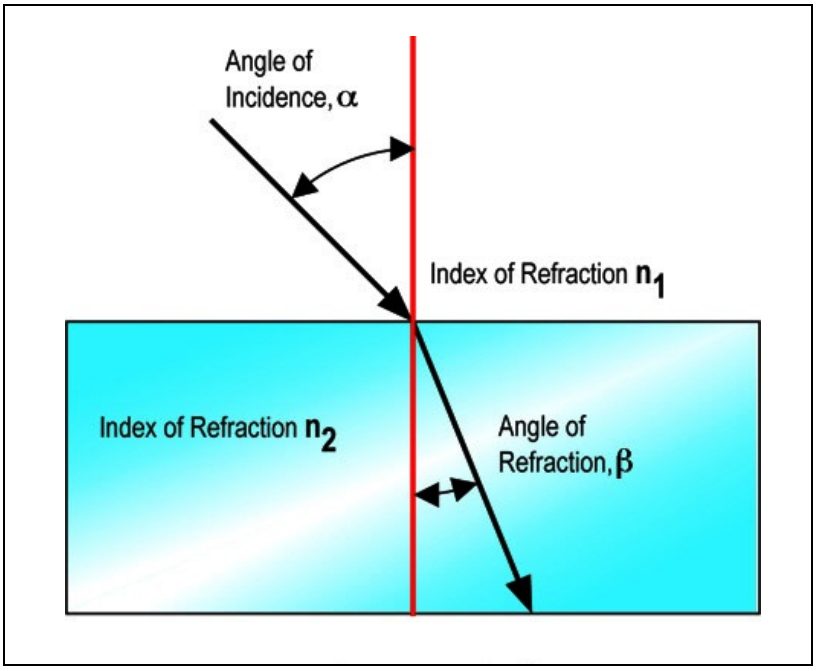

Figure 1.1: The index of refraction

$$n = \frac{\sin \alpha}{\sin \beta} = \frac{c}{\upsilon} \qquad 1.1$$

The index of refraction (Figure 1.1) is dependent upon wavelength. If the incident light is not monochromatic, the substituent rays will experience varying amounts of refraction. This effect is known as dispersion. Consequently, measurements of refractive indices require the use of monochromatic incident light. Generally for optical plastics experimental values of refractive indices compiled were measured at the Na-*D* line, which has a wavelength of 5893 Å.

The index of refraction is usually measured via an Abbe refractometer. This instrument has a fixed telescope and two right-angle prisms. A thin film of the sample being measured is placed in the gap between the hypotenuses of the right-angled prisms. The monochromatic incident light is refracted through the first prism, the sample, and the second prism. The refracted beam emerges parallel to the incident beam and is viewed with the telescopic eyepiece. The prism assembly is rotated to create a field of view as seen through the telescope in which exactly one-half of the field is dark and the other half is light, with a sharp interface between the two. The refractive index of the sample is read from a graduated scale on the prism assembly. Imperfect alignment of the prisms can increase the error.

The optical density of any transparent medium is a measure of its refractive index. A medium with a relatively high refractive index is said to have a high optical density, while one with a low index is said to have a low optical density.[23]

1.5.1 Polarisability and index of refraction

The refractive index of a material is intimately related to its polarisability *(α)*. The two are related to each other through the molar refractivity (R_{LL}), which is given as:

$$R_{LL} = \frac{M}{\rho}\frac{n^2 - 1}{n^2 + 2} \quad 1.2$$

where M is the molar mass and ρ is the density of the material. This definition of molar refraction is due to Lorentz and Lorenz[24]. Equation can be represented as:

$$n = \sqrt{\frac{V + 2R_{LL}}{V - R_{LL}}} \quad 1.3$$

Gladstone and Dale have also proposed a relationship between molar refraction and refractive index:

$$n = 1 + \frac{R_{GD}}{M/\rho} \quad 1.4$$

The relationship between polarisability and molar refractivity is:

$$3\varepsilon_0 R = N_A \alpha(\omega) \quad 1.5$$

where ε_0 is the dielectric constant and N_A is Avogadro's number. The dynamic polarisability $\alpha(\omega)$ is a function of frequency and is given as:

$$\alpha(\omega) = \frac{2}{3h}\sum_n \frac{\omega_{n0}\left|\langle 0|\mu|n\rangle\right|^2}{\omega_{n0}^2 - \omega^2} \quad 1.6$$

where ω is frequency, the subscript *0* denotes the ground state, the subscript *n* denotes the excited state, and μ is the electric transition dipole moment from ground to excited states.

1.5.2 Refractive index of polymers

Denbigh established that the molar refraction may be considered as the sum of the bond refractions that make up the molecule. Van Krevelen[24] assigned chemical group refractivities that can be used to calculate refractive indices of polymers. If the crystalline

and noncrystalline densities and their refractive indices are known then a similar additivity approach can be used to calculate the refractive indices of semicrystalline polymers of known density as follows:

$$n = v_{cr} n_{cr} + (1 - v_{cr}) n_{cr} \quad 1.7$$

$$v_{cr} = (\rho - \rho_{nc}) / (\rho_{cr} - \rho_{nc}) \quad 1.8$$

The refractive index is also a function of frequency, temperature, and degree of polymerisation. While predicting the refractive index of a material, it is important to consider both the intrinsic refractivity and density as the key physical factors determining the refractive index. For example, fluorinated polymers have very high densities but very low intrinsic refractivity and therefore very low refractive indices. The densities of many polymers containing aromatic rings[25-29] are not very high but they have large intrinsic refractivity and therefore high refractive indices. Amorphous polytetrafluoroethylene has a density of 2.00 g/cm^3 but a refractive index of only 1.350. Amorphous polystyrene has a density of only 1.05 g/cm^3 and a refractive index of 1.59.[30]

R_{LL} and R_{GD} have very little dependence on temperature and percent crystallinity while molar volume '*V*' changes significantly with changing temperature. Refractive index '*n*' decreases with increasing molar volume in asymptotic manner and approaches the absolute minimum value of 1.0.

Temperature is another parameter on which the refractive index is dependent. The temperature dependence of refractive index is similar for all polymers. A very simple and empirical rule of thumb is that refractive index decreases by about 1.10 x 10^{-4} when temperature increases by 2.0 x 10^{-4} K for transparent polymers and for isotropic amorphous polymers, refractive index decreases by about 3.10^{-4} with increase of

temperature by to 5.10^{-4} K. Since refractive index can never become smaller than 1.0, the rate of decrease of refractive index with increasing temperature above glass transition temperature must eventually level off and asymptotically approach zero for refractive index to remain greater than 1.0.

Molar refraction of a polymer can be predicted if both the refractive index and the density are known. The refractive indices of polymers can be predicted by using group contributions to estimate V and either R_{LL} or R_{GD}. Refractive index can be estimated in terms of V and either R_{LL} or R_{GD}.

Group contributions for R_{LL} were developed from data on liquid organic compounds rather than polymers.[31,32] This is because the intrinsic refractive power of a given structural unit is affected only very slightly whether it is located in a small molecule or in a polymer chain. Changes in the molar volume account for most of the difference between the refractive indices of liquid organic compounds and high polymers containing the same structural units.

1.5.3 Strategies to obtain high refractive index materials

The desired characteristics in a material need to design. For obtaining high refractive index, element to be incorporated should have high mean polarisability and low molar volume. Copolymerisation of monomers and homopolymers that have $n > 1.5$ can also lead to polymers having a high refractive index. To obtain polymers with high refractive index and Abbe number, polymers incorporating structural elements an aromatic group, a halogenated aromatic group[25-29] and an alicyclic condensed ring were synthesised, but refractive index and Abbe number values improved moderately.

Polyacrylates, that are composed of specific organic polymer chains and inorganic moieties, showed a remarkably high refractive index (due to polymer chain) and Abbe values (due to inorganic moiety). Based on molar refraction and molar dispersion, sulphur[33-35] and oxygen containing polymers would be expected to have higher refractive index and Abbe number values.[31-32] Refractive index can also be achieved through polarisabilities of the combined groups in a molecule.[33-35]

Contributions to the refractive indices are higher for carbon atoms than for hydrogen atoms. Since carbon atoms dominate the structure of most polymers have a refractive index near 1.50. Polymers with strongly electronegative substituents such as fluorine will have lower refractive indices. Substituents having high polarisabilities over a large atomic area such as sulphur, phosphorous, bromine, chlorine and iodine tend to have higher refractive indices.[36] Bulky, conjugated aromatic substituents, particularly hetero-aromatic substituents, such as carbazole have high refractive indices. Carbazole based polymers[32] have good optical properties and are easy to process.

Polymethacrylates and polyacrylates are used commercially in many optical applications. A family of novel methacrylates, acrylates and dimethacrylates were synthesised incorporating the carbazole moiety along with aromatic substituents. Polymerisation of these monomers generated high refractive index materials.[37-41]

Increasing the polarisability of substituent groups increases the refractive index of materials. Thus, the refractive index depends on the movements of the electron cloud of atoms forming the polymer.[42] On transition from one hydrocarbon polymer to another, the polarisability does not change and hence, the refractive index does not change much. It is well known that the refractive index of polymers is within the limits of 1.36 – 1.70.

Very few polymers have a refractive index close to 1.70 while most polymers incorporating hydrocarbon chain have refractive index value close to 1.5. Higher refractive index can only be achieved by incorporation of groups with higher molar refraction. Aromatic structural elements contribute to increased refractive index and increased dispersion. Low dispersion is desirable, in order to minimise chromatic aberration of the polymer.[68-70]

Optical materials with refractive indices not less than 1.55 may be obtained from polymers containing only C, H, O and N.[43-48] Further increase in index is achieved by:

a. Copolymerisation of monomers having high refractive index.
b. Introduction of atoms such as metal atoms having high ionic size and polarisability into the system.
c. Introduction of nano fillers into the system.

1.5.3.1 Copolymerisation of monomers

The refractive index of polymers depends on the refractive index of monomers constituting the polymers. Monomers have been suitably modified to obtain copolymers having a refractive index in range 1.49 to 1.56.[49-51] The refractive index of these polymers match refractive index that of crown glasses and hence are preferred alternate materials for optical applications.

Polyimides are a class of polymers extensively used in microelectronics because of their outstanding key properties such as high thermal stability, chemical resistance and good mechanical properties.[52] You et al. reported sulphur polyimides (Figure 1.2 a) with high refractive index, good transparency and low birefringence.[53-55] However these polymers are expensive and some times produce coloured product.

Sulphur containing polyamides

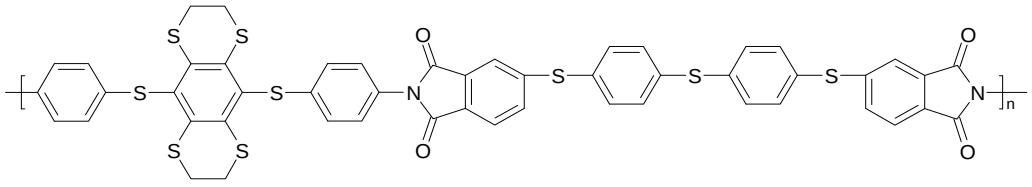

(a)

Polystyrene

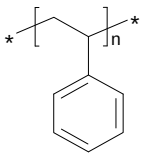

(b)

Polythiourethanes

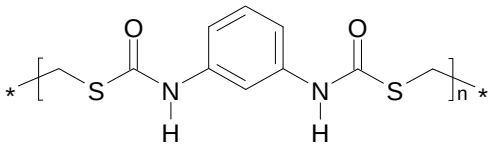

(c)

Poly(N-vinyl carbazole)

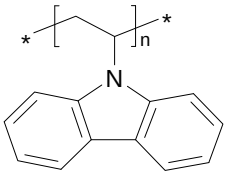

(d)

Aromatic polysulphone

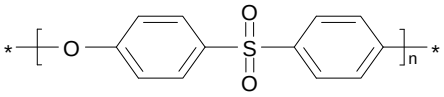

(e)

Polycarbonate

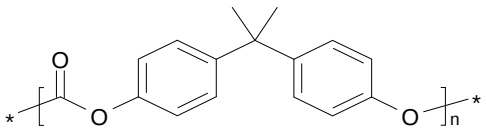

(f)

Sulphur containing methacrylate

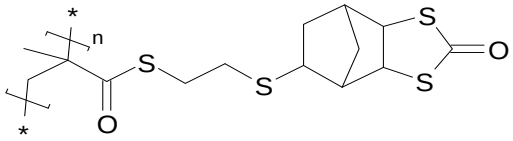

(g)

Figure 1.2 (a-g): Structures of high refractive index polymers

Copolymerisation of styrene with monomers having a refractive index greater than 1.6, leads to the formation of polymers with higher refractive index. For example, refractive index of a copolymer of styrene with vinyl carbazole is 1.669.[56]

So far, the reported work shows that copolymerisation can be successfully carried out by thermal polymerisation technique. The notable examples of polymers with good refractive index values of 1.55-1.58, good strength, rigidity and weather resistance[57] are obtained this way.

Sulphur containing monomers are good candidates for producing high refractive index optical materials.[58-60] Ready polarisability of sulphur produces a strong interaction between the material and incident light, resulting in high refractive index.[60] Sulphur containing polymers including polythiourethanes (Figure 1.2 c) are therefore, nowadays, being developed as optical materials.[61-67] Thio(meth)acrylates (Figure 1.2 g) are well known to provide an optical resin composition that can be rapidly polymerised. Thus it exhibits good handling properties, excellent optical properties, particularly a high refractive index and excellent impact resistance and also generates less unpleasant odour during processing. The polymerisation and copolymerisation of vinyl thioacetate in the presence of radical catalysts does not lead to high molecular weight because its exhibits a high chain transfer constant.[71] Subsequent hydrolysis of the thioacetate functional group requires alkaline conditions and is accompanied by oxidative cross-linking. Copolymerisation of thioacetate with vinylene carbonate, methyl methacrylate, N-vinyl succinamide, N-vinyl phthalamide, N-vinyl carbazole, styrene and methacrylate led to high refractive index materials.[72-74] Sulphur containing substituents including linear

thioether, sulfone, cyclic thiophene, thiadiazole, thianthrene etc., are commonly used for increasing a polymer's refractive index.

Sulphur containing O-(meth) acrylate resins have been prepared,[71] mainly for eyeglasses and cameras by the dithioacetalisation, thio-esterification or thiourethanisation of a novel thiol compound followed by dehydrohalogenation. A sulphur containing O-(meth)acrylate resin or a thio(meth)acrylate resin can be prepared by rapid polymerisation by using of either UV rays, thermal methods or both. Thus, thio(meth)acrylate are used to provide an optical resin composition which has good handling properties and can be rapidly polymerised to give excellent optical properties, including a high refractive index and excellent impact resistance, as well as generating less unpleasant odour during processing. Sulphur based PMMA polymers have been used for plastic lens, films and optical components due to high transparency, high refractive index and good adhesion.[75,76]

Phosphorous containing groups, such as phosphonates and phosphazenes exhibit high molar refractions and good optical transmittance in the visible light region. Thus, phosphorous containing polymers might be good candidates as high refractive index polymers for optical applications. Phosphazenes contain inorganic phosphorous-nitrogen backbone; afford dense molecular packing and a high molar refraction of the repeating unit. In addition, the films exhibit good optical transparency with maximum absorption wave lengths of around 270-280 nm.[77-81]

Eyeglass lenses with high refractive index were prepared from a copolymer comprising methacryl thioester, triethylpropane tris (2–mercapto propionate) and methacrylic acid ester. The lens obtained from the copolymer showed a refractive index

of 1.648 and Abbe No. 29.[82] Optical lenses with high refractive indexes of 1.620 are prepared by the copolymerisation of benzene thiol (dimethacrylic thioester), di (meth)acrylic esters (eg. diethylene glycol diacrylate), thio (dimercaptoethyl) and aromatic vinyl compounds such as styrene.

Optical lenses with high refractive index of 1.654 were also prepared by the copolymerisation of methacrylic thioesters (4,4'–thiobisbenzene thiol dimethacrylic thioester), pentacrylthritol tetrakis (thioglycol), thiodi (mercaptoethyl) and divinyl benzene.[83] Reaction of thiols with methacrylic acid gave resins having a refractive index of 1.61 and Abbe number 30.[84]

A copolymer comprising 1,4–bis(2–mercaptoethylene methylene) benzene dimethacrylate, 1,4–bis(2–mercaptoethylene thiomethylene) benzene and α-methyl styrene were used for the production of high refractive index lenses. Schmitt et al. prepared highly transparent methacrylate copolymers for optical lenses by reacting methacrylic acid anhydride with sodium 1,2-ethanedithiolate, combining this with diisocyanate, dithiol, methacrylate and polymerised to yield a polymer having refractive index of 1.60, Abbe No. 37.2 and impact strength of 3.85 kJ/m^2.[83]

Copolymerisation yields flexible, soft high refractive index materials having low glass transition temperature for intraocular lens applications.[85-87]

1.5.3.2 Introduction of metallic atoms of high polarisability

Polymer materials containing metal atoms have always been of special interest for optics.[88-89] Use of metals having high polarisablity and low ionic radius like barium, strontium, lead and lanthanum has resulted in materials having a refractive index of 1.62 – 1.65.[90-92]

Metals are incorporated into the polymerisable unsaturated acid, which leads to transparent polymers with high refractive indices.[90] Unsaturated acids and systems such as divinyl benzene have also been used to generate high refractive index plastics.[89] The value of refractive index has been shown to depend on the type of polymerisation. Laser polymerisation leads to a higher refractive index than polymerisation by thermal methods.[93] Such changes in the refractive index are related to the difference in the chemical structure due to reconfiguration of bonds. The other important development, which would perhaps become a preferred technique in future for polymerisation, especially of high refractive index, pertains to the use of radiation for polymerisation.

1.5.3.3 Introduction of nano filler

In recent years, nanoparticles have been used to make transparent nanocomposite structures having high refractive indices. Polymers dispersed inorganic particles in range 1 to 100 nm do not scatter light and are potential materials. Using nano particles, refractive indices over the entire range of 1 to 3, which is the lowest and the highest possible refractive index in polymer matrices can be obtained.[94] Transparent polymeric materials can be coated with surface layers of UV absorbing nanoparticles to inhibit degradation of the polymer.[95]

The technological challenge in creating near transparent high refractive index, organic/inorganic nanocomposites lies in the creation of nanoparticles in the size of 20 to 40 nm, to produce high refractive index nanoparticles. Lead sulphide (PbS), Indium phosphide (InP), Gallium phosphide (GaP), Germanium (Ge) and Silicon (Si) particles in a gelatin matrix have been prepared in this way.[96]

Particles useful for nanocomposites are prepared by a variety of techniques ranging from mechanical attrition to colloidal processing. Mixing, spin coating or casting suspension of nanoparticles in appropriate organic solvents are technologies used to prepare nanocomposites. Reverse micelle technology has been used to prepare UV curable, transparent, acrylic resin and titania compositions by controlled hydrolysis of titanium tetrabutoxide (TTB).

We have utilised a technique for making polymers of controlled refractive index through copolymerisation. Any refractive index, within the limits 1.50 to 1.62**,** can be obtained by this method using newly synthesised monomers. Using two monomers bracketing the desired RI, a copolymer can be synthesised in which the RI of the copolymer can be varied with the monomer feed composition. The relationship between RI and copolymer composition can be expressed by a simple rule of mixtures to a first approximation. Fine tuning of the monomer feed results in polymers with controlled RI. The focus of the work presented in Chapter 4 and 5 is to prepare precisely controlled high RI materials using this technique.

One of the objectives of the thesis is to synthesise high refractive index materials for Intraocular Lens (IOL) application. We will quickly review various aspects related to IOLs.

1.6 The Eye

The structure of the eye (Figure 1.3) is remarkable being able to receive light and to transmit it as pulses recognised as images by the brain. The eye is housed in an eye socket (or orbit) within the skull. The size of the orbit largely exceeds that one of the soft tissue eyeball. The space between the eyeball and the orbit is filled with fat and lined with a sheet of connective tissue, which allows the free motion of the globe.

The eye is a nearly spherical hollow globe with an average diameter of about 2.5 cm filled with fluids. The three layer wall consists of (i) a peripheric fibrous protective envelope, known as the sclerocorneal layer, whose posterior part, i.e. the sclera, is white and covers approximately five sixths of the eye surface, (ii) the anterior sclerocorneal layer, known as the cornea, and (iii) the middle vascular layer, that contains the choroid and the iris.

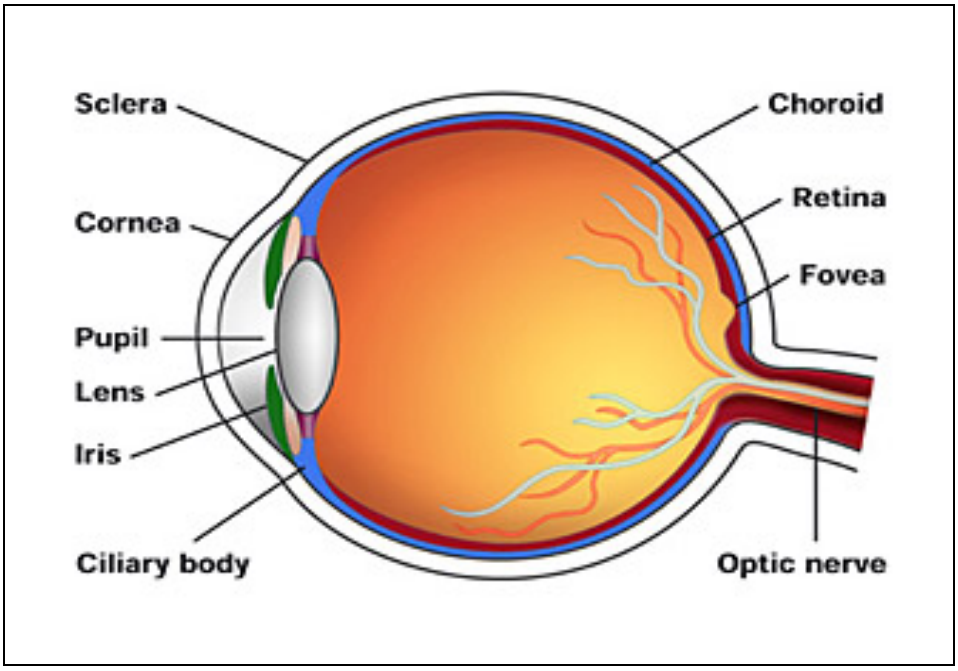

Figure 1.3: Eye anatomy

The lens is a 4 mm thick transparent biconvex body, with an average diameter of 9 mm. It is attached to the ciliary body via a network of elastic fibres, the zonules. No cell loss and long lived proteins in a light-saturated environment are key features of the lens. However, the lens core proteins are exposed to environmental damage, such as age related environmental issues, sudden physical trauma, radiation pulse or poor nutrition, which often results in the opacification of the lens, known as 'Cataract'.[97-99]

1.7 Cataract

Cataract is a clouding of the lens of the eye which impedes the passage of light (Figure 1.4). Most cases of cataract are related to the aging process. However, children can be born with a cataract or develop it in their teenage years. Furthermore, a cataract may develop after eye injuries, inflammation, and some other eye diseases. According to studies of the World Health Organisation (WHO), more than 50 million people suffer from cataract worldwide which makes cataract the cause for about half of all worldwide cases of blindness.[143] Although cataracts can be surgically removed, in many countries surgical services are inadequate, and cataract remains the leading cause of blindness. With an increase in average life expectancy, the number of people suffering from cataract is growing.

Cataract is thus an important cause of bad vision in both developed and developing countries. Comprehensive prevention of cataract development is not known yet. The treatment of cataract through an operation is very successful in restoring sight. The opaque lens is removed and replaced by an artificial intraocular lens (IOL).[100] Even though the first successful implantation of an IOL was accomplished, yet some significant drawbacks related to IOL surgery still exist today. A typical post-operative

complication is posterior capsule opacification (PCO), the so-called secondary cataract. PCO is caused by proliferation and migration of retained lens epithelial cells into the optical axis, and leads to a progressive deterioration and disturbances in visual activity.[101-107]

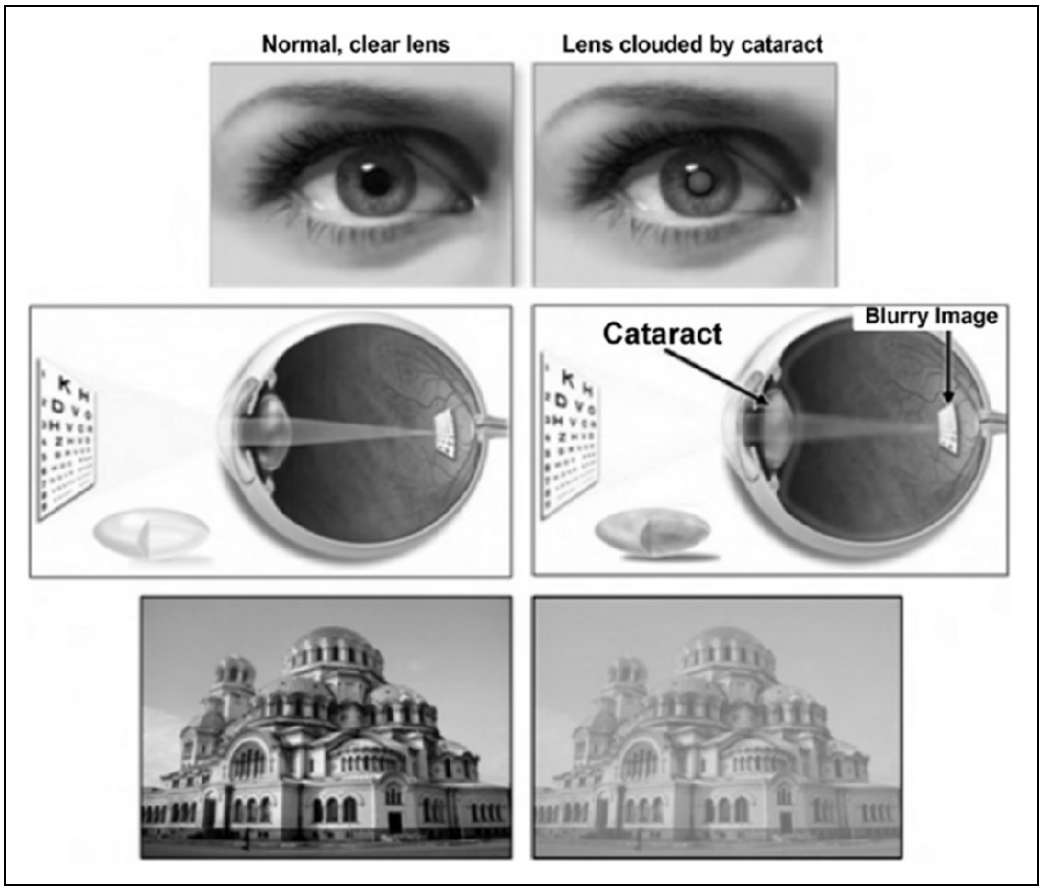

Figure 1.4: Comparison of normal and cataractous lenses

1.8 Intraocular Lens Development

Dr. Harold Ridley implanted the first intraocular lens (IOL) on November 29, 1949.[108-112] In so doing he changed the practice of ophthalmology. Not only will Ridley's invention provide superior visual rehabilitation to cataract patients for generations to come, but also, without his having realised it, the IOL has been a major factor in changing the way ophthalmology is practiced. Ridley would rely on his World War II

experiences to obtain a suitable material for his first artificial lens. During the war, British freighter cockpit canopies made of poly(methyl methacrylate) (PMMA) would fragment due to gunfire. The fragments from some of the canopies would penetrate the eyes of the flight crew. These fragmented PMMA splinters did not irritate the eyes, and caused very little reaction. Having examined several of these fliers, Ridley made the observation that, "Unless a sharp edge of the plastic material rests in contact with a sensitive and mobile portion of the eye, the tissue reaction is insignificant".[108]

As Ridley considered which material would best be suited for IOL development, he learned that commercial PMMA was not pure enough to be implanted into the human eye.[113] With the help of his friend John Holt at Imperial Chemical Industries, Perspex CQ (Clinical Quality) was synthesised which is still in use today. Perspex CQ has a refractive index of 1.49 and a specific gravity of 1.19.[108]

The first IOL was made by Rayners of London.[113] The dimensions of the circular lens were 8.35 mm in diameter, 2.40 mm in thickness and 112 mg in weight. These dimensions were about 1mm less than those of the human lens. The refractive power of the lens was 24 diopters.[113]

Ridley implanted his first IOL into the capsular bag of the posterior chamber following extra capsular cataract extraction (ECCE). The procedure was performed on a 45 year old woman at St. Thomas Hospital in London on November 29, 1949.[114] Ridley's IOL implantations were a success, but left the patients severely myopic. Ridley continued to improve his IOLs and procedures. Soon others were improving and implanting IOLs as well. From the first implantation to present day, the evolution of IOLs can be roughly broken down into six generations.

1.8.1 Generation I: Original Ridley posterior chamber lens

Generation I IOLs were made and implanted during 1949-1954.[108] These lenses were designed to be similar in size and shape to the human crystalline lens, which is anatomically planted in the posterior chamber of the eye. An adult crystalline lens measures approximately 4 mm in thickness and 9 mm in diameter.

There were several postoperative complications associated with the first generation IOLs. These included inflammation, pupillary occlusion, thickening of the posterior capsule, loss of anterior chamber, secondary glaucoma, iris atrophy caused by IOL pressure, decentration and dislocation of the lens.[115]

1.8.2 Generation II: Early anterior chamber lenses

One of the major problems with the original Ridley lens was dislocation. The anterior chamber of the eye was considered for the new implantation site due to its narrow confines.[115] This generation of lenses was developed and implanted from 1952 to 1962.[108] PMMA was still the material of choice for IOL optics. Anterior placement of the IOL was also considered an easier technical procedure than posterior placement.

Unlike the original lens developed by Ridley, many anterior chamber lens designs were developed from ideas of many different surgeons who worked with IOLs. Notable during this time were Baron, who implanted the first anterior chamber IOL, Strampelli, Choyce, and Bober-Ans of Denmark.[115]

Contact with endothelial cells and corneal decompensation were the two major problems with anterior chamber IOLs. These IOLs had serious long term complications and many surgeons abandoned IOL implantation all together.[116]

1.8.3 Generation III: Iris support lenses

This generation of lenses were developed and implanted during 1953-1973.[108] Iris support IOLs were designed in an attempt to overcome the problems associated with Ridley's posterior chamber lens and the anterior chamber lenses developed in the 1950s. Iris support IOL optics were made of PMMA. In 1953, Epstein introduced the collar stud lens.[117] The central post was 3 mm in diameter and the IOL was placed in the iris plane. The major complication with the iris support lenses was erosion or chafing of the iris stroma and pigment epithelium at the IOL contact sites.[118] Cornelius Binkhorst of Holland tried improving on the designs of Epstein and Copeland by minimising the amount of surface area the IOL had in contact with the iris. He hypothesised that contact with the posterior side of the iris would not cause complications; this was later seen to be an incorrect assumption.

1.8.4 Generation IV: Later model anterior chamber IOLs

This generation of lenses was designed and implanted from around 1963 until the mid 1980s.[108] Iris support IOLs underwent many different design changes from the early 1950s until the early 1980s. During this time, many new anterior chamber fixated IOLs were being introduced. If the anterior IOL design was correctly vaulted and properly sized, long term success could be achieved. PMMA was still the material of choice for these later model anterior chamber IOLs, but many of the IOLs developed during this period had to be removed from the market due to manufacturing defects and design flaws.

1.8.5 Generation V: Modern PMMA posterior chamber IOLs

Modern PMMA posterior chamber IOLs were designed and implanted from about 1975 until the mid 1990's. During this period, the evolution of extracapsular cataract extraction was marked by four major milestones: Microscopic surgery, phacoemulsification for cataract removal, iridocapsular fixation, and use of flexible haptics.[116]

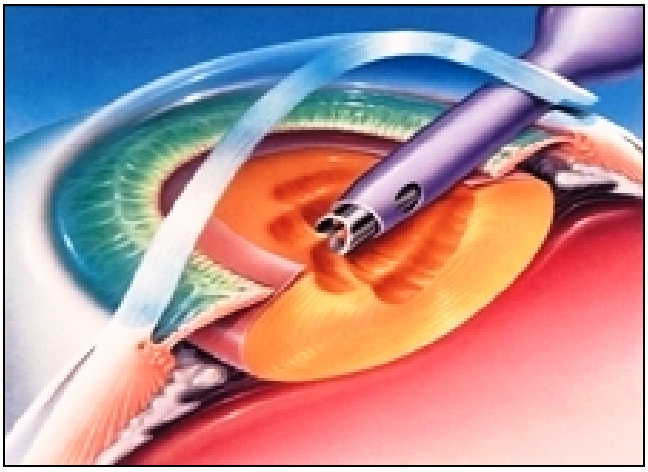

Figure 1.5: Phacoemulsification for cataract removal

Phacoemulsification was first introduced by Kelman in 1967.[119] This technique used an ultrasonic vibrating tip to liquefy the natural cataractous crystalline lens (Figure 1.5). The lens could then be extracted by aspiration through a much smaller incision than with nonultrasonic methods.

Iridocapsular fixation was heavily influenced by Cornelius Binkhorst. He was one of the pioneers in the return to the Extra Capsular Cataract Opacification (ECCE) procedure.[120] Binkhorst realised that an intact posterior capsule enhanced stability and provided many advantages for IOL implantation.

In previous IOL designs, the optics were made of PMMA and remained inflexible. Most IOLs were made as one piece rigid structures that were abrasive and damaging to the tissues of the eye. Flexible haptics made of polypropylene (PP) reduced the surface area and damage to the supporting tissue. The most common designs with flexible haptics were the C-looped and J-looped designs. Figure 1.6 illustrates common flexible haptic IOL design.

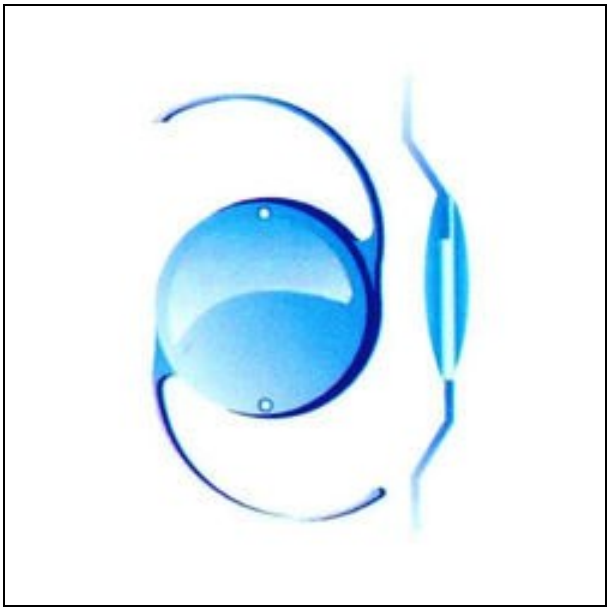

Figure 1.6: Flexible haptic IOL design

A significant modification that took place during the early 1980s was the addition of UV radiation absorbing molecules to the IOL optic (PMMA) to prevent retinal damage by solar exposure.[121] The addition of UV absorbing molecules was done to mimic the UV absorbing properties of the natural crystalline lens. Ultraviolet radiation below 400 nm is absorbed by the eye and passes to the retina after the natural crystalline lens is removed. This UV radiation is thought to cause cystoid macular edema and age related macular degeneration.[122] UV absorbing molecules are added to all present day IOLs.

1.8.6 Generation VI: Foldable IOLs

This generation of IOLs began in the mid 1980s and is the most common type of IOL implanted today. The major advantage of foldable IOLs is the ability to insert the lens through a 2.5 mm corneal incision. Prior to foldable IOLs, the corneal incision had to be minimally the width of the PMMA optic. The small incision allows the wound to heal without the need of sutures. Figure 1.7 illustrates the foldable intraocular lens implant insertion through tiny incision into eye and unfolded lens set into its permanent position.

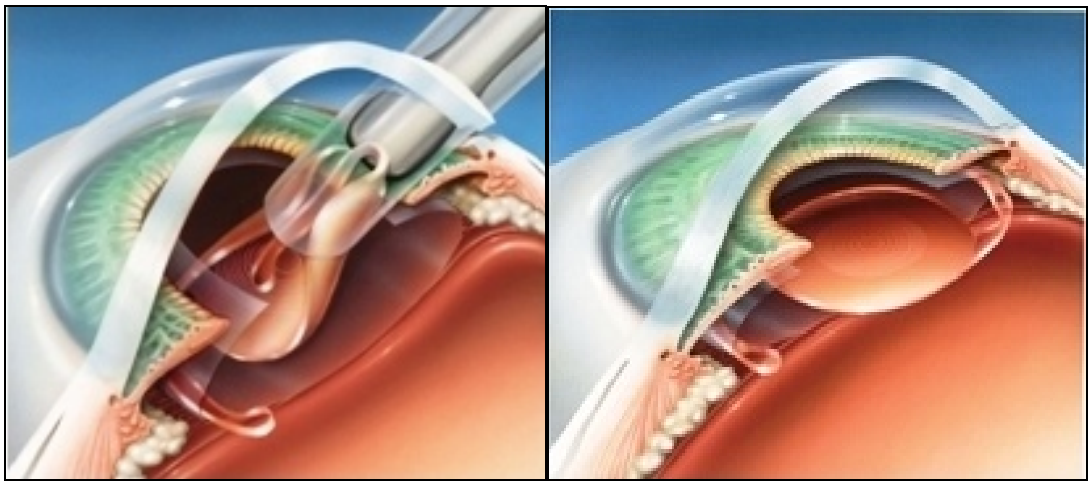

(a) **(b)**

Figure 1.7 (a-b): (a) IOL insertion through tiny incision into eye, (b) unfolded lens

1.9 Materials for IOL

From the above discussion, it is quite obvious that the IOLs are designed to remain inserted in the eye as an integral part of eye playing the role of a naturally existing crystalline lens of the eye. Thus, it is essential that the material to be used for making IOLs must meet the following basic criteria mentioned in Table 1.1.

Table 1.1: Essential properties of material for IOL application

Property	Discription
Transparent	The polymer may not be opaque. Otherwise scattering will be caused by the polymer or embedded particles generating glare.
Colourless	The material should be without colour. Only a slight yellowish tone caused by absorption of blue light can be tolerated. Coloured materials are not suitable.
Elastomeric	The material should have elastomeric properties to obtain a foldable IOL and avoid plastic deformation.
Cross-linked	To afford elastomeric properties the polymer must be a cross-linked network. A cross-linking procedure that does not involve a photochemical process is favorable to avoid undesired changes in refractive index.
Bulk polymerisable	The corresponding monomer should be polymerisable to a plate by bulk polymerisation. Bulk polymerisation is the conversion of monomer into a polymer without the aid of a solvent.
Suitable for turning	The mechanical properties of the polymer must allow the fabrication of IOLs by diamond turning.
Biocompatible	The polymer must not have any toxic or injurious effects on the eye.
Non-degradable	Despite being biocompatible the polymer should not be biodegradable. Otherwise, the IOL would degrade over the long time it needs to stay in the eye.
Thermally stable	Polymeric material should be thermally stable.
Immune to sunlight	The overall IOL must be designed in such a way that light from the sun or other common light sources cannot change the refractive power even after extended periods of time.

1.10 Types of IOL

These are several types of IOLs.[123] The following subsections are devoted to specific cases.

1.10.1 Monofocal IOL

Monofocal, or single vision lenses, are the standard lenses that have been implanted at the time of routine cataract surgery for many years. These lenses take the place of cataract and can help one to see distant objects. However, these lenses will not

correct astigmatism and will not correct near vision, so it is likely that one will need to wear glasses at least part-time for distance visions and full-time for near work.

1.10.2 Toric IOL

In addition to correcting nearsightedness or farsightedness, toric lenses have the ability to correct astigmatism. If one has significant astigmatism before surgery, then this lens option will provide you with a better opportunity to have clear distance vision without glasses. Toric lenses still correct primarily distance vision and will not correct near vision.

1.10.3 Multi-focal IOL

Multi-focal lenses are appropriate for some patients who have a strong desire to see distant and near objects without glasses and are willing to potentially somewhat compromise the quality of their vision to obtain freedom from glasses. In appropriate candidates, multifocal lenses can improve distance, intermediate (computer distance), and near vision and can reduce their dependency on spectacles at all of these distances; however, neither lens restores the natural vision at all distances one had as a youth, and the person may experience some problems with these lenses. These include, but are not limited to: poor night vision, including glare and halos, less sharpness of vision than may be obtained with a monofocal IOL and spectacles, and inadequate near and intermediate vision that still may require the use of glasses. Multi-focal lenses may require some time for adaptation, and in very rare cases, the vision obtained with multi-focal lenses may be so poor that replacement of the lens with a monofocal lens may be necessary. This is a separate procedure, and it carries additional surgical risks.

1.10.4 Pseudo-accommodative IOL

These IOLs are designed to provide good distance acuity and a moderate amount of intermediate and near correction. Most patients would find that they still require reading glasses for most near tasks.

1.11 Manufacture of IOL

1.11.1 Polymerisation techniques to make materials for IOLs

The process for the production of IOLs consists of the following steps:

(a) Copolymerisation of monomers

(b) Casting into lenses

(c) Machining, cutting and grinding

(d) Fixing of the haptic to the optic.

1.11.1.1 Copolymerisation

The polymers for foldable intraocular lenses and rigid intraocular lenses are made by the conventional polymerisation. Mixtures of the liquid monomers in the desired proportion, and a conventional thermal free radical initiator are injected into a suitable mold consisting of the optic and haptic portions.

1.11.1.2 Cast polymerisation

The mixture is then subjected to a heating cycle to activate the initiator. Free radical initiator such as peroxides, peroxydicarbonates and azonitriles are used. To facilitate the polymerisation, conventional photo initiator compounds are also used.

Optional additives such as UV absorbing materials are used so that the lenses may have an ultraviolet absorbance imitating that of the natural lens of the eye. The ultraviolet absorbing material can be any compound that absorbs ultraviolet light but does not

absorb substantial amounts of visible light. The ultraviolet absorbing compound is incorporated into the monomer mixture and entrapped in the polymer matrix when the monomer mixture is polymerised.[124] To prevent leaching out of the ultraviolet absorbing compound, compounds that can covalently bond to the polymer matrix are chosen.

IOLs can also be cast into sheet form by a conventional two step procedure.[125] In the first step, the casting mixture is prepared by heating the mixture of monomers, cross-linking agent and initiator at 80 °C. In the second step the mixture is transferred to a cell suitable for casting sheets and polymerised by subjecting the cell to suitable heating. IOLs are lathe cut from sheets while holding the temperature of sheets below 0 °C.[126]

1.11.1.3 Cutting, grinding and machining

After the polymerisation cycle, molding and drilling operations are carried out. The mold containing the optical material is placed on a lathe and the desired optic chamber is lathe cut. The lathing and drilling operation is carried out by cooling the mold/optic in a freezer to less than 10 °C and preferably less than 0 °C.[127]

1.11.1.4 Attachment of the haptics

The next step involves the attachment of the haptic to the optic in the case of a multipiece IOL. Two holes are drilled into the side of the lens. The haptic is then inserted into the optic with the help of a laser source. Suitable haptic materials are polypropylene and PMMA.

1.11.1.5 Techniques of making IOLs from base materials

Rigid intraocular lens made of PMMA and soft intraocular lens made of modified acrylates or silicones can be manufactured by:

1. Cast molding: - A method of injecting a monomer into a casting mold designed to produce lenses of a desired shape. Cast molding is also used to cast optical blanks, which are further processed into lenses.

2. Lathe cutting: - A method of cutting a sheet obtained by polymerising and curing of a monomer into an intraocular lens of a desired shape. Another alternative is to use the optical blanks and subjecting it to the lathe machine to cut lenses out.

Sometimes in the IOLs manufactured by the methods indicated above, voids formation was observed. These voids get filled up with the vitreous humor of the eye and results in the formation of luminescent spots which do not affect the visual activity, but influence the contrast sensitivity of the IOL.[128]

Ichikawa, et al.[130] developed a multi-step process to overcome the void formation as detailed below:

- Step 1: The monomer mixed solution is polymerised to produce a base material.
- Step 2: One part of the base material produced in the first step is heated in oven to complete the polymerisation.
- Step 3: The completely polymerised material is immersed into the second portion of the base material produced during step1. In case any voids formed in the polymerised material can be filled by the base material during this step.
- Step 4: The impregnated material from the above step is taken out and excess of unpolymerised base material is removed from the surface.
- Step 5: The setting of a protective coating is done after removing excess of unpolymerised material from the surface of the base material as in step 4.

Basically, this method was earlier tried for preparation of other polymeric materials such as Poly(vinyl chloride) to eliminate the voids, also termed as fish eye. The multistep process of making IOLs is useful in that respect. By adopting suitable methodology for preparation of IOLs, certain biocompatibility problems could be resolved. For example, according to Hung et al., a bicomposite IOL optic comprising an anterior surface material consisting of an ophthalmically acceptable lens-forming material and a posterior surface material, different from the anterior surface material, for reducing the risk of posterior capsule opacification is prepared.[142] The posterior surface material consisted essentially of two or more aryl acrylic hydrophobic functional monomers. The method of preparation of IOLs involves the following steps:

(a) Forming a posterior surface layer of material by polymerising a posterior surface material composition consisting essentially of two or more aryl acrylic hydrophobic monomers and a cross-linking agent in a mold having the desired IOL posterior surface shape and by

(b) Forming an anterior surface layer by adding a liquid anterior composition consisting of an ophthalmically acceptable IOL material to the top of the posterior surface layer and polymerising the liquid anterior composition.

Yet another method for producing IOLs include a combination of steps which helped to increase the pull strength between the fixation member of the IOL and the optic of the IOL without requiring sophisticated high frequency corona discharge activation or plasma activation of the fixation member or primer coating of the fixation member.

While it may appear simple, achieving the complete polymerisation to obtain a material of desired characteristics without any optical flaws remains a subject of research

and development, in spite of the existing experience of so many years and for several types of materials.

Attempts to resolve the biocompatibility related issues by developing novel methods of preparation of IOLs are a welcome trend. As far as the concept of providing a single material with completely different surfaces is concerned, it presents several opportunities if one looks at the challenges.

1.12 Literature

The first foldable IOL was a silicone based lens developed by Mazzoco. These lenses were of the plate design without loops. This lens was made of the silicone elastomer, poly(dimethyl siloxane) or PDMS. Silicone IOLs have the lowest glass transition temperatures of any IOLs produced.[129] Initially, people were skeptical in predicting that all of the silicone lenses would turn brown and become cataractous with time.[130] This problem was remedied through quality control processes and complete material polymerisation. Others reported difficulty in performing yttrium-aluminum-garnet (YAG) laser posterior capsulotomy and a significant increase in capsular opacification and inflammation in the eye with respect to PMMA.[131] Appropriate understanding of new techniques for capsulotomy with the silicone lens has reduced YAG laser pitting to a minimum. Silicone IOLs are hydrophobic and have contact angle in excess 110^{o}.[129] Table 1.2 provides structures of some IOL materials.

Table 1.2: Chemical composition and structures of IOL materials

Chemical composition	Structure
Poly(dimethyl siloxane)	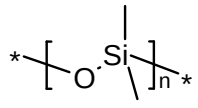
Poly(dimethyl diphenyl siloxane)	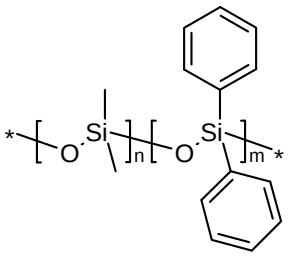
Poly(methyl methacrylate)	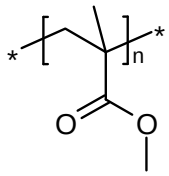
Poly(EA-co- EMA-co-TFEMA)	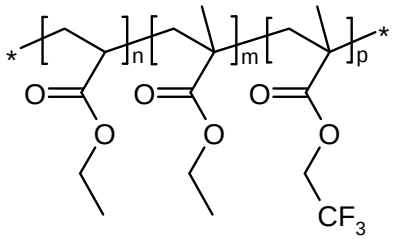
Poly(PEA-co-PEMA)	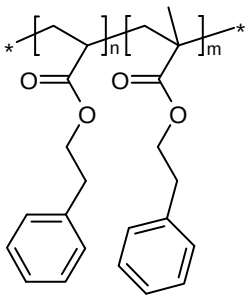
Poly(PEA-co-HEMA)	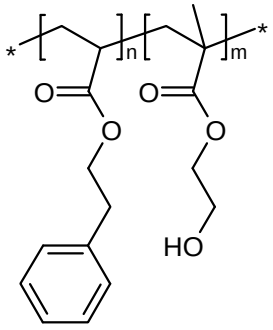

Another foldable IOL material that is in extensive use today includes the hydrogel poly(hydroxyl ethylmethacrylate) or HEMA. Poly(HEMA) is hydrophilic with contact angles ranging from 59 to 69°.[130] The hydroxyl containing monomer can be copolymerised free radically with a variety of different materials such as high refractive index acrylates, cross-linkers and UV-absorbers to obtain the final desired product. PDMS and poly(HEMA) produced suitable foldable IOL materials. The drawback was the low refractive index these materials possessed. Higher refractive index allows for a thinner IOL optic. The desire for thin profile lenses required a higher refractive index material.[132,133]

The most common lens on the market today is the hydrophobic acrylic lens 'AcrySof' developed by Alcon in the early 1990's. This IOL was the first foldable acrylic IOL approved by the FDA. The approach was to build on the success of the PMMA IOLs and specifically design a new, high refractive index, foldable IOL biomaterial. This IOL material is an acrylic copolymer consisting of 2-phenylethyl acrylate, 2-phenylethyl methacrylate, diacrylate cross-linker and a polymerisable benzotriazole UV absorber. The UV absorbing benzotriazole is covalently bonded to the polymer backbone. The reaction is initiated by the thermal degradation of a peroxide initiator. The IOL optic is formed by reactive extrusion. When polymerisation is complete, the material is washed free of any byproducts with an exhaustive solvent extraction process. This IOL has many favourable properties that are required for a foldable IOL. These properties include high refractive index (~1.55), chemical stability, absence of leachable monomers, and biocompatibility. Due to the high refractive index, these lenses have the thinnest optic for a given power and optic size. Contact angles for the 'AcrySof' IOLs range from 73 to 80°.[129]

Continued implantation of the 'AcrySof' IOL revealed a significant reduction in posterior capsule opacification (PCO). Paul Ursell and colleagues reported less PCO with the acrylic lens compared with silicone and PMMA lenses after two post-operative years.[134] The PCO rate for the 'AcrySof' IOL is approximately 11%. PCO for silicone and PMMA range from 36% to 65%.[135] The decrease in PCO was related to two factors. The hydrophobic acrylic adhered to the capsular bag in which it was implanted. This prevented the growth of excess lens epithelial cells (LECs) between the IOL and the capsular bag. Reijo Linnola hypothesised that the adherence of the IOL to the capsular bag allowed only a single layer of LECs to form. With only a single layer of LECs behind the IOL, the visual axis remains clear.[136] Over time, some of the LECs die, forming a bioactive bond between the capsular bag and the IOL optic. Dr. Linnola and colleagues pursued this theory and determined that fibronectin, an extra-cellular protein, was responsible for this bioactive bond.[137,138]

A second characteristic of the 'Acrysof' IOL that prevented PCO was a sharp, keen, square edge on the optic. Previous silicone and PMMA IOLs had rounded edges. Okihiro Nishi and colleagues investigated the effect of a square edge and PCO reduction.[139] Okihiro concluded that the square edge created a discontinuous bend in the capsular bag. The discontinuous bend combined with the adhesiveness of the acrylic material to the capsular bag were the factors that significantly reduced PCO.

The 'Sensar Ar-40' by Allergan Surgical was the second hydrophobic foldable acrylic IOL approved by the FDA. The 'Sensar' IOL is a three-piece foldable acrylic terpolymer with blue core PMMA haptics.[140] The terpolymer optic is composed of ethyl acrylate (EA), ethyl methacrylate (EMA), and 2,2,2-trifluoroethyl methacrylate

(TFEMA). The material is cross-linked with ethylene dimethacrylate (EGDM). Due to the aliphatic and fluorinated nature of the 'Sensar' acrylics, the refractive index is lower (η_D~1.47) than the 'AcrySof' IOL (η_D ~1.55). The fluorinated methacrylate component decreases the surface energy of the IOL and reduces tackiness to itself and surgical instruments. The 'Sensar' lens is lathe cut from polymer sheets. Since the glass transition temperature of the 'Sensar' lens is less than room temperature, the lathe cutting must be done cryogenically. The surface smoothness and round edges of the 'Sensar' IOL are a result of tumble polishing.[150] Table 1.3 detailed material composition and characteristic properties of some currently available IOLs.

It has been more than half a century since Ridley implanted the first IOL. Since then, more than 100 million IOLs have been implanted with remarkable success.[141] The IOL has become one of the most successful long term implants of the twentieth century. Cataract surgery has been transformed from a one week procedure with hospitalisation to an outpatient procedure with less than ten minutes of surgery time for skilled surgeons. This improvement in ophthalmology has been achieved by continuous advances in surgical technique, instrumentation, and IOL design.

Despite the enormous success of the intraocular lens, there is considerable opportunity for newer polymers with higher refractive index and lower glass transition temperature. Higher refractive index would allow for the use of the thinner IOLs. This coupled with lower glass transition temperature (and hence greater flexibility) will allow for smaller incision and quicker healing after surgery, generating higher through-puts and lower costs. One of the objectives of this thesis is to provide polymeric material having enhanced properties over existing materials.

Table 1.3: Characteristics of some currently available hydrophobic IOLs

IOL/manufacturer (country)	Material composition*	Refractive index	T_g
Three-piece and one-piece AcrySof/Alcon Laboratories, Inc. (US)	Copolymer of phenylethyl acrylate and phenylethyl methacrylate, cross-linked with butanediol diacrylate	1.555	14.0
Sensar AR40 and AR40e one-piece Tecnis/Abbott Medical Optics Inc. (US)	Copolymer of ethyl acrylate, ethyl methacrylate, and 2,2,2-trifluoroethyl methacrylate, cross-linked with ethylene glycol dimethacrylate	1.470	12.21
AF-1 series iMics 1/Hoya Surgical Optics (Japan)	Cross-linked copolymer of phenylethyl methacrylate and n-butyl acrylate, fluoroalkyl methacrylate	1.520	11
XACT/Advanced Vision Science, Inc. (US)	Copolymer of hydroxyethyl methacrylate, polyethylene glycol phenyl ether acrylate, and styrene, cross-linked with ethylene glycol dimethacrylate	1.540	15–20
HP 757SQ/Aurolab (India)	Copolymer of ethylacrylate and ethylmethacrylate, cross-linked with a difunctional acrylate/methacrylate	1.470	11 ±2
Acrylmex/Ophthalmic Innovations International (now Aaren Scientific) (US)	Terpolymer of butyl acrylate, ethyl methacrylate, and N-benzyl-N-isopropylpropenamide, cross-linked with ethylene glycol dimethacrylate	1.490	NP
Matrix Acrylic Aurium/Medennium (US)	Poly(2-phenyloxyethyl acrylate), cross-linked with phenyl-containing dimethacrylate (IOL has a photochromic chromophore)	1.560	NP
Hydromax/Carl Zeiss Meditec (Germany)	Homopolymer of 2-phenoxy ethyl acrylate, cross-linked with ethoxylated (2) bisphenol A dimethacrylate	1.560	16
SeeLens HP/Hanita (Israel)	Ethoxyethyl methacrylate and methyl methacrylate with incorporated violet-filtering chromophore	1.480	10
Mediflex/Mediphacos (Brazil)	Copolymer of acrylate/methacrylate with blue-light filtering chromophore nonaromatic acrylic rubber	1.480	5
* All models have ultraviolet light blockers, NP = not provided			

1.13 Applications of high refractive materials

Table 1.4 illustrates various applications of high refractive index materials in optical devices.

Table 1.4: Applications of high refractive index materials

Optical Device	Type of Material
Intraocular lenses	Polymethacrylates and copolymers of modified acrylates Silicones and modified silicones
Spectacles	Glass; Polymethacrylates; Polycarbonates; Polythiourethanes
Sun glasses	Glass; Polymethacrylates
Contact lenses	Polymethacrylates and copolymers of modified acrylates Silicones and modified silicones
Binoculars	Glass; Polymethacrylates; Polycarbonates
Telescopes	Glass; Polymethacrylates; Polycarbonates
Magnifying Lenses	Glass; Polymethacrylates; Polycarbonates
Optical waveguides	Lithium niobate; Potassium titanyl phosphate
Optical fibres	Glass; Polymethacrylates
Optical modulators	Lithium niobate; Potassium titanyl phosphate
Optical interconnectors	Lithium niobate; Potassium titanyl phosphate
Liquid crystal displays (LCDs)	Glass; Polymethacrylates

1.14 References

[1] M. Jalie, *Optimtry Today/Optics Today*, **2005,** 45, 6, 38-46.

[2] M. Jalie, *Principle of Ophthalmic Lenses*, 5th edition, ABDO, London, **1984**.

[3] J. C. Seferis, *Refractive Indices of Polymers in Polymer Handbook*, 4th edition, (Brandrup, J., Immergut, E. H. & Grulke, E. A.), **1999,**Vol. 1, 571 (Wiley, New York).

[4] G. Keiser, *Optical Fiber Communications*, MacGraw Hill, New York, **1983.**

[5] H. Lan, F. Robert, H. Encai, M. Taun, L. Radcliffe, *WO 2010002562,* Innovative Properties Company, USA, **2010**.

[6] H. Lan, F. Robert, H. Encai, M. Taun, L. Radcliffe, *US 20100003501,* Innovative Properties Co., USA, **2010**.

[7] L. Chance, F. Charles *WO 2009137525*, Alcon, Inc., Switz., **2009**.

[8] F. Parra,B. Vazquez, L. Benito, J. Barcenilla, S. Roman, *Biomacromolecules*, **2009**, 10(11), 3055-3061.

[9] F. H. Namdaran, A. R. LeBoeuf, *EP 0485197*, Nestle S. A., **1991**.

[10] F. H. Namdaran, A. R. LeBoeuf, *US 5403901*, Nestle S. A., **1995**.

[11] M. D. Determan, A. I. Everaerts, C. L. Moore, D. B. Olson, *US 20100048804,* Innovative Properties Company, USA, **2010**.

[12] S. M. Hong, A. J. Nam, K. G. Yong, *KR 2009098121*, Dongwoo Fine-Chem Co., Ltd., S. Korea, **2009**.

[13] G. S. Jha, G. Seshadri, R. K. Khandal, *e-Polymers*, **2007**, 120.

[14] W. L. C. Rasmussen, *Ph. D. Thesis*, **2001.**

[15] M. Roger, *Vision Council of America*, Arlington, Va, **1988**, Vol. 2.

[16] J. D. Lytle, *Handbook of optics*, McGraw Hill. Inc., **1995,** 2nd edition.

[17] W. F. Frank, *Precision Plastics Optics for Optical Storage*, *SPIE*, **1997**, Vol. 3135, 30-31.

[18] H. D. Wolpert, *The photonic Design and Application Handbook,* **1991**, H-300 to H-307.

[19] R. T. Hebert, *Design, Fabrication and Application of precision Plastic optics, SPIE* 1995, vol. **2600**, 23-24.

[20] T. Moss, *Advance in replicated and plastic optics*, *SPIE*, **1977**, 115, 23-24.

[21] D. L. Wise, *Photonic polymer System; Fundamentals, Methods and Application,* New York, **1998**.

[22] V. Galiatsatos, R. O. Neaffer, S. Sen, B. J. Sherman, *Physical Properties of Polymers Handbook*, edited by J. E. Mark, AIP Press, New York, **1996**.

[23] F. A. Jenkins, H. E. White, *Fundamentals of optics,* 4th edition, Tata McGraw-Hill, **2011**.

[24] D. W. Van Krevelen, *Properties of Polymers*, Elsevier Science Pub. Co., **1990.**

[25] A. A. Akadskil, M. Yu, I. K. Stronie, *Fisicheskie svoistva polimerobv (Chemical structure and physical properties of polymers),* Moscow, **1983**, 284.

[26] N. Amaya, K. Anan, Y. Muruta, R. Seita, *US* 60,092,313 A2, **1985**.

[27] M. S. Misura, E. J. Sare, *EP*. 224,123 A2, **1987**.

[28] I. D. Torbin, Y. F. Damino, *(Optical parts made from polymers) Optiko-nukh. Prom-St*, **1974**, 10.

[29] H. Dislich, *Ange. Want. Chemie.,* **1976**, 18, 2.

[30] E. I. Shepurev, *Optiko-mekh. Prom.*, **1998**, 1.

[31] H. Lorkonski, *J. Plast.Kaut. Schuk.*, **1976**, 23, 318-320.

[32] V. G. Ruyshev, M. P. Invanko, T. I. Koslova, *Plast. Mas.*, **1987,** 58-59.

[33] W. E. Degenhard, *Encyclopedia of IndustrialChemical Analysis General Techniques*, (F.D. Smlt, C. L. Hilton. edition) Interscience, New york, **1966**, P-2, Vol. 3, 392-407.

[34] J. Saint-Just, O. A. Larson, *Anal. Chem.*, **1979**, 51, 1097**.**

[35] S. Tabata, W. Yan, K. Yokata, N. Kushibiki, Y. Kawae, N. Kamako, *Polym.Prepr. Jpn.,* **1987**, 36, 1163.

[36] A. Sugio, T. Miki, *JP 6279210*, Japan, MKI: CO8F220130, **1987**.

[37] L. F. Kosyanchuk, Y. N. Mizelskii, Y. S. Lipatov, *Polim. Mater.,* **1992**, 53.

[38] M. Shimuta, T. Takahashi, H. Abe, *US 5543482*, **1996**.

[39] P. Nakatsuka, K. Hanabusa, *JP 5412774458*, RZh Khimiya , **1980**.

[40] T. Nagata, K. Okazaki, T. Miura, *EP* 351073, **1990**.

[41] B. Schmitt, W. Klesse,V. R. Kerscher, P. Hartmann, *WO* 41775, **2004**.

[42] P. Jiang, *EP* 745621, Essilor International Compagnie Generale Optique., **1997**.

[43] Y. Kitahar, J. Jiang, *US 015669*, **2002.**

[44] K. Okaniwa, T. Sugishita, T. Yamanaka, *WO 2007013230*, Hitachi Chemicals, Japan, **2007**.

[45] Y. Kitahara, J. Jiang, *EP 972772*, Hoya Corp., Japan, **2000**.

[46] T. Kobayashi, T. Murakami, *JP 2002343137*, Conica Co., Japan, **2002**.

[47] P. Jiang, G. Widawski, G. Menduni, *WO 9902575*, Essilor International Compagnie Generale Optique., Japan, **1999**.

[48] S. Nishiyama, O. Abe, H. Tanaka, M. Taniguchi, *JP 62185053*, Nippon Kogaku, Japan, **2003**.

[49] K. Okazaki, Y. Kanemura, T. Nagata, *EP* 665219 (Cl. C07C321/14) **1994**.

[50] K. Sasagawa, K. Fuji, N. Kawasaki, T. Suzuki, *EP 659790*, (Cl. CO8 G 18/38), **1995**.

[51] J. Jiang, M. Kosaka, *EP 803504*, **1997**.

[52] Y. Suzuki, J. Liu, Y. Nakamura, Y. Shibasaki, S. Ando, M. Ueda, *Polym. J.,* **2008**, 40, 414.

[53] N. You, Y. Suzuki, D. Yurifuji, S. Ando, M. Ueda, *Macromolecules*, **2008**, 41, 6361.

[54] J. Liu, Y. Nakamura, Y. Suzuki, Y. Shibasaki, S. Ando, M. Ueda, *Macromolecules*, **2007**, 40, 7902.

[55] J. Liu, Y. Nakamura, Y. Suzuki, Y. Shibasaki, S. Ando M. Ueda, *Macromolecules*, **2007**, 40, 4614.

[56] Z. Yang, Z. Yin-Niah, R. Zhenya , G. Brian, *US 525123*, **1995**.

[57] T. Fukuda, *JP 005956*, MKI 3, **1982**.

[58] C. Allam, J. L. Kuo, J. E. Mcgrath, D. K. Mohanty, *Macromol. Chem. Phys.,* **1999**, 200(8), 1854.

[59] H. Elias, *Encyclopedia of Industrial chemistry*, 5th ed., (B. Elvers, S. Hawkins, G. Schultz, Edision) VHS: New York, **1992**, A20, 643.

[60] B. Martina, K. Volkar, *US 5488128*, **1993**.

[61] Y. Kanemura, K. Sasagawa, S. Kabayashi, *EP 528590 A1*, **1993**.

[62] L. Yean, C. Bochu, *EP 408459* A1, **1990**.

[63] A. Nagai, T. Miyagawa, H. Kudo, T. Endo, *Macromolecules,* **2003**, 36, 9335.

[64] A. Nagai, M. Sato, B. Ochaiai, T. Endo, *Macromolecules,* **2004**, 37, 3523.

[65] A. Nagai, M. Sato, B. Ochaiai, T. Endo, *Macromolecules* **2004**, 37, 7538.

[66] T. Okubo, S. Kohmoto, M. Yamamoto, *J. Appl. Polm. Sci.,* **1998**,68,1791.

[67] B. Jaffrennou, N. Droger, F. Mechin, *e-polymers*, **2005**, 82.

[68] A. A. Akadskil, M. Yu, I. K. Stronie, *Fisicheskie svoistva polimerobv (Chemical structure and physical properties of polymers),* Moscow, **1983**, 284.

[69] N. Amaya, K. Anan, Y. Muruta, R. Ikebe, *US 60092313* A2, **1985**.

[70] H. Dislich, *Ange wan. Chemie.,* **1976**, 18, 2 .

[71] S. Kobayashi, N. Kawayuchi, T. Suzuki, M. Imai, K. Fujii, *US 20010044555*, **2001**.

[72] C. G. Overberger, H. Biletech, R. G. Nickerson, *Polymer Sci.,* **1958**, 27, 381.

[73] J. T. Ferraro, F. W. Orttung, *J. Org. Chem.*, **1961**, 3458.

[74] G. Hardy, J. Vargu, K. Nytrai, I. Czajlik, L. Zubonyai, *Vysokomolekul. Soedin.,* **1964**, 6, 758.

[75] Y. Liu, Y. Nakamura, S. Shibasaki, S. Ando, M. Ueda, *Polym. J.*, **2007**, 39, 543.

[76] T. Matsuda, Y. Funae, M. Yoshida, Y. Yamamoto,T. Takaya, *J. Appl. Poly. Sci*., **2000**, 76, 45.

[77] T. Fushimi, H. F. Allcock, *Dalton. Trans*., **2009**, 2477.

[78] M. A. Olshavsky, H. R. Allcock, *Macromolecules*, **1996**, 28, 6188.

[79] M. A. Olshavsky, H. R. Allcock, *Macromolecules,* **1997**, 30, 4179.

[80] H. K. Shobha, H. Johnson, M. Sankarapandian, Y. S. Kim, P. Rangarajan, D. G. Baird, J. E. McGrath, *J. Polym. Sci. Part A Polym. Chem*., **2001**, 39, 2904.

[81] H. K. Shobha, V. Sekharipuram, J. E. Mcgrath, A. Bhatnagar, *US 7375178*, **2008.**

[82] T. Honda, I. Kaitsu, *Chem. Abstr.*, **1994** 120,173551.

[83] B. Schmitt, W. Klesse, V. R. Kerscher, P. Hartmann, *WO* 200441775, **2004.**

[84] A. Sugis, T. Kawaki, O. Aoki, M. Miura, T. Watanabe, *JP 61123614 Jpn. Kokai Tokkyo Koho*., **1986.**

[85] H. C. Makker, *US 7928171*, Abbot Medical Optics Inc., US, **2011.**

[86] C. Freeman, D. L. Jinkerson, *US 6353069*, Alcon, TX**, 2000.**

[87] C. Freeman, *US 7790824*, Alcon, TX, **2010**.

[88] D. Nauti, S. Minami, *JP 62261305*, Japan, MKI4 C 08 F 30/04, **1989**.

[89] T. Abe, S. Eugti, N. Tokotani, *JP 6228618*, Japan, MKI4 C 08 G 220/14, C08 C222: 04, **1987**.

[90] T. Abe, I. Okabe, H. Terao, *JP 6226518*, Japan, MKI4 C 08 F 220/06, **1988**.

[91] H. Selsakashl, K. Eguchi, *JP 6094410*, Japan, MKI4 C 08 F 20/06, **1987**.

[92] H. Selsakashl, K. Eguchi, *JP 6092306*, Japan, MKI4 C 08 F 20/06, C02 B1/04, **1983**.

[93] S. Eguchi, S. Tann, H. Asano, *Mater. Sci. and Eng.*, **1986,** Vol. 55, 654-658.

[94] H. Slmmrock, A. Mathy, M. Dominguez, G. Wegner, *Adv. Material*, **1989**, 1, 294.

[95] E. J. Pope, M. Asani, O. Liardon, E. Kovats, *Mat. Res. Soc. Symp. Proc.*, **1989**, 132, 105.

[96] M. Weibe, W. Caseri, U. Suter, H. Kiess, E. Wehrli, *Polym. Advn. Techn.*, **1991**, 2, 75-80.

[97] R.A. Weale, J. Physiol., **1988**, 395, 577–587.

[98] S. Zigman, in: H. Maisel (Ed.), *The Ocular Lens: Structure, Function and Pathology*, Academic Press, London, **198**5, pp. 117–150.

[99] K.R. Hightower, *Curr. Eye Res*., **1994**, 14, 71–78.

[100] G. Brian, H. Taylor, *Cataract blindness - challenges for the 21st century*, *Bull. World Health Organ.*, **2001**, 79(3), 249–256.

[101] D. Apple, N. Mamalis, K. Loftfield, J. M. Googe, L. C. Novak, D. Kavka-Van Norman, S. E. Brandy, R. *J. Olson, Surv. Ophthalmol*., **1984**, 29, 1–54.

[102] D. J. Apple, K. D. Solomon, M. R. Tetz, E. I. Assia, E. Y. Holland, U. F. Legler, J. C. Tsai, V. E. Casteneda, J. P. Hoggatt, A. M. Kosick, *Surv. Ophthalmol.*, **1992**, 37, 73–116.

[103] D. A. Schaumberg, M. R. Dana, W. G. Christen, R. J. Glynn, *Ophthalmology*, **1998**, 105, 1213–1221.

[104] M. E. Wilson, *Ophthalmology*, **1996**, 103, 1719–1720.

[105] S. K. Pandey, M. E. Wilson, R. H. Trivedi, A. M. Izak, T. A. Macky, L. Werner, D. J. Apple, *Int. Ophthalmol. Clin*., **2001**, 41, 175–196.

[106] T. Kohnen, R. Pena-Cuesta, D. D. Koch, *Ger. J. Ophthalmol.*, **1996**, 5, 171–175.

[107] J. Zwaan, P. B. Mullaney, A. Awad, S. al Mefser, D. T. Wheeler, *Ophthalmology*, **1998**, 105, 112–118.

[108] N. H. L. Ridley, *Trans. Ophthalmol. Soc*., **1951**, 71, 617–621.

[109] N. H. L. Ridley, *St. Thomas' Hospital Reports* **1951**, 7 (2nd series), 12–14.

[110] N. H. L. Ridley, *Lancet*, **1952**, 19, 118–129.

[111] N. H. L. Ridley, *Trans. Am. Academy Ophthalmol. Otolaryngol.*, **1953**, 57, 98–106.

[112] N. H. L. Ridley, *Br. J. Ophthalmol*., **1954**, 38, 156–162.

[113] D. T. Azar, *Intraocular Lenses in Cataract and Refractive Surgery*, **2001**, Philadelphia, Pennsylvania: W.B. Saunders Company.

[114] N. S. Jaffe, G. F. Jaffe, *Cataract Surgery and Its Complications*. 5th edition, **1990**, Philadelphia, Pennsylvania.

[115] D. J. Apple, R. J. Olson, M. C. Kincaid, *Intraocular Lenses: Evolution, Designs, Complications, and Pathology*, **1989**, Baltimore, Maryland: Williams & Wilkins.

[116] S. P. Shearing, *Journal of the American Intraocular Implant Society*, **1984**, 10**,** 343-346.

[117] E. Epstein, *British Journal of Ophthalmology,* **1959**. 43, 29-33.

[118] H. Hirschman, *Transactions of the American Academy of Ophthalmology and Otolaryngoogyl*, **1976**. 81, 89-92.

[119] C. D. Kelman, *American Journal of Ophthalmology*, **1967**, 64, 23-25.

[120] C. D. Binkhorst, *Ophthalmology*, **1980**, 87, 609-617.

[121] S. Lerman, *Ultraviolet radiation protection. CLAO J*., **1985**. 11, 39-45.

[122] L. M. Jampol, *Archives of Ophthalmology*, **1985**, 14, 1134-1135.

[123] *www.eyecenter.emory.edu*, on May **2012.**

[124] K. Inomata, K. Nakazato, N. Nakabayashi, K. Ishihara, *JP 169526,* **2000**.

[125] F. Oener, S. Hakan, A. Osman, S. D. Sarioglu, K. Ismet, C. Sueleyman, *Ophthalmologica ,* **2003** , 217(2), 124.

[126] A. R. Leboeuf, M. Karakelle, *WO9907756*, **1999**.

[127] K. Mentak, *WO0061646*, **2000**.

[128] N. Ichikawa, Y. Akahata,T. Sunada, US *7160488*, **2007**.

[129] M. Tehrani, D. Burkhard, W. Beate, P. Tadeusz, E. Wolf, *Ophthalmologica,* **2004**, 218, 57-63.

[130] A. T. Milauskas, *Archives of Ophthalmology*, **1991**, 109**,** 913-915.

[131] P.E. Bath, C.F.B., Y. Dang, *Journal of Cataract and Refractive Surgery*, **1987**, 13**,** 47-49.

[132] T. Oshika, *Journal of Cataract and Refractive Surgery*, **1996**, 22**,** 1360-1364.

[133] S. Milazzo, H. Blin, *Journal of Cataract and Refractive Surgery*, **1996**, 22, 1351-1354.

[134] P. G. Ursell, D. J. Spalton, M. V. Pande, E. J. Hollick, S. Barman, J. Boyce, K. Tilling, *Journal of Cataract and Refractive Surgery*, **1998**, 22, 352-360.

[135] E. J. Hollick, D. J. Spalton, P. G. Ursell, M. V. Pande, British Journal of Ophthalmology, **1998**, 82**,** 1182-1188.

[136] R. J. Linnola, *Journal of Cataract and Refractive Surgery*, **1997**, 23, 1539-1542.

[137] R. J. Linnola, J.I. Salonen, R.P. Happonen, *Journal of Cataract and Refractive Surgery*, **1999**, 25, 1480-1485.

[138] R. J. Linnola, J.I. Salonen, R.P. Happonen, *Journal of Cataract and Refractive Surgery*, **1999**, 25**,** 1486-1491.

[139] O. K. Nishi, K. Sakanishi, *Ophthalmic Surgery and Lasers*, **1998**, 29, 587-594.

[140] S. Lane, *Ophthalmic Hyperguide*., **2005**, 1-8.

[141] R. L. Lindstrom, N. Doddi, *Journal of Cataract and Refractive Surgery*, **1986**, 12**,** 285-289.

[142] X. D Hung, K. Yao, Z. Zhang, Y. Zhang, Y. Wang, *Journal of Cataract and Refractive Surgery,* **2010**, 36(2), 290-8.

[143] www.who.int/mediacentre/factsheets/fs282/en/, cited on May **2012**

Chapter II

Aims and Objectives

2.1 Aims

Prime aim of this thesis is the synthesis and study of novel high refractive index polymers. For biomedical optical articles, high refractive index polymers having low birefringence, high transparency and good biocompatibility are needed.

Transparent acrylic materials are becoming increasingly important in optical design. Amongst several optical properties, refractive index is the most important criteria for selection of materials suitable for application in optics. One of the possible candidates for this purpose is plastic materials. Other than the essential properties like light transmission, transparency and refractive index (RI), plastics are also known for their light weight. High refractive index is important for transparent synthetic polymers to be suitable as optical materials. Polymers with high refractive index will need to be thinner than those having lower refractive index, for the same focal length. The use of thin lenses contributes to reducing the volume of space occupied by lenses in optical assemblies, which can advantageously make an optical apparatus light weight and small sized. Additional requirement for greater through-put during operative procedures is the material's flexibility. This is addressed by tweaking the polymer back-bone to lower the glass transition temperature. While thin lenses reduce the space occupied by lenses in optical assemblies, flexible materials require shorter operative lengths for insertion.

Optical products can be prepared from high index of refraction materials, including high index of refraction (meth)acrylates monomers. The monomers can be polymerised to take the form of a product capable of modifying or controlling the flow of light. The refractive index of materials can be increased by increasing the polarisability of

substituent groups. High refractive index polymers can be obtained by incorporating oxygen and sulphur containing groups as well as aromatic rings.

Current high RI plastics include polyurethanes, polyesters, epoxy and episulphide resins. Most of the high RI plastics use thiourethane and episulphide chemistries with highly polarisable chemical moieties such as aromatics and sulphur. However, optical articles produced from these materials suffer from after-cure yellowing and strong odours during lens processing. In addition, these monomers have inherently long production cycles due to prolonged curing times needed to maintain optical homogeneity. There is, therefore, a need for monomers which offer fast cure, high RI, low colour, and low odour when cured or upon cutting and grinding, while maintaining optical homogeneity.

Copolymerisation is the most successful and powerful method for effecting systematic changes in polymer properties. The incorporation of two different monomers, having diverse physical and chemical properties in the same polymer molecule in varying proportions leads to the formation of new materials with scientific technical importance. Copolymerisation modulates both the intramolecular and intermolecular forces exercised between like and unlike polymer segments and consequently properties such as glass transition temperature, refractive index, melting point, solubility, crystallinity, permeability, adhesion, elasticity and chemical reactivity may be varied within wide limits. Co- and terpolymerisation are used effectively to increase the amorphous character of the polymer which increases the transparency and the flexibility of the polymer chains. Copolymers tend to have a set of properties uniquely their own, setting them apart from that of their parent homopolymers. In copolymers, the sequence distribution of the different monomers is a key parameter to ensure homogeneity. Copolymerisation studies

and estimation of reactivity ratios are of utmost importance due to the need of predicting, designing, and properly controlling polymeric material properties. Therefore, having a good knowledge of polymerization parameters, among which reactivity ratios are the most important ones, would be very helpful.

In human contact applications it is an intrinsic requirement that the level of residual monomers to be extremely low. One way to ensure this is to follow polymerisation kinetics till the very end so as to ensure sufficient time is given for all the monomers to be converted into polymers. However, since both monomers in a copolymerisation will have differing relative rate of addition to the copolymer chain, one of the monomers will be depleted ahead of the other and the final several percentage of the copolymerisation will be essentially homopolymerisation of the less reactive monomer. In such a case the copolymer and homopolymer may phase separate leading to inhomogenity, thereby affecting transparency. Thus, investigation of copolymerisation kinetics is of paramount importance.

Cataract is the opacification of the lens due to age or other causes such as ocular trauma or inflammation which do not allow light rays to pass through the eye. It is a common surgical procedure for the cataract treatment to remove the opaque natural crystalline lens and replace it with an intraocular lens (IOL). Despite the enormous success of the intraocular lens, there is considerable opportunity for newer polymers with higher refractive index and lower glass transition temperature. Higher refractive index would allow for the use of the thinner IOLs. This, coupled with lower glass transition temperature (and hence greater flexibility), will allow for smaller incision and quicker healing after surgery, generating higher through-puts and lower costs.

In the present investigation a thorough study was carried out to synthesise different, new high refractive index (meth)acrylate monomers. This was followed by study of solution and bulk polymerisation, characterisation and evaluations.

2.2 Objectives

- Synthesis of new (meth)acrylic monomers with potentially higher refractive indices.
- Synthesis of homopolymers and evaluation of their optical and thermal properties.
- Copolymerisation studies of newer monomers to determine reactivity ratios.
- Synthesis and evaluation of new cross-linked (meth)acrylate polymer networks.
- Bulk polymerisation kinetics of 2-phenylethyl (meth)acrylate using photo and thermal initiators.

Objectives of thesis explored in detail were as follows:

Standard procedure for synthesising novel high refractive index monomers was established. Initially, reaction of achiral styrene oxide with phenol was conducted to synthesise aromatic based alcohols. Newly synthesised alcohol was thoroughly purified, reacted with acryloyl and methacryloyl chloride to obtain respective acrylates and methacrylates. Sulphur containing aromatic based alcohol was synthesised by reacting thiophenol with styrene oxide and converted to corresponding acrylate and methacrylate by reacting with acryloyl and methacryloyl chloride, respectively. 2-Phenylethyl acrylate and 2-phenylethyl methacrylate were synthesised using 2-phenylethanol and corresponding acid chlorides. Characterisation of newer monomers was carried out using ^{1}H NMR, ^{13}C NMR, IR and mass spectroscopic techniques to confirm their structure.

Homopolymers of newer monomers were prepared by free radical solution polymerisation using 2,2'-azobisisobutyronitrile (AIBN). Newer monomers were characterised for their thermal and optical properties.

Copolymerisation studies of newer monomers were done by free radical solution polymerisation using 2,2'-azobisisobutyronitrile (AIBN). ^{1}H NMR spectroscopy was used to determine compositions of copolymers. Chain copolymerisation is important to study the relationship between the chemical structure and reactivity of monomer. Estimation of reactivity ratios was done using Fineman-Ross (FR), Kelen-Tudos (KT), extended Kelen-Tudos (Ex KT) and Mao-Huglin (MH) graphical methods. From estimated reactivity ratios of the monomer combinations, azeotropic composition for some monomer sets were calculated. Structural parameters of the copolymers were obtained by calculating dyad monomer sequence fractions and the mean sequence length. Optical properties of copolymers like refractive index (RI) and transmittance was determined by Abbe refractometer and spectrophotometer, respectively. Solubility of copolymers was tested in common solvents. The molecular weights [weight-average molecular weight (M_w) and number-average molecular weight (M_n)] of the polymers were determined with gel permeation chromatography (GPC). Thermal data was obtained with a DSC and TGA instruments.

Novel polymeric flexible, high refractive index systems of chemically cross-linked aromatic and sulphur containing aromatic based acrylate/methacrylate copolymer networks were developed and characterised. Glass moulds were designed and fabricated for polymerisation. Binary copolymer networks based on different compositions were

synthesised by radical copolymerisation in bulk using bifunctional radical initiator like Luperox–256. Various divinyl monomers were used as cross-linkers.

The thermomechanical properties, refractive index, transparency, and surface wettability as well as cytotoxicity were systematically evaluated to mimic the *in vivo* situation by differential scanning calorimetry (DSC), tensile tester, Abbe refractometer, spectrophotometer, contact angle measurements, and MTT assay, respectively.

Photopolymerisation of 2-phenylethyl (meth)acrylates were carried out to estimate their kinetic parameters. Different compositions of photoinitiators were used to study the effect of concentration of photoinitiator on cure kinetics. These compositions obtained were tested for photo-curing performance using differential photocalorimetry (DPC) or photo DSC under polychromatic radiation. Rates of polymerisation as well as the percentage conversions were estimated. Other parameters such as induction time, maximum rate and conversion attained as well as the time to attain peak maximum were obtained.

Thermal free radical bulk polymerisation kinetics of 2-phenylethyl acrylate and 2-phenylethyl methacrylate monomers were carried out. Free radical bulk polymerisation kinetics of 2-phenylethyl (meth)acrylate were determined by differential scanning calorimetry in the non-isothermal mode. The polymerisation was investigated with varying ramp rate at different monomer to initiator concentrations**.** Kissinger and Ozawa methods were applied to determine the activation energy (E_a).

Chapter III

Monomer Synthesis and Homopolymerisation

3.1 Monomer Synthesis

2-Phenoxy-2-phenylethanol and 2-phenyl-2-(phenylthio)ethanol were the precursors for syntheses of the novel aromatic and sulphur containing aromatic (meth)acrylates, respectively. To synthesise 2-phenoxy-2-phenylethanol, molar excess of phenol was reacted with styrene oxide in the presence of a base, such as sodium hydroxide, and with moderate heat. The nucleophilic oxygen of the phenol attacks and opens the ring of the styrene oxide. Several reports are available about the reaction of styrene oxide with phenol.[1-4] Reaction yields mixture of structural isomers of primary and secondary alcohol. We modified the procedure to yield primary alcohol (2-phenoxy-2-phenylethanol) as the major product. The intermediate alcohol was reacted slowly with an excess of acryloyl chloride or methacryloyl chloride at low temperatures, while solvated in methylene chloride, in the presence of triethylamine (TEA) to produce 2-phenoxy-2-phenylethyl acrylate and 2-phenoxy-2-phenylethyl methacrylate, respectively.

The refractive index of the resulting polymer can be increased by increasing the polarisability of substituent groups. By incorporating oxygen, sulphur and aromatic rings high refractive index polymers have been synthesised. Incorporating sulphur into acrylates and methacrylates is expected to increase the refractive index further. An analogous reaction was performed using an excess of thiophenol rather than phenol with styrene oxide in presence of mild acidic condition, to produce 2-phenyl-2-(phenylthio)ethanol.[5] In presence of acid catalyst such as zinc chloride reaction yielded primary alcohol as the major product. Sulphur containing acrylate and methacrylate were synthesised by reacting 2-phenyl-2-(phenylthio)ethanol with acryloyl chloride and methacryloyl chloride, respectively.

2-phenylethyl acrylate and 2-phenylethyl methacrylate were synthesised by modified procedures.[6] Synthesised alcohols and monomers were characterised by different spectroscopic techniques to confirm structures.

3.2 Materials

Acryloyl chloride and methacryloyl chloride were prepared by reacting acrylic acid and methacrylic acid with benzoyl chloride.[7] Styrene oxide, acrylic acid, methacrylic acid and deuterated chloroform were procured from Sigma-Aldrich. Phenol, thiophenol, ethyl methyl ketone, methylene chloride, methanol and triethylamine were purchased from Merck. All solvents and reagents were purified and dried by according to procedures given in Vogel's Text Book of Practical Organic Chemistry.[8] Silica gel (60–120) mesh was used for column chromatography and was purchased from ACME Chemical Company, Mumbai, India.

3.3 Characterisation Techniques

3.3.1 Nuclear magnetic resonance (NMR) spectroscopy

Nuclear magnetic resonance (NMR) spectra were recorded on a Bruker AC200 instrument, using deuterated chloroform as solvent and tetramethylsilane (TMS) as the references for ^{1}H nuclei. Chemical shifts are given in hertz (Hz).

3.3.2 Infrared spectroscopy

A fourier transform infrared spectrometer (Model 68B – Perkin Elmer, USA) was used to identify functional groups in the structure of monomers.

3.3.3 Mass spectrometry

EI Mass spectra were recorded on Finngan MAT-1020 spectrometer at 70 *eV* using a direct inlet system. Sample preparation was carried out using methanol as solvent.

3.3.4 Microanalysis

The microanalysis for carbon, hydrogen and oxygen were carried out using a FLASH-EA (Thermo Finnigan – 1112 series) elemental analyser.

3.3.5 X-ray crystallography

The X-ray Crystal data were collected on Bruker SMART APEX CCD diffractometer using M_o K_α radiation with fine focus tube with 50 kV and 30 MA**.**

3.4 Synthetic Procedures

3.4.1 Synthesis of 2-phenoxy-2-phenylethanol

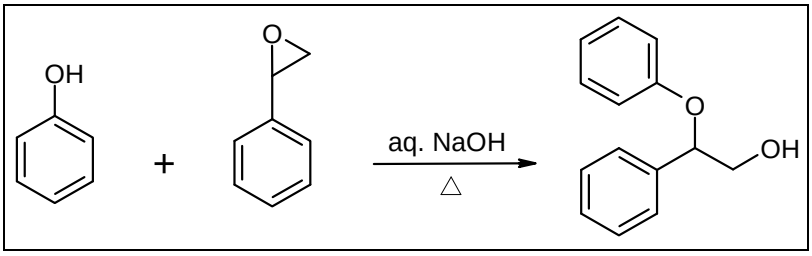

Scheme 3.1: Synthesis of 2-phenoxy-2-phenylethanol

In a three necked round bottom flask equipped with stirrer, condenser and a dropping funnel was charged 28.2 g (0.3 mol) of phenol, 4 g (0.1 mol) of sodium hydroxide (NaOH) and 15 mL of water. Mixture was kept stirring at 80 ^oC for 10 min. As soon as mixture became homogeneous, 12.01 g (0.1 mol) of styrene oxide was added drop-wise. Reaction mixture was refluxed with stirring at 100 ^oC for 3 h. After completion of reaction amber coloured reaction mixture was cooled to 20 ^oC and added

drop-wise to cold 5% NaOH (150 mL) solution to remove excess of free phenol. The insoluble material then taken up into 100 mL of dichloromethane. Organic layer was washed with 5% NaOH (100 mL) solution followed by brine and water. Further organic layer was dried over anhydrous sodium sulphate and dichloromethane was removed under reduced pressure. Viscous amber coloured liquid turned into light brown solid on cooling. Crude product was purified by recrystallisation with petroleum ether: dichloromethane (90:10) mixture to obtain 15.0 g of pure 2-phenoxy-2-phenylethyl alcohol as white solid.

Mol. Formula	**:**	$C_{14}H_{14}O_2$
Mol. Weight	**:**	214.27
ESI-MS (m/z)	**:**	237.28 $[M+Na]^+$
Melting Point	**:**	78 °C
IR (KBr, cm^{-1})	**:**	3403, 3032, 2921, 1591, 1491, 1552, 1238, 1077, 1042, 915, 885, 847, 748, 690
Elemental Analysis	**:**	Calculated : C, 78.48; H, 6.59; O, 14.93 % Found : C, 78.39; H, 6.60
^{1}H NMR (200 MHz, $CDCl_3$)	**:**	δ / ppm : 6.9-7.5 (m, 10H), 5.30 (dd, 1H), 3.91 (m, 2H), 2.34 (m, 1H)
^{13}C NMR (200 MHz, $CDCl_3$)	**:**	δ / ppm : 157.70, 137.73, 129.39, 128.73, 126.14, 126.24, 121.18, 115.85, 81.01, 67.56

3.4.2 Synthesis of 2-phenoxy-2-phenylethyl acrylate

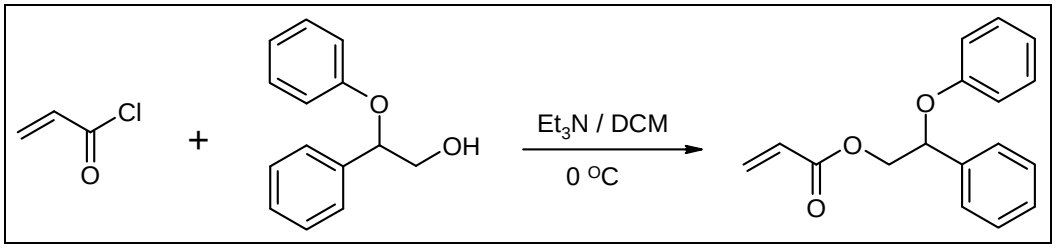

Scheme 3.2: Synthesis of 2-phenoxy-2-phenylethyl acrylate

In a three necked flask equipped with a mechanical stirrer, nitrogen inlet, and guard tube was charged with 32.8 g (0.15 mol) of 2-phenoxy-2-phenylethanol and 100 mL of dry distilled dichloromethane. The reaction flask was cooled in an ice bath under nitrogen. 23.7 g (0.23 mol) triethylamine was added by dropping funnel under stirring. Acryloyl chloride 21.04 g (0.23 mol) in 100 mL dry dichloromethane was taken in dropping funnel, added slowly, drop-wise with stirring, maintaining temperature around 0-5 ^{o}C throughout the addition. After the addition, reaction mixture was kept stirring at the same temperature for 2 h. Reaction was allowed to proceed at room temperature for 24 h. Reaction was monitored by TLC (30 % DCM in hexane). After the completion of reaction, 3.20 g (0.1 mol) of methanol was added drop-wise to deactivate the unreacted acryloyl chloride while keeping the temperature below 20 ^{o}C. Then, 200 mL of water was added to wash the mixture, followed by separation of the mixture into layers. Thereafter, organic layer washed with 4 % NaOH solution, brine solution and distilled water. Organic layer was dried over sodium sulphate and dichloromethane was removed under reduced pressure to obtain liquid 2-phenoxy-2-phenylethyl acrylate. Crude product was purified by column chromatography (silica gel) using petroleum ether: ethyl acetate (90:10) mixture to yield 39.0 g of colourless transparent liquid. The yield was 95% based on the charged 2-phenoxy-2-phenylethanol.

Mol. Formula	**:**	$C_{17}H_{16}O_3$
Mol. Weight	**:**	268.32
ESI-MS (m/z)	**:**	291.09 $[M+Na]^+$
IR (KBr, cm^{-1})	**:**	3062, 3032, 2960, 2470, 1950, 1727, 1689, 1632, 1596, 1492, 1452, 1405, 1232, 1192, 1058, 980, 935, 882, 808, 735, 753, 696
Elemental Analysis	**:**	Calculated : C, 76.10; H, 6.01; O, 17.89 % Found : C, 76.12; H, 6.00 %
^{1}H NMR (200 MHz, $CDCl_3$)	**:**	δ / ppm : 7.26 (m, 7H), 6.84 (m, 3H), 6.33 (d, 1H), 6.10 (dd, 1H), 5.71 (d, 1H), 5.40 (t, 1H), 4.45 (d,2H)
^{13}C NMR (200 MHz, $CDCl_3$)	**:**	δ / ppm : 165.59, 157.61, 137.33, 131.02, 129.17, 128.55, 128.13, 127.84, 126.19, 120.99, 115.79, 77.87, 67.53

3.4.3 Synthesis of 2-phenoxy-2-phenylethyl methacrylate

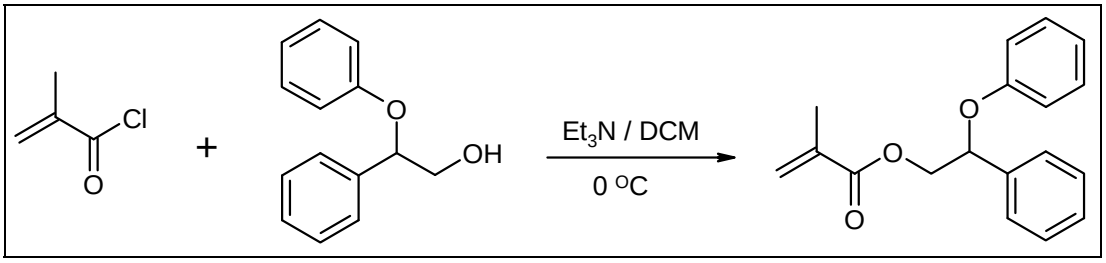

Scheme 3.3: Synthesis of 2-phenoxy-2-phenylethyl methacrylate

In a three necked flask equipped with a mechanical stirrer, nitrogen inlet, and guard tube was charged 32.8 g (0.15 mol) of 2-phenoxy-2-phenylethanol, and 100 mL of dry distilled dichloromethane. The reaction flask was cooled in an ice bath under nitrogen. 24.28 g (0.24 mol) triethylamine was added by dropping funnel under stirring. Methacryloyl chloride 24.04 g (0.23 mol) in 100 mL dry dichloromethane was taken in

dropping funnel, added slowly, drop-wise with stirring while maintaining temperature between 0-5 ^{o}C throughout the addition. After the addition, reaction mixture was kept stirring at same temperature for 2 h. Reaction was allowed to proceed at room temperature for 24 h. Reaction was monitored by TLC (30 % DCM in hexane). After completion of reaction 3.20 g (0.1 mol) of methanol was added drop-wise to deactivate the unreacted methacryloyl chloride while keeping the temperature below 20 ^{o}C. Then, 200 mL of water was added to wash the mixture, followed by separation of the mixture into layers. Thereafter organic layer was washed with 4 % NaOH solution, brine solution and distilled water. Organic layer was dried over sodium sulphate and dichloromethane was removed under reduced pressure to obtain liquid 2-phenoxy-2-phenylethyl methacrylate. Crude product was purified by column chromatography (silica gel) using petroleum ether: ethyl acetate (90:10) mixture to yield 39.7 g of colourless transparent liquid. The yield was 92% based on the charged 2-phenoxy-2-phenylethanol. It is found that compound forming crystals at 0 °C in hexane: ethyl acetate (95: 05) mixture.

Mol. Formula	**:**	$C_{18}H_{18}O_3$
Mol. Weight	**:**	282.34
ESI-MS (m/z)	**:**	305.26 $[M+Na]^+$
IR (KBr, cm^{-1})	**:**	3024, 2963, 2406, 1719, 1638, 1598, 1492, 1454, 1295, 1215, 1166, 1080, 1022, 946, 883, 756, 698
Elemental Analysis	**:**	Calculated : C, 76.57; H, 6.43; O, 17.00 % Found : C, 76.45; H, 6.51%
^{1}H NMR (200 MHz, $CDCl_3$)	**:**	δ / ppm : 7.30 (m, 7H), 6.89 (m, 3H), 6.10 (s, 1H), 5.54 (s, 1H), 5.43 (t, 1H), 4.45 (d, 2H), 1.19 (s, 3H)

^{13}C NMR (200 MHz, $CDCl_3$) **:** δ / ppm : 167.07, 157.82, 137.60, 135.86, 129.29, 128.66, 128.24, 126.32, 126.00, 121.10, 115.95, 78.09, 67.87, 18.18

Single crystal X-ray crystallography analysis confirmed the assigned structure (Figure 3.1)

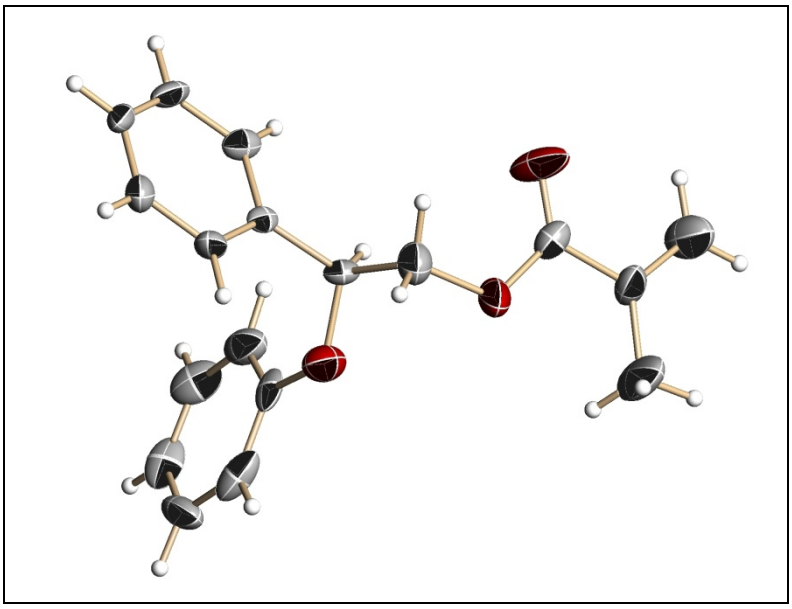

Figure 3.1: ORTEP diagram of 2-phenoxy-2-phenylethyl methacrylate

3.4.4 Synthesis of 2-phenyl-2-(phenylthio)ethanol

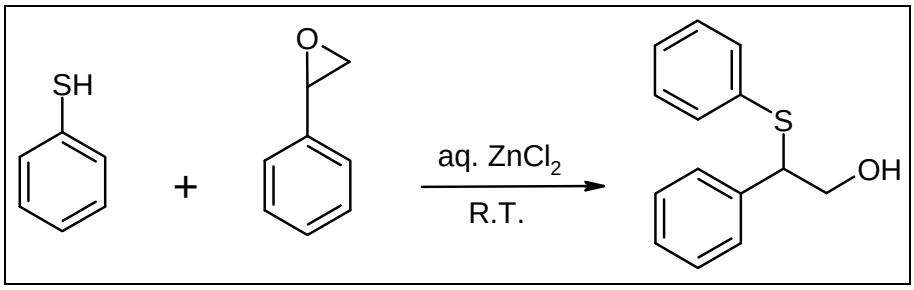

Scheme 3.4: Synthesis of 2-phenyl-2-(phenylthio)ethanol

In a three necked round bottom flask thermostated at 30 °C and equipped with a magnetic stirrer, dropping funnel and a pH electrode, thiophenol (0.15 mL, 1.5 mmol)

and 0.5 mL of a 0.1 M aqueous solution of zinc chloride (ZnCl2, 0.05 mmol) were added to 0.7 mL of water. The resulting pH was adjusted to 4.0 by adding 0.05 mL of aqueous 5 M NaOH. The styrene oxide (1.0 mmol) was then added under stirring. After the reaction, 5 M NaOH was added to the resulting mixture to achieve a pH of 9.0–9.5 and the reaction mixture was extracted with ethyl acetate. Further, organic layer was dried over anhydrous sodium sulphate and ethyl acetate was removed under reduced pressure. Viscous light yellow coloured liquid product was obtained. Crude product was purified by column chromatography (silica gel) using hexane: ethyl acetate (90:10) mixture.

Mol. Formula	**:**	$C_{14}H_{14}OS$
Mol. Weight	**:**	230.33
ESI-MS (m/z)	**:**	253.23 $[M+Na]^+$
IR (KBr cm^{-1})	**:**	3414, 3021, 2932, 2408, 1950, 1730, 1584, 1477, 1377, 1215, 1054, 908, 749, 699,
Elemental Analysis	**:**	Calculated : C, 73.01; H, 6.13; O, 6.95; S, 13.92 % Found : C, 72.80; H, 6.25; S, 13.37%
^{1}H NMR (200 MHz, $CDCl_3$)	**:**	δ / ppm : 7.27 (m, 10H), 4.28 (t, 1H), 3.86 (m, 2H), 2.28 (bs, 1H)
^{13}C NMR (200 MHz, $CDCl_3$)	**:**	δ / ppm : 138.88, 132.29, 128.77, 127.96, 127.58, 127.32, 65.10, 55.71

3.4.5 Synthesis of 2-phenyl-2-(phenylthio)ethyl acrylate

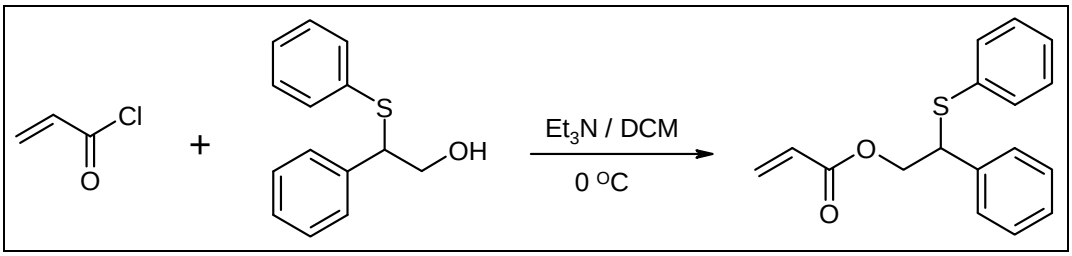

Scheme 3.5: Synthesis of 2-phenyl-2-(phenylthio)ethyl acrylate

In a three necked flask equipped with a mechanical stirrer, nitrogen inlet, and guard tube was charged with 30.0 g (0.13 mol) of 2-phenyl-2-(phenylthio)ethanol and 100 mL of dry distilled dichloromethane. The reaction flask was cooled in an ice bath under nitrogen. 17.13 g (0.17 mol) triethylamine was added by dropping funnel under stirring. 15.56 g (0.17 mol) of acryloyl chloride in 100 mL dry dichloromethane was taken in dropping funnel and added slowly, drop-wise with stirring, maintaining a temperature of 0-5 ^{o}C throughout the addition. After the addition, reaction mixture was kept stirring at same temperature for 2 h. Reaction was further allowed to proceed at room temperature for 24 h. Reaction was monitored by TLC (30 % DCM in hexane). After completion of reaction 3.20 g (0.1 mol) of methanol was added drop-wise to deactivate the unreacted acryloyl chloride while keeping the temperature below 20 ^{o}C. Then, 200 mL of water was added to wash the mixture, followed by separation of the mixture into layers. Thereafter organic layer was washed with 4 % NaOH solution, brine solution and distilled water. Organic layer was dried over sodium sulphate and dichloromethane was removed under reduced pressure to obtain liquid 2-phenyl-2-(phenylthio)ethyl acrylate. Crude product was purified by column chromatography (silica gel) using petroleum ether: ethyl acetate (95:05) mixture to yield 34.78 g of colourless

transparent liquid. The yield was 93% based on the charged 2-phenyl-2-(phenylthio)ethanol.

Mol. Formula	**:**	$C_{17}H_{16}O_2S$
Mol. Weight	**:**	284.38
ESI-MS (m/z)	**:**	307.48 $[M+Na]^+$
IR (KBr, cm^{-1})	**:**	3021, 2950, 2403,1721, 1636, 1616, 1582, 1481, 1406, 1268, 1215, 1069, 981, 756, 696
Elemental Analysis	**:**	Calculated : C, 71.80; H, 5.67; O, 11.25; S, 11.28 % Found : C, 72.01; H, 5.80; S, 11.13 %
^{1}H NMR (200 MHz, $CDCl_3$)	**:**	δ / ppm : 7.27 (m, 10H), 6.24 (dd, 1H), 5.91 (dd, 1H), 5.71 (dd, 1H), 4.53 (m, 3H)
^{13}C NMR (200 MHz, $CDCl_3$)	**:**	δ / ppm : 165.82, 138.34, 133.87, 132.56, 131.31, 130.18, 129.05, 128.70, 128.06, 127.67, 126.72, 66.62, 51.37

3.4.6 Synthesis of 2-phenyl-2-(phenylthio)ethyl methacrylate

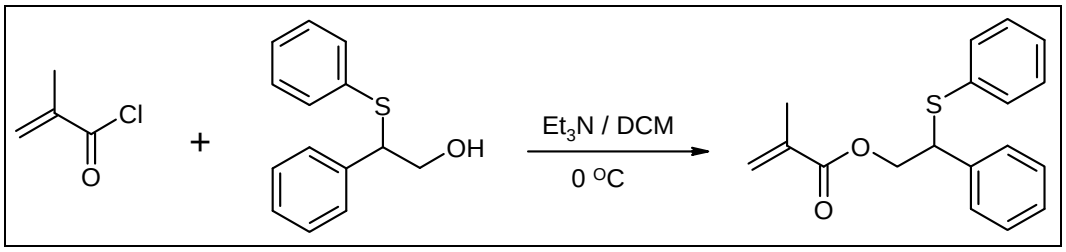

Scheme 3.6: Synthesis of 2-phenyl-2-(phenylthio)ethyl methacrylate

In a three necked flask equipped with a mechanical stirrer, nitrogen inlet, and guard tube was with charged 12.30 g (0.043 mol) of 2-phenyl-2-(phenylthio)ethanol and 30 mL of dry distilled dichloromethane. The reaction flask was cooled in an ice bath under nitrogen. 5.69 g (0.056 mol) triethylamine was added by dropping funnel under

stirring. Methacryloyl chloride 5.14 g (0.056 mol) in 20 mL dry dichloromethane was taken in dropping funnel and added slowly, drop-wise with stirring, maintaining a temperature of 0-5 ^{o}C throughout the addition. After the addition reaction mixture was kept stirring at same temperature for 2 h. Reaction was further allowed to proceed at room temperature for 24 h. Reaction was monitored by TLC (30 % DCM in hexane). After completion of reaction 1.60 g (0.05 mol) of methanol was added drop-wise to deactivate the unreacted methacryloyl chloride while keeping the temperature below 20 ^{o}C. Then, 50 mL of water was added to wash the mixture, followed by separation of the mixture into layers. Thereafter organic layer was washed with 4 % NaOH solution, brine solution and distilled water. Organic layer was dried over sodium sulphate and dichloromethane was removed under reduced pressure to obtain liquid 2-phenyl-2-(phenylthio)ethyl methacrylate. Crude product was purified by column chromatography (silica gel) using petroleum ether: ethyl acetate (95:05) mixture to yield 13.98 g of colourless transparent liquid. The yield of monomer was 92% based on the charged 2-phenyl-2-(phenylthio)ethanol.

Mol. Formula	**:**	$C_{18}H_{18}O_2S$
Mol. Weight	**:**	298.41
ESI-MS (m/z)	**:**	331.39 $[M+Na]^+$
IR (KBr, cm-1)	**:**	3025, 2953, 2400, 1723, 1637, 1612, 1511, 1407, 1217, 1061, 762, 669
Elemental Analysis	**:**	Calculated : C, 72.45; H, 6.08; O, 10.72; S, 10.75 % Found : C, 72.10; H, 6.20; S, 10.58 %
^{1}H NMR	**:**	δ / ppm : 7.11 (m, 10H), 5.95 (s, 1H), 5.35 (s, 1H), 4.50 (m,

(200 MHz, $CDCl_3$)		3H), 176 (s, 3H)
^{13}C NMR (200 MHz, $CDCl_3$)	**:**	δ / ppm : 166.30, 138.07, 135.43, 133.58, 131.82, 128.55, 128.15, 127.58, 127.35, 127.03, 125.47, 66.30, 50.87, 17.73

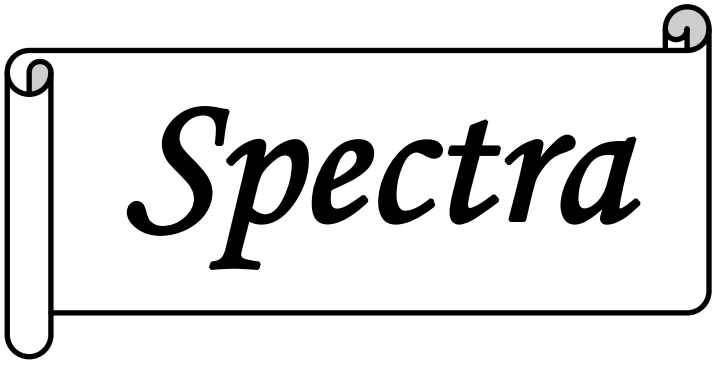
Spectra

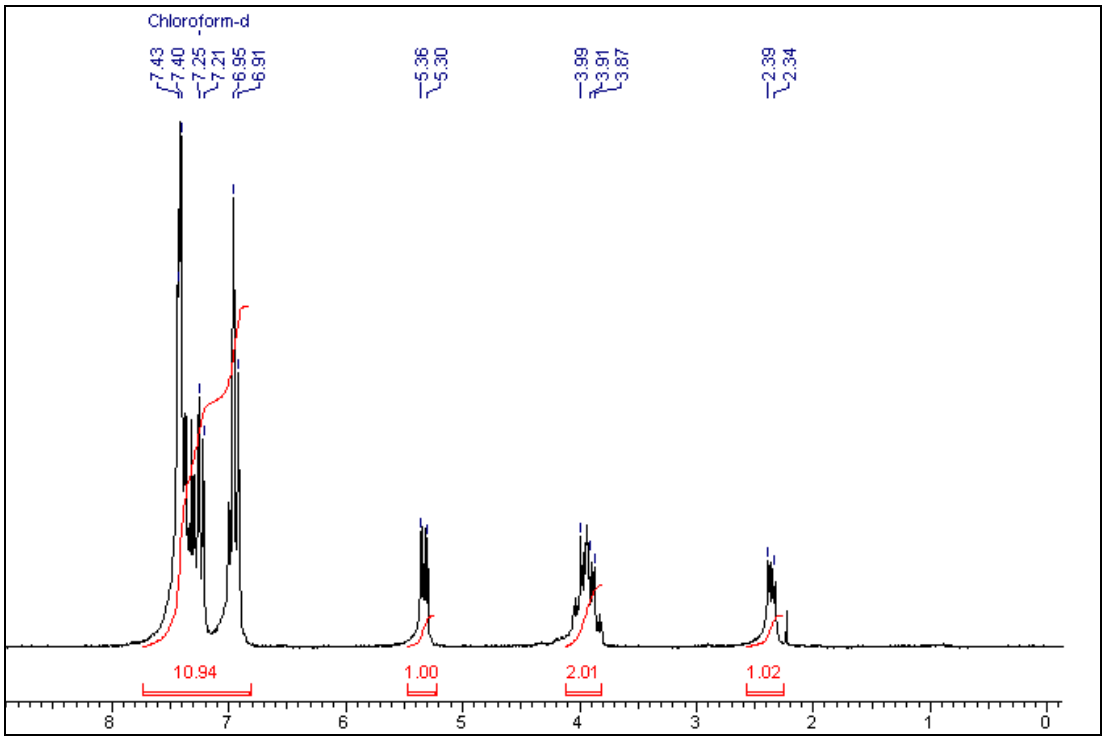

Figure 3.2: ^{1}H NMR spectrum of 2-phenoxy-2-phenylethanol

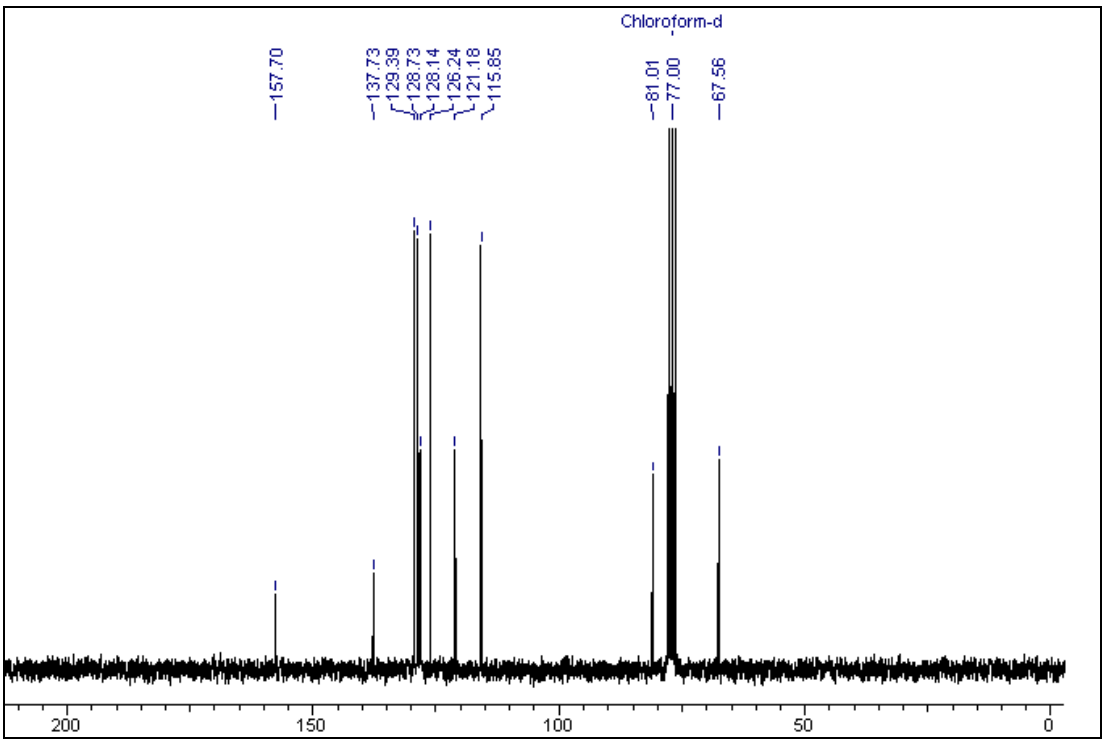

Figure 3.3: ^{13}C NMR spectrum of 2-phenoxy-2-phenylethanol

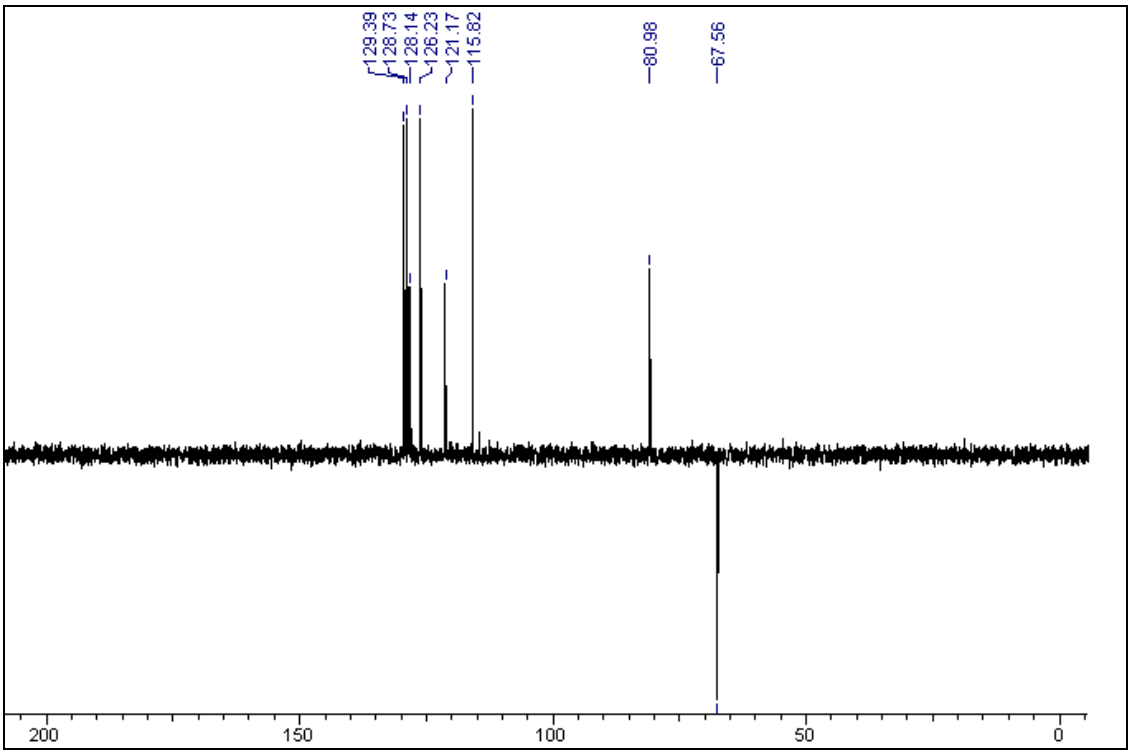

Figure 3.4: ^{13}C DEPT NMR spectrum of 2-phenoxy-2-phenylethanol

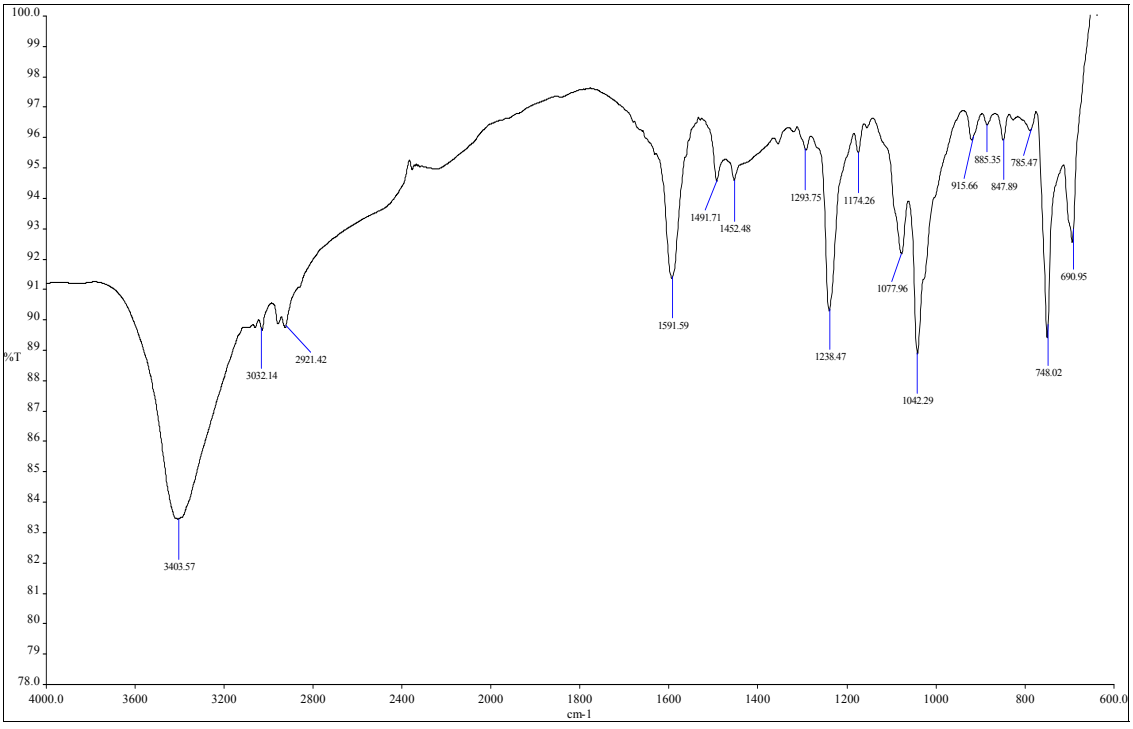

Figure 3.5: IR spectrum of 2-phenoxy-2-phenylethanol

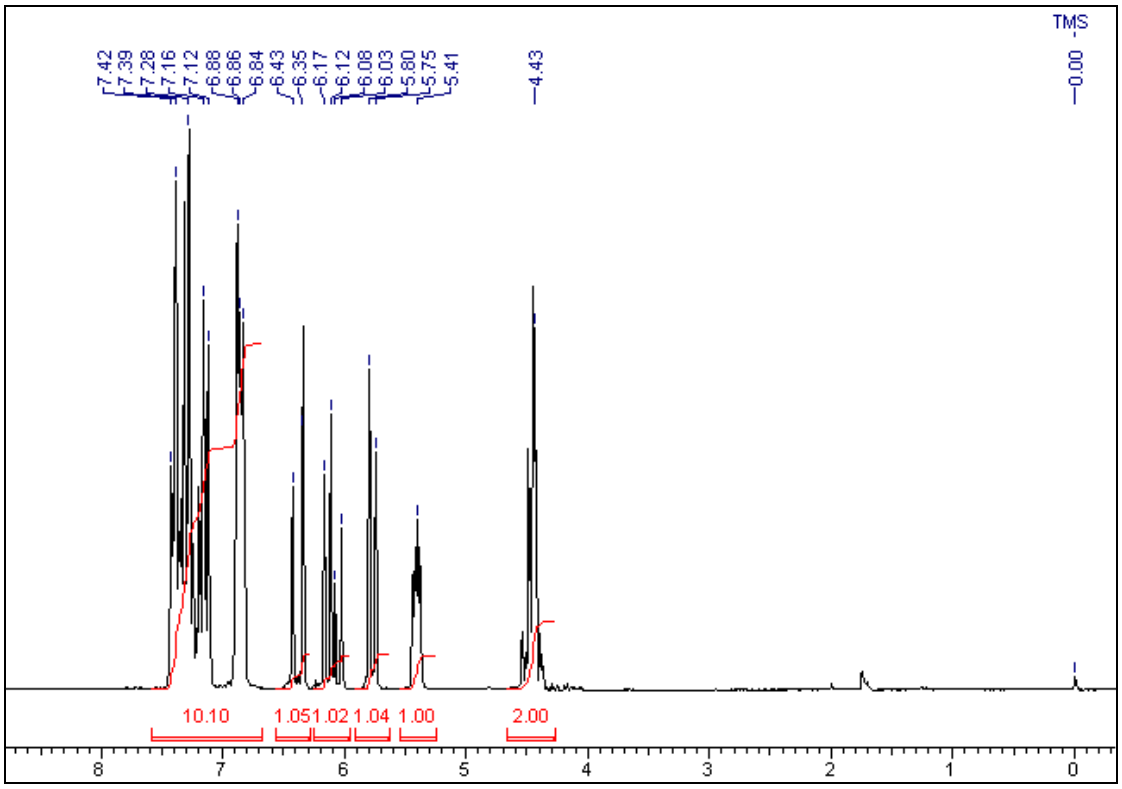

Figure 3.6: ^{1}H NMR spectrum of 2-phenoxy-2-phenylethyl acrylate

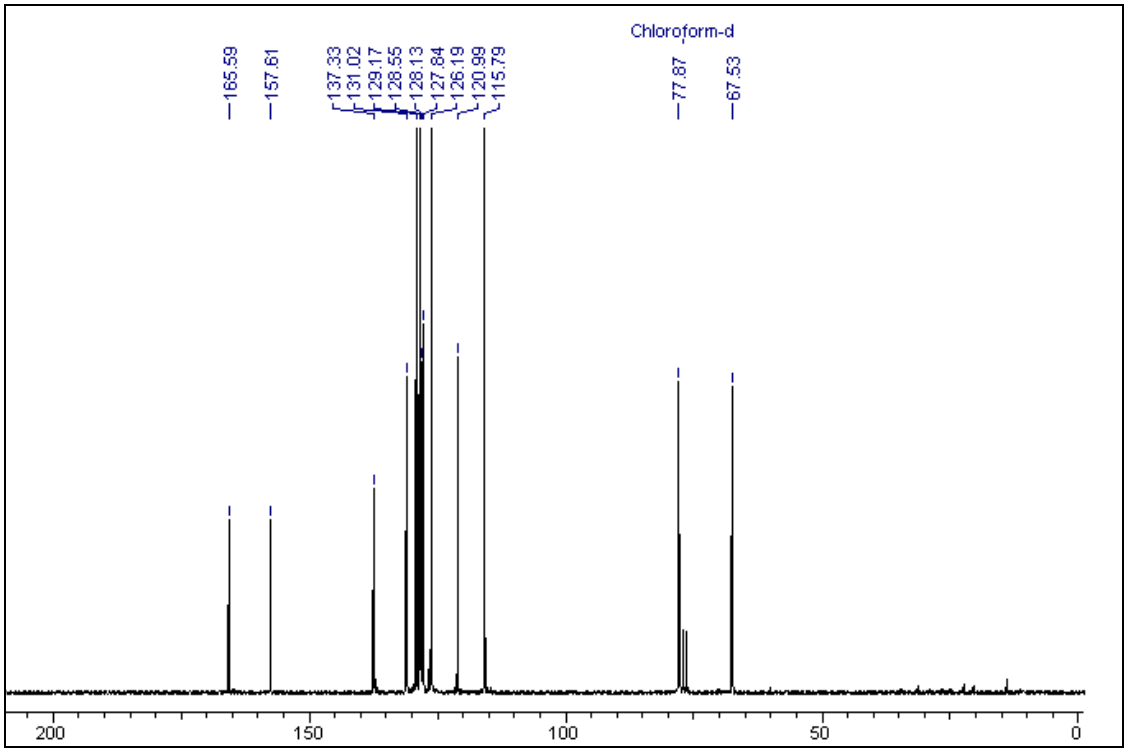

Figure 3.7: ^{13}C NMR spectrum of 2-phenoxy-2-phenylethyl acrylate

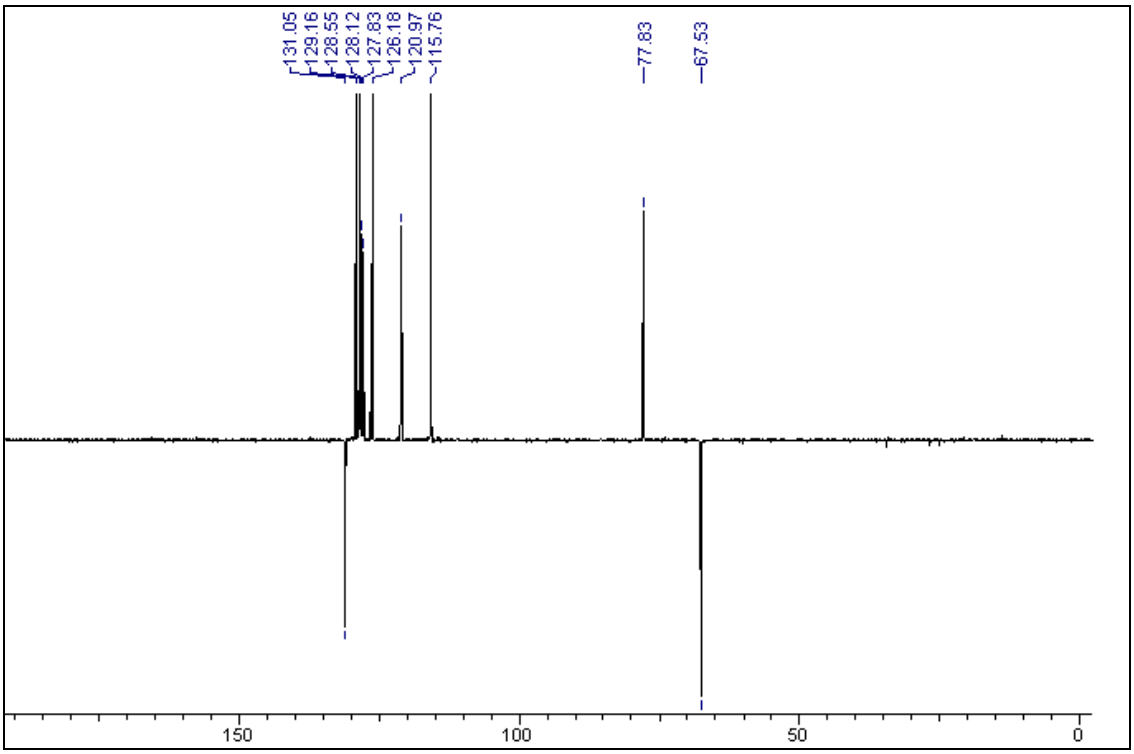

Figure 3.8: ^{13}C DEPT NMR spectrum of 2-phenoxy-2-phenylethyl acrylate

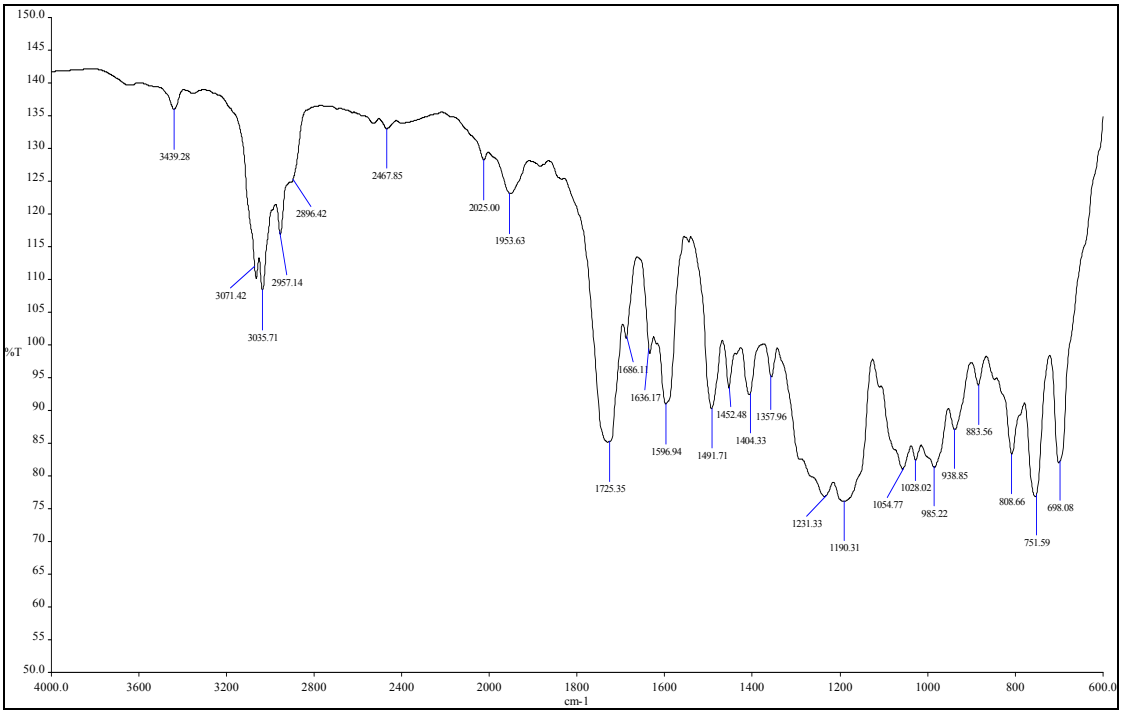

Figure 3.9: IR spectrum of 2-phenoxy-2-phenylethyl acrylate

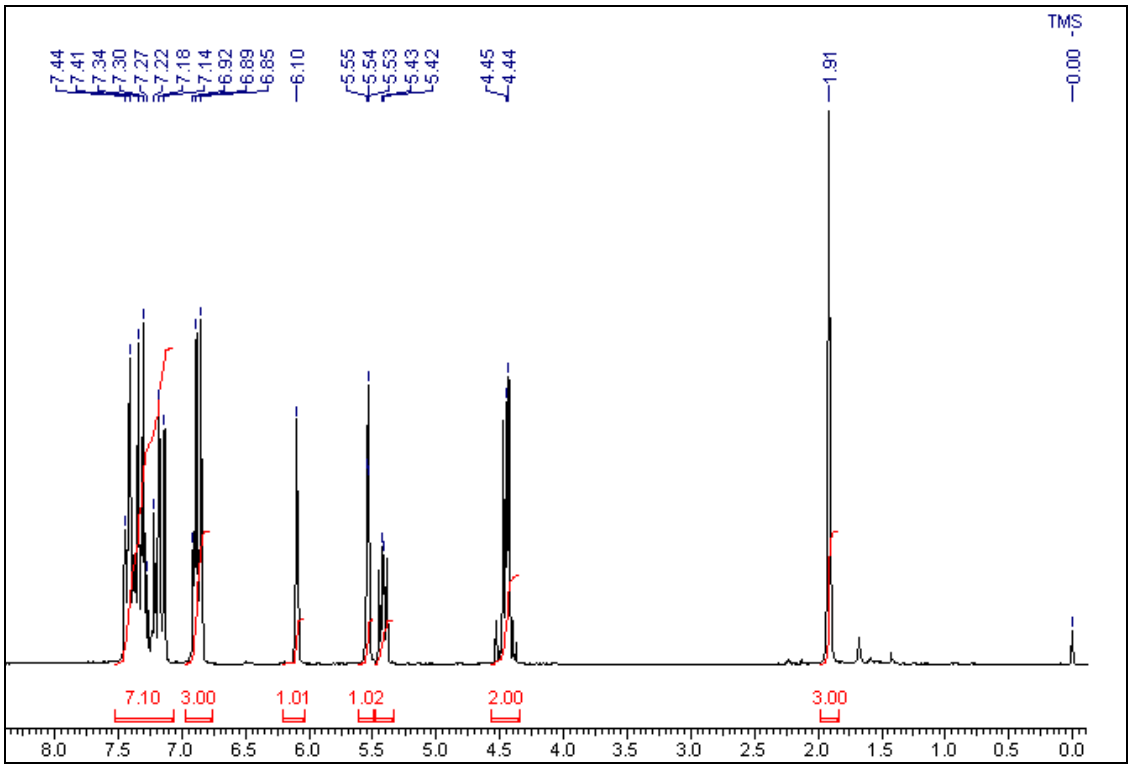

Figure 3.10: ^{1}H NMR spectrum of 2-phenoxy-2-phenylethyl methacrylate

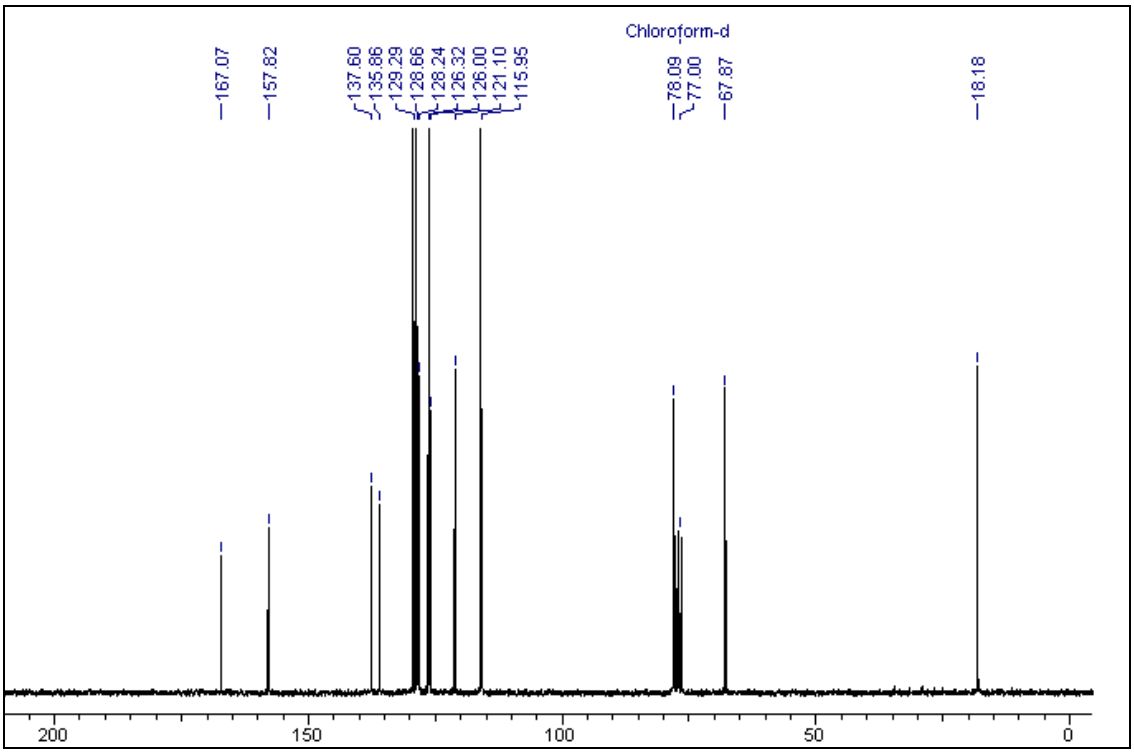

Figure 3.11: ^{13}C NMR spectrum of 2-phenoxy-2-phenylethyl methacrylate

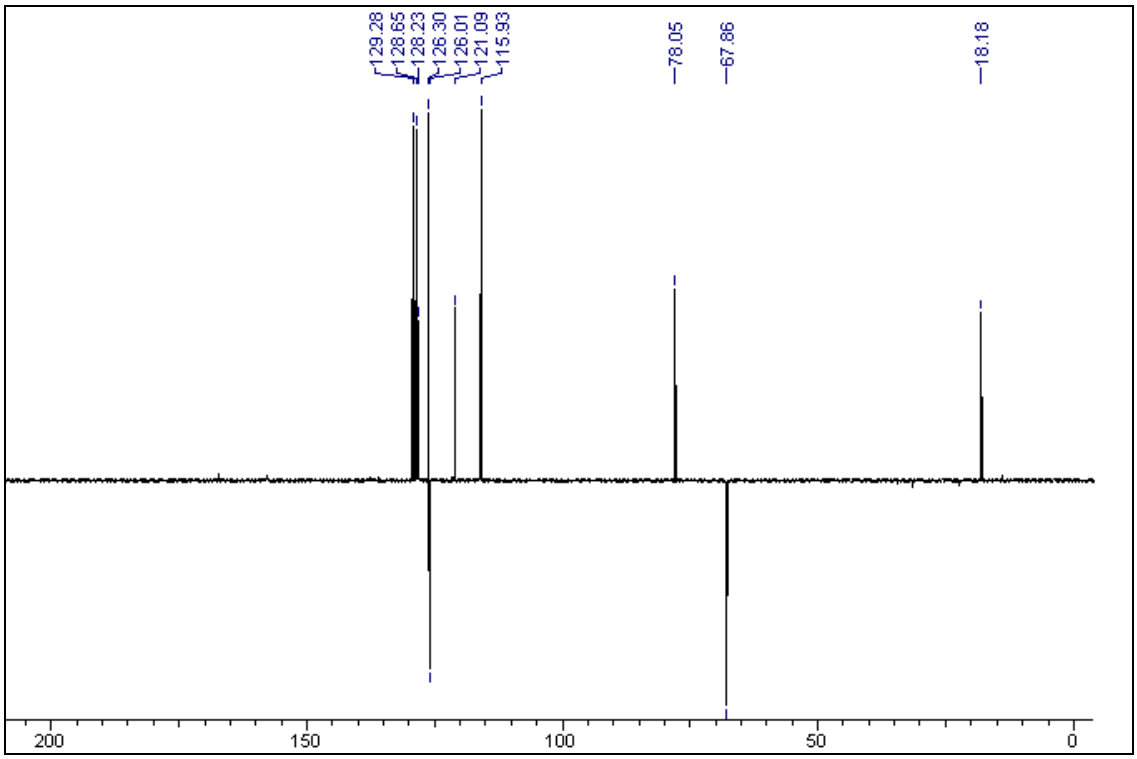

Figure 3.12: ^{13}C DEPT NMR spectrum of 2-phenoxy-2-phenylethyl methacrylate

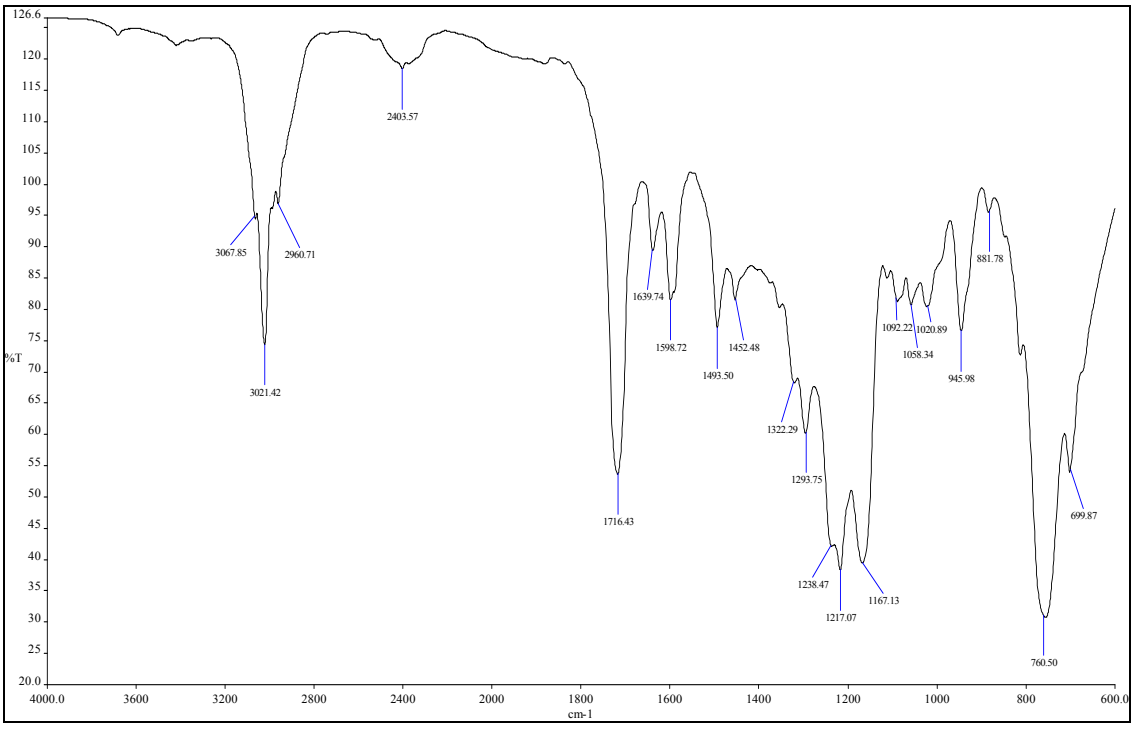

Figure 3.13: IR spectrum of 2-phenoxy-2-phenylethyl methacrylate

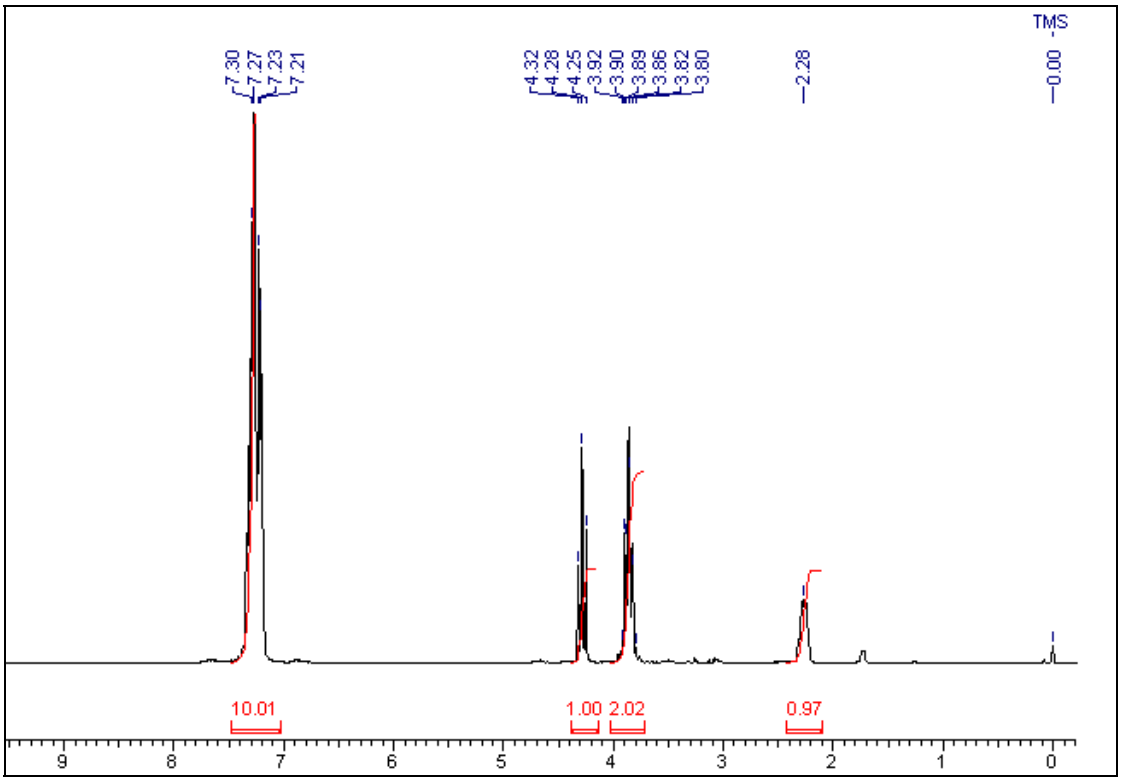

Figure 3.14: ^{1}H NMR spectrum of 2-phenyl-(2-phenylthio)ethanol

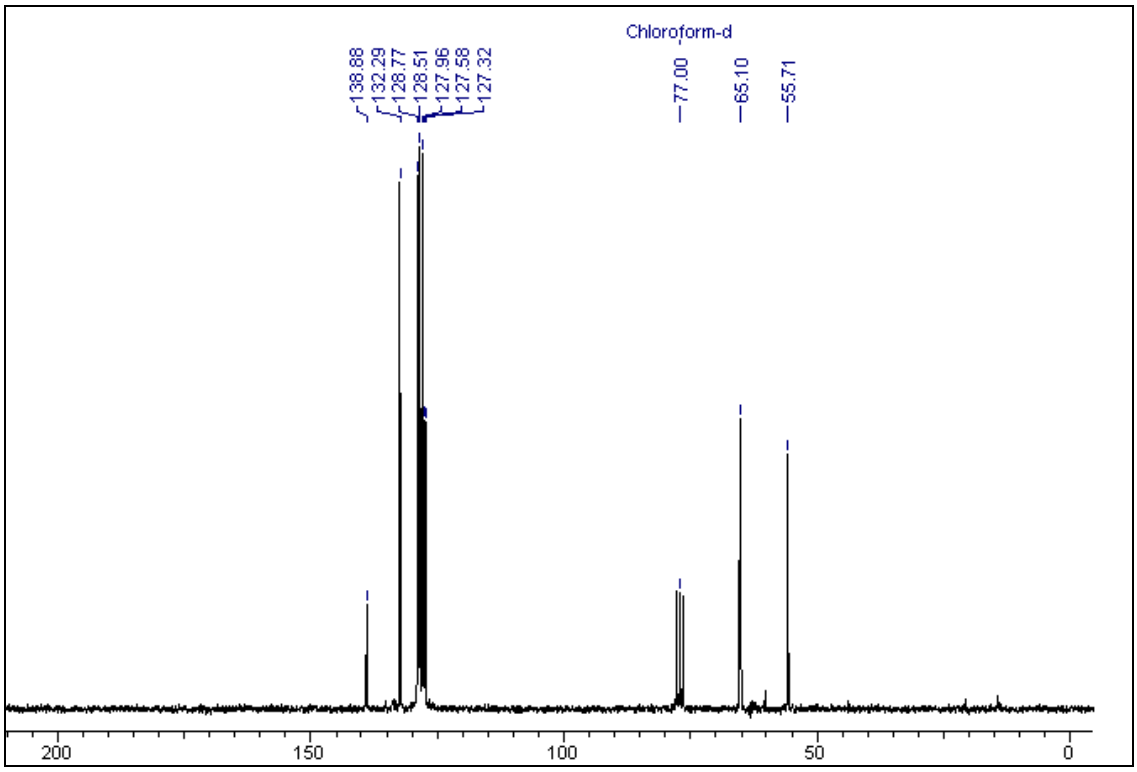

Figure 3.15: ^{13}C NMR spectrum of 2-phenyl-(2-phenylthio)ethanol

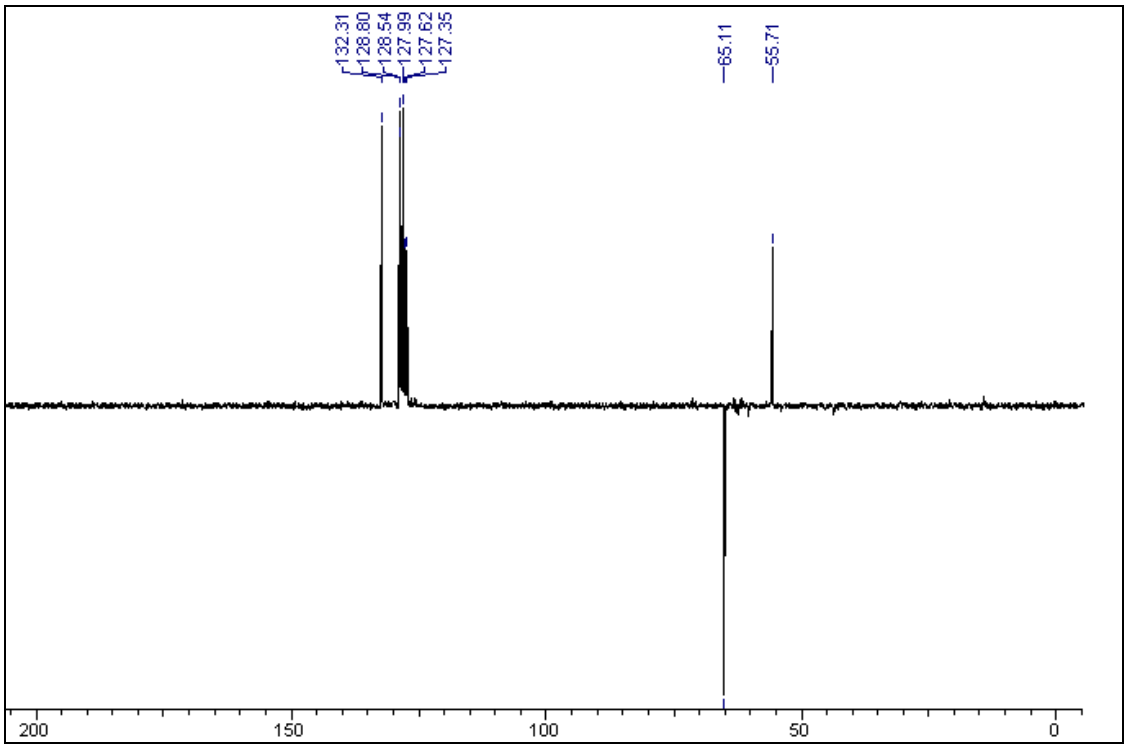

Figure 3.16: ^{13}C DEPT NMR spectrum of 2-phenyl-(2-phenylthio)ethanol

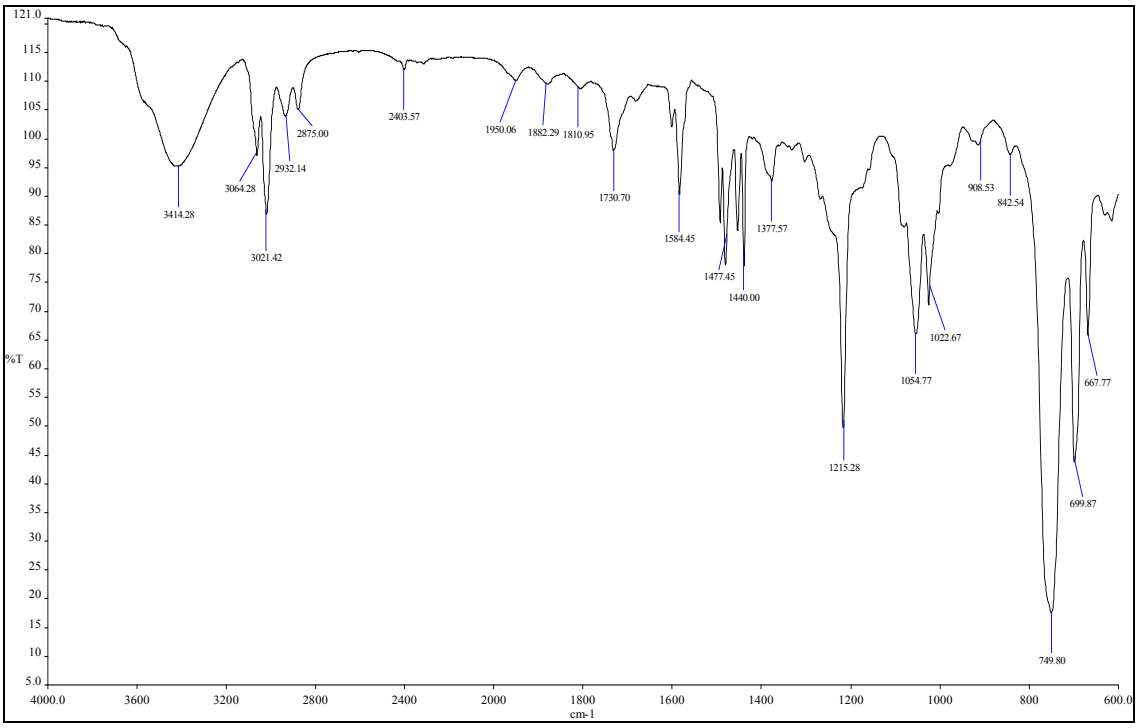

Figure 3.17: IR spectrum of 2-phenyl-(2-phenylthio)ethanol

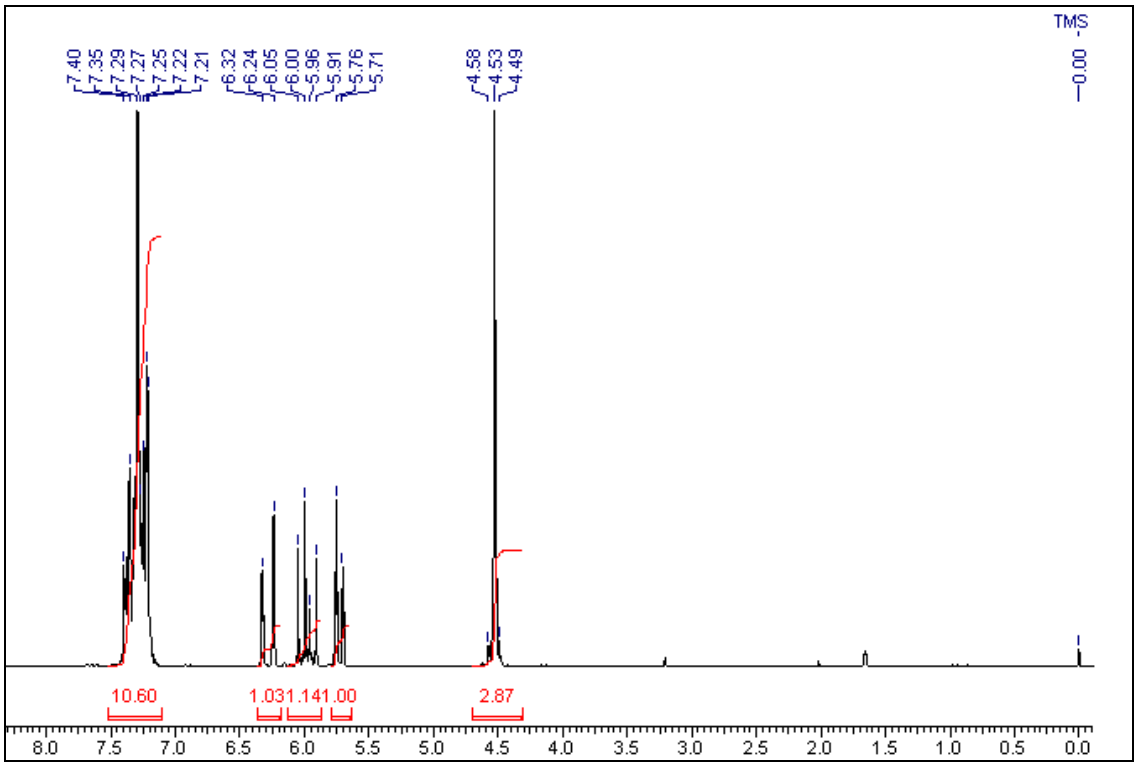

Figure 3.18: ^{1}H NMR spectrum of 2-phenyl-(2-phenylthio)ethyl acrylate

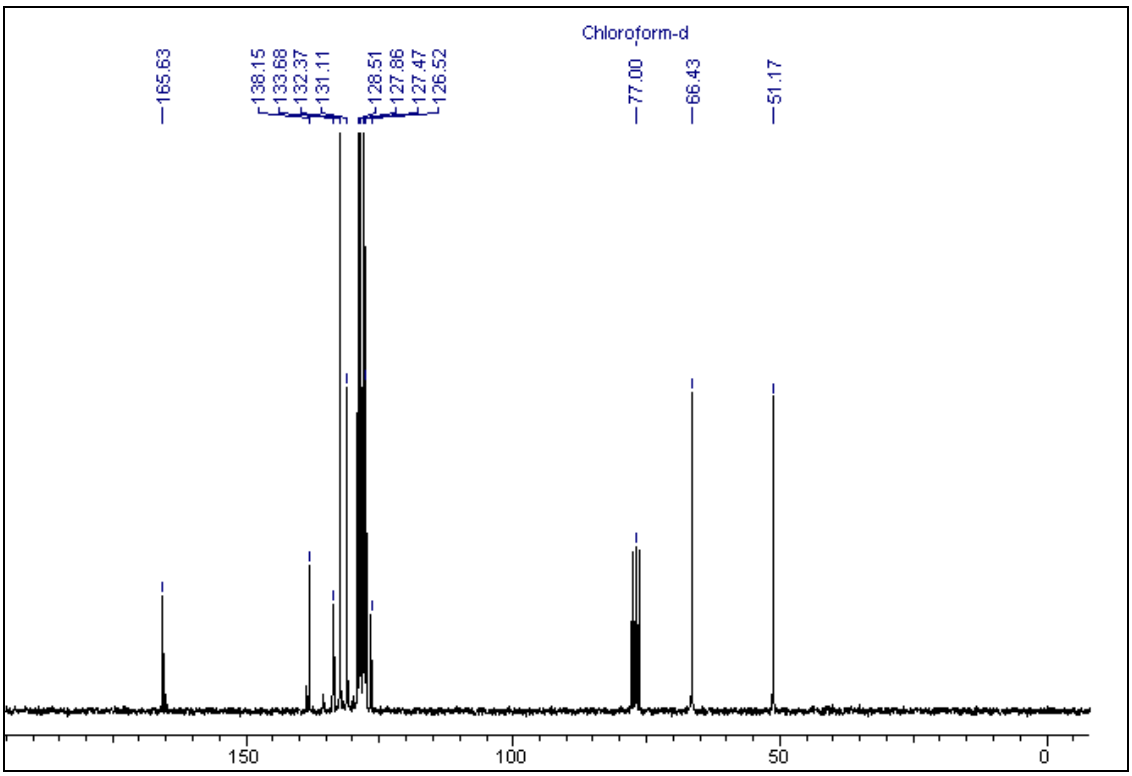

Figure 3.19: ^{1}H NMR spectrum of 2-phenyl-(2-phenylthio)ethyl acrylate

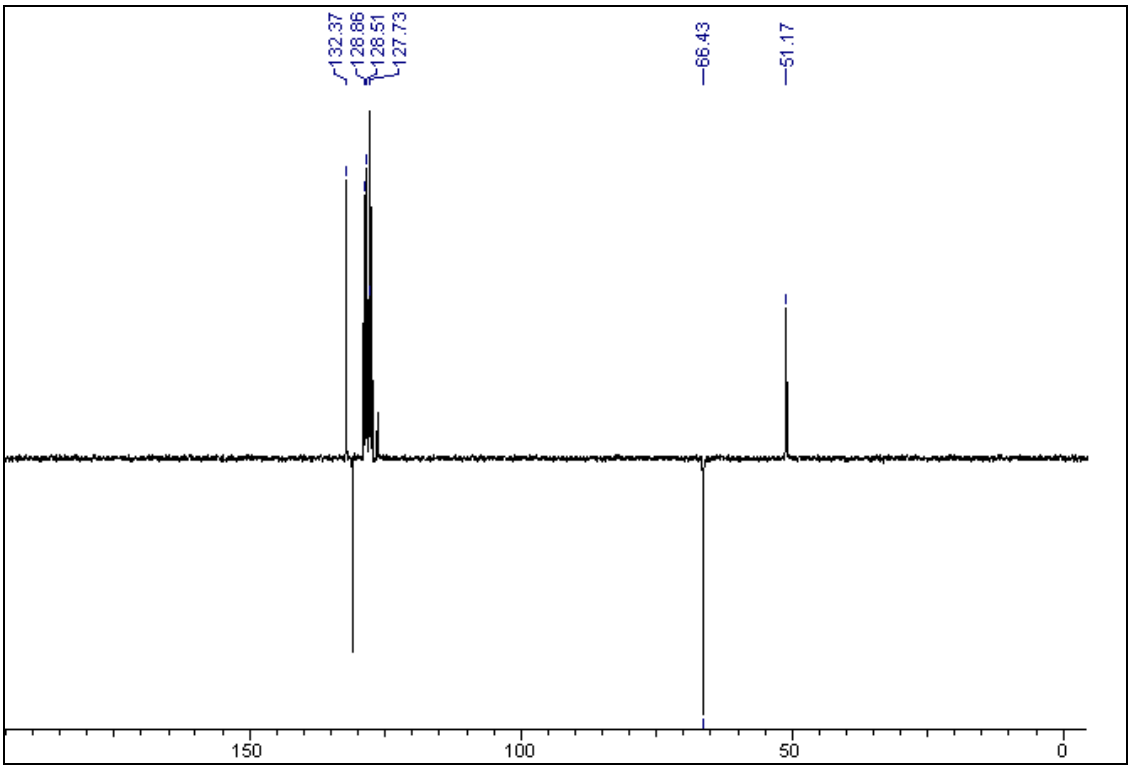

Figure 3.20: ^{13}C DEPT NMR spectrum of 2-phenyl-(2-phenylthio)ethyl acrylate

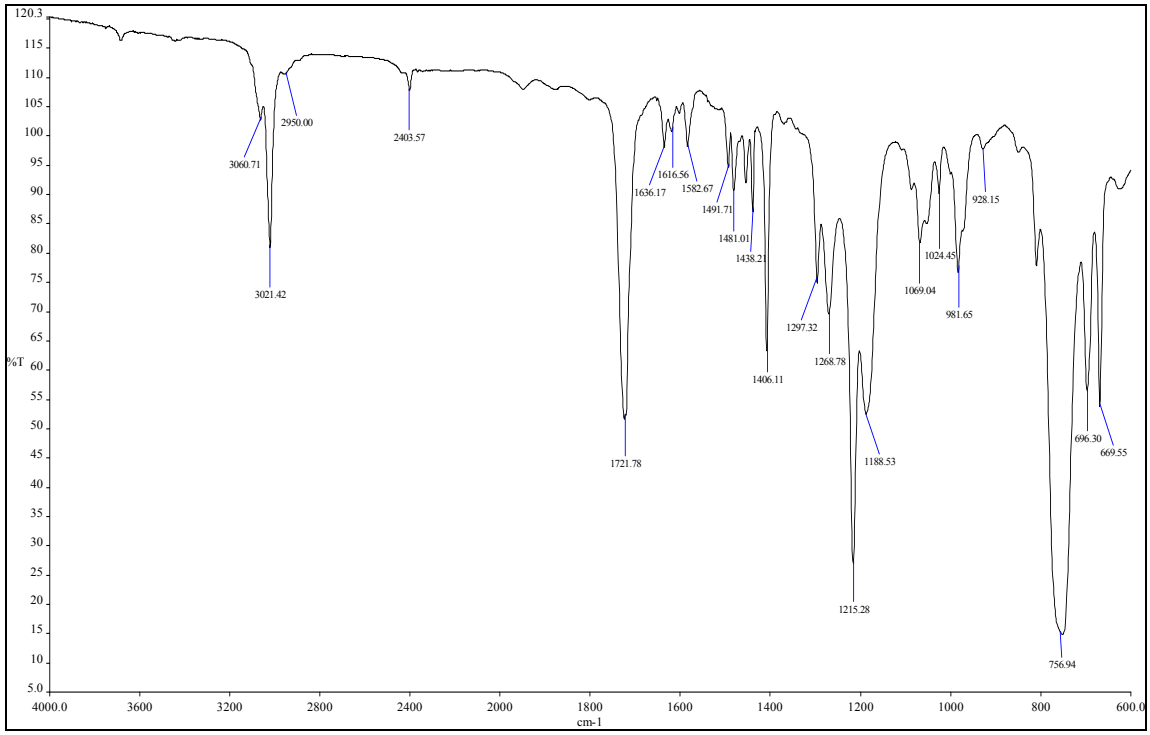

Figure 3.21: IR spectrum of 2-phenyl-(2-phenylthio)ethyl acrylate

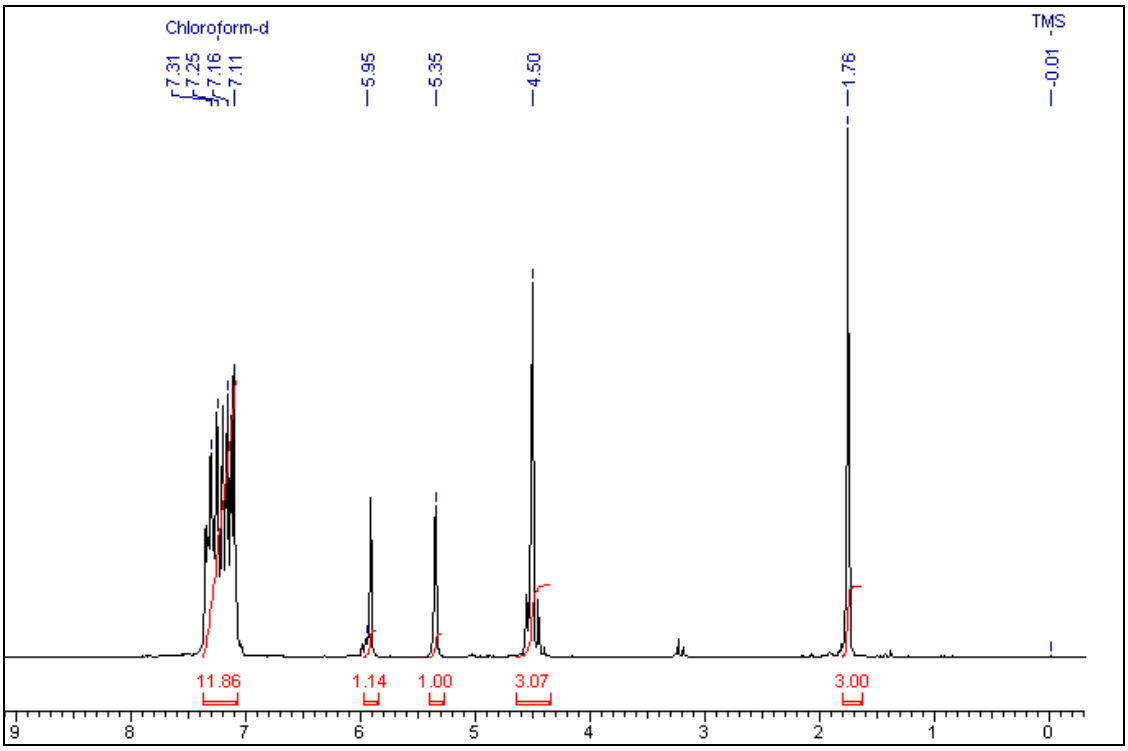

Figure 3.22: ^{1}H NMR spectrum of 2-phenyl-(2-phenylthio)ethyl methacrylate

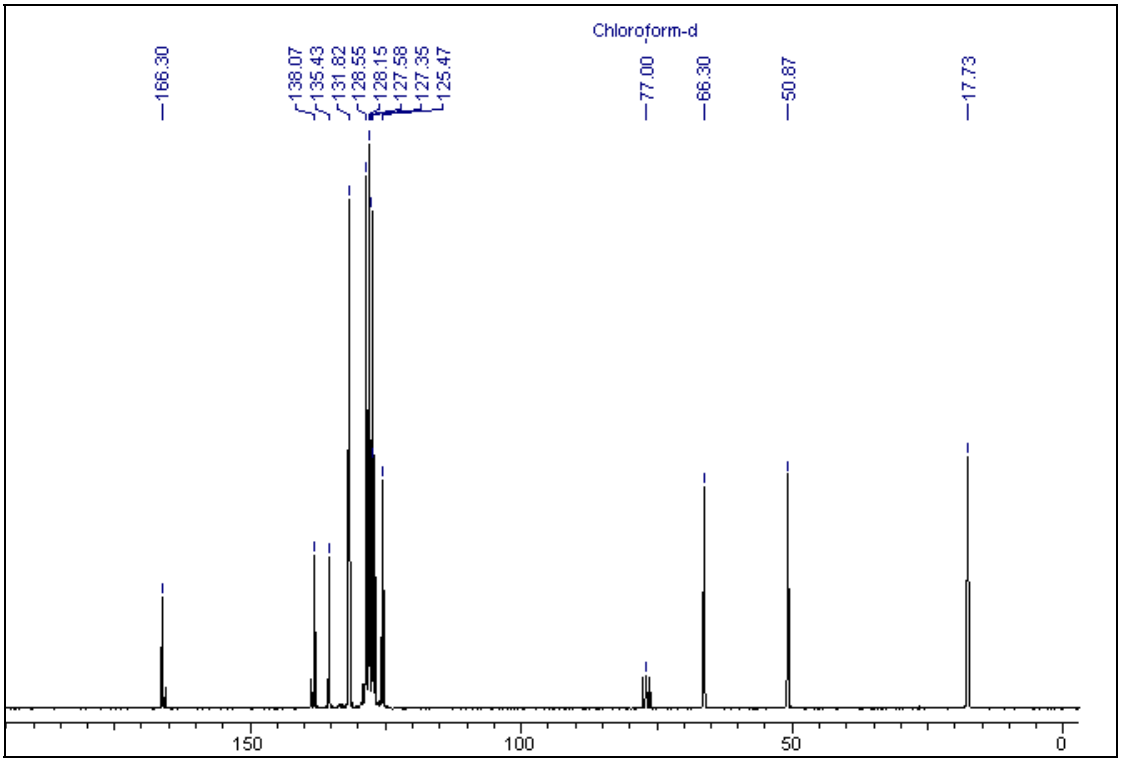

Figure 3.23: ^{13}C NMR spectrum of 2-phenyl-(2-phenylthio)ethyl methacrylate

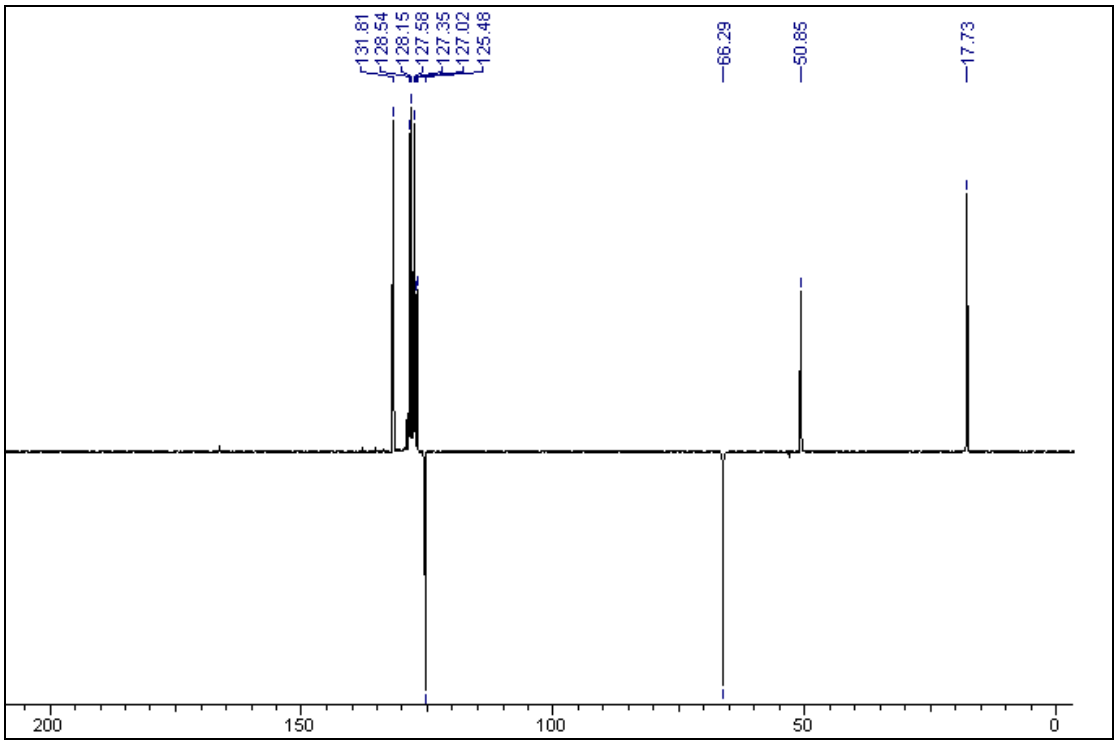

Figure 3.24: ^{13}C DEPT NMR spectrum of 2-phenyl-(2-phenylthio)ethyl methacrylate

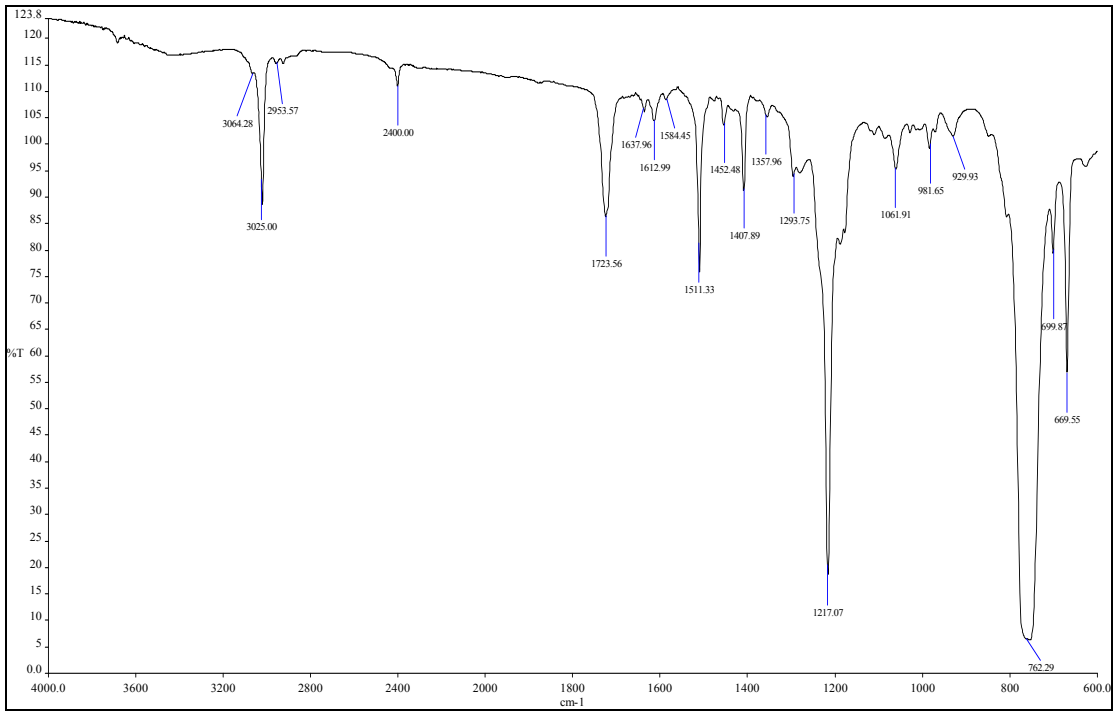

Figure 3.25: IR spectrum of 2-phenyl-(2-phenylthio)ethyl methacrylate

3.5 Homopolymerisation

Predetermined quantities of monomer, ethyl methyl ketone (EMK) and 2,2'-azobisisobutyronitrile (AIBN) (1 mol % of total monomers) were placed in a Pyrex tube. The mixture was deoxygenated by flushing with oxygen free nitrogen for at least 10 min. The tube was tightly sealed and immersed in a thermostated water bath at 70 °C. After the reaction times, the polymers were precipitated in methanol, filtered off, and purified by reprecipitations from chloroform solution into methanol and finally dried under reduced pressure for 24 h.

3.5.1 Characterisation techniques

Differential scanning calorimetry (DSC) was analysed by TA Q100 instrument under nitrogen atmosphere at a heating rate of 10 °C/min. Refractive index measurements were performed with an Automatic Refractometer, model PTR 46 X.

3.5.2 Results and discussion

3.5.2.1 Refractive index

Refractive Indices (RI) of all homopolymers are represented in Table 3.1. RI of poly(PPEA) and poly(PPEM) are higher than that of poly(PEA) and poly(PEMA). This is due to additional aromatic ring which contributes to increase in polarisability and subsequently RI of homopolymer. It was also observed that the RI of poly(PTEA) and poly(PTEM) are higher than all other homopolymers. Polarisability of sulphur atom is higher than oxygen, by replacing 'O' with 'S' in the polymer backbone, polymers with high refractive indices have been produced.

Table 3.1: Structures, T_g and RI of homopolymers

No	Name	Polymer structure	T_g (°C)	RI
1	Poly(2-phenoxy-2-phenyl ethyl acrylate)	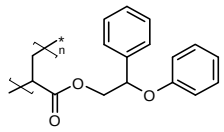	56.00	1.574
2	Poly(2-phenoxy-2-phenyl ethyl methacrylate)	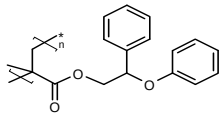	80.85	1.578
3	Poly[2-phenyl-2-(phenylthio)ethyl acrylate]	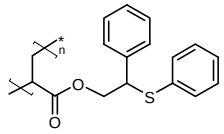	25.63	1.620
4	Poly[2-phenyl-2-(phenylthio)ethyl methacrylate]	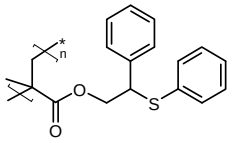	68.60	1.618
5	Poly(2-phenylethyl acrylate)	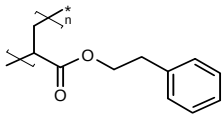	-3.00	1.553
6	Poly(2-phenylethyl methacrylate)	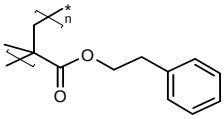	42.97	1.559

3.5.2.2 Glass transition temperature (T_g)

Table 3.1 and Figure 3.26 summarise the T_g values of all homopolymers. T_g of poly(methacrylates) are higher than corresponding poly(acrylates) due to α-methyl group in polymer backbone. T_g of poly(PPEA) and poly(PPEM) are higher than corresponding sulphur containing poly(PTEA) and poly(PTEM), due to larger volume of sulphur atom than oxygen.

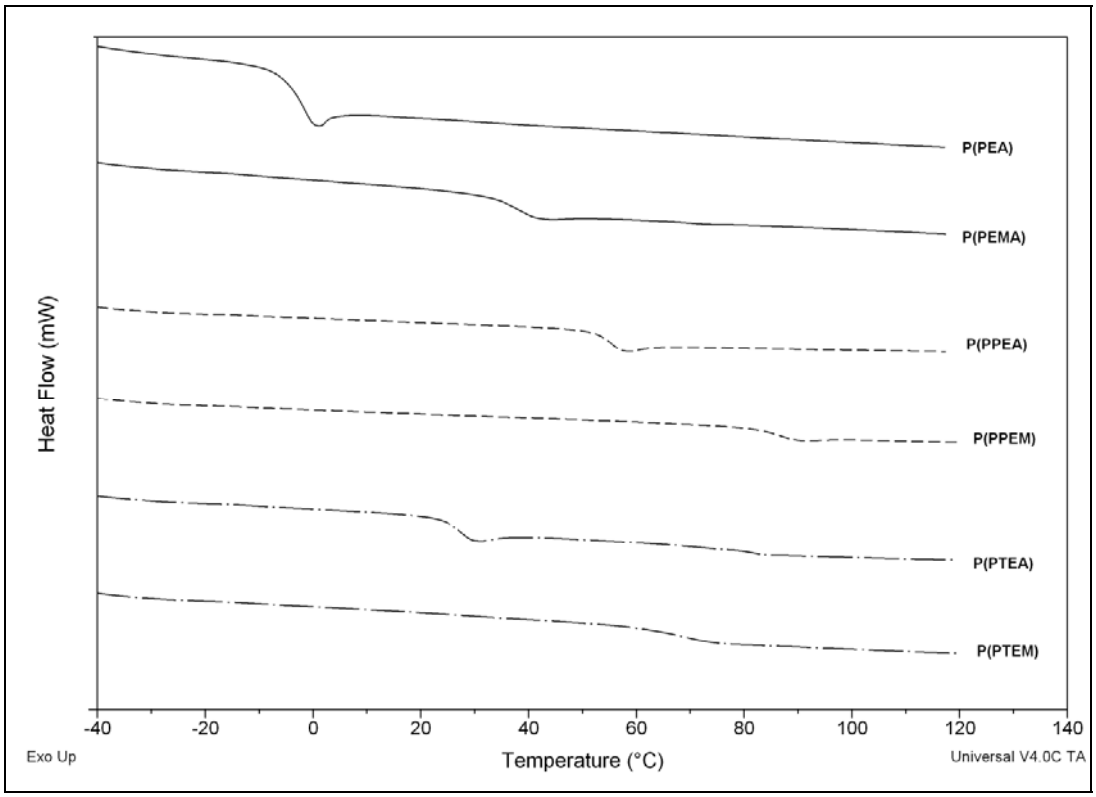

Figure 3.26: DSC thermograms of homopolymers

Copolymerisation studies of newly synthesised monomers with 2-phenylethyl (meth)acrylates are discussed in detailes in next chapter.

3.6 References

[1] C. O. Guss, *J. Am. Chem. Soc.,* **1949**, 71, 3460.

[2] C. O. Guss, *J. Am. Chem. Soc.,* **1950,** 72, 3878.

[3] B. Das, M. Krishnaiah, P. Thirupathi, *Tetrahedron Lett*., **2007**, 48, 4263–4265.

[4] M. B. Hocking, *Can. J. Chem*., **1974**, 52, 2730.

[5] D. Amantini, F. Fringuelli, F. Pizzo, *Synlett*., **2003**, 15, 2292–2296.

[6] U. Senthilkumar, K. Ganesan, B. S. R. Reddy *J. Polym. Res.,* **2003**, 10, 21–29.

[7] G. H. Stempel, R. P. Cross, R. P. Mariella, *J. Am. Chem. Soc.*, **1950**, **72**, 2299.

[8] A. I. Vogel, *Practical Organic Chemistry*, Third Ed., Longman Group Ltd. London, **1974.**

Chapter IV

Copolymerisation Studies

4.1 Introduction

Copolymer is a polymer derived from two (or more) monomeric species. Copolymerisation refers to methods used to chemically synthesise a copolymer, and is the most useful methodology to tailor make a polymer product with specially desired properties. Copolymerisation modifies the symmetry of the polymer chain and modulates both intermolecular and intramolecular forces, so properties of the polymer may vary within the wide limits. Free-radical binary copolymerisation reactions are important from both practical and theoretical point of view. Theoretically, it is interesting to focus on the effect of the chemical structure on the reactivity of monomers and radicals. Practically, radical copolymerisation is the most recommendable process to prepare an unlimited number of polymers by changing the nature and relative proportions of monomers in the reaction medium.

For many free radical vinyl polymerisations, two monomers are used and the copolymer chain formed contains both of the structural elements from both monomers. This type of reaction that employs two comonomers is a copolymerisation. The reactivity and the relative concentrations of the two monomers should determine the concentration of each comonomer that is incorporated into the copolymer chain.

The application of chain copolymerisations has produced much important fundamental information. Most of the knowledge of the reactivities of monomers via carbocations, free radicals, and carbanions in chain polymerisations has been derived from chain copolymerisation studies. The chemical structure of these monomers strongly influences reactivity during copolymerisation. Furthermore, from the technological viewpoint, copolymerisation has been critical to the design of the copolymer product with

a variety of specifically desired properties. As compared to homopolymers, the synthesis of copolymers can produce an unlimited number of different sequential arrangements where the changes in relative amounts and chemical structures of the monomers produce materials of varying chemical and physical properties.

Several different types of copolymers are known and the process of copolymerisation can often be changed in order to obtain these structures. A statistical or random copolymer may obey some type of statistical law which relates to the distribution of each type of comonomer that has been incorporated into the copolymer, Thus, for example, it may follow zero or first or second order Markov statistics.[1] Copolymer chains that are formed via a zero order Markov process, or Bernoullian, contain two monomer structures that are from two monomers A and B randomly distributed, termed random copolymers:[2]

–A-A-B-B-B-A-B-A-B-B-A-A-B-A-

Alternating, block and graft copolymers are the other three types of copolymer structures. Equimolar compositions with a regularly alternating distribution of monomer units are alternating copolymers:[3-7]

–A-B-A-B-A-B-A-B-A-B-A-B-A-B-A-

A linear copolymer that contains one or more long uninterrupted sequences of each of the comonomer species is a block copolymer:[8-9]

-A-A-A-A-A-A-A-A–B-B-B-B-B-B-B-B-B-

A graft copolymer[10-11] contains a linear chain of one type of monomer structure and one or more side chains that consist of linear chains of another monomer structure.

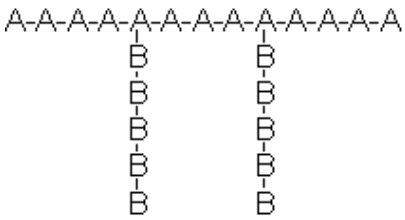

For this discussion, the main focus will be on randomly distributed or statistical copolymers.

Copolymer composition is usually different from the molar composition of the starting materials charged into the polymerisation system. Therefore, monomers have different tendencies to be incorporated into the copolymer, which also means that each type of comonomer reacts at different rate with the two free radical species present. Even in the early work by Staudinger,[12] it was noted that the copolymer that was formed had almost no characteristics similar to those of the homopolymers derived from each of the monomers. Furthermore, the relative reactivities of monomers in a copolymerisation were also quite different from their reactivities in homopolymerisation. Thus, some monomers were more while some were less reactive during copolymerisation than during their homopolymerisation. Even more interesting was that some monomers that would not homopolymerise at all would copolymerise relatively well with a second monomer to form copolymers. It was concluded that the homopolymerisation features do not easily directly relate to those of the copolymerisation.

Alfrey, Mayo-Lewis and Walling,[13-15] demonstrated that the copolymer composition can be determined by chemical reactivity of free radical propagating chain terminal unit during copolymerisation. Application of the first order Markov statistics was used and the terminal model of copolymerisation was proposed. The use of two monomers, M_1 and M_2, during copolymerisation leads to two types of propagating

species. The first of these species is a propagating chain that ends with a monomer of structure M_1 and the second species is a propagating chain that ends with a monomer of structure M_2. For radically initiated copolymerisations, the two structures can be represented by $-M_1\cdot$ and $-M_2\cdot$, where the dash (-) represent the chain and the $M\cdot$ represents the radical at the growing end of the chain. The assumption that the reactivity of these propagating species only depends on the monomer unit at the end of the chain is called the terminal unit model.[16] If this is so, only four propagation reactions are possible for a two monomer system. The propagating chain that ends in $M_1\cdot$ can either add a monomer of type M_1 or of type M_2. Also, the propagating chain that ends in $M_2\cdot$ can add a monomer unit of type M_2 or of type M_1. Therefore, these equations can be written with the rate constants of reactions:[7]

$$-M_1\cdot + M_1 \xrightarrow{k_{11}} -M_1\cdot \qquad 4.1$$

$$-M_1\cdot + M_2 \xrightarrow{k_{12}} -M_2\cdot \qquad 4.2$$

$$-M_2\cdot + M_1 \xrightarrow{k_{21}} -M_1\cdot \qquad 4.3$$

$$-M_2\cdot + M_2 \xrightarrow{k_{22}} -M_2\cdot \qquad 4.4$$

The rate constant for the reaction of the propagating chain that ends in M_1 and adds another M_1 to the end of the chain is k_{11}, and the rate constant for the reaction of the propagating chain that ends in M_2 and adds M_1 to the end of the chain is k_{21}, and so on. The term self-propagation refers to the addition of a monomer unit to the chain that ends with the same monomer unit and the term cross-propagation refers to a monomer unit that is added to the end of a propagating chain that ends in a different monomer unit. These

irreversible reactions can propagate by free radical, anionic or cationic processes, although active lifetimes could be very different.

As indicated by reactions 4.1 and 4.3, monomer M_1 is consumed and as indicated by reactions 4.2 and 4.4, monomer M_2 is consumed. The rates of disappearance of the two monomers in species are given by:

$$-\frac{d[M_1]}{dt} = k_{11}[-M_1\cdot][M_1] + k_{21}[-M_2\cdot][M_1] \quad 4.5$$

$$-\frac{d[M_2]}{dt} = k_{12}[-M_1\cdot][M_2] + k_{22}[-M_2\cdot][M_2] \quad 4.6$$

In order to find the rate at which the two monomers enter into the copolymer, equation 4.5 is divided by equation 4.6 to give the copolymer composition equation:

$$\frac{d[M_1]}{d[M_2]} = \frac{k_{11}[-M_1\cdot][M_1] + k_{21}[-M_2\cdot][M_1]}{k_{12}[-M_1\cdot][M_2] + k_{22}[-M_2\cdot][M_2]} \quad 4.7$$

The low concentrations (below 10 mol L^{-1}) of the radical chains in the systems are very hard to experimentally determine. So, to remove these from the equation, the steady state approximation is normally employed. Therefore, a steady state concentration is assumed for both of the species -$M_1\cdot$ and -$M_2\cdot$ separately. The interconversion between the two species must be equal in order for the concentrations of each to remain constant and hence the rates of reactions 4.2 and 4.3 must be equal:

$$k_{21}[-M_2\cdot][M_1] = k_{12}[-M_1\cdot][M_2] \quad 4.8$$

Rearrangement of equation 4.8 and combination with equation 4.7 gives:

$$\frac{d[M_1]}{d[M_2]} = \frac{\frac{k_{11}k_{21}[-M_1\cdot][M_1]^2}{K_{12}[M_2]} + k_{21}[-M_2\cdot][M_1]}{k_{22}[-M_2\cdot][M_2] + k_{21}[-M_2\cdot][M_1]} \quad 4.9$$

This equation can be further simplified by dividing the right side and the top and bottom by k_{21} [$-M_2^{\cdot}$] [M_1]. The results are then combined with the parameters r_1 and r_2, which are defined as the reactivity ratios:

$$r_1 = \frac{k_{11}}{k_{12}} \quad , \quad r_2 = \frac{k_{22}}{k_{21}} \tag{4.10}$$

The most familiar form of copolymerisation composition equation is then obtained as:

$$\frac{d[M_1]}{d[M_2]} = \frac{r_1[M_1]^2 + [M_1][M_2]}{r_2[M_2]^2 + [M_1][M_2]} \tag{4.11}$$

The ratio of the rates of addition of each monomer can also be considered as the ratio of the molar concentrations of the two monomers incorporated in the copolymer, which is denoted by (m_1/m_2). The copolymer composition equation can then be written as:

$$\frac{m_1}{m_2} = \frac{r_1[M_1]^2 + [M_1][M_2]}{r_2[M_2]^2 + [M_1][M_2]} \tag{4.12}$$

The copolymer composition equation defines the molar ratios of the two monomers that are incorporated into the copolymer, $d[M_1]/d[M_2]$. As seen in the equation, this term is directly related to the concentration of the monomers that were in the feed, $[M_1]$ and $[M_2]$, and also the monomer reactivity ratios, r_1 and r_2. The ratio of the rate constant for the addition of its own type of monomer to the rate constant for the addition of the other type of monomer is defined as monomer reactivity ratio for each monomer in the system. When $-M_1^{\cdot}$ prefers to add monomer M_1 instead of monomer M_2, the r_1 value is greater than one. When $-M_1^{\cdot}$ prefers to add monomer M_2 instead of monomer M_1, the r_1 value is less than one. When the r_1 value is equal to zero, the

monomer M_1 is not capable of adding to itself, which means that homopolymerisation is not possible.

The copolymer composition equation can also be expressed in mole fractions instead of concentrations, which helps to make the equation more useful for experimental studies. In order to put the equation into these terms, F_1 and F_2 are the mole fractions of M_1 and M_2 in the copolymer, and f_1 and f_2 are the mole fractions of monomers M_1 and M_2 in the feed. Therefore:

$$f_1 = 1 - f_2 = \frac{[M_1]}{[M_1]+[M_2]} \qquad 4.13$$

and

$$F_1 = 1 - F_2 = \frac{d[M_1]}{d[M_1]+d[M_2]} \qquad 4.14$$

then combining equation 4.13, 4.14 and 4.11 gives

$$F_1 = \frac{r_1 f_1^2 + f_1 f_2}{r_1 f_1^2 + 2 f_1 f_2 + r_2 f_2^2} \qquad 4.15$$

This form of the copolymer equation gives the mole fraction of monomer M_1 introduced into the copolymer.[6]

4.2 Methods to Determine of Reactivity Ratios

The kinetics and mechanisms involved in the free-radical binary copolymerisation of vinyl monomers have been a research topic of interest for many years. The copolymerisation of two monomers, A and B, give rise to the formation of a copolymer chain having composition and sequence distribution, which are dependent on the relative proportion of applied monomers as well as the monomer and radical reactivities.[16] The

composition of a copolymer produced by simultaneous polymerisation of two monomers is usually different from the composition of the comonomer feed from which it is produced. This shows that different monomers have different tendencies to undergo copolymerisation. These tendencies often have little or no resemblance to their behaviour in homopolymerisation. Different models have been put forth to visualise the mechanism of addition of growing chains and the factors influencing them.

Estimation of reactivity ratios are important because of following reasons. Primarily to predict copolymer composition and microstructure for any starting mixture and secondly to classify the relative reactivities of different monomers toward free microradicals and finally to understand issues related to the rate of copolymerisation and molecular weight distribution.

Copolymerisation reactivity ratios were originally measured for the purpose of describing the relative reactivities of various monomers towards various radicals. Nowadays it is being treated as quantitative data and hence the necessity of accurate measurement arises. Several methods have been developed to estimate reactivity ratios. Some of these methods require labourious calculation procedures and so the digital computer can be put to use in an efficient manner to estimate reactivity ratios.

The estimation methods developed to determine reactivity ratio are based on the binary copolymer composition equation 4.16:[16,18-20]

$$\frac{dM_1}{dM_2} = \frac{r_1 M_1^2 + M_1 M_2}{r_2 M_2^2 + M_1 M_2} \qquad 4.16$$

where r_1 and r_2 are the monomer reactivity ratios and dM_1/dM_2 is the relative rate of addition of the two monomers to the chain. The copolymer composition may not be

independent of conversion. This means the disappearance of monomer one may be faster than the disappearance of monomer two, if monomer one is being incorporated into the copolymer at a faster rate and therefore it has a larger reactivity ratio than monomer two. Different types of monomers show different types of copolymerisation behaviour. Depending on the reactivity ratios of the monomers, the copolymer can incorporate the comonomers in different ways. The three main types of behaviour that copolymerisations tend to follow correspond to the conditions when both r_1 and r_2 are equal to one, $r_1.r_2 < 1$ and $r_1.r_2 > 1$.

A perfectly random copolymerisation is achieved when the both r_1 and r_2 values are equal to one. This type of copolymerisation will occur when the two different types of propagating species, $-M_1^{\cdot}$ and $-M_2^{\cdot}$, show the exact same preference for the addition of each type of monomer. In other words, the growing radical chains do not prefer to add one of the monomers more than the other, which results in perfectly random incorporation into the copolymer.

An alternating copolymerisation is defined as $r_1 = r_2 = 0$. The polymer product in this type of copolymerisation shows a non-random equimolar amount of each comonomer that is incorporated into the copolymer. This may occur because the growing radical chains will not add to its own monomer. Therefore, the opposite monomer will have to be added to produce a growing chain and a perfectly alternating chain is obtained.

When $r_1 > 1$ and $r_2 > 1$, both of the monomers want to add to themselves and in theory could produce block copolymers. But actually, because of the short lifetime of the propagating radical, the product of such copolymerisations produces very undesirable heterogeneous products that include homopolymers. Therefore, macroscopic phase

separation could occur and desirable physical properties such as transparency would not be achieved.

In order to determine the amount of the comonomer that has been incorporated into the copolymer, various analytical methods must be used. Proton Nuclear Magnetic Resonance, Carbon 13 NMR and Fourier Transform Infrared Spectroscopy are three sensitive instruments that can determine the copolymer composition.

Many methods have been used to estimate reactivity ratios of a large number of comonomers.[21] Tidwell and Mortimer distinguished four different procedures for the calculation of the monomer reactivity ratios in copolymerisation, namely, approximation, linearisation, intersection, and curve fitting. We will quickly review few of them which still have importance in today's context.

4.2.1 Approximation methods

4.2.1.1 Tidwell and Mortimer method

This approximation method based on differential copolymerisation equation, probably first mentioned by Tidwell and Mortimer[31], depends on the fact that at extremely low concentrations of either monomer the consumption of both monomers occurs almost entirely by chain-end radicals which leads to:

$$\frac{d[M_1]}{d[M_2]} = r_1 \frac{M_1}{M_2} \qquad 4.17$$

This method requires extremely sensitive analytical techniques, and, in addition, it is simply assumed that the experiments can be described by the usual Alfrey-Mayo model.

4.2.1.2 Volker Jaack method

This method[50] uses an integrated form of the Mayo equation:

$$\log \frac{[M_1]}{[M_1]_0} = r_1 \log \frac{[M_2]}{[M_2]_0} \qquad 4.18$$

where the subscript zero again denotes initial conditions. Equation 4.18 is valid for high monomer conversions in copolymerisation, provided an excess of monomer M_1 remains enough throughout the copolymerisation.

4.2.2 Linearisation methods

4.2.2.1 The Intersection method

One can calculate reactivity ratios for binary copolymerisation only by performing two experiments.[22] Following linear equation 4.19 is given below:

$$r_2 = \frac{[M_1]}{[M_2]}\left[\frac{m_1}{m_2} - 1\right] + \frac{m_2[M_1]^2}{m_1[M_2]^2} \qquad 4.19$$

where $[M_1]$, $[M_2]$ are the molar concentrations in the feed and m_1 and m_2 in the copolymer. A graphic representation of equation gives a set of straight lines in r_1, r_2 coordinate, each line representing one experiment. The point whose coordinates are located at the intersection of two different experiments represents r_1 and r_2 values.

4.2.2.2 Joshi and Joshi method

This method[23,24] is an improvement of the Mayo Lewis intersection method. The best point of intersection was given a mathematical significance in this method. The best point of intersection was defined as the one which was statistically closest to all experimental lines and which if it were not for experimental errors would lie on every line of the Mayo Lewis plot, resulting ideally in an unique intersection point. A condition was set up to make the sum of the squares of the perpendicular distances from all the

lines to the best point of intersection to a minimum. This method does not suffer from the errors of reindexing the monomers.

4.2.2.3 The Fineman-Ross method

The first method to balance successfully the entire set of experiments and to estimate the experimental error was that developed by Fineman and Ross.[25] This method offers a simple graphical method to evaluate reactivity ratios. A simpler method of estimation would involve carrying out the copolymerisations to low conversions and using the approximate form of differential copolymerisation equation to estimate the reactivity ratios. However, a simpler technique, which permits the use of data in the intermediate concentration regions and reduces the uncertainties in the r values, is possible. If $f = (m_1/m_2)$ and $F = (M_1/M_2)$, then the differential equation 4.16 can be rewritten as:

$$\frac{F(1-f)}{f} = r_2 - \frac{F^2}{f} r_1 \qquad 4.20$$

Equation 4.20 can be represented as:

$$G = r_1 H - r_2 \qquad 4.21$$

where $G = (f-1)/F$ and $H = f/F^2$. A plot of G as ordinate and H as abscissa is a straight line whose slope is $-r_1$ and intercept is r_2. The method of least squares can be employed to find the line of best fit. The slope of the line of best fit is influenced very much by the points which are nearer to the origin, so it does not give an uniform weightage to the points and hence it suffers from errors of reindexing the monomers. The validity is only qualitative and the estimates of r_1 and r_2 can change with each experiment by weighing

the data in different ways. Furthermore, the high and low experimental composition data are unequally weighed, which produces large effects on the calculated values of r_1 and r_2.

4.2.2.4 Yezrielev- Brokhina-Roskin (YBR) method

To overcome lack of symmetry in the FR method Yezrielev et al.[26] derived the following symmetric equation 4.22:

$$\left[1-\frac{m_2}{m_1}\right]\sqrt{\frac{m_1}{m_2}} = \frac{M_1}{M_2}\sqrt{\frac{m_1}{m_2}}r_1 - \frac{M_1}{M_2}\sqrt{\frac{m_1}{m_2}}r_2 \qquad 4.22$$

The values of reactivity ratios can be determined by least square method.

4.2.2.5 Kelene-Tudos (KT) method

A refinement of the linearisation method was introduced by Kelen and Tudos[27-29] by adding an arbitrary positive constant α into the Fineman and Ross equation. This technique spreads the data more evenly over the entire composition range to produce equal weighting to all the data. The Kelen and Tudos refined form of the copolymer equation 4.23 is as follows:

$$\eta = \left[r_1 + r_2/\alpha\right]\ \xi\ -\ r_2/\alpha \qquad 4.23$$

where
$$\eta = G/(\alpha + H) \quad and \quad \xi = H/(\alpha + H) \qquad 4.24$$

By plotting η versus ξ, a straight line is produced that gives $-r_2/\alpha$ and r_1 as the intercepts on extrapolation to $\xi=0$ and $\xi=1$, respectively. Distribution of the experimental data symmetrically on the plot is performed by choosing the α value to be $(H_m \cdot H_M)^{1/2}$ where H_m and H_M are the lowest and highest H values, respectively.

4.2.3 Nonlinear methods

4.2.3.1 Curve – Fitting method

The non-linear or curve-fitting[30] method is based on the copolymer composition equation in the form:

$$\frac{m_1}{m_2} = \frac{r_1 M_1^2 + M_1 M_2}{r_2 M_2^2 + M_1 M_2} \qquad 4.25$$

This equation is based on the assumptions that the monomer concentrations do not change much throughout the reaction and the molecular weight of the resulting polymer is relatively high. In order to determine reactivity ratios from the experimental data, a graph must be generated for the comonomer amount incorporated into the copolymer, m_1, versus the feed comonomer amount, M_1, for the entire range of comonomer concentration. Then, a curve can be drawn through the points for selected r_1 and r_2 values and the validity of the chosen reactivity ratio values can be checked by changing the r_1 and r_2 values until the experimenter can demonstrate that the curve best fits the data points.

4.2.3.2 Nonlinear Tidwell Mortimer method

The Tidwell and Mortimer[31-35] (TM) method employs the nonlinear least squares procedure to estimate the reactivity ratios. Briefly, the method consists of the following: given initial estimates of r_1 and r_2 a set of computations is performed which on repetition rapidly leads to a pair of values of the reactivity ratios that yields the minimum value of the sum of the squares of the differences between the observed and computed polymer composition.

This method has a disadvantage. If the initial estimates are quite different from the actual values of r_1 and r_2, the value of the sum of square of deviations does not reach a minimum. In order to get rid of this, Gauss Newton nonlinear least square procedure was subjected to modifications as suggested by Box. If the initial estimates are very good then the number of iterations required for the value of the sum of square of deviations to converge is less.

4.2.3.3 The Kuo-Chen (KC) method

The Kuo-Chen method[36] is a simple nonlinear extrapolation method derived from Fineman-Ross Method. Equation 4.26 is as follows:

$$\frac{M_1}{m_1} = \frac{r_1 M_1^2 + 2M_1 M_2 + r_2 M_2^2}{r_1 M_1 + M_2} \qquad 4.26$$

where M_1 and M_2 are molar concentrations of the monomers in feed and m_1 and m_2 are copolymer compositions. By plotting the ratio M_1M_2/m_1m_2 against M_1, the extrapolation to $M_1=0$ and $M_1=1.0$, respectively, gives r_1 and r_2.

4.2.3.4 Error in Variable method (EVM)

Error in variable method is an extension of nonlinear TM method which correctly accounts for the error in the variables.[37,38] Using a principle of least squares, the sum of the weighted squares of the residuals is made a minimum.[39,40] To estimate reactivity ratios using the nonlinear least square error in variable method, initial estimation of reactivity ratios are necessary and can be found by KT method.

In the calculation of reactivity ratios, the weights that should be assigned to an experimental point are proportional to the derivatives of the response, with respect to the

parameters evaluated under experimental conditions used to generate experimental points.

4.2.4 Methods to estimate reactivity ratios at higher conversions

Since composition of the copolymer changes with conversion, the copolymer should be isolated at a conversion as low as possible so as to use approximately the initial composition of the feed monomers. Such a limiting conversion is dependent on the initial feed composition and the reactivity ratios of the comonomers. However, even at low conversion a certain composition change is recorded, and what is measured is the average molar copolymer composition, not the instantaneous composition.

Montgomy and Fry[41] showed that the classical methods of determining monomer reactivity ratios from the differential copolymer composition equation are erroneous. The low molecular weight species formed by termination through side reaction and impurities and the handling of small quantities of copolymer magnify the errors. Purification by dissolution and precipitation entails the loss of low molecular weight species. Polymer conversions are also generally high, violating the low conversion requirement. The differential form of copolymer composition equation does not take into consideration about the drift of the monomer feed, due to the unequal reactivities of the monomers, with conversion. The copolymers obtained at high conversion are the true representatives of the reaction dictated by the monomer reactivity ratios, while the initial copolymers are governed to a large extent by the monomer feed.

The integrated copolymer composition equation is represented as:[14]

$$r_2 = \frac{\log\left[\frac{M_2}{m_2}\right] - \frac{1}{P}\log\left[\frac{1-P(M_1/M_2)}{1-P(m_1/m_2)}\right]}{\log\left[\frac{M_1}{m_1}\right] + \frac{1}{P}\log\left[\frac{1-P(M_1/M_2)}{1-P(m_1/m_2)}\right]} \quad 4.27$$

where M_1 and M_2 are the mole fractions of monomer 1 and 2 present initially and m_1 and m_2 mole fractions of the monomer remaining unreacted when the reaction is stopped. P is the integration variable, expressed as the function of the reactivity ratios:

$$P = \frac{(1-r_1)}{(1-r_2)} \quad 4.28$$

4.2.4.1 Extended Kelen-Tudos method (Ex KT)

Kelen and Tudos[42,43] modified their low conversion equation for high conversion data by redefining η and ξ. This is probably the most useful and widely accepted method presently. If copolymerisations are carried to higher conversions the determination of copolymerisation parameters involves labourious calculations because the integrated equation must be applied. The Extended Kelen-Tudos method is used to estimate reactivity ratios with data even at high conversions. The equation may be derived by computing the partial molar monomer conversions, ζ_1 and ζ_2 and the integral z, where:

$$\varsigma_2 = w\left[\frac{\mu + x_0}{\mu + y}\right] \quad and \quad \varsigma_1 = \varsigma_2 y / x_0 \quad 4.29$$

$$z = \frac{\log(1-\varsigma_1)}{\log(1-\varsigma_2)} \quad 4.30$$

where x_0 is M_1/M_2, the initial mole ratio in feed; y is m_1/m_2, the final mole ratio in the copolymer; w is weight fraction conversion; and μ = *Mol. Wt. of* M_2 */ Mol. Wt. of* M_1. The variable H and G and the plotting parameters η and ξ can be computed as:

$$H = y/z^2 \quad and \quad G = (y-1)/z \tag{4.31}$$

$$\eta = G/(\alpha + H) \quad and \quad \xi = H/(\alpha + H) \tag{4.32}$$

The final equation for Extended Kelen Tudos method is represented as:

$$\eta = [r_1 + r_2/\alpha]\ \xi - r_2/\alpha \tag{4.33}$$

where $\alpha = (H_{min} \times H_{max})^{1/2}$. By plotting η versus ξ, a straight line is produced that gives $-r_2/\alpha$ and r_1 as the intercepts on extrapolation to $\xi=0$ and $\xi=1$, respectively.

4.2.4.2 Mao-Huglin (MH) method

Mao and Huglin[44] in 1993 proposed an iterative linear method based on KT method. By considering the corresponding equations, computer simulation can be used to a series of data at low and high conversions.[45] A small number of copolymerisation systems can be placed in simplified conditions to study high conversions. This method gives a solution for simultaneous estimation of both reactivity ratios for feed composition range large enough to generate results applicable over entire range of comonomer compositions.

In this method corresponding instantaneous monomer feed composition f^c may be calculated back from the calculated value, F^c of the copolymer composition.

$$f^c = \frac{(F^c - 1) + \sqrt{(1 + F^c)^2 + 4r_1 r_2 F^c}}{2r_1} \tag{4.34}$$

F^c can be calculated from the assumed reactivity ratios by the integrated copolymerisation equation. The convergence criterion of iteration is that the recalculated reactivity ratios should become equal to the assumed ones.

In the absence of experimental data on copolymerisation at higher conversion values, all that remains is to compare actual results with those of the MH method. Other investigators have previously employed many of the aforementioned linearisation methods, but the approach which is taken here, to estimate more reliable and statistically sound monomer reactivity ratios, is different.

In the present work reactivity ratios of all monomer combinations at any conversion as well as 95% joint confidence intervals were calculated using the terminal model computer program FORTRAN 77, kindly offered by Dr. R. Mao.[44]

4.2.4.3 The Intersection method

Reactivity ratios at significantly higher conversion level were initially estimated by Mayo and Lewis.[14] They did this through an intersection method and the integral equation 4.27. Monomer reactivity ratios can be estimated by determining the straight lines in an r_1-r_2 diagram for each experiment.

Binary polymerisations have become increasingly important technologically and a good knowledge of polymerisation parameters, including reactivity ratios, is very essential. Our research also looked at potential enhancements in reactivity ratio estimation for binary systems. Another related issue in multicomponent polymerisations is the existence of an azeotropic point. The feed composition of such a point would result in copolymer products with a homogeneous composition. Predicting the existence and also calculating the composition of the azeotropic point can reduce the effort of running costly experiments, in that computational results can be used to narrow the experimental search space.

4.2.5 Statistical distribution of dyad monomer sequences

Igarashi[46] has developed the relation of copolymer composition with the distribution of bonds between the same and different monomer units in a binary copolymer molecule. The statistical distribution of two monomers M_1-M_1, M_2-M_2 and M_1-M_2 can be calculated by employing following equations:

$$X = \phi_1 - \frac{2\phi_1(1-\phi_1)}{1+\left[(2\phi_1-1)^2 + 4r_1r_2\phi(1-\phi_1)\right]^{1/2}} \quad 4.35$$

$$Y = (1-\phi_1) - \frac{2\phi_1(1-\phi_1)}{1+\left[(2\phi_1-1)^2 + 4r_1r_2\phi(1-\phi_1)\right]^{1/2}} \quad 4.36$$

$$Z = \frac{4\phi_1(1-\phi_1)}{1+\left[(2\phi_1-1)^2 + 4r_1r_2\phi(1-\phi_1)\right]^{1/2}} \quad 4.37$$

where X, Y, and Z are the mole fractions of the M_1-M_1, M_2-M_2 and M_1-M_2 dyads in the copolymer, respectively, and ϕ_1 is the mole fraction of monomer 1 in copolymer.

Mean sequence lengths μ_1 and μ_2 were also calculated using the following equations:[47]

$$\mu_1 = 1 + r_1\frac{[M_1]}{[M_2]} \quad 4.38$$

$$\mu_2 = 1 + r_2\frac{[M_2]}{[M_1]} \quad 4.39$$

4.3 Copolymerisation Studies

To study the copolymerisation of a monomer combination, a set of nine experiments was conducted. Different feed ratios were employed each time (monomer molar ratios: 90/10 to 10/90), and the copolymerisation reactions were quenched at rather low or moderate yields. The conversions were controlled and determined by gravimetric measurements. Weight fraction conversions were calculated with respect to total weight of feed monomers. The copolymerisation procedure was monitored by ^{1}H NMR spectroscopy. The experimental results were processed on the basis of the Fineman-Ross (FR), Kelen-Tudos (KT), Extended Kelen-Tudos (Ex KT) and Mao-Huglin (MH) equations.

4.3.1 Materials

Ethyl methyl ketone, chloroform, methanol, and dichloromethane (Merck) were freshly distilled over molecular sieves before use. All monomers were purified by column chromatography before use. 2,2'-Azobisisobutyronitrile (AIBN) was recrystallised from methanol.

4.3.2 Characterisation techniques

4.3.2.1 Nuclear magnetic resonance (NMR) spectroscopy

Nuclear magnetic resonance (NMR) spectra were recorded on a Bruker AC400 instrument, using deuterated chloroform as solvent and tetramethylsilane (TMS) as the references for ^{1}H nuclei. Chemical shifts are given in part per million δ (ppm). The experimental conditions for recording ^{1}H NMR spectra were as follows: flip angle 90°, acquisition time 4.5 s , pulse delay 2 s, number of scans 128.

4.3.2.2 Differential scanning calorimetry (DSC)

Differential scanning calorimetry (DSC) measurements were conducted using a TA 2920 analyser from TA Instruments DA 73085, a RCS DA cooler. All samples were run against an aluminium reference in crimped aluminium pans. A temperature range of -50 to 120 °C was used to determine glass transition temperature (T_g) of copolymers. Scans were recorded at a heating rate of 10 °C /min. A second scan was required for the assessment of glass transition temperature (T_g), defined as the inflection point in the heat capacity jump.

4.3.2.3 Solubility

The solubility of homopolymer and copolymers were tested by mixing 20 mg with 2 mL of various solvents in test tubes. After setting aside the closed tubes for a day solubility was estimated.

4.3.2.4 Refractometry (R.I.)

Refractive index measurements were performed with an Automatic Refractometer, model PTR 46 X, from Index Instrument and calibrated with a standard. 30 wt% polymer solutions made in methylene chloride and films were casted on prism. Solvent was allowed to evaporate. Each sample was allowed to equilibrate to 20 °C prior to the measurements. The measurements were done in triplicate and the average results recorded.

4.3.2.5 Gel permeable chromatography (GPC)

Size Exclusive Chromatography (SEC) analysis were carried out to know molecular weight and molecular weight distribution at 40 °C using LDC Analytical GPC system consisting of a Thermoseparation P4000 solvent delivery system, auto injector, A

1000, refractomonitor IV (refractive index detector range 0.020), using Phenomenex-Phenogel GPC column (300 x 7.8 mm). THF was the carrier solvent at a flow rate of 1 mL/min. The system was calibrated with polystyrene standards having molecular weights in the range 970–600,000.

4.3.2.6 UV-Vis spectroscopy

Ultraviolet–visible (UV–vis) spectra were recorded on a Perkin Elmer Lambda-950 Spectrometer in the wavelengths range of 200–800 nm. As these polymers needed to be transparent over long distances (cm) for the optical experiments, solutions were used (10% over 1 cm may be equated to 1 mm of polymer) rather than films (< 10 μm thick).

4.3.2.7 Thermogravimetric analysis (TGA)

The thermal stability of the copolymers was studied by thermogravimetric analysis (TGA) employing a STA 6000 TGA model from Perkin Elmer instruments. The samples were heated at a rate of 10 °C /min under nitrogen atmosphere in the temperature range of 30 to 900 °C.

4.4 Copolymerisation of 2-phenylethyl acrylate (PEA) and 2-phenoxy-2-phenylethyl acrylate (PPEA)

4.4.1 Synthesis of poly(PEA-*co*-PPEA)

Copolymers of PEA with PPEA having different composition were synthesised in ethyl methyl ketone (EMK) solution using 2,2'-azobisisobutyronitrile (AIBN) as free radical initiator. The feed compositions of the monomers are presented in Table 4.1. Appropriate quantities of the monomer, comonomer, EMK and AIBN (1 mol % of monomer) were taken in a polymerisation tubes and flushed with oxygen free nitrogen gas for 10 min. The tubes were tightly sealed and immersed in a thermostatic water bath at 70 °C. The reaction time was selected so as to yield moderate copolymer conversions in order to be within the realm of applicability of differential copolymerisation equation. The conversions were controlled and determined by gravimetric measurements. After the reaction times, the copolymers were precipitated in methanol, filtered off, and purified by reprecipitations from chloroform solution into methanol and finally dried under reduced pressure for 24 h. Synthesis of the statistical copolymers poly(PEA-*co*-PPEA) is depicted in Scheme 4.1.

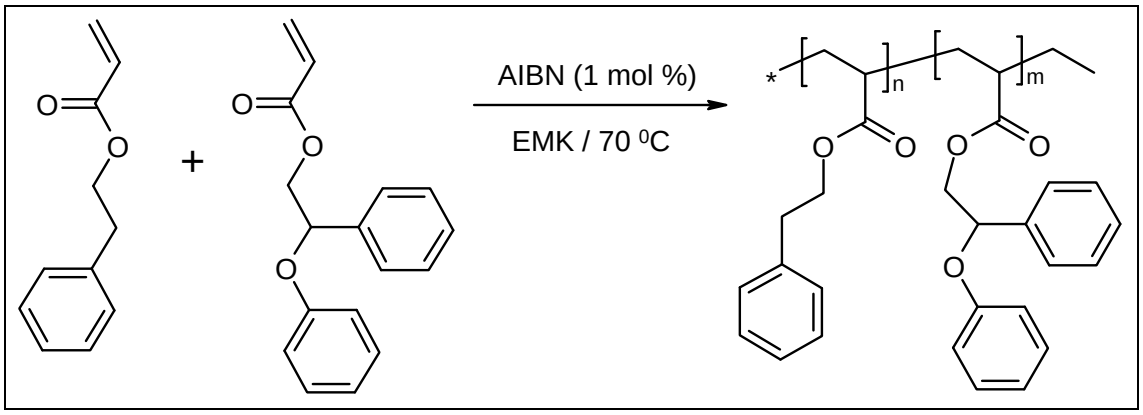

Scheme 4.1: Synthesis of poly(PEA-*co*-PPEA)

The entire range of data provided for a systematic study, with 10% intervals, of the copolymerisation of 2-phenylethyl acrylate and 2-phenoxy-2-phenylethyl acrylate over a range of 90/10 to 20/80 of PEA/PPEA monomer mole percent feed ratios.

The copolymers were soluble in solvents like tetrahydrofuran, acetone, dimethyl formamide, dimethyl sulphoxide, chloroform, methylene dichloride, toluene but were insoluble in hydrocarbons like n-hexane, petroleum ether and hydroxyl group containing solvents such as methanol, ethanol and 2-propanol.

Table 4.1: Composition data for copolymerisation of PEA with PPEA

Polymer Code	Mole fraction				Wight fraction conversion
	in feed		in polymer		
	M_1	M_2	m_1	m_2	
P(PEA)	1	0	1	0	-
PEA-PPEA-1	0.9011	0.0989	0.8888	0.1112	0.5038
PEA-PPEA-2	0.8013	0.1987	0.7965	0.2035	0.4654
PEA-PPEA-3	0.7016	0.2984	0.7001	0.2999	0.3925
PEA-PPEA-4	0.6084	0.3916	0.6071	0.3929	0.4822
PEA-PPEA-5	0.5185	0.4815	0.5098	0.4902	0.5500
PEA-PPEA-6	0.4116	0.5884	0.3939	0.6061	0.5327
PEA-PPEA-7	0.3118	0.6882	0.3528	0.6472	0.4532
PEA-PPEA-8	0.2230	0.7770	0.2832	0.7168	0.4563
P(PPEA)	0	1	0	1	-

In order to determine the amount of each comonomer that was incorporated into the copolymer, proton nuclear magnetic resonance (^{1}H NMR) was performed on each copolymer using deuterated chloroform as solvent. Figure 4.1 shows the ^{1}H NMR spectra of all PEA/PPEA copolymers and the assigned peaks that were used in the calculations to determine the amount of each comonomer.

The assignment of the resonance peaks of each kind of monomeric unit in the copolymer chains leads to the accurate evaluation of the composition of copolymer. The Methylene group (-CH_2-**CH_2**-Ph) of the PEA was used to determine the copolymer composition. The integrated intensity of this peak was compared to the peak area of methylene ester group (>CH-**CH_2**-O-) of PPEA in the copolymer spectrum.

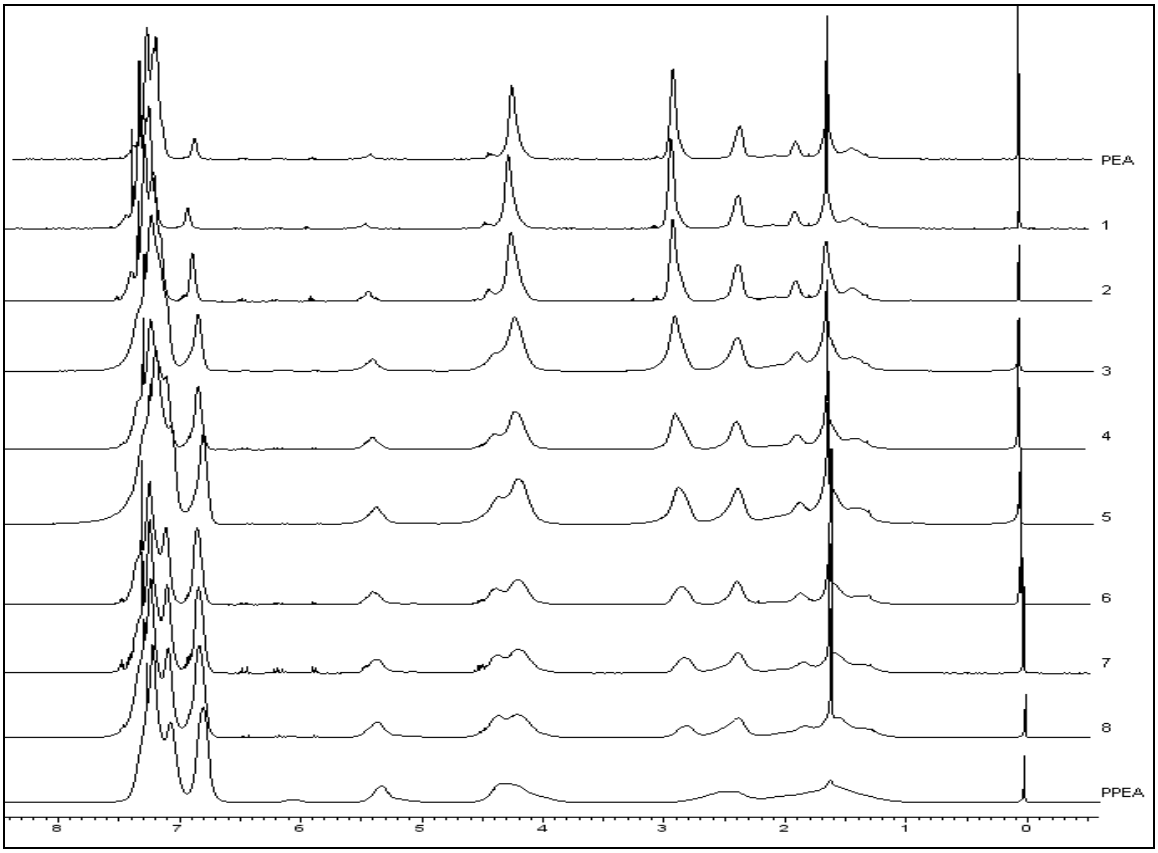

Figure 4.1: ^{1}H NMR spectra of poly(PEA), poly(PPEA) and poly(PEA-*co*-PPEA)

The following expression is used to calculate the composition of copolymers. Let F_1 be the mole fraction of PEA.

$$F_1 = \frac{\int 2.8(-CH_2-\underline{CH}2-Ph)/2}{\int 2.8(-CH_2-\underline{CH}2-Ph)/2 \; + \; \int 4.3(\;\rangle CH-\underline{CH}2-O-)/2} \qquad 4.40$$

From equation 4.40, the mole fraction of PEA was determined by measuring the intensities of corresponding aliphatic proton signals. The compositions of the poly(PEA-*co*-PPEA) copolymers assessed from ^{1}H NMR and gravimetrically determined weight fraction conversions are presented in Table 4.1.

4.4.2 Reactivity ratio determination for poly(PEA-*co*-PPEA) system

From the monomer feed ratios and the copolymer composition, the reactivity ratios of PEA and PPEA were determined by Finemann-Ross (FR), Kelen-Tudos (KT), extended Kelen-Tudos (Ex KT) and Mao-Huglin (MH) methods. The significance of the parameters of FR and KT for the copolymers is presented in Table 4.3 and that of extended KT is shown in Table 4.4. The reactivity ratios of PEA and PPEA are denoted as r_{PEA} (or r_1) and r_{PPEA} (or r_2) respectively and the values obtained from various methods are presented in Table 4.2.

Table 4.2: Reactivity ratios of PEA and PPEA computed by different models

Method	r_{PEA}	r_{PPEA}
Finemann-Ross	0.847	0.753
Kelen-Tudos	0.838	0.745
Extended Kelen-Tudos	0.773	0.651
Mao-Huglin	0.787	0.668
Average	0.811	0.704

The r_1 and r_2 values obtained from four methods are in good agreement with each other. Since the r_1 and r_2 values are less than one, this system gives rise to azeotropic polymerisation at a particular composition of the monomers which is calculated using the following equation:

$$N_1 = \frac{(1 - r_{PEA})}{(2 - r_{PEA} - r_{PPEA})} \qquad 4.41$$

The azeotropic polymerisation forms at a particular composition 0.389, when the mole fraction of the monomer PEA in the feed is 0.389, the copolymer formed will have the same composition as that of the feed. When the mole fraction of the feed is less than 0.389 with respect to PEA, the copolymer formed will be relatively richer in this monomer unit than the feed. When the mole fraction of the monomer PEA in the feed is above 0.389, the copolymer will be relatively richer in PPEA unit than that in the feed. However, the product of r_{PEA} and r_{PPEA} is less than 1, which indicates that the system leads to the formation of random copolymers.

Table 4.3: FR and KT parameters for the copolymerisation of PEA with PPEA

Polymer Code	$F=M_1/M_2$	$f=m_1/m_2$	$H=F^2/f$	$G=F(f-1)/f$	$\xi=H/(\alpha+H)$	$\eta=G/(\alpha+H)$
PEA-PPEA-1	9.1112	7.9928	10.3861	7.9713	0.7764	2.7281
PEA-PPEA-2	4.0327	3.9140	4.1550	3.0024	0.8516	0.6154
PEA-PPEA-3	2.3512	2.3344	2.3681	1.3440	0.7658	0.4347
PEA-PPEA-4	1.5536	1.5452	1.5621	0.5482	0.6833	0.2398
PEA-PPEA-5	1.0768	1.0400	1.1150	0.0414	0.6063	0.0225
PEA-PPEA-6	0.6995	0.6499	0.7529	-0.3768	0.5098	-0.2551
PEA-PPEA-7	0.4531	0.5451	0.3766	-0.3781	0.3421	-0.3435
PEA-PPEA-8	0.2870	0.3951	0.2085	-0.4394	0.2236	-0.4712

Table 4.4: Extended Kelen-Tudos parameters for PEA-PPEA copolymer system

Polymer Code	ζ_1	ζ_2	Z	H	G	ξ	η
PEA-PPEA-1	0.4939	0.5630	0.8226	11.8108	8.5004	0.8971	0.6457
PEA-PPEA-2	0.4616	0.4756	0.9592	4.2542	3.0380	0.7585	0.5417
PEA-PPEA-3	0.3914	0.3942	0.9908	2.3782	1.3469	0.6372	0.3609
PEA-PPEA-4	0.4809	0.4835	0.9923	1.5692	0.5494	0.5368	0.1879
PEA-PPEA-5	0.5388	0.5579	0.9482	1.1567	0.0422	0.4607	0.0168
PEA-PPEA-6	0.5062	0.5449	0.8964	0.8087	-0.3906	0.3739	-0.1806
PEA-PPEA-7	0.5210	0.4330	1.2972	0.3240	-0.3507	0.1930	-0.2090
PEA-PPEA-8	0.5927	0.4306	1.5952	0.1553	-0.3792	0.1029	-0.2512

The graphical plots concerning the methods FR, KT and Ex-KT are given in Figure 4.2 (a-c). The plots were linear in all cases and for all graphical methods, thus indicating that these copolymerisations follow conventional copolymerisation kinetics and that the reactivity of a polymer radical is determined only by the terminal monomer unit. As for some copolymers moderate yields were obtained, the extended KT and Mao-Huglin methods were employed as well. It is obvious that all methods provide similar data concerning the reactivity ratios for both monomers.

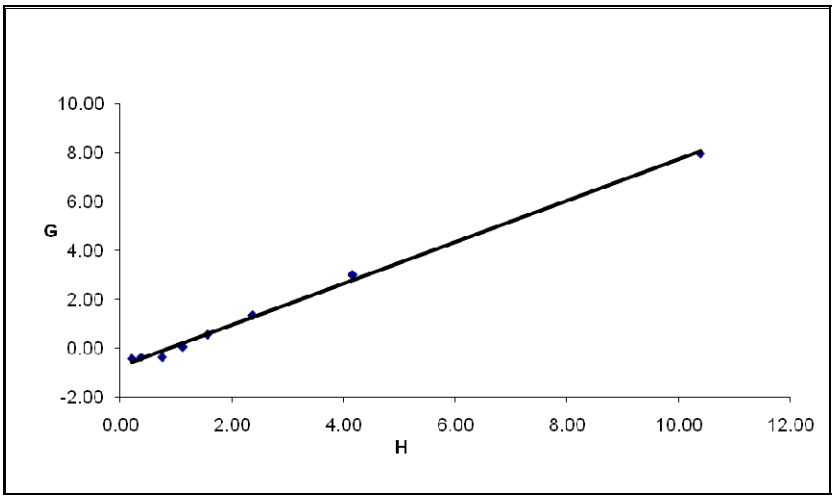

(a)

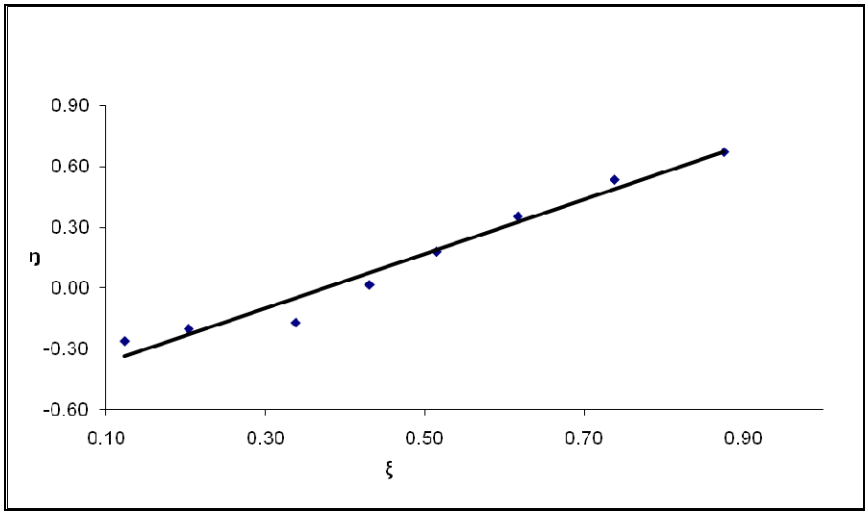

(b)

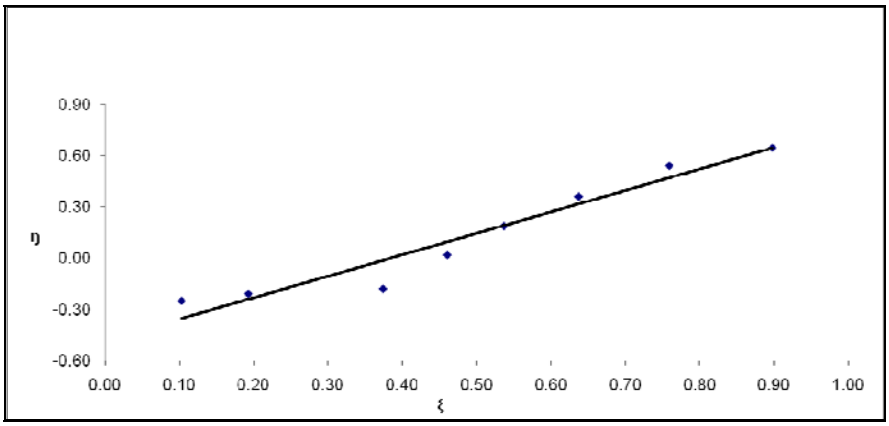

(c)

Figure 4.2: (a) FR, (b) KT and (c) Extended KT plots for the PEA and PPEA copolymer system

The 95 % joint confidence limit of the reactivity ratio values was calculated for Mao-Huglin method and has been plotted in Figure 4.3. Its equation is,

$2.3560\ (r_1 - 0.7872)^2 - 2.0455\ (r_1 - 0.7872)\ (r_2 - 0.6676) + 1.2802\ (r_2 - 0.6676)^2 = 0.0411$

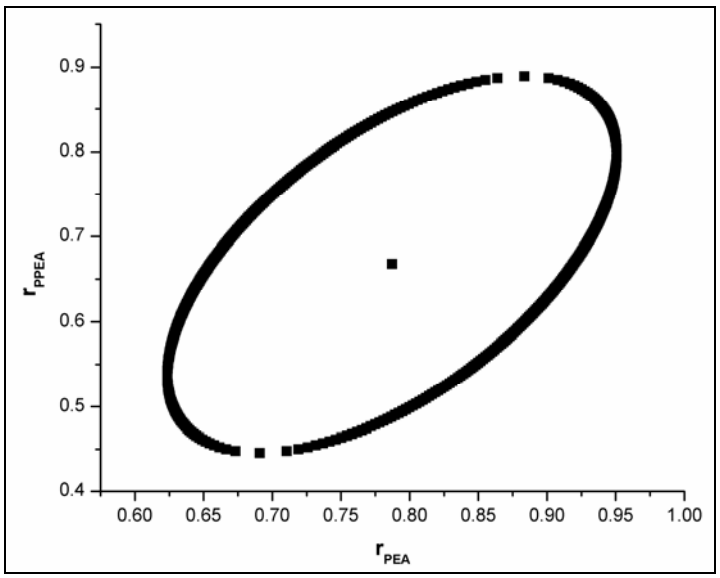

Figure 4.3: 95% Joint confidence interval of r_{PEA} and r_{PPEA} values by Mao-Huglin method for PEA-PPEA copolymer system

The statistical distribution of dyad monomer sequences M_{PEA}-M_{PEA}, M_{PPEA}-M_{PPEA} and M_{PEA}-M_{PPEA} were calculated using the method proposed by Igarashi. Mean sequence

lengths μ_{PEA} and μ_{PPEA} were also calculated. The data summarise in Table 4.5, and the variation of the dyad fractions with the PEA mole fraction in the copolymers is displayed in Figure 4.4.

Table 4.5: Structural data for poly(PEA-*co*-PPEA) system

Polymer Code	M_1-M_1	M_2-M_2	M_1-M_2	μ_{M1}	μ_{M2}
PEA-PPEA-1	0.7862	0.0086	0.2052	8.3892	1.0773
PEA-PPEA-2	0.6262	0.0332	0.3406	4.2705	1.1746
PEA-PPEA-3	0.4813	0.0811	0.4376	2.9068	1.2994
PEA-PPEA-4	0.3651	0.1509	0.4840	2.2600	1.4531
PEA-PPEA-5	0.2670	0.2474	0.4857	1.8733	1.6538
PEA-PPEA-6	0.1764	0.3886	0.4350	1.5673	2.0064
PEA-PPEA-7	0.1499	0.4443	0.4058	1.3674	2.5539
PEA-PPEA-8	0.1105	0.5441	0.3454	1.2328	3.4530

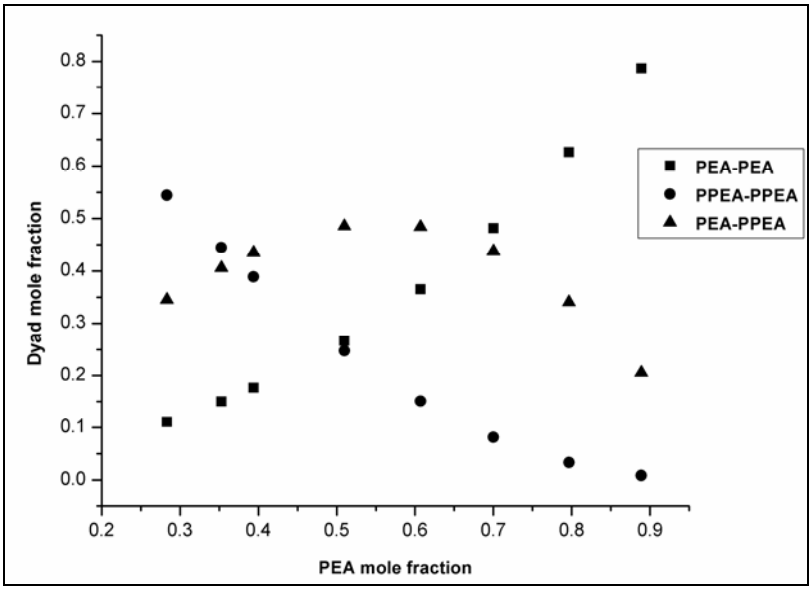

Figure 4.4: Dyad monomer sequence fractions versus the PEA mole fraction for poly(PEA-*co*-PPEA)

4.4.3 Characterisation

Refractive index of thin copolymer films was determined in triplicate using refractometer. All of the polymer films were solvent cast from methylene chloride (30 wt

% polymer to solvent) and dried slowly. The results are listed in Table 4.6. The PPEA homopolymer has a refractive index of 1.574, which is higher than the refractive index of 1.553 for PEA. The refractive index of copolymer increases with increase in PPEA content in the copolymer.

Table 4.6: Refractive index, glass transition temperature and molecular weight data for poly(PEA), poly(PPEA) and poly(PEA-*co*-PPEA)

Polymer Code	R. I.	T_g (°C)	Molecular weight		P.D.I.
			M_n x 10^4	M_w x 10^4	
P(PEA)	1.553	-3.00	3.44	7.22	2.10
PEA-PPEA-1	1.556	2.79	2.779	5.53	1.99
PEA-PPEA-2	1.558	11.79	2.802	5.24	1.87
PEA-PPEA-3	1.560	18.36	3.211	5.78	1.80
PEA-PPEA-4	1.561	21.40	2.867	5.56	1.94
PEA-PPEA-5	1.564	27.56	2.629	4.92	1.87
PEA-PPEA-6	1.564	32.11	2.882	5.25	1.82
PEA-PPEA-7	1.566	38.32	2.858	5.43	1.90
PEA-PPEA-8	1.565	43.53	3.076	5.91	1.92
P(PPEA)	1.574	56.00	6.40	12.61	1.97

The T_g of the homopolymers and copolymers were determined using DSC. Table 4.6 and Figure 4.5 summarise the T_g values of the copolymers. All the copolymers showed a single T_g indicating a homogeneous structure. The T_g of p(PEA) homopolymer is -3.0 °C and that of p(PPEA) is 56.0 °C. The T_g values of the copolymers were decreased proportionally with increase in the mole fraction of PEA in the copolymer. For intraocular lens low T_g's are required to improve material performance, particularly during the surgical procedures, where some sample folding is required. Copolymers

PEA-PPEA-1 to 5 showed relatively low glass transition temperatures (2.7 to 27°C), which are desirable in the IOL composite material.

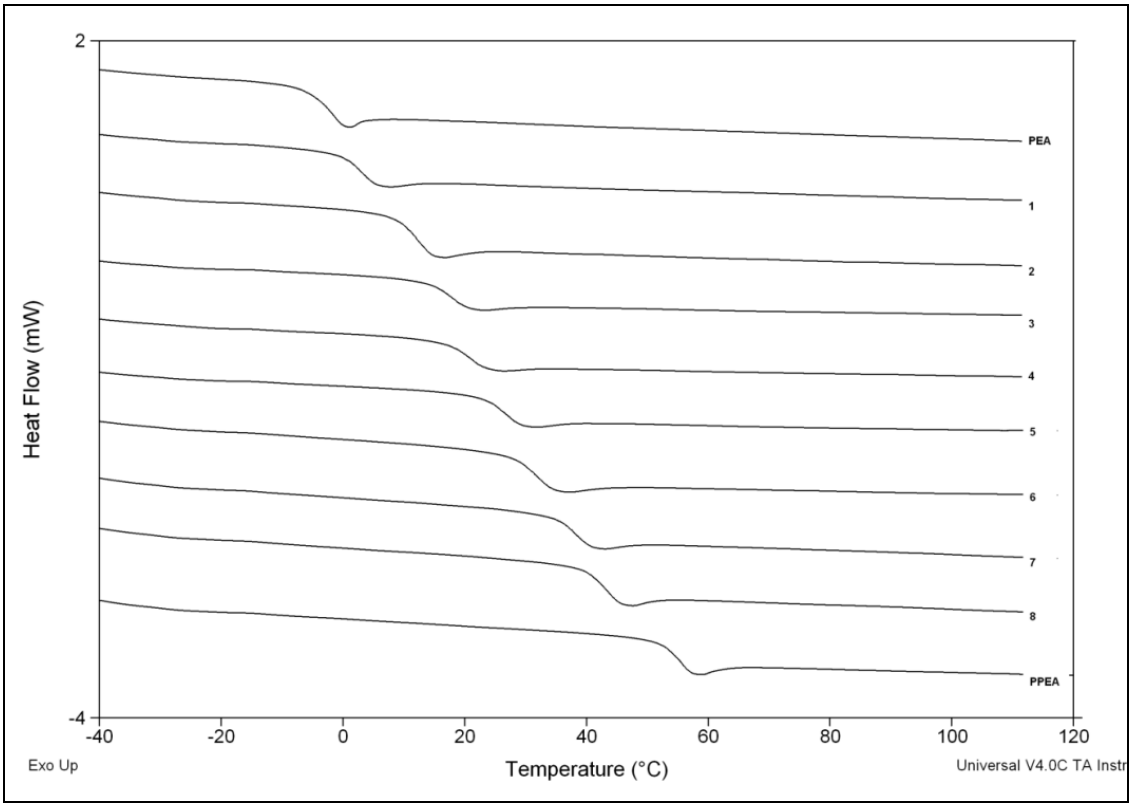

Figure 4.5: DSC thermograms of poly(PEA), poly(PPEA) and poly(PEA-*co*-PPEA)

The weight-average (M_w) and number-average (M_n) molecular weights and the polydispersity indices (PDI) of copolymers are presented in Table 4.6. The polydispersity index of copolymers ranges between 1.80 and 1.99. The theoretical values of PDI for polymers produced via radical recombination and disproportionation are 1.5 and 2.0, respectively.[48,49] This suggests that polymers were produced mainly via termination of growing chain by disproportionation.

Figure 4.6 shows the UV-Visible absorption spectra of the polymer solutions in chloroform. All polymers exhibited good transparency in visible region (wavelengths: 400-800 nm). Nearly identical spectra could be seen for copolymers.

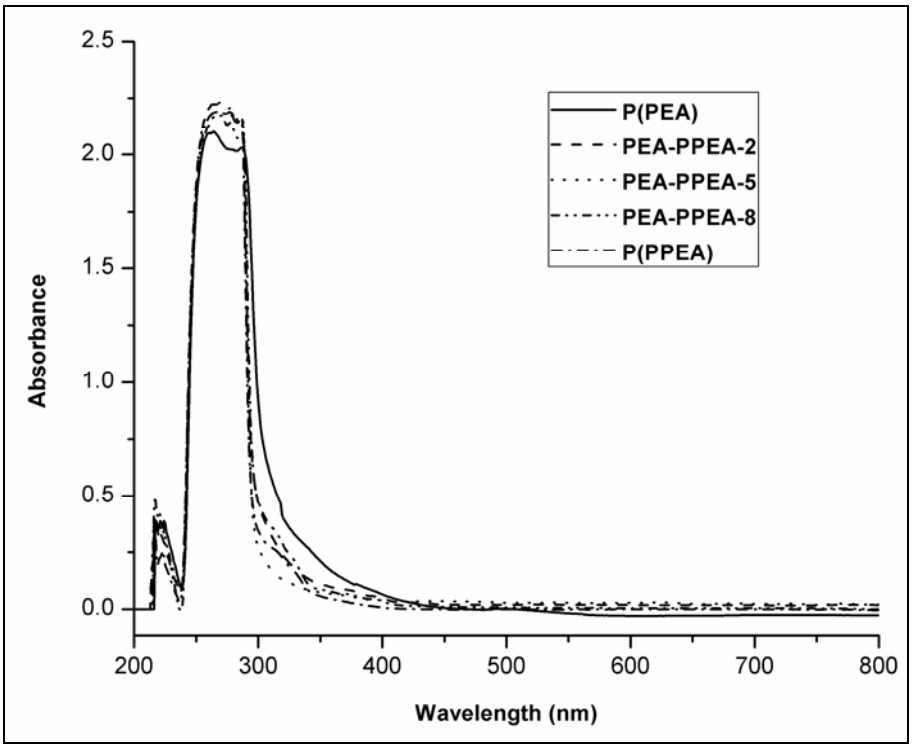

Figure 4.6: UV-visible spectra of poly(PEA), poly(PPEA) and poly(PEA-*co*-PPEA)

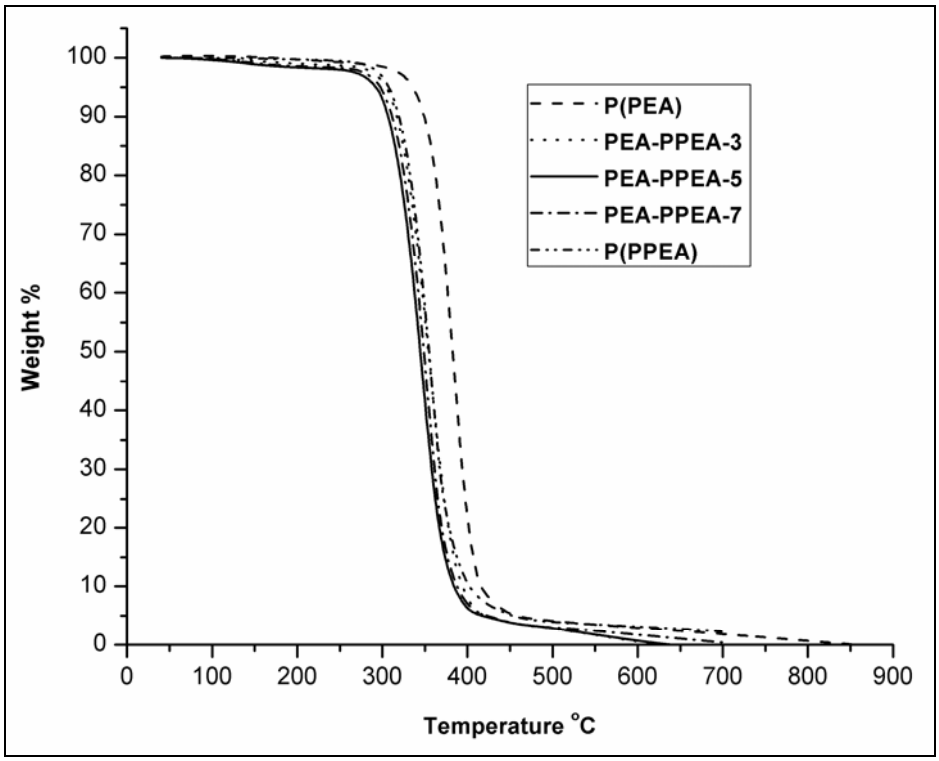

Figure 4.7: TGA thermograms of poly(PEA), poly(PPEA) and poly(PEA-*co*-PPEA)

The thermal degradation of copolymers was characterised using TGA. TGA curves (Figure 4.7) clearly indicates that all polymers undergo single step degradation. In all polymers the weight loss was found to occur in a single step, starting at ~300 °C and ending at ~600 °C.

4.5 Copolymerisation of 2-phenylethyl acrylate (PEA) and 2-phenoxy-2-phenylethyl methacrylate (PPEM)

4.5.1 Synthesis of poly(PEA-*co*-PPEM)

Predetermined quantities of 2-phenylethyl acrylate, 2-phenoxy-2-phenylethyl methacrylate, ethyl methyl ketone (EMK) and 2,2'-azobisisobutyronitrile (AIBN) (1 mol % of total monomers) were placed in Pyrex tubes. The mixtures were deoxygenated by flushing with oxygen free nitrogen for at least 10 min. The tubes were tightly sealed and immersed in a thermostated water bath at 70 °C. The reaction time was selected so as to yield moderate copolymer conversions in order to be within the realm of applicability of the differential copolymerisation equation. The conversions were controlled and determined by gravimetric measurements. After the reaction times, the copolymers were precipitated in methanol, filtered off, and purified by reprecipitations from chloroform solution into methanol and finally dried under reduced pressure for 24 h. Synthesis of the statistical copolymers, poly(PEA-*co*-PPEM) is depicted in Scheme 4.2.

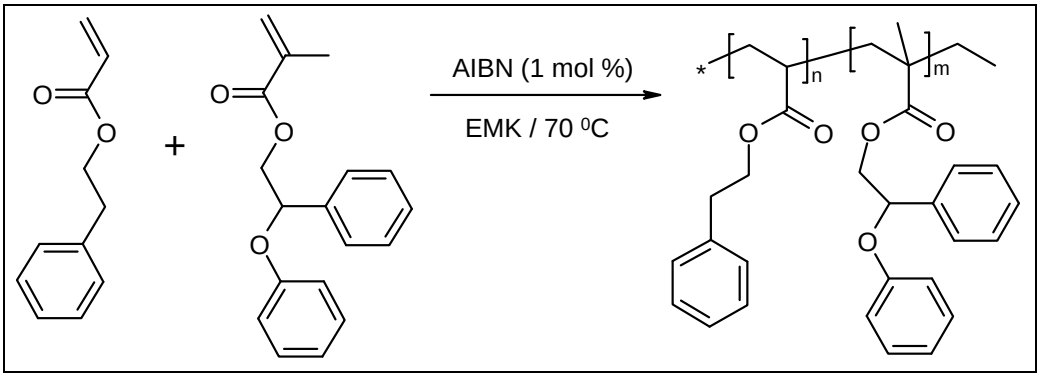

Scheme 4.2: Synthesis of poly(PEA-*co*-PPEM)

Table 4.7 indicates the amounts of each monomer in mol % that were used to produce a methodical study of the copolymer composition. The entire range of data provided for a systematic study, with 10% intervals, of the copolymerisation of 2-

phenylethyl acrylate and 2-phenoxy-2-phenylethyl methacrylate over a range of 90/10 to 10/90 of PEA/PPEM monomer mole percent feed ratios.

The copolymers were soluble in solvents like tetrahydrofuran, acetone, dimethyl formamide, dimethyl sulphoxide, chloroform, methylene dichloride, toluene but were insoluble in hydrocarbons like n-hexane, petroleum ether and hydroxyl group containing solvents such as methanol, ethanol and 2-propanol.

Table 4.7: Composition data for copolymerisation of PEA with PPEM

Polymer Code	Mole fraction				Wight fraction conversion
	in feed		in polymer		
	M_1	M_2	m_1	m_2	
P(PEA)	1	0	1	0	-
PEA-PPEM-1	0.8991	0.1009	0.7241	0.2759	0.2286
PEA-PPEM-2	0.8029	0.1971	0.6442	0.3558	0.4292
PEA-PPEM-3	0.6975	0.3025	0.5191	0.4809	0.4684
PEA-PPEM-4	0.5933	0.4067	0.4124	0.5876	0.4962
PEA-PPEM-5	0.5006	0.4994	0.2999	0.7001	0.4147
PEA-PPEM-6	0.4080	0.5920	0.2369	0.7631	0.4189
PEA-PPEM-7	0.2985	0.7015	0.1886	0.8114	0.5077
PEA-PPEM-8	0.1943	0.8057	0.1071	0.8929	0.4437
PEA-PPEM-9	0.1086	0.8914	0.0687	0.9313	0.3654
P(PPEM)	0	1	0	1	-

In order to determine the amount of each comonomer that was incorporated into the copolymer, proton nuclear magnetic resonance (^{1}H NMR) was performed on each copolymer. All of the ^{1}H NMR samples were dissolved in deuterated chloroform and placed into a warm water ultrasonic bath. An ultrasonic bath was used to quickly dissolve the copolymers that afforded the required copolymer solutions. ^{1}H NMR experiments produced well-resolved peaks. Figure 4.8 shows the ^{1}H NMR spectra of all PEA/PPEM

copolymers and the assigned peaks that were used in the calculations to determine the amount of each comonomer.

The assignment of the resonance peaks of each kind of monomeric unit in the copolymer chains leads to the accurate evaluation of the composition of copolymer. All ^{1}H NMR spectra show some signals specific to both comonomers. Methylene group (-CH_2-**CH_2**-Ph) of the PEA led to a signal centered at 2.8 ppm. While the methylene ester group (>CH-**CH_2**-O-) of PPEM showed a signal at 4.2 ppm. The integrated intensities of these peaks were used to calculate composition of copolymers.

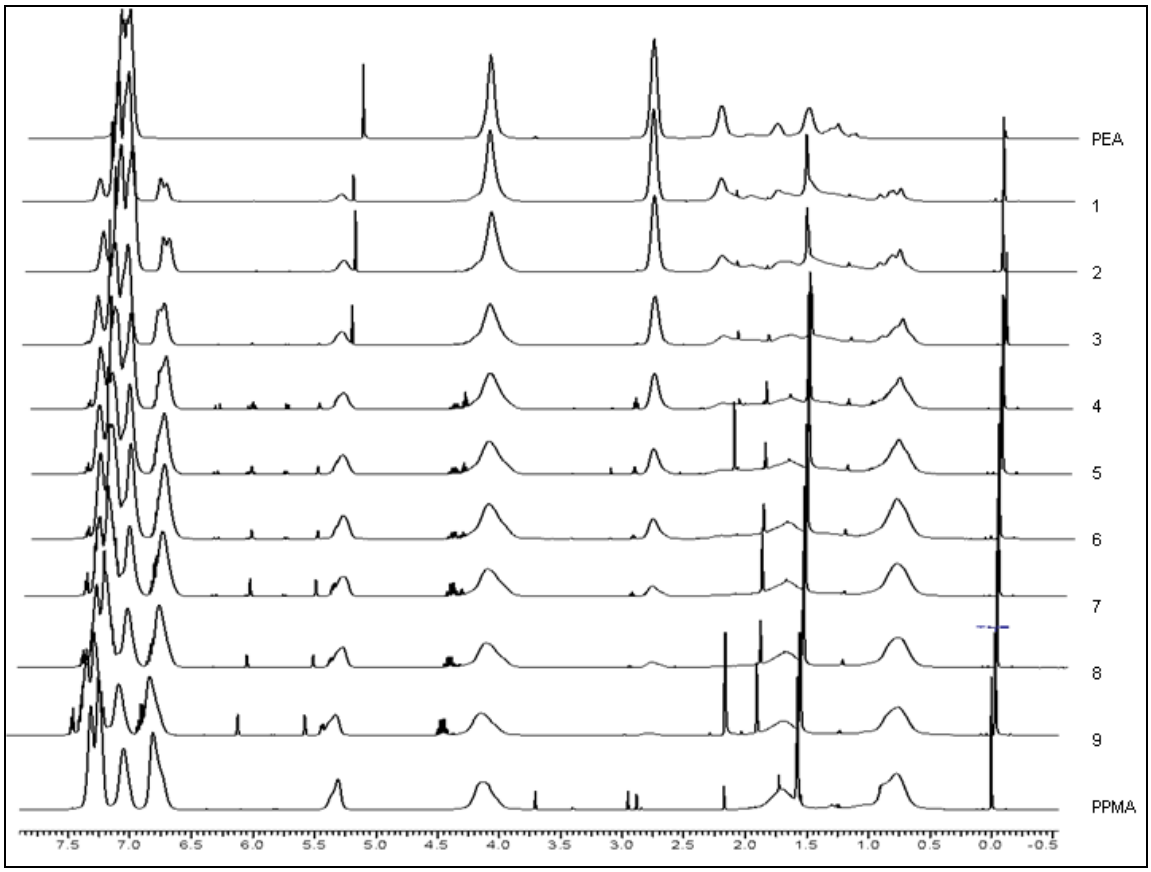

Figure 4.8: ^{1}H NMR spectra of poly(PEA), poly(PPEM) and poly(PEA-*co*-PPEM)

The following expression is used to calculate the composition of copolymers. Let F_1 be the mole fraction of PEA.

$$F_1 = \frac{\int 2.8(-CH_2 - \underline{CH}_2 - Ph)/2}{\int 2.8(-CH_2 - \underline{CH}_2 - Ph)/2 \; + \; \int 4.2(\rangle CH - \underline{CH}_2 - O-)/2} \qquad 4.42$$

From equation 4.42 the mole fraction of PEA was determined by measuring the intensities of corresponding aliphatic proton signals. The compositions of the poly(PEA-*co*-PPEM) copolymers assessed from ^{1}H NMR and gravimetrically determined weight fraction conversions are presented in Table 4.7.

4.5.2 Reactivity ratio determination for poly(PEA-*co*-PPEM) system

From the monomer feed ratios and the copolymer compositions, the reactivity ratios of PEA and PPEM were determined by Finemann-Ross (FR), Kelen-Tudos (KT), extended Kelen-Tudos (Ex KT) and Mao-Huglin (MH) methods. The significance of the parameters of FR and KT for the copolymers is presented in Table 4.9 and that of extended KT is shown in Table 4.10. The reactivity ratios of PEA and PPEM are denoted as r_{PEA} (or r_1) and r_{PPEM} (or r_2) respectively and the values obtained from various methods are presented in Table 4.8.

Table 4.8: Reactivity ratios of PEA and PPEM computed by different models

Method	r_{PEA}	r_{PPEM}
Finemann-Ross	0.246	1.543
Kelen-Tudos	0.305	1.743
Extended Kelen-Tudos	0.192	2.064
Mao-Huglin	0.192	2.017
Average	0.234	1.842

The value of r_{PEA} is less than 1 and that of r_{PPEM} is greater than 1, which indicates presence of higher incorporation of PPEM units in the copolymer than feed. The product

r_{PEA} x r_{PPEM} is less than 1, suggesting that there is a tendency for the formation of a random copolymer system; the copolymer will be relatively richer in PPEM monomeric unit.

Table 4.9: FR and KT parameters for the copolymerisation of PEA with PPEM

Polymer Code	$F=M_1/M_2$	$f=m_1/m_2$	$H=F^2/f$	$G=F(f-1)/f$	$\xi=H/(\alpha+H)$	$\eta=G/(\alpha+H)$
PEA-PPEM-1	8.9090	2.6249	30.2377	5.5150	0.9246	0.1686
PEA-PPEM-2	4.0735	1.8104	9.1653	1.8235	0.7880	0.1568
PEA-PPEM-3	2.3053	1.0794	4.9236	0.1695	0.6663	0.0229
PEA-PPEM-4	1.4588	0.7018	3.0321	-0.6198	0.5515	-0.1127
PEA-PPEM-5	1.0024	0.4284	2.3456	-1.3375	0.4875	-0.2780
PEA-PPEM-6	0.6893	0.3104	1.5303	-1.5309	0.3829	-0.3831
PEA-PPEM-7	0.4255	0.2324	0.7791	-1.4053	0.2401	-0.4331
PEA-PPEM-8	0.2412	0.1199	0.4849	-1.7695	0.1643	-0.5997
PEA-PPEM-9	0.1218	0.0738	0.2011	-1.7695	0.0754	-0.5731

Table 4.10: Extended Kelen-Tudos parameters for PEA-PPEM copolymer system

Polymer Code	ζ_1	ζ_2	Z	H	G	ξ	η
PEA-PPEM-1	0.5685	0.1675	0.2181	55.1764	7.4498	0.9375	0.1266
PEA-PPEM-2	0.7139	0.3173	0.3050	19.4599	2.6570	0.8409	0.1148
PEA-PPEM-3	0.6825	0.3196	0.3356	9.5849	0.2365	0.7225	0.0178
PEA-PPEM-4	0.6593	0.3172	0.3544	5.5892	-0.8415	0.6029	-0.0908
PEA-PPEM-5	0.5319	0.2273	0.3397	3.7115	-1.6825	0.5021	-0.2276
PEA-PPEM-6	0.5019	0.2261	0.3677	2.2963	-1.8754	0.3842	-0.3137
PEA-PPEM-7	0.5611	0.3065	0.4444	1.1770	-1.7272	0.2423	-0.3556
PEA-PPEM-8	0.4750	0.2362	0.4183	0.6856	-2.1041	0.1570	-0.4819
PEA-PPEM-9	0.3758	0.2277	0.5483	0.2456	-1.6892	0.0625	-0.4302

The graphical plots concerning the methods FR, KT and ex-KT are given in Figure 4.9 (a-c). The plots were linear in all cases and for all graphical methods, thus

indicating that these copolymerisations follow conventional copolymerisation kinetics and that the reactivity of a polymer radical is determined only by the terminal monomer unit. As for some copolymers moderate yields were obtained, the extended KT and Mao-Huglin methods were employed as well. It is obvious that all methods provide similar data concerning the reactivity ratios for both monomers.

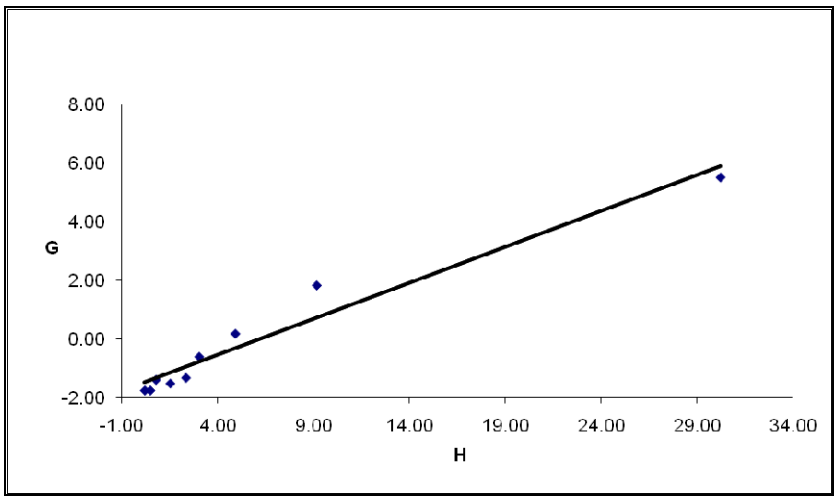

(a)

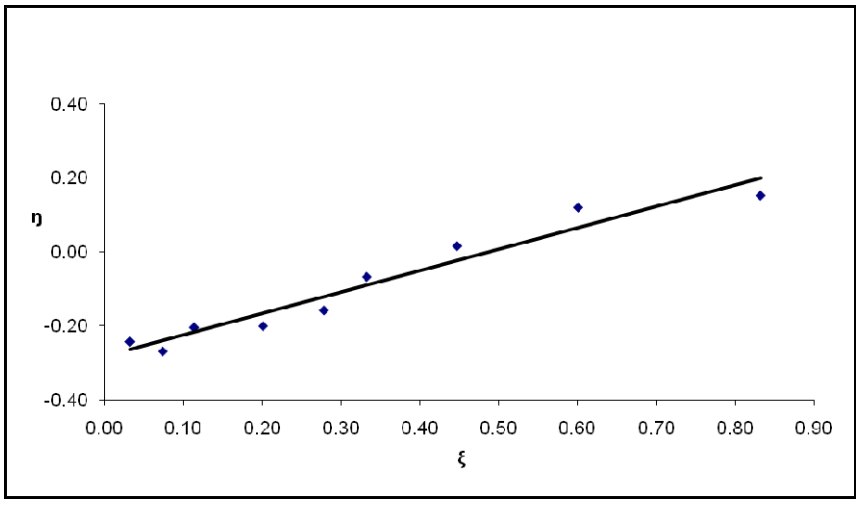

(b)

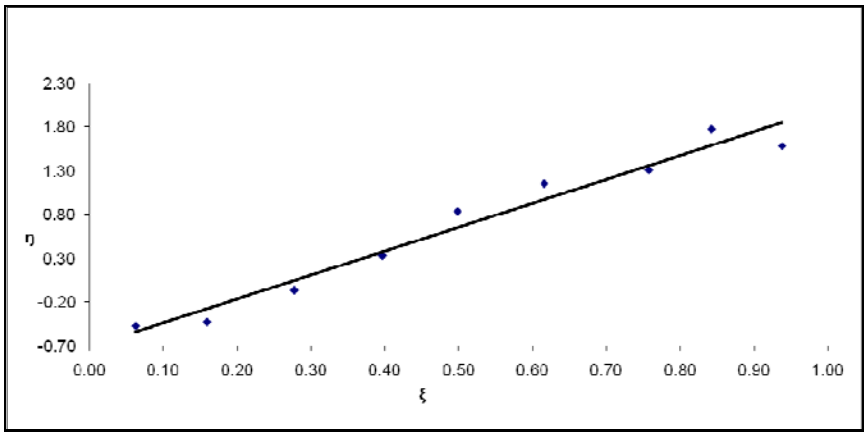

(c)

Figure 4.9: (a) FR, (b) KT and (c) Extended KT plots for the PEA and PPEM copolymer system

95 % joint confidence limit of the reactivity ratio values was calculated for Mao-Huglin method and has been plotted in Figure 4.10. Its equation is,

$$2.9756\,(r_1 - 0.1923)^2 - 0.8121(r_1 - 0.1923)(r_2 - 2.0171) + 0.2298(r_2 - 2.0171)^2 = 0.0154$$

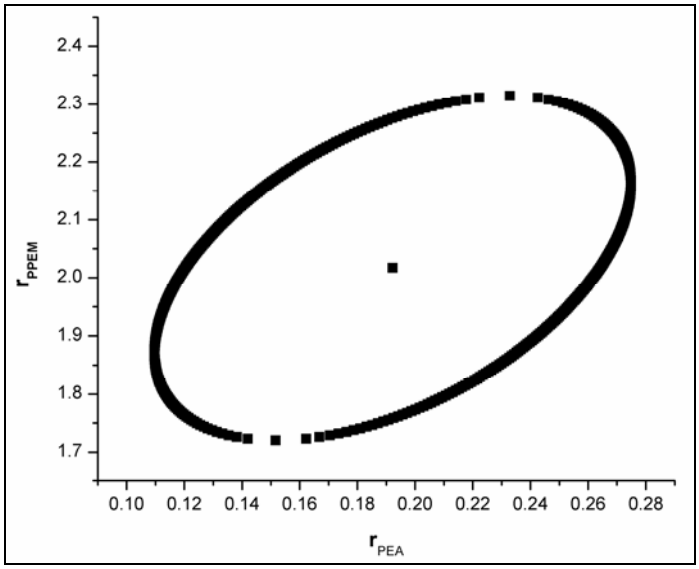

Figure 4.10: 95% Joint confidence interval of r_{PEA} and r_{PPEM} values by Mao-Huglin method for PEA-PPEM copolymer system

The statistical distribution of dyad monomer sequences M_{PEA}-M_{PEA}, M_{PPEM}-M_{PPEM} and M_{PEA}-M_{PPEM} were calculated using the method proposed by Igarashi. Mean sequence lengths μ_{PEA} and μ_{PPEM} were also calculated. The data summarise in Table 4.11,

and the variation of dyad fractions with the PEA mole fraction in the copolymers is displayed in Figure 4.11.

Table 4.11: Structural data for poly(PEA-*co*-PPEM) system

Polymer Code	M_1-M_1	M_2-M_2	M_1-M_2	μ_{M1}	μ_{M2}
PEA-PPEM-1	0.5049	0.0567	0.4384	3.08	1.21
PEA-PPEM-2	0.3943	0.1059	0.4997	1.95	1.45
PEA-PPEM-3	0.2579	0.2197	0.5224	1.54	1.80
PEA-PPEM-4	0.1727	0.3479	0.4795	1.34	2.26
PEA-PPEM-5	0.1063	0.5065	0.3872	1.23	2.84
PEA-PPEM-6	0.0771	0.6033	0.3197	1.16	3.67
PEA-PPEM-7	0.0576	0.6804	0.2619	1.10	5.33
PEA-PPEM-8	0.0296	0.8154	0.1549	1.06	8.64
PEA-PPEM-9	0.0182	0.8807	0.1011	1.03	16.12

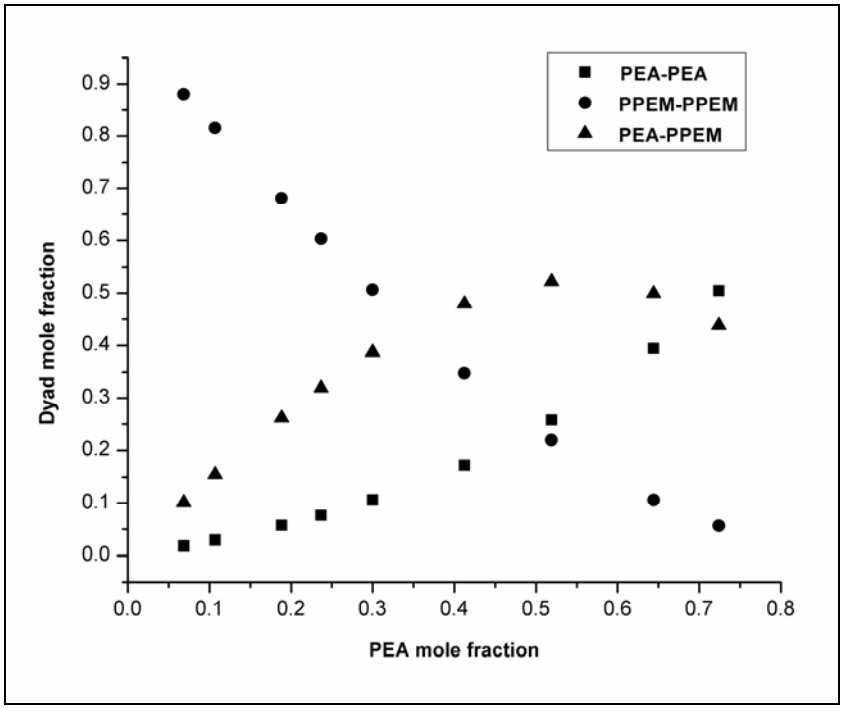

Figure 4.11: Dyad monomer sequence fractions versus the PEA mole fraction for the poly(PEA-*co*-PPEM)

4.5.3 Characterisation

Refractive index of thin copolymer films was determined in triplicate using refractometer. All of the polymer films were solvent cast from methylene chloride (30 wt % polymer to solvent) and dried slowly. The PPEM homopolymer has a refractive index of 1.576, which is higher than the refractive index of 1.553 for PEA. The copolymer refractive index increased with increasing PPEM content.

Table 4.12: Refractive index, glass transition temperature and molecular weight data for poly(PEA), poly(PPEM) and poly(PEA-*co*-PPEM)

Polymer Code	R. I.	T_g (°C)	Molecular weight		P.D.I.
			M_n x 10^4	M_w x 10^4	
P(PEA)	1.553	-3	3.44	7.22	2.1
PEA-PPEM-1	1.560	12.31	2.63	6.58	2.5
PEA-PPEM-2	1.563	14.54	2.64	6.07	2.3
PEA-PPEM-3	1.565	25.54	2.90	7.54	2.6
PEA-PPEM-4	1.568	46.56	3.99	9.18	2.3
PEA-PPEM-5	1.571	56.34	4.75	9.98	2.1
PEA-PPEM-6	1.571	60.14	5.50	10.45	1.9
PEA-PPEM-7	1.573	67.37	5.31	10.62	2.0
PEA-PPEM-8	1.572	74.03	5.60	11.20	2.0
PEA-PPEM-9	1.575	73.13	9.53	15.25	1.6
P(PPEM)	1.576	80.87	8.96	15.23	1.7

Glass transition temperature is important depending on the application of the RI-controlled polymer material. For intraocular lens low T_g's were required to improve material performance, particularly during the surgical procedures where some sample folding is required. Copolymers PEA-PPEM-1 to 3 showed relatively low glass transition temperatures (12 to 25 °C), which were desirable in the optical composites. Figure 4.12 represents the glass transition temperature curves for the PEA/PPEM system. The

copolymer glass transition temperature increased with increasing PPEM content as expected.

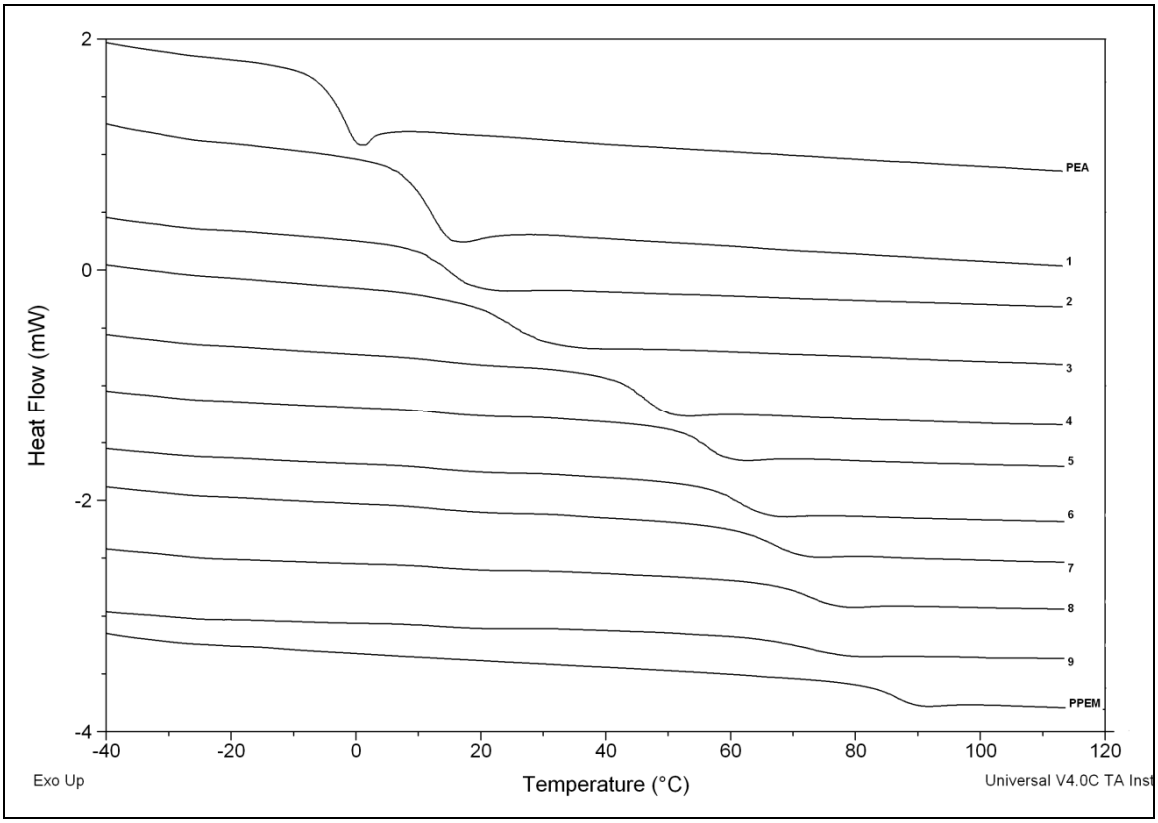

Figure 4.12: DSC thermograms of poly(PEA), poly(PPEM) and poly(PEA-*co*-PPEM)

The number and weight average molecular weights of PEA, PPEM homopolymer and PEA-PPEM copolymers were estimated by gel permeation chromatography and presented in Table 4.12. M_n and M_w ranges from 26,300 to 95,300 and 60,700 to 1,52,300, respectively. The polydispersity indices (PDI)s of the polymers produced via radical combination and disproportionation are close to 1.5–2.0.[48,49] The values of M_w/M_n of the copolymers suggest that for most of the copolymers there is a tendency for chain

termination by disproportionation. The data clearly indicated that molecular weight increased as content of PPEM in the copolymer is increased.

Figure 4.13 represents the UV–Vis absorption spectra of representative copolymers. Polymers show high transparency in the visible region (λ = 400–800 nm). Nearly identical spectra could be seen for copolymers.

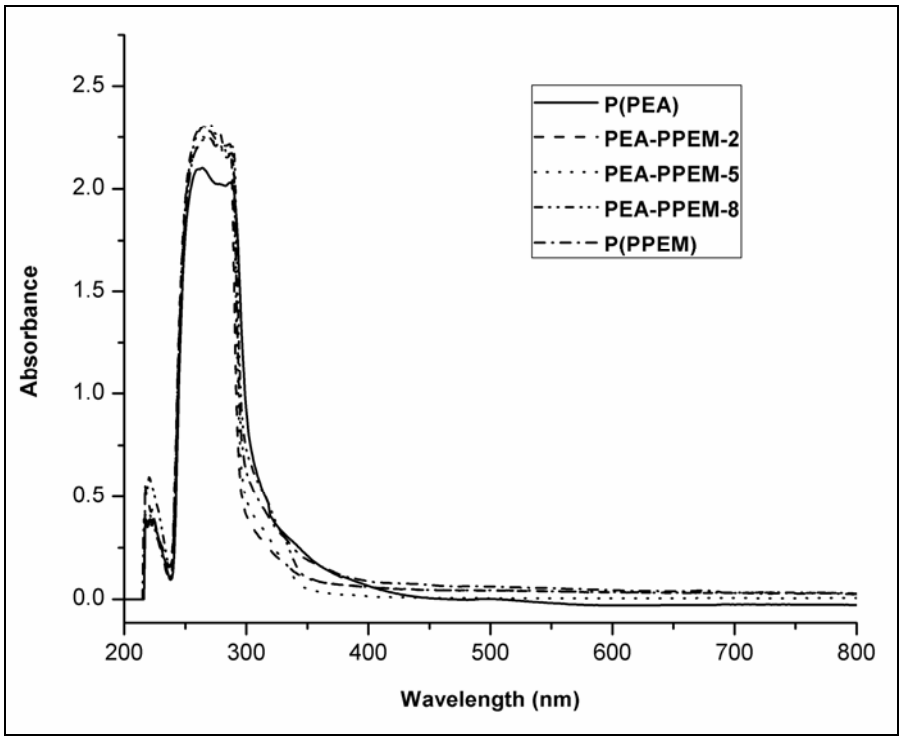

Figure 4.13: UV-visible spectra of poly(PEA), poly(PPEM) and poly(PEA-*co*-PPEM)

The thermal degradation of representative copolymers was characterised using TGA. The TGA curves (Figure 4.14) clearly indicate that all polymers undergo single step degradation. In all polymers the weight loss was found to occur in a single step. It is observed that the initial thermal degradation temperature shifted to higher side as PEA content increases in copolymer, which indicates thermal stability of the copolymer increases with an increase in PEA content in the copolymer.

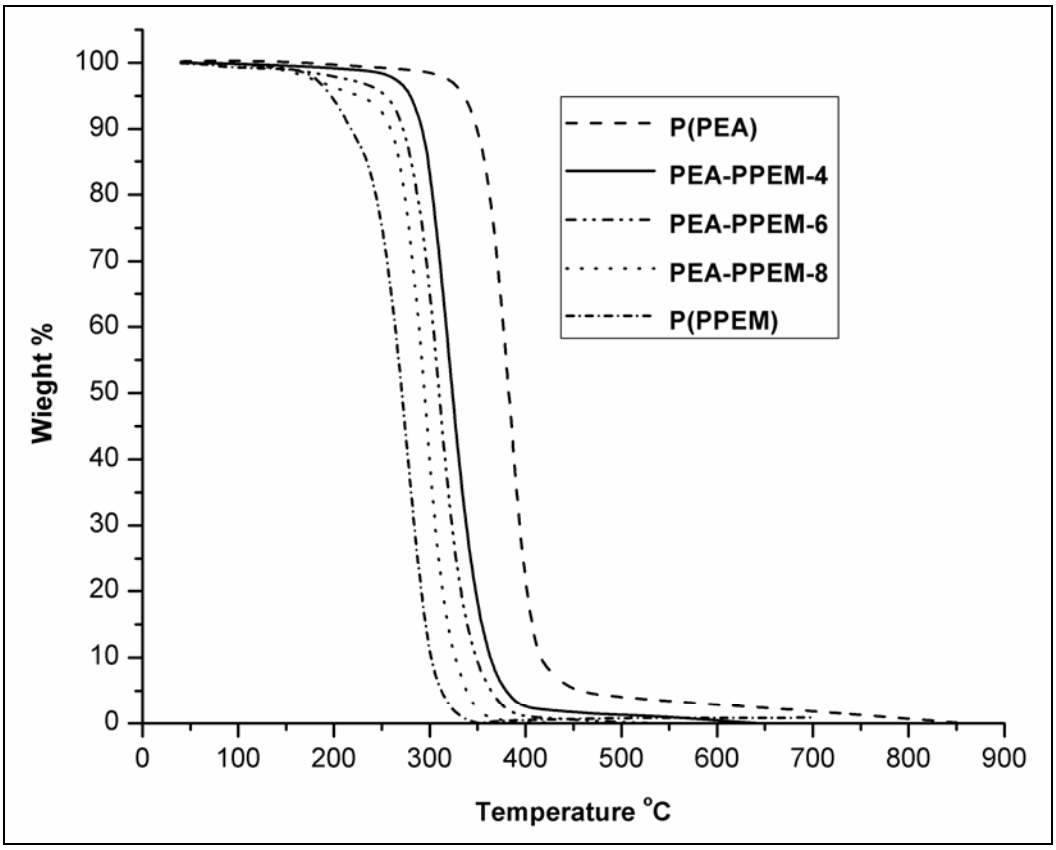

Figure 4.14: TGA thermograms of poly(PEA), poly(PPEM) and poly(PEA-*co*-PPEM)

4.6 Copolymerisation of 2-phenylethyl methacrylate (PEMA) and 2-phenoxy-2-phenylethyl acrylate (PPEA)

4.6.1 Synthesis of poly(PEMA-*co*-PPEA)

Copolymers of PEMA with PPEA having different compositions were synthesised in ethyl methyl ketone (EMK) solution using 2,2'-azobisisobutyronitrile (AIBN) as free radical initiator. The feed compositions of the monomers are presented in Tables 4.13. Appropriate quantities of the monomer, comonomer, EMK and AIBN (1 mol % of monomer) were taken in a polymerisation tubes and flushed with oxygen free nitrogen gas for 10 min. The tubes were tightly sealed and immersed in a thermostatic water bath at 70 °C. The reaction time was selected so as to yield moderate copolymer conversions in order to be within the realm of applicability of the differential copolymerisation equation. The conversions were controlled and determined by gravimetric measurements. After the reaction times, the copolymers were precipitated in methanol, filtered off, and purified by reprecipitations from chloroform solution into methanol and finally dried under reduced pressure for 24 h. Synthesis of the statistical copolymers, poly(PEMA-*co*-PPEA), is depicted in Scheme 4.3.

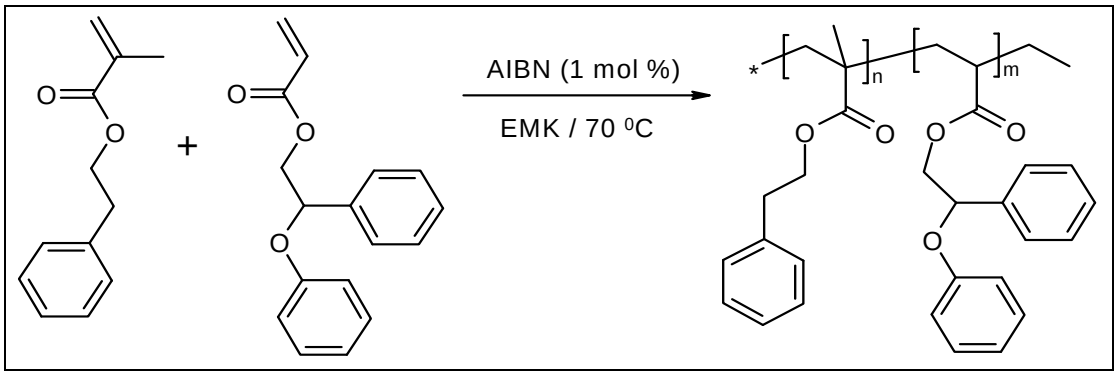

Scheme 4.3: Synthesis of poly(PEMA-*co*-PPEA)

The copolymerisation of 2-phenylethyl methacrylate with 2-phenoxy-2-phenylethyl acrylate in EMK solution was studied in a wide composition interval with the mole fractions of PEMA ranging from 0.2 to 0.9 in the feed.

The copolymers were soluble in solvents like tetrahydrofuran, acetone, dimethyl formamide, dimethyl sulphoxide, chloroform, methylene dichloride, toluene but were insoluble in hydrocarbons like n-hexane, petroleum ether and hydroxyl group containing solvents such as methanol, ethanol and 2-propanol.

Table 4.13: Composition data for copolymerisation of PEMA with PPEA

Polymer Code	Mole fraction				Wight fraction conversion
	in feed		in polymer		
	M_1	M_2	m_1	m_2	
P(PEMA)	1	0	1	0	-
PEMA-PPEA-2	0.8034	0.1966	0.8850	0.1150	0.2412
PEMA-PPEA-3	0.7059	0.2941	0.8197	0.1803	0.2508
PEMA-PPEA-4	0.6040	0.3960	0.7463	0.2537	0.2797
PEMA-PPEA-5	0.4996	0.5004	0.6536	0.3464	0.3188
PEMA-PPEA-6	0.4046	0.5954	0.5525	0.4475	0.3467
PEMA-PPEA-7	0.3229	0.6771	0.4566	0.5434	0.4182
PEMA-PPEA-8	0.2295	0.7705	0.3436	0.6564	0.4012
PEMA-PPEA-9	0.1155	0.8845	0.1862	0.8138	0.4453
P(PPEA)	0	1	0	1	-

Proton nuclear magnetic resonance (^{1}H NMR) is performed on each copolymer using deuterated chloroform as solvent to determine the amount of each comonomer that is incorporated into the copolymer. Figure 4.15 shows the ^{1}H NMR spectra of all PEMA/PPEA copolymers and the assigned peaks that were used in the calculations to determine the amount of each comonomer.

The assignment of the resonance peaks of each kind of monomeric unit in the copolymer chains leads to the accurate evaluation of the composition of copolymer. The resonance for methylene protons at 2.8 ppm (-CH_2-**CH_2**-Ph) of PEMA and combined resonance for methylene protons (-O-**CH_2**-CH_2-) of PEA and methylene protons (>CH-**CH_2**-O-) of PPEM at 4.3 ppm are well separated hence, their relative resonance areas can be measured and used to calculate the mole fraction of PEMA in copolymer.

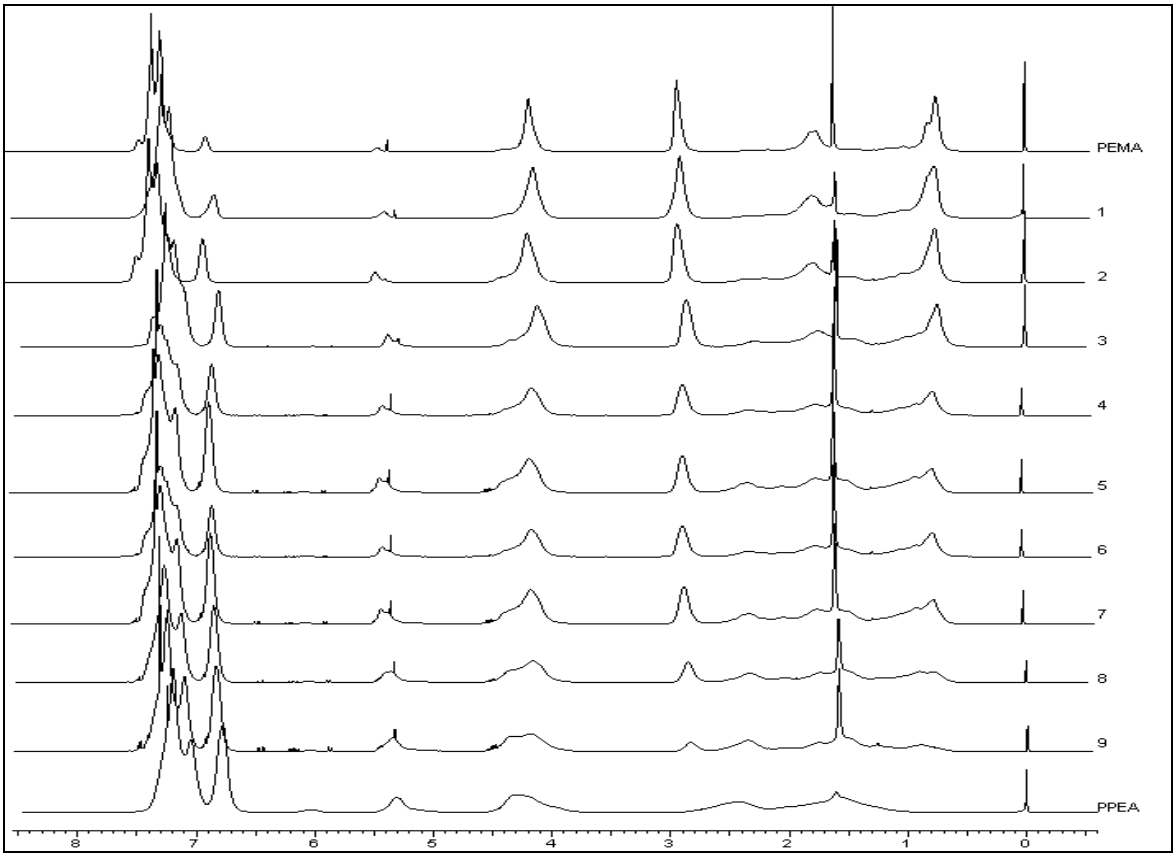

Figure 4.15: ^{1}H NMR spectra of poly(PEMA), poly(PPEA) and poly(PEMA-*co*-PPEA)

The following expression is used to calculate the composition of copolymers. Let F_1 be the mole fraction of PEMA.

$$F_1 = \frac{\int 2.8(-CH_2 - \underline{CH}_2 - Ph)/2}{\int 2.8(-CH_2 - \underline{CH}_2 - Ph)/2 \; + \; \int 4.3(\rangle CH - \underline{CH}_2 - O-)/2} \qquad 4.43$$

From equation 4.43, the mole fraction of PEMA was determined by measuring the intensities of corresponding aliphatic proton signals. The compositions of the poly(PEMA-*co*-PPEA) copolymers assessed from ^{1}H NMR and gravimetrically determined weight fraction conversions presented in Table 4.13.

4.6.2 Reactivity ratio determination for poly(PEMA-*co*-PPEA) system

From the monomer feed ratios and the copolymer composition, the reactivity ratios of PEMA and PPEA were determined by Finemann-Ross (FR), Kelen-Tudos (KT), extended Kelen-Tudos (Ex KT) and Mao-Huglin (MH) methods. The significance of the parameters of FR and KT for the copolymers is presented in Table 4.15 and that of extended KT is shown in Table 4.16. The reactivity ratios of PEMA and PPEA are denoted as r_{PEMA} (or r_1) and r_{PPEA} (or r_2) respectively and the values obtained from various methods are presented in Table 4.14.

Table 4.14: Reactivity ratios of PEMA and PPEA computed by different models

Method	r_{PEMA}	r_{PPEA}
Finemann-Ross	1.969	0.595
Kelen-Tudos	1.949	0.592
Extended Kelen-Tudos	2.009	0.407
Mao-Huglin	2.043	0.438
Average	1.993	0.508

The use of the obtained average reactivity ratio values gives $r_{PEMA} \times r_{PPEA} = 1.01$, indicative of an ideal copolymerisation. Because $r_{PEMA} > 1$and $r_{PPEA} < 1$, a heterogeneous copolymer structure may be expected in which one end (the initial part) of the chain will

be richer in PEMA than the rest of the chain. At later stages of the polymerisation the amount of PEMA monomers will be minor or totally consumed; however, the solution still contains PPEA monomers that can be initiated and propagated.

Table 4.15: FR and KT parameters for the copolymerisation of PEMA with PPEA

Polymer Code	$F=M_1/M_2$	$f=m_1/m_2$	$H=F^2/f$	$G=F(f-1)/f$	$\xi=H/(\alpha+H)$	$\eta=G/(\alpha+H)$
PEMA-PPEA-2	4.0865	7.6957	2.1700	3.5555	0.9307	1.5249
PEMA-PPEA-3	2.4002	4.5463	1.2672	1.8723	0.8868	1.3103
PEMA-PPEA-4	1.5253	2.9417	0.7908	1.0068	0.8302	1.0569
PEMA-PPEA-5	0.9984	1.8868	0.5283	0.4693	0.7657	0.6801
PEMA-PPEA-6	0.6795	1.2346	0.3740	0.1291	0.6982	0.2411
PEMA-PPEA-7	0.4769	0.8403	0.2707	-0.0907	0.6260	-0.2097
PEMA-PPEA-8	0.2979	0.5235	0.1695	-0.2712	0.5118	-0.8187
PEMA-PPEA-9	0.1306	0.2288	0.0745	-0.4401	0.3155	-1.8632

Table 4.16: Extended Kelen-Tudos parameters for PEMA-PPEA copolymer system

Polymer Code	ζ_1	ζ_2	Z	H	G	ξ	η
PEMA-PPEA-2	0.2742	0.1456	2.0366	1.8554	3.2876	0.8741	1.5489
PEMA-PPEA-3	0.3039	0.1604	2.0715	1.0595	1.7120	0.7986	1.2904
PEMA-PPEA-4	0.3639	0.1887	2.1636	0.6284	0.8974	0.7017	1.0020
PEMA-PPEA-5	0.4401	0.2329	2.1878	0.3942	0.4053	0.5960	0.6129
PEMA-PPEA-6	0.4977	0.2739	2.1510	0.2668	0.1091	0.4997	0.2043
PEMA-PPEA-7	0.6179	0.3507	2.2278	0.1693	-0.0717	0.3879	-0.1643
PEMA-PPEA-8	0.6228	0.3544	2.2283	0.1054	-0.2139	0.2829	-0.5739
PEMA-PPEA-9	0.7335	0.4186	2.4382	0.0385	-0.3163	0.1259	-1.0347

The graphical plots concerning the methods FR, KT and ex-KT are given in Figures 4.16 (a-c). The plots were linear in all cases and for all graphical methods, thus indicating that these copolymerisations follow conventional copolymerisation kinetics and that the reactivity of a polymer radical is determined only by the terminal monomer

unit. As for some copolymers moderate yields were obtained, the extended KT and Mao-Huglin methods were employed as well. It is obvious that all methods provide similar data concerning the reactivity ratios for both monomers.

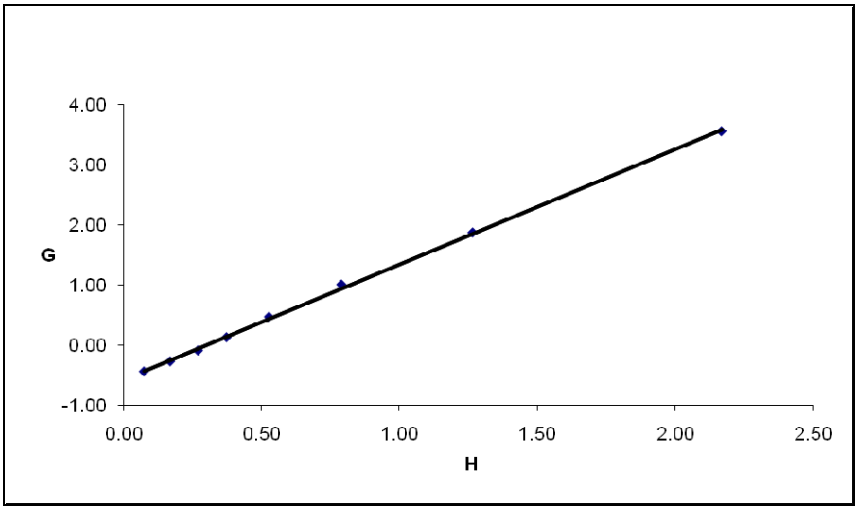

(a)

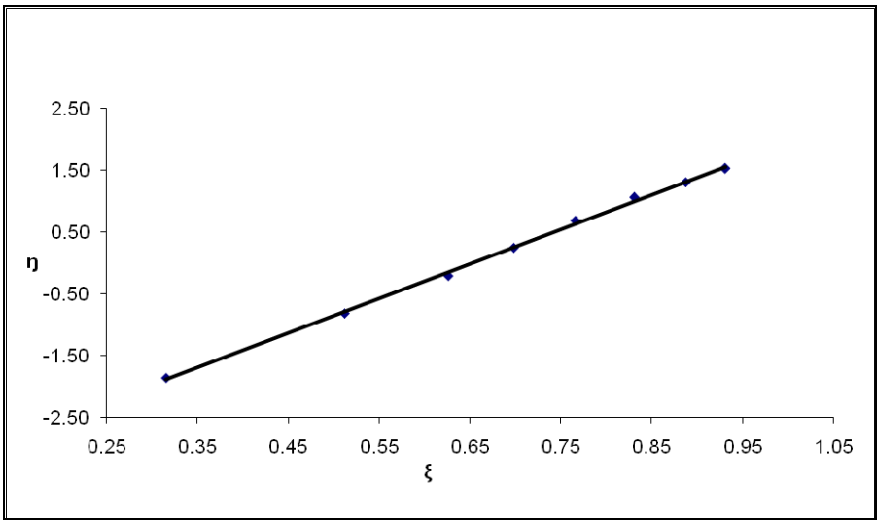

(b)

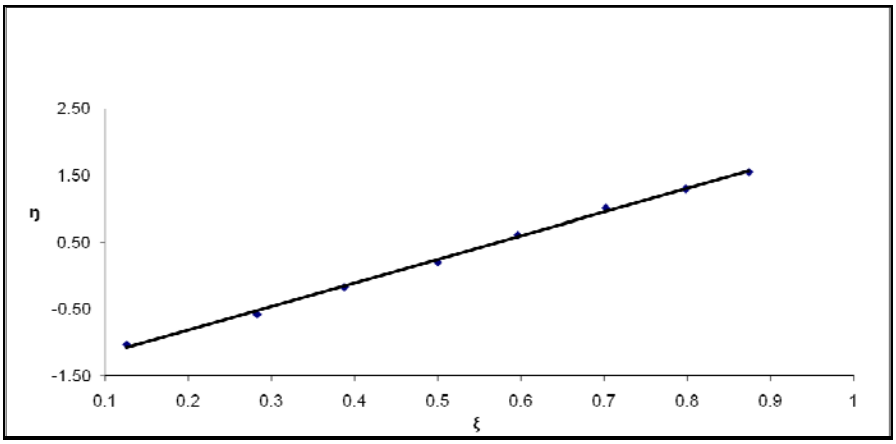

(c)

Figure 4.16: (a) FR, (b) KT and (c) Extended KT plots for the PEMA and PPEA copolymer system

95 % joint confidence limit of the reactivity ratio values was calculated for Mao-Huglin method and has been plotted in Figure 4.17. Its equation is,

$2.2329\ (r_1 - 0.4094)^2 - 0.8270\ (r_1 - 0.4094)\ (r_2 - 2.0124) + 0.2007\ (r_2 - 2.0124)^2 = 0.0006$

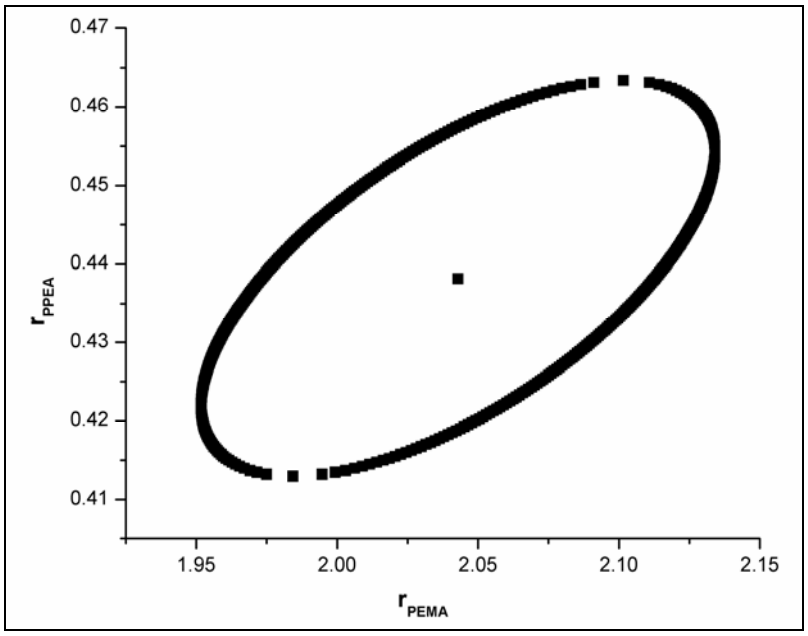

Figure 4.17: 95% Joint confidence interval of r_{PEMA} and r_{PPEA} values by Mao-Huglin method for PEMA-PPEA copolymer system

The statistical distribution of dyad monomer sequences M_{PEMA}-M_{PEMA}, M_{PPEA}-M_{PPEA} and M_{PEMA}-M_{PPEA} were calculated using the method proposed by Igarashi. Mean

sequence lengths μ_{PEMA} and μ_{PPEA} were also calculated. The data summarise in Table 4.17, and the variation of dyad fractions with PEMA mole fraction in the copolymers is displayed in Figure 4.18.

Table 4.17: Structural data for poly(PEMA-*co*-PPEA) system

Polymer Code	M_1-M_1	M_2-M_2	M_1-M_2	μ_{M1}	μ_{M2}
PEMA-PPEA-2	0.7844	0.0144	0.2012	9.14	1.12
PEMA-PPEA-3	0.6761	0.0367	0.2871	5.78	1.21
PEMA-PPEA-4	0.5673	0.0747	0.3579	4.04	1.33
PEMA-PPEA-5	0.4487	0.1415	0.4098	2.99	1.51
PEMA-PPEA-6	0.3406	0.2356	0.4237	2.35	1.75
PEMA-PPEA-7	0.2555	0.3423	0.4021	1.95	2.07
PEMA-PPEA-8	0.1728	0.4856	0.3416	1.59	2.71
PEMA-PPEA-9	0.0817	0.7093	0.2090	1.26	4.89

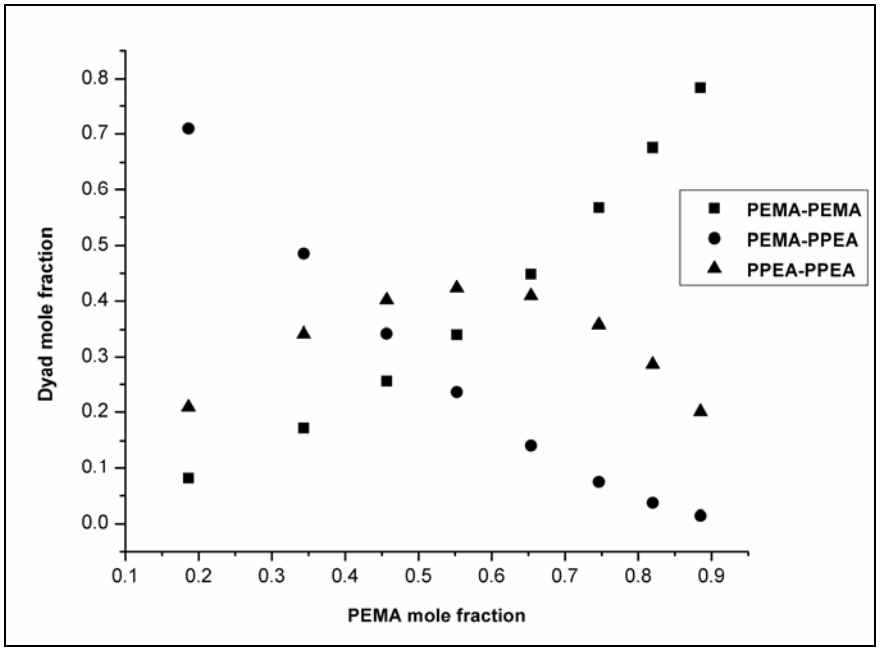

Figure 4.18: Dyad monomer sequence fractions versus PEMA mole fraction for poly(PEMA-*co*-PPEA)

4.6.3 Characterisation

As shown in Table 4.18, the magnitude of the refractive index increases with increasing PPEA content in copolymer. The refractive index values of the polymer vary from 1.559 to 1.574.

Table 4.18: Refractive index, glass transition temperature and molecular weight data for poly(PEMA), poly(PPEA) and poly(PEMA-*co*-PPEA)

Polymer Code	R. I.	T_g (°C)	Molecular weight		P.D.I.
			M_n x 10^4	M_w x 10^4	
P(PEMA)	1.559	42.97	4.10	9.02	2.20
PEMA-PPEA-2	1.560	40.39	4.929	9.07	1.84
PEMA-PPEA-3	1.560	42.48	4.809	9.19	1.91
PEMA-PPEA-4	1.561	43.24	5.151	9.99	1.94
PEMA-PPEA-5	1.563	43.33	5.260	9.57	1.82
PEMA-PPEA-6	1.563	43.39	5.250	9.61	1.83
PEMA-PPEA-7	1.565	44.49	4.716	8.91	1.89
PEMA-PPEA-8	1.568	45.49	4.814	9.00	1.87
PEMA-PPEA-9	1.570	47.69	4.543	6.86	1.51
P(PPEA)	1.574	56.00	6.40	10.88	1.70

The glass transition temperatures (T_g) of copolymers were determined by differential scanning calorimetry, and the data is presented in Table 4.18 and figure 4.19. The T_g of poly(PEMA) is 42.9 °C, and that of poly(PPEA) is 56.0 °C. The results clearly indicate that the T_g values of copolymers depend on the composition of comonomers and increase with increasing PPEA content in the polymer chain.

The weight-average (M_w) and number-average (M_n) molecular weights and the polydispersity indices (PDI) of polymer samples are presented in Table 4.18. The polydispersity index of the polymers ranges between 1.84 and 1.94. The theoretical

values of PDI for polymers produced via radical recombination and disproportionation are 1.5 and 2.0, respectively. This suggests that polymers were produced mainly via termination of growing chain by disproportionation.

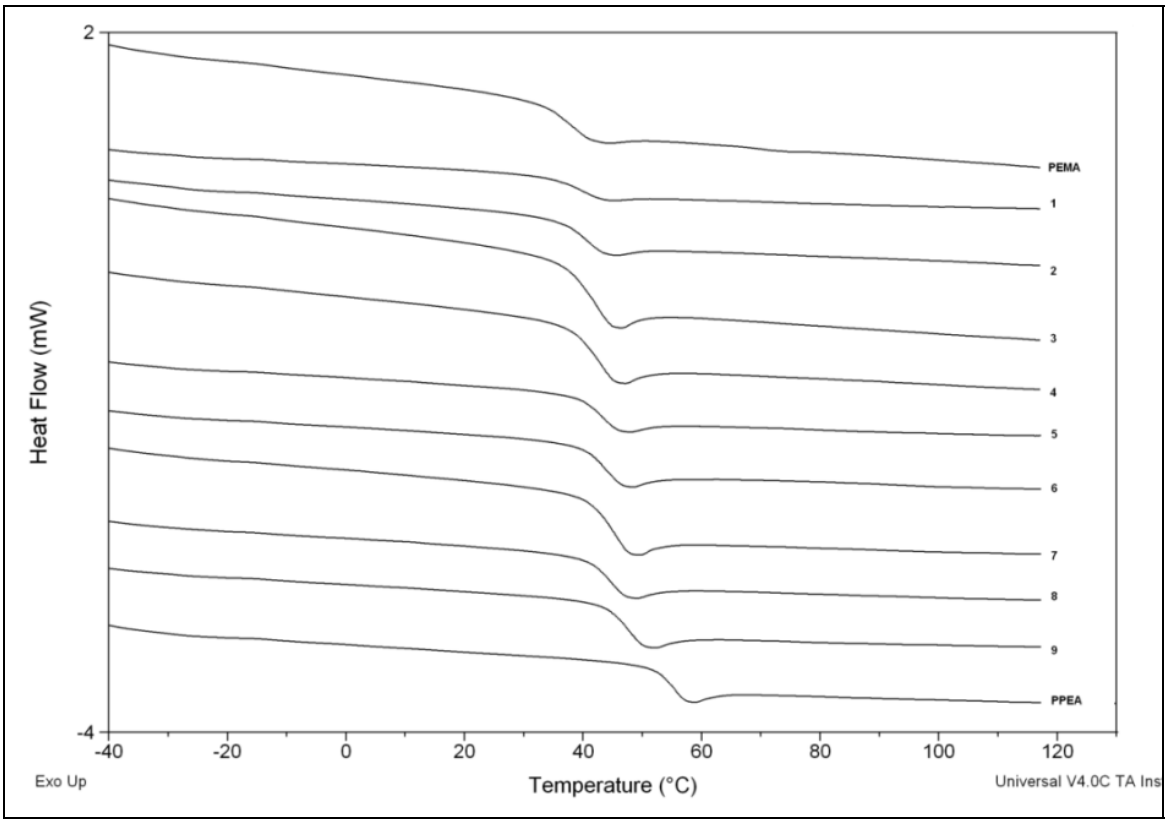

Figure 4.19: DSC thermograms of poly(PEMA), poly(PPEA) and poly(PEMA-*co*-PPEA)

Figure 4.20 shows the UV–vis absorption spectra of representative copolymers. Polymers show high transparency in the visible region (λ = 400–800 nm).

Thermal stability of the copolymers was measured by TGA under inert conditions, and the thermograms are presented in Figure 4.21. The copolymers underwent decomposition in single step except homopolymer of PEMA which decomposed in two steps. As the content of PPEA increases in copolymer, degradation temperature shifted to higher side.

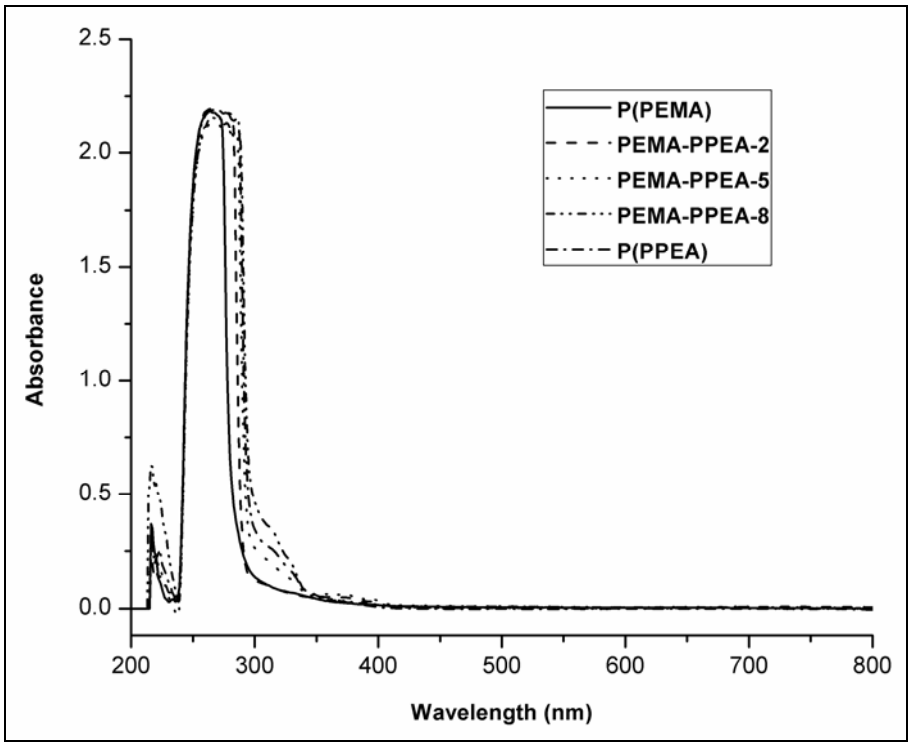

Figure 4.20: UV-visible spectra of poly(PEMA), poly(PPEA) and poly(PEMA-*co*-PPEA)

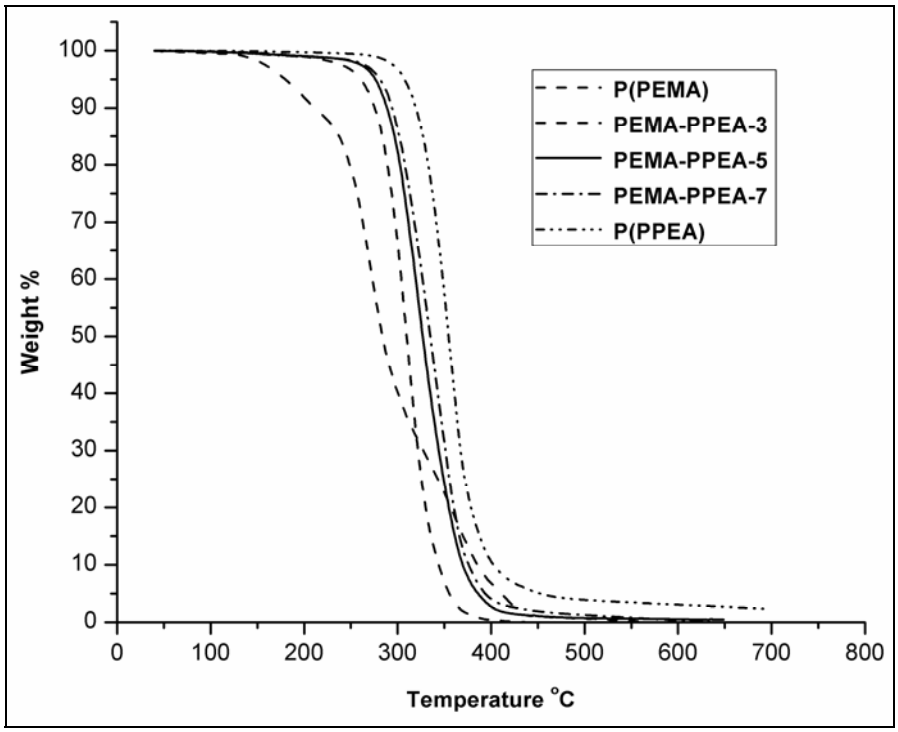

Figure 4.21: TGA thermograms of poly(PEMA), poly(PPEA) and poly(PEMA-*co*-PPEA)

4.7 Copolymerisation of 2-phenylethyl methacrylate (PEMA) and 2-phenoxy-2-phenylethyl methacrylate (PPEM)

4.7.1 Synthesis of poly(PEMA-*co*-PPEM)

Copolymers of PEMA with PPEM having different composition were synthesised in ethyl methyl ketone (EMK) solution using 2,2'-azobisisobutaronitrile (AIBN) as free radical initiator. The feed compositions of the monomers are presented in Tables 4.19. Appropriate quantities of the monomer, comonomer, EMK and AIBN (1 mol % of monomer) were taken in a polymerisation tubes and flushed with oxygen free nitrogen gas for 10 min. The tubes were tightly sealed and immersed in a thermostatic water bath at 70 °C. The reaction time was selected so as to yield moderate copolymer conversions in order to be within the realm of applicability of the differential copolymerisation equation. The conversions were controlled and determined by gravimetric measurements. After the reaction times, the copolymers were precipitated in methanol, filtered off, and purified by reprecipitations from chloroform solution into methanol and finally dried under reduced pressure for 24 h. Synthesis of the statistical copolymers, poly(PEMA-*co*-PPEM), is depicted in scheme 4.4.

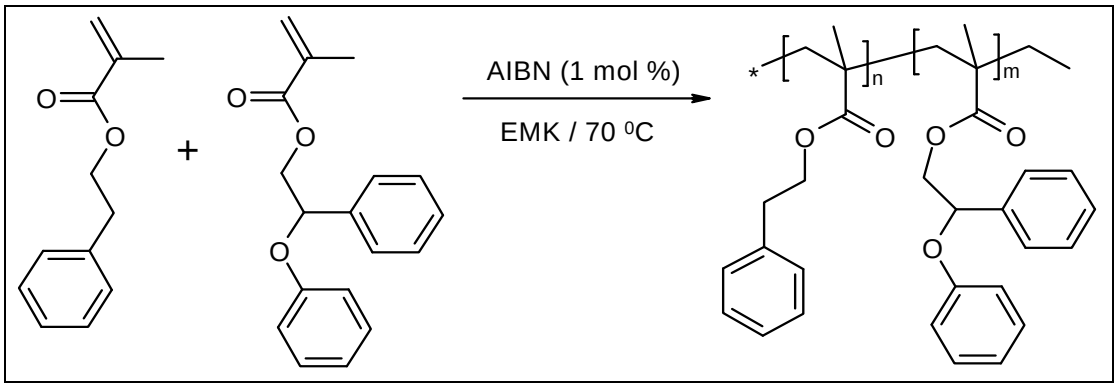

Scheme 4.4: Synthesis of poly(PEMA-*co*-PPEM)

The entire range of data provided for a systematic study, with 10% intervals, of the copolymerisation of 2-phenylethyl methacrylate and 2-phenoxy-2-phenylethyl methacrylate over a range of 90/10 to 10/90 of PEMA/PPEM monomer mole percent feed ratios.

The copolymers were soluble in solvents like tetrahydrofuran, acetone, dimethyl formamide, dimethyl sulphoxide, chloroform, methylene dichloride, toluene but were insoluble in hydrocarbons like n-hexane, petroleum ether and hydroxyl group containing solvents such as methanol, ethanol and 2-propanol.

Table 4.19: Composition data for copolymerisation of PEMA with PPEM

Polymer Code	Mole fraction				Wight fraction conversion
	in feed		in polymer		
	M_1	M_2	m_1	m_2	
P(PEMA)	1	0	1	0	-
PEMA-PPEM-1	0.9014	0.0986	0.9141	0.0859	0.3236
PEMA-PPEM-2	0.8018	0.1982	0.8153	0.1847	0.3709
PEMA-PPEM-3	0.6994	0.3006	0.7189	0.2811	0.4100
PEMA-PPEM-4	0.5995	0.4005	0.6213	0.3787	0.4390
PEMA-PPEM-5	0.4963	0.5037	0.5256	0.4744	0.4610
PEMA-PPEM-6	0.4321	0.5679	0.4330	0.5670	0.4391
PEMA-PPEM-7	0.3113	0.6887	0.3190	0.6810	0.5180
PEMA-PPEM-8	0.2092	0.7908	0.2107	0.7893	0.6598
PEMA-PPEM-9	0.1306	0.8694	0.0997	0.9003	0.6625
P(PPEM)	0	1	0	1	-

In order to determine the amount of each comonomer incorporated into the copolymer, proton nuclear magnetic resonance (^{1}H NMR) was performed on each copolymer using deuterated chloroform as solvent. An ultrasonic bath was used to quickly dissolve the copolymers that afforded the required copolymer solutions. ^{1}H NMR

experiments produced well resolved peaks. Figure 4.22 shows the ^{1}H NMR spectra of all PEMA/PPEM copolymers and the assigned peaks that were used in the calculations to determine the amount of each comonomer.

The assignment of the resonance peaks of each kind of monomeric unit in the copolymer chains leads to the accurate evaluation of the composition of copolymer. Thus, the composition of copolymers was calculated by comparing the integral peak areas of the methylene protons (-CH_2-**CH_2**-Ph) of PEMA, exhibiting resonance signal at around at 2.8 pmm, to that of the methylene protons (>CH-**CH_2**-O-) of PPEM showing signal at 4.1 ppm, which is overlapping with signal for methylene protons (-O-**CH_2**-CH_2-) of PEMA (Figure 4.22).

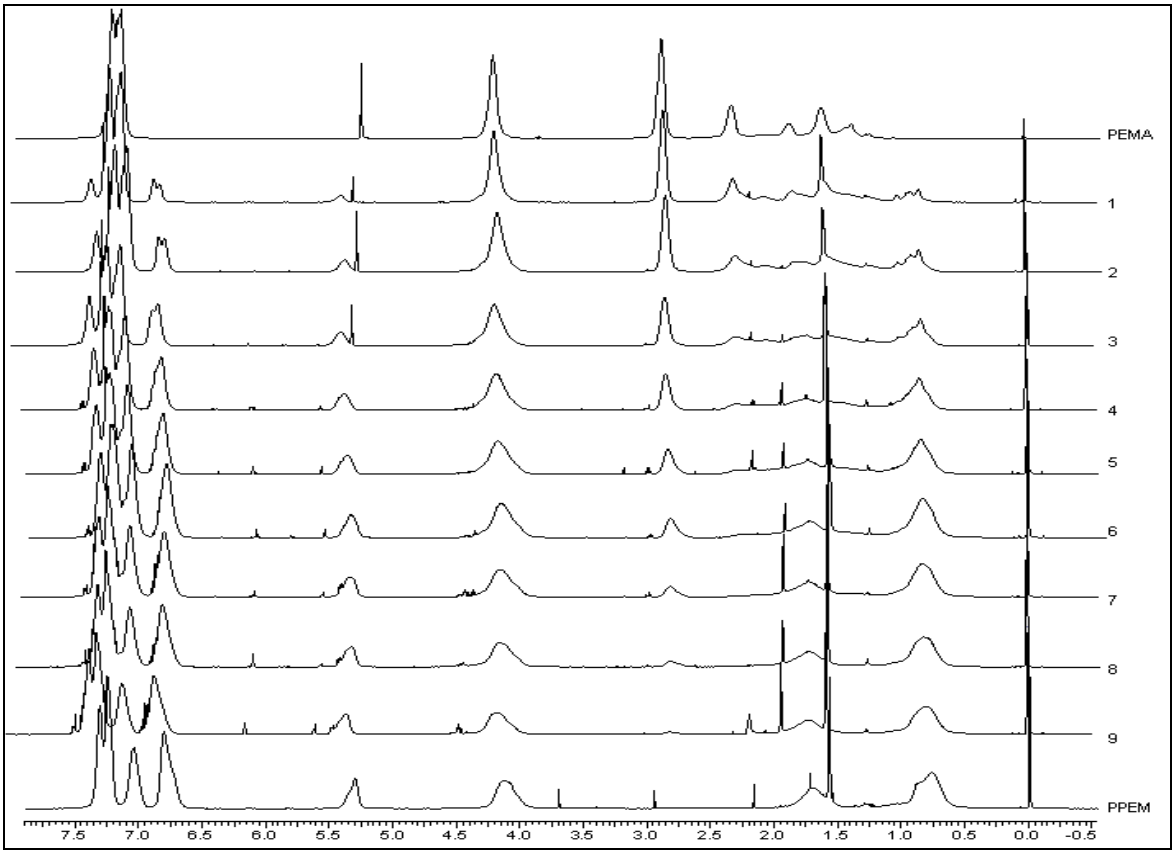

Figure 4.22: ^{1}H NMR spectra of poly(PEMA), poly(PPEM) and poly(PEMA-*co*-PPEM)

The following expression is used to calculate the composition of copolymers. Let F_1 be the mole fraction of PEMA.

$$F_1 = \frac{\int 2.8(-CH_2 - \underline{CH}2 - Ph)/2}{\int 2.8(-CH_2 - \underline{CH}2 - Ph)/2 \; + \; \int 4.1(\rangle CH - \underline{CH}2 - O-)/2} \qquad 4.44$$

From equation 4.44, the mole fraction of PEMA was determined by measuring the intensities of corresponding aliphatic proton signals. The compositions of the poly(PEMA-*co*-PPEM) copolymers assessed from ^{1}H NMR and gravimetrically determined weight fraction conversions are presented in Table 4.19.

4.7.2 Reactivity ratio determination for poly(PEMA-*co*-PPEM) system

From the monomer feed ratios and the copolymer composition, the reactivity ratios of PEMA and PPEM were determined by Finemann-Ross (FR), Kelen-Tudos (KT), extended Kelen-Tudos (Ex KT) and Mao-Huglin (MH) methods. The significance of the parameters of FR and KT for the copolymers is presented in Table 4.21 and that of extended KT is shown in Table 4.22. The reactivity ratios of PEMA and PPEM are denoted as r_{PEMA} (or r_1) and r_{PPEM} (or r_2) respectively and the values obtained from various methods are presented in Table 4.20.

Table 4.20: Reactivity ratios of PEMA and PPEM computed by different models

Method	r_{PEMA}	r_{PPEM}
Finemann-Ross	1.193	1.127
Kelen-Tudos	1.219	1.159
Extended Kelen-Tudos	1.298	1.248
Mao-Huglin	1.309	1.259
Average	1.255	1.198

In the PEMA-PPEM copolymer system the reactivity ratios of both monomers are similar and greater than one as well as the r_1 x r_2 product is greater than unity. Hence, both monomers showed the same preference for adding one or the other of the two monomers. This indicates that the copolymers are weak orders with predominantly random distribution of monomeric units in the copolymer chain.

Table 4.21: FR and KT parameters for the copolymerisation of PEMA with PPEM

Polymer Code	$F=M_1/M_2$	$f=m_1/m_2$	$H=F^2/f$	$G=F(f-1)/f$	$\xi=H/(\alpha+H)$	$\eta=G/(\alpha+H)$
PEMA-PPEM-1	9.1420	10.6446	7.8515	8.2832	0.9246	0.1686
PEMA-PPEM-2	4.0454	4.4153	3.7065	3.1292	0.7880	0.1568
PEMA-PPEM-3	2.3267	2.5570	2.1171	1.4168	0.6663	0.0229
PEMA-PPEM-4	1.4969	1.6403	1.3660	0.5843	0.5515	-0.1127
PEMA-PPEM-5	0.9853	1.1079	0.8763	0.0960	0.4875	-0.2780
PEMA-PPEM-6	0.7609	0.7637	0.7581	-0.2354	0.3829	-0.3831
PEMA-PPEM-7	0.4520	0.4685	0.4361	-0.5128	0.2401	-0.4331
PEMA-PPEM-8	0.2645	0.2669	0.2621	-0.7265	0.1643	-0.5997
PEMA-PPEM-9	0.1502	0.1108	0.2036	-1.2054	0.0754	-0.5731

Table 4.22: Extended Kelen-Tudos parameters for PEMA-PPEM copolymer system

Polymer Code	ζ_1	ζ_2	Z	H	G	ξ	η
PEMA-PPEM-1	0.3301	0.2835	1.2017	7.3711	8.0257	0.8423	0.9171
PEMA-PPEM-2	0.3794	0.3476	1.1169	3.5392	3.0577	0.7194	0.6216
PEMA-PPEM-3	0.4249	0.3866	1.1318	1.9961	1.3757	0.5912	0.4075
PEMA-PPEM-4	0.4590	0.4188	1.1319	1.2804	0.5657	0.4812	0.2126
PEMA-PPEM-5	0.4938	0.4392	1.1772	0.7994	0.0916	0.3668	0.0420
PEMA-PPEM-6	0.4402	0.4386	1.0050	0.7561	-0.2351	0.3539	-0.1101
PEMA-PPEM-7	0.5324	0.5136	1.0546	0.4213	-0.5040	0.2339	-0.2798
PEMA-PPEM-8	0.6648	0.6589	1.0162	0.2585	-0.7214	0.1577	-0.4402
PEMA-PPEM-9	0.5005	0.6789	0.6111	0.2965	-1.4550	0.1769	-0.8678

The graphical plots concerning the methods FR, KT and ex-KT are given in Figures 4.23 (a-c). The plots were linear in all cases and for all graphical methods, thus indicating that these copolymerisations follow conventional copolymerisation kinetics and that the reactivity of a polymer radical is determined only by the terminal monomer unit. As for some copolymers moderate yields were obtained, the extended KT and Mao-Huglin methods were employed as well.

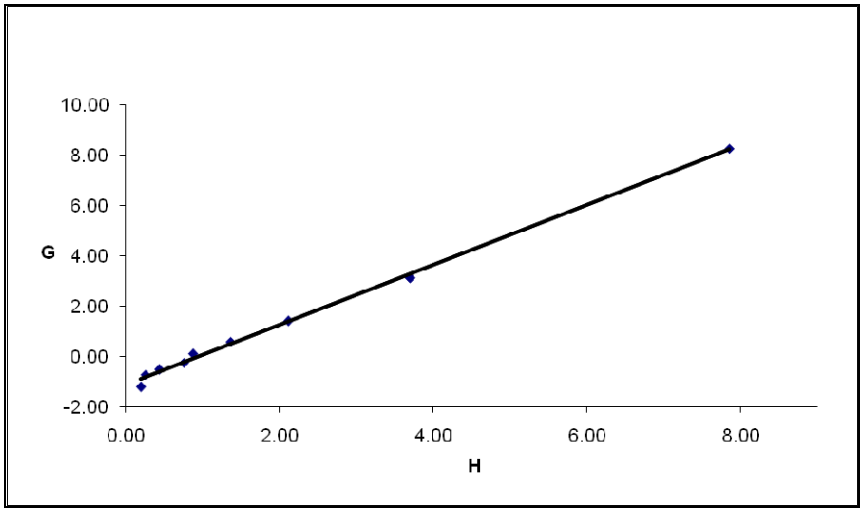

(a)

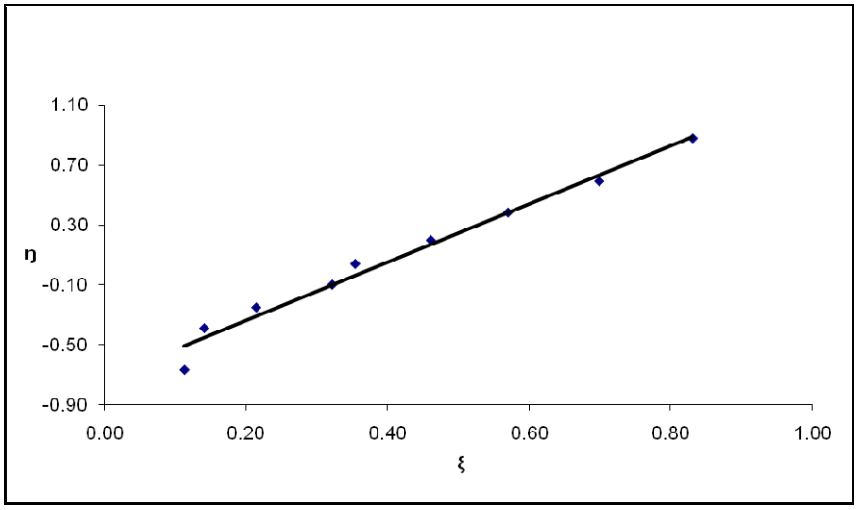

(b)

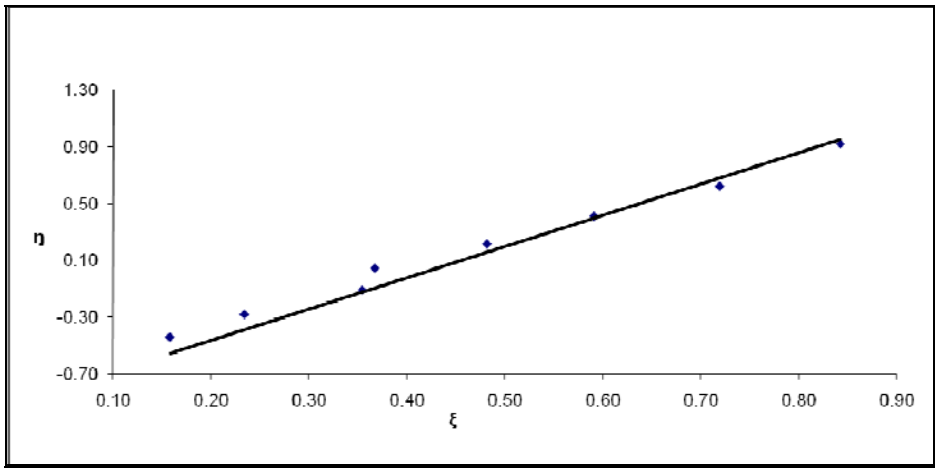

(c)

Figure 4.23: (a) FR, (b) KT and (c) Extended KT plots for the PEMA and PPEM copolymer system

The 95 % joint confidence limit of the reactivity ratio values was calculated for Mao-Huglin method and has been plotted in Figure 4.24. Its equation is,

$2.2841(r_1\text{-}1.3094)^2 - 2.6967(r_1\text{-}1.3094)(r_2\text{-}1.2585) + 1.8796(r_2\text{-}1.2585)^2 = 0.1021$

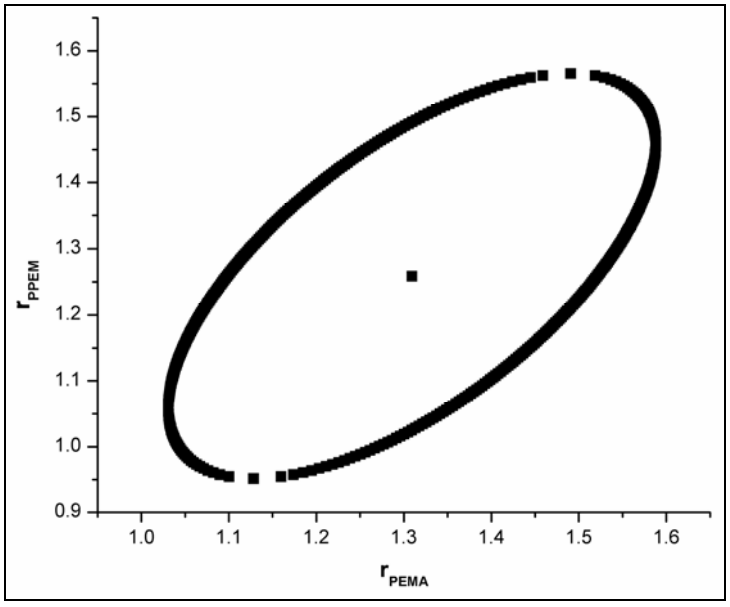

Figure 4.24: 95% Joint confidence interval of r_{PEMA} and r_{PPEM} values by Mao-Huglin method for PEMA-PPEM copolymer system

The statistical distribution of the dyad monomer sequences M_{PEMA}-M_{PEMA}, M_{PPEM}-M_{PPEM} and M_{PEMA}-M_{PPEM} were calculated using the method proposed by Igarashi.

Mean sequence lengths μ_{PEMA} and μ_{PPEM} were also calculated. The data summarise in Table 4.23, and the variation of the dyad fractions with the PEMA mole fraction in the copolymers is displayed in Figure 4.25.

Table 4.23: Structural data for poly(PEMA-*co*-PPEM) system

Polymer Code	M_1-M_1	M_2-M_2	M_1-M_2	μ_{M1}	μ_{M2}
PEMA-PPEM-1	0.8392	0.0110	0.1498	12.47	1.13
PEMA-PPEM-2	0.6802	0.0495	0.2703	6.08	1.30
PEMA-PPEM-3	0.5485	0.1107	0.3408	3.92	1.51
PEMA-PPEM-4	0.4351	0.1926	0.3722	2.88	1.80
PEMA-PPEM-5	0.3402	0.2890	0.3708	2.24	2.22
PEMA-PPEM-6	0.2608	0.3948	0.3444	1.95	2.57
PEMA-PPEM-7	0.1769	0.5388	0.2844	1.57	3.65
PEMA-PPEM-8	0.1085	0.6871	0.2044	1.33	5.53
PEMA-PPEM-9	0.0478	0.8484	0.1038	1.19	8.98

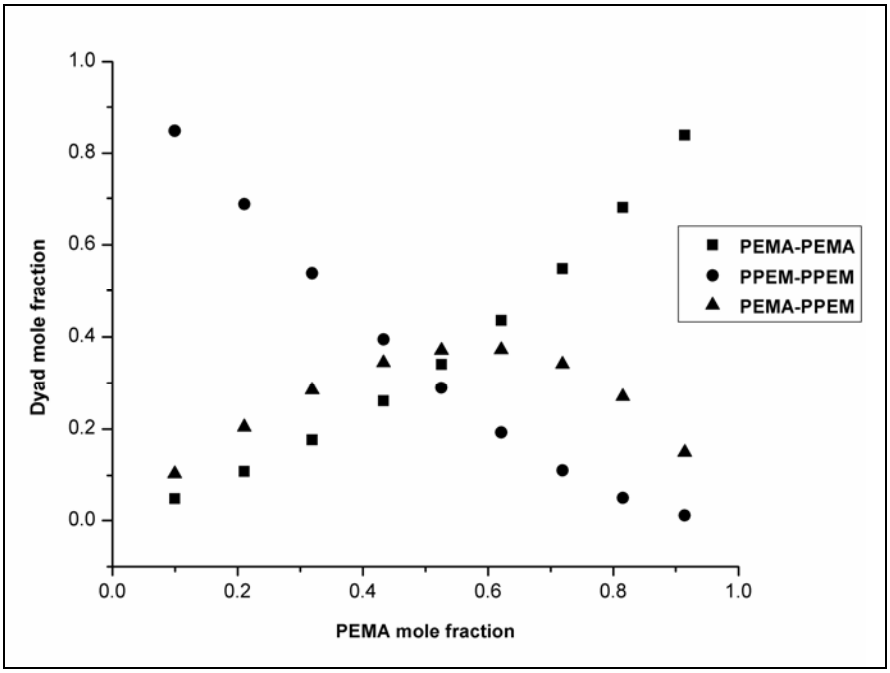

Figure 4.25: Dyad monomer sequence fractions versus PEMA mole fraction for poly(PEMA-*co*-PPEM)

4.7.3 Characterisation

Refractive index of thin copolymer films was determined in triplicate using refractometer. All of the polymer films were solvent cast from methylene chloride (30 wt % polymer to solvent) and dried slowly. The results are listed in Table 4.24. The PPEM homopolymer has a refractive index of 1.576, which is higher than the refractive index of 1.559 for PEMA. The refractive index of copolymer increases with increase in PPEM content.

Table 4.24: Refractive index, glass transition temperature and molecular weight data for poly(PEMA), poly(PPEM) and poly(PEMA-*co*-PPEM)

Polymer Code	R. I.	T_g (°C)	Molecular weight		P.D.I.
			M_n x 10^4	M_w x 10^4	
P(PEMA)	1.559	42.97	4.10	9.02	2.20
PEMA-PPEM-1	1.564	45.45	3.42	7.15	2.09
PEMA-PPEM-2	1.565	51.69	3.52	7.32	2.08
PEMA-PPEM-3	1.568	56.48	16.45	18.92	1.15
PEMA-PPEM-4	1.569	61.21	15.51	16.60	1.07
PEMA-PPEM-5	1.570	67.68	15.72	17.13	1.09
PEMA-PPEM-6	1.570	68.69	18.12	19.21	1.06
PEMA-PPEM-7	1.571	71.78	18.24	20.06	1.10
PEMA-PPEM-8	1.571	75.55	19.89	23.47	1.18
PEMA-PPEM-9	1.573	79.46	16.12	17.89	1.11
P(PPEM)	1.578	80.87	8.96	15.23	1.70

The DSC curves presented in Figure 4.26 shows the evolution of the glass transition temperatures of the poly(PEMA-*co*-PPEM) copolymers. The glass transition temperatures of the copolymers are ranging from 42 to 80 °C (Table 4.24) and increases with increase in PPEM content. The observed thermal behavior can be explained by the mobile hindrance of the bulky side chain of the PPEM due to additional aromatic ring.

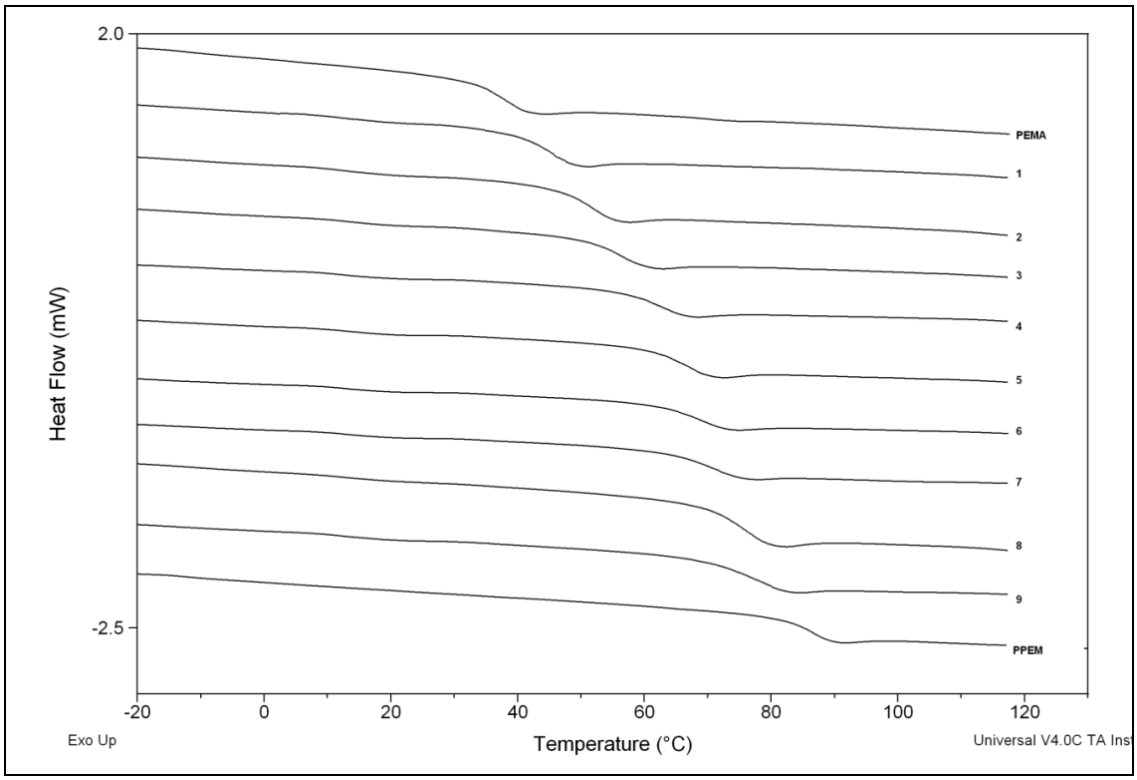

Figure 4.26: DSC thermograms of poly(PEMA), poly(PPEM) and poly(PEMA-*co*-PPEM)

The molecular weights and polydispersity indices of the poly(PEMA-*co*-PPEM) copolymers were assessed by size exclusion chromatography and presented in Table 4.24. PDI values indicated that in the homopolymerisation of PEMA and PPEM, the growing chains terminate by disproportionation and tendency for termination by disproportionation is greater for PEMA than for PPEM.

UV-Visible absorption spectra were measured for representative polymers. Polymers exhibited good transparency in the visible region, as shown in Figure 4.27.

The thermal stabilities of the polymers were investigated by thermogravimetric analysis (TGA). In Figure 4.28 the TGA thermograms of representative copolymers are shown. It is clear that the copolymers underwent decomposition in two distinguished stages. In case of all polymers the starting of weight loss was found to occur at ~200 °C.

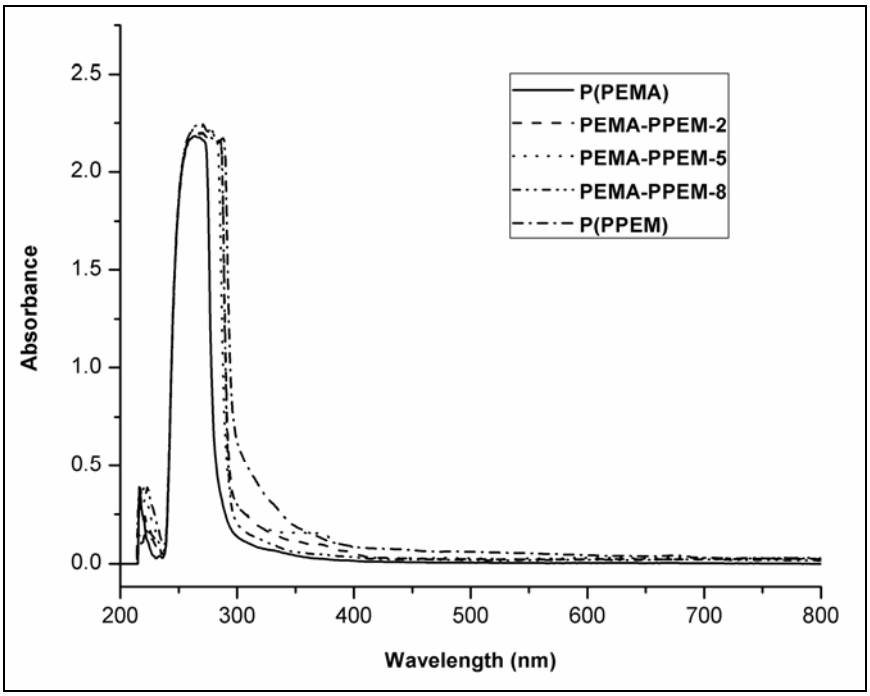

Figure 4.27: UV-visible spectra of poly(PEMA), poly(PPEM) and poly(PEMA-*co*-PPEM)

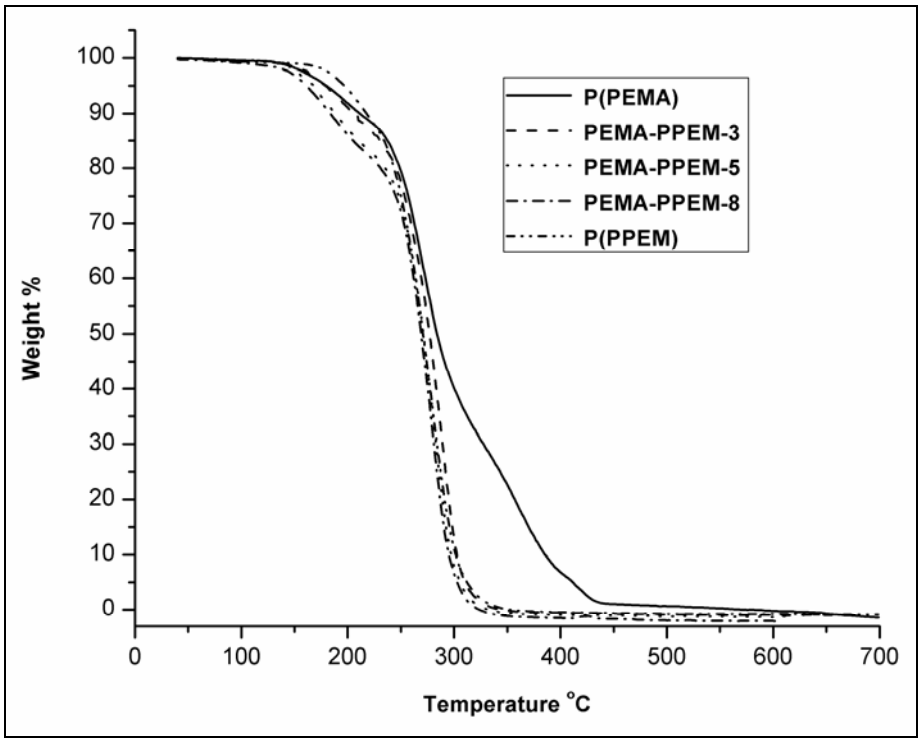

Figure 4.28: TGA thermograms of poly(PEMA), poly(PPEM) and poly(PEMA-*co*-PPEM)

4.8 Copolymerisation of 2-phenylethyl acrylate (PEA) and 2-phenyl-(2-phenylthio)ethyl acrylate (PTEA)

4.8.1 Synthesis of poly(PEA-*co*-PTEA)

Copolymers of PEA with PTEA having different composition were synthesised in EMK solution using 2,2'-azobisisobutyronitrile (AIBN) as free radical initiator. The feed compositions of the monomers are presented in Tables 4.25. Appropriate quantities of the monomer, comonomer, EMK and AIBN (1 mol % of monomer) were placed in a polymerisation tubes and flushed with oxygen free nitrogen gas for 10 min. The tubes were tightly sealed and immersed in a thermostatic water bath at 70 °C. The reaction time was selected so as to yield moderate copolymer conversions in order to be within the realm of applicability of the differential copolymerisation equation. The conversions were controlled and determined by gravimetric measurements. After the reaction times, copolymers were precipitated in methanol, filtered off, and purified by reprecipitations from chloroform solution into methanol and finally dried under reduced pressure for 24 h. Synthesis method for the statistical copolymers, poly(PEA-*co*-PTEA), is depicted in Scheme 4.5.

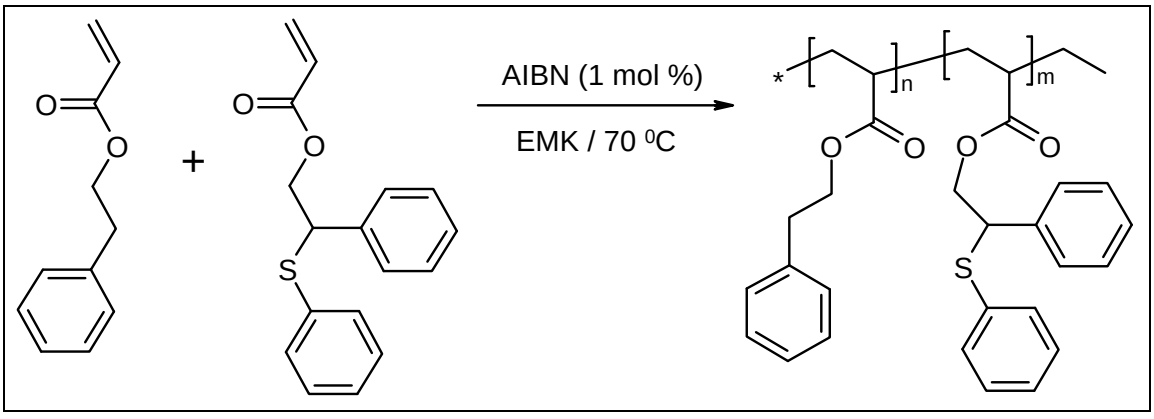

Scheme 4.5: Synthesis of poly(PEA-*co*-PTEA)

The copolymerisation of 2-phenylethyl acrylate with 2-phenyl-(2-phenylthio)ethyl acrylate in EMK solution was studied in a composition interval with the mole fractions of PEA ranging from 0.2 to 0.9 in the feed.

The copolymers were soluble in solvents like tetrahydrofuran, dimethyl formamide, dimethyl sulphoxide, chloroform, methylene dichloride, toluene but were insoluble in hydrocarbons like n-hexane, petroleum ether and hydroxyl group containing solvents such as methanol, ethanol and 2-propanol.

Table 4.25: Composition data for copolymerisation of PEA with PTEA

Polymer Code	Mole fraction				Wight fraction conversion
	in feed		in polymer		
	M_1	M_2	m_1	m_2	
P(PEA)	1	0	1	0	-
PEA-PTEA-2	0.7919	0.2081	0.8021	0.1979	0.5324
PEA-PTEA-3	0.7005	0.2995	0.7109	0.2891	0.3154
PEA-PTEA-4	0.6100	0.3900	0.6198	0.3802	0.3854
PEA-PTEA-5	0.5146	0.4854	0.5226	0.4774	0.3726
PEA-PTEA-6	0.4100	0.5900	0.4190	0.5810	0.3616
PEA-PTEA-7	0.3272	0.6728	0.3352	0.6648	0.4197
PEA-PTEA-8	0.1880	0.8120	0.1898	0.8102	0.4132
PEA-PTEA-9	0.0991	0.9009	0.0984	0.9016	0.4362
P(PTEA)	0	1	0	1	-

The structures of the copolymers was characterised by ^{1}H NMR spectroscopy. ^{1}H NMR spectra of poly(PEA-*co*-PTEA) obtained from comonomer with different feed ratios are shown in Figure 4.29. The chemical shift assignments of copolymers were based on those obtained for poly(PEA) and poly(PTEA). The copolymer composition was determined from ^{1}H NMR spectral analysis of the copolymer. The peak at 2.8 ppm should be assigned to the methylene group (-CH_2-**CH_2**-Ph) of the PEA. The broad

resonance observed at signal at 4.4 ppm is for the methylene proton (-CH-**CH_2**-O-) and methine protons (-S-**CH**(Ph)-CH_2-) of PTEA. Intensities of these well separated peaks were used to determine copolymer composition.

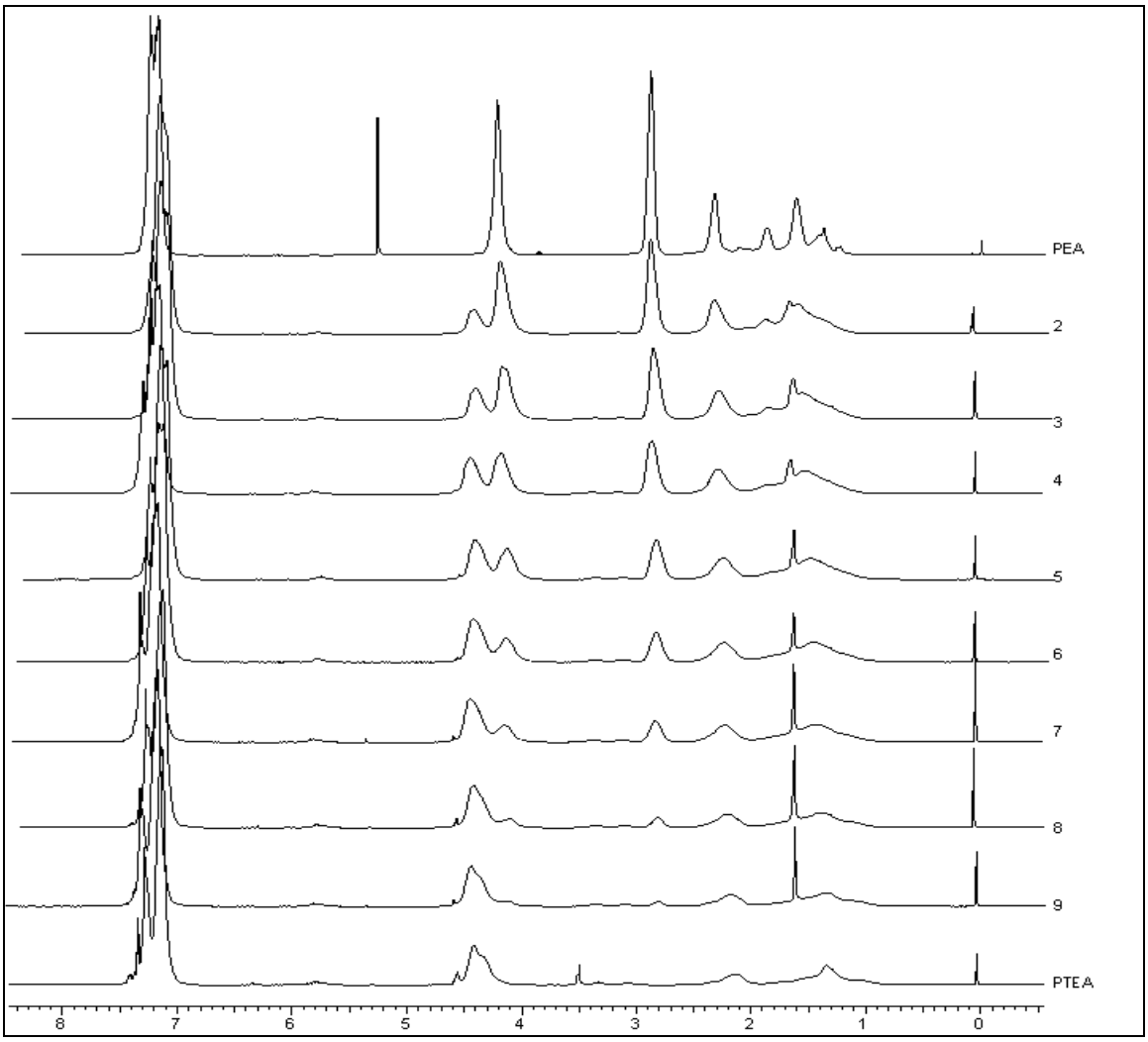

Figure 4.29: ^{1}H NMR spectra of poly(PEA), poly(PTEA) and poly(PEA-*co*-PTEA)

The following expression is used to calculate the composition of copolymers. Let F_1 be the mole fraction of PEA.

$$F_1 = \frac{\int 2.8(-CH_2 - \underline{CH}2 - Ph)/2}{\int 2.8(-CH_2 - \underline{CH}2 - Ph)/2 \; + \; \int 4.4(-S - \underline{CH}(Ph) - \underline{CH}2 - O-)/3} \qquad 4.45$$

From equation 4.45, the mole fraction of PEA was determined by measuring the intensities of corresponding aliphatic proton signals. The compositions of the poly(PEA-*co*-PTEA) copolymers assessed from ^{1}H NMR and gravimetrically determined weight fraction conversions are presented in Table 4.25.

4.8.2 Reactivity ratio determination for poly(PEA-*co*-PTEA) system

From the knowledge of the copolymer composition, the reactivity ratios of PEA and PTEA were determined by Finemann-Ross (FR), Kelen-Tudos (KT), extended Kelen-Tudos (Ex KT) and Mao-Huglin (MH) methods. The significance of the parameters of FR and KT for the copolymers is presented in Table 4.27 and that of extended KT is shown in Table 4.28. The reactivity ratios of PEA and PTEA are denoted as r_{PEA} (or r_1) and r_{PTEA} (or r_2) respectively and the values obtained from various methods are presented in Table 4.26.

Table 4.26: Reactivity ratios of PEA and PTEA computed by different models

Method	r_{PEA}	r_{PTEA}
Finemann-Ross	1.081	1.006
Kelen-Tudos	1.084	1.007
Extended Kelen-Tudos	1.114	1.011
Mao-Huglin	1.119	1.011
Average	1.100	1.009

In the PEA-PTEA copolymer system the value of r_{PEA} is slightly more than r_{PTEA}, in this system PEA is found to have higher reactivity than PTEA. The values of r_{PEA} and r_{PTEA} are greater than 1 and the product r_{PEMA} x r_{PPEM} is also greater than 1. This indicates that the copolymers are weak orders with predominantly random distribution of monomeric units in the copolymer chain.

Table 4.27: FR and KT parameters for the copolymerisation of PEA with PTEA

Polymer Code	$F=M_1/M_2$	$f=m_1/m_2$	$H=F^2/f$	$G=F(f-1)/f$	$\xi=H/(\alpha+H)$	$\eta=G/(\alpha+H)$
PEA-PTEA-2	3.8054	4.0541	3.5720	2.8667	0.8637	0.6931
PEA-PTEA-3	2.3389	2.4590	2.2246	1.3877	0.7978	0.4977
PEA-PTEA-4	1.5641	1.6304	1.5005	0.6048	0.7269	0.2930
PEA-PTEA-5	1.0602	1.0949	1.0265	0.0919	0.6455	0.0578
PEA-PTEA-6	0.6949	0.7212	0.6696	-0.2687	0.5429	-0.2178
PEA-PTEA-7	0.4863	0.5042	0.4691	-0.4782	0.4541	-0.4630
PEA-PTEA-8	0.2315	0.2342	0.2289	-0.7571	0.2887	-0.9550
PEA-PTEA-9	0.1100	0.1091	0.1109	-0.8983	0.1644	-1.3314

Table 4.28: Extended Kelen-Tudos parameters for PEA-PTEA copolymer system

Polymer Code	ζ_1	ζ_2	Z	H	G	ξ	η
PEA-PTEA-2	0.5090	0.5423	1.0986	3.3589	2.7799	0.8458	0.7000
PEA-PTEA-3	0.3061	0.3218	1.0627	2.1774	1.3729	0.7806	0.4922
PEA-PTEA-4	0.3775	0.3935	1.0550	1.4650	0.5976	0.7053	0.2877
PEA-PTEA-5	0.3678	0.3799	1.0420	1.0085	0.0911	0.6223	0.0562
PEA-PTEA-6	0.3575	0.3710	1.0480	0.6566	-0.2661	0.5175	-0.2097
PEA-PTEA-7	0.4162	0.4315	1.0493	0.4579	-0.4725	0.4279	-0.4416
PEA-PTEA-8	0.4126	0.4174	1.0153	0.2272	-0.7543	0.2707	-0.8987
PEA-PTEA-9	0.4364	0.4328	0.9889	0.1116	-0.9009	0.1542	-1.2449

The graphical plots concerning the methods FR, KT and ex-KT are given in Figures 4.30 (a-c). The plots were linear in all cases and for all graphical methods, thus indicating that these copolymerisations follow conventional copolymerisation kinetics and that the reactivity of a polymer radical is determined only by the terminal monomer unit. As for some copolymers moderate yields were obtained, the extended KT and Mao-Huglin methods were employed as well. It is obvious that all methods provide similar data concerning the reactivity ratios for both monomers.

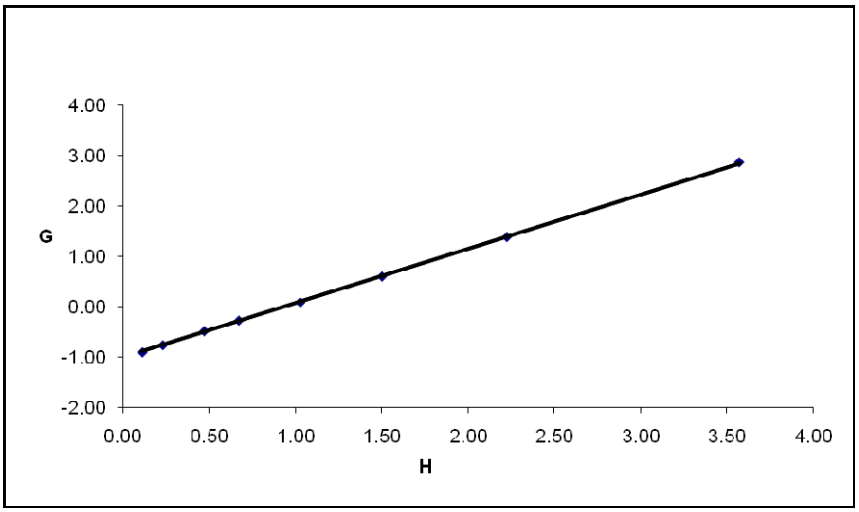

(a)

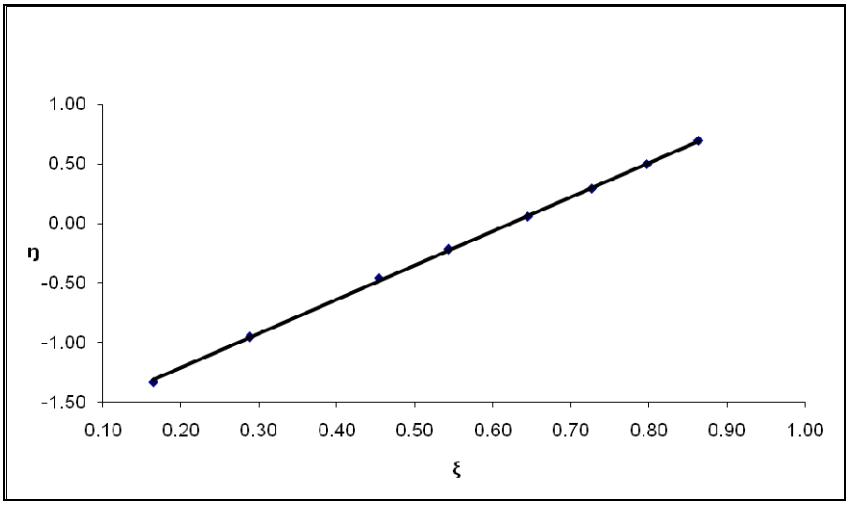

(b)

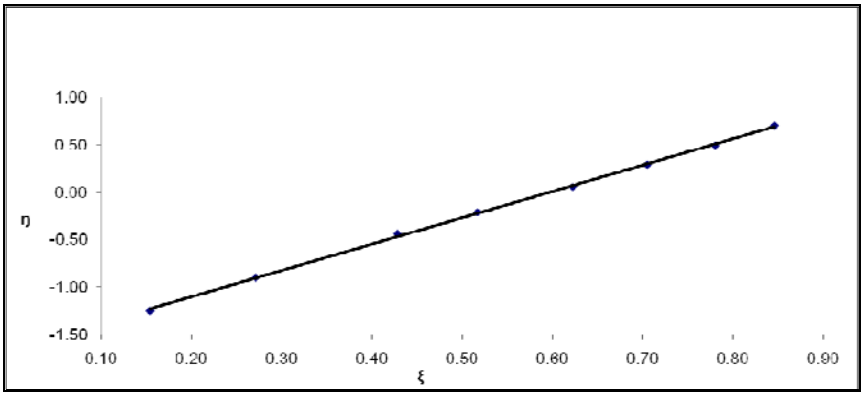

(c)

Figure 4.30: (a) FR, (b) KT and (c) Extended KT plots for the PEA and PTEA copolymer system

95 % joint confidence limit of the reactivity ratio values was calculated for Mao-Huglin method and has been plotted in Figure 4.31. Its equation is,

$$2.7580\ (r_1 - 1.1119)^2 - 5.1169\ (r_1 - 1.1119)\ (r_2 - 1.0107) + 5.6206\ (r_2 - 1.0107)^2 = 0.0018$$

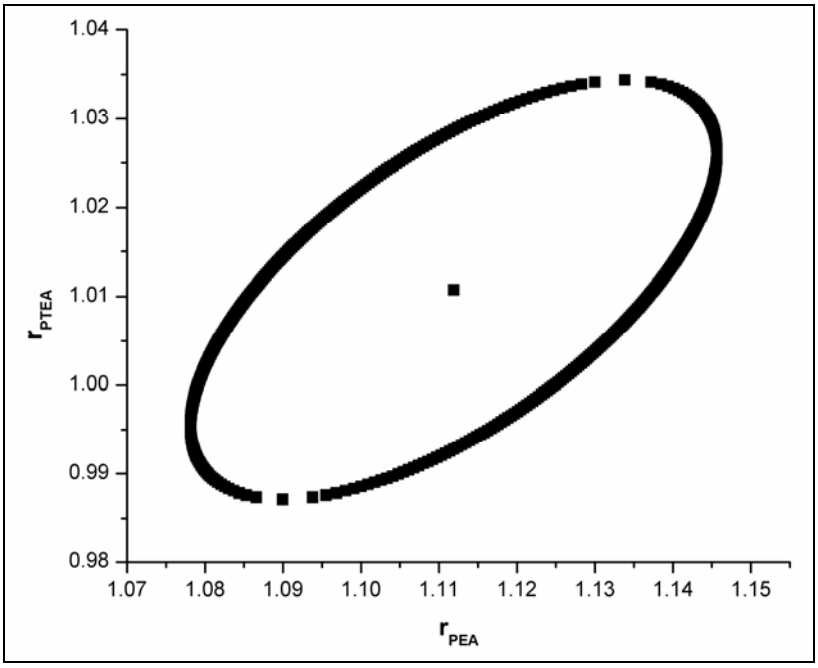

Figure 4.31: 95% Joint confidence interval of r_{PEA} and r_{PTEA} values by Mao-Huglin method for PEA-PTEA copolymer system

The statistical distribution of the dyad monomer sequences M_{PEA}-M_{PEA}, M_{PTEA}-M_{PTEA} and M_{PEA}-M_{PTEA} were calculated using the method proposed by Igarashi. Mean sequence lengths μ_{PEA} and μ_{PTEA} were also calculated. The data summarise in Table 4.29, and the variation of the dyad fractions with the PEA mole fraction in the copolymers is displayed in Figure 4.32.

Table 4.29: Structural data for poly(PEA-*co*-PTEA) system

Polymer Code	M_1-M_1	M_2-M_2	M_1-M_2	μ_{M1}	μ_{M2}
PEA-PTEA-2	0.6521	0.0478	0.3001	5.19	1.27
PEA-PTEA-3	0.5248	0.1030	0.3722	3.57	1.43
PEA-PTEA-4	0.4168	0.1771	0.4061	2.72	1.65
PEA-PTEA-5	0.3195	0.2742	0.4063	2.17	1.95
PEA-PTEA-6	0.2328	0.3948	0.3725	1.76	2.45
PEA-PTEA-7	0.1731	0.5027	0.3242	1.53	3.07
PEA-PTEA-8	0.0871	0.7076	0.2053	1.25	5.36
PEA-PTEA-9	0.0422	0.8454	0.1124	1.12	10.17

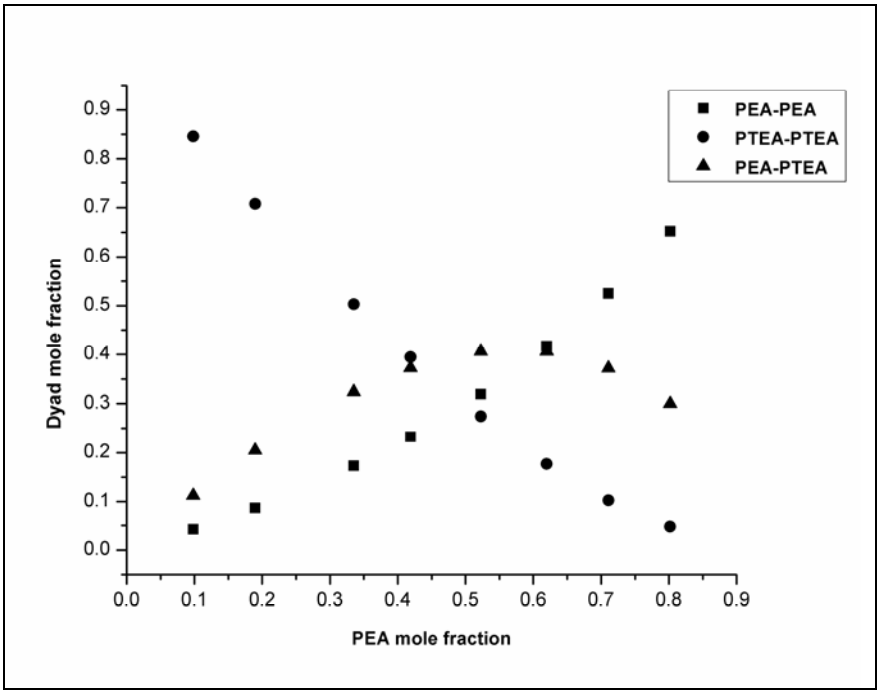

Figure 4.32: Dyad monomer sequence fractions versus PEA mole fraction for poly(PEA-*co*-PTEA)

4.8.3 Characterisation

The refractive index of an optical material can be increased by incorporating polarisable group into acrylate polymers. We attempted to enhance the refractive index of an acrylic polymer by introducing sulfur atom into the polymer. The refractive indices of

all copolymers were observed at 589 nm and summarise in Table 4.30. Results indicating that refractive index significantly increased with increase in the sulphur containing comonomer content in the resulting copolymer.

Table 4.30: Refractive index, glass transition temperature and molecular weight data for poly(PEA), poly(PTEA) and poly(PEA-*co*-PTEA)

Polymer Code	R. I.	T_g (°C)	Molecular weight		P.D.I.
			M_n x 10^4	M_w x 10^4	
P(PEA)	1.553	-3.00	3.44	7.22	2.10
PEA-PTEA-2	1.571	7.92	2.13	4.17	1.96
PEA-PTEA-3	1.575	11.47	2.80	5.04	1.80
PEA-PTEA-4	1.585	14.51	2.73	4.91	1.80
PEA-PTEA-5	1.598	16.52	2.46	4.80	1.95
PEA-PTEA-6	1.603	20.31	2.95	5.02	1.70
PEA-PTEA-7	1.608	21.73	2.72	4.87	1.79
PEA-PTEA-8	1.610	23.16	2.79	4.83	1.73
PEA-PTEA-9	1.612	25.63	2.82	5.27	1.87
P(PTEA)	1.620	27.11	5.17	9.77	1.89

The glass transition temperatures (T_g) of these polymers were determined using DSC, values are represented in Table 4.30. Figure 4.33 shows the DSC curves for various compositions of poly(PEA-*co*-PTEA) copolymers and corresponding homopolymers. The T_g values lie in the range of -3.0 to 27.1 °C. Most of the polymers have T_g blow 20 °C, which provides flexibility to the polymeric chain.

The weight-average (M_w) and number-average (M_n) molecular weights and the polydispersity indices (PDI) of all copolymers are presented in Table 4.30. The PDI of the polymers ranges between 1.70 and 1.96. The theoretical values of PDI for polymers produced via radical recombination and disproportionation are 1.5 and 2.0, respectively.

This suggests that polymers were produced mainly via termination of growing chain by disproportionation.

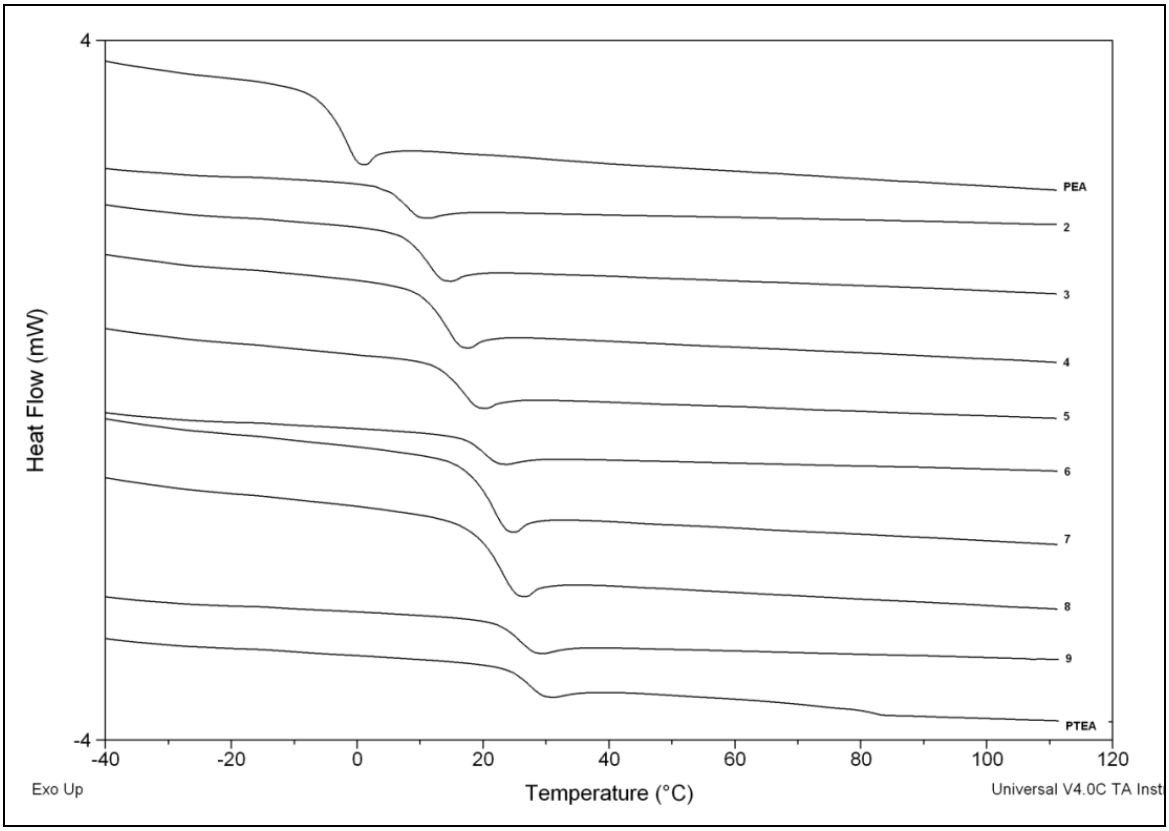

Figure 4.33: DSC thermograms of poly(PEA), poly(PTEA) and poly(PEA-*co*-PTEA)

UV-visible spectra of homopolymers and representative copolymers were acquired in solution. As can be observed in Figure 4.34 polymers exhibiting good transparency in visible region (wavelengths: 400-800 nm).

Thermal stability of the copolymers was measured by TGA under inert conditions, and the thermograms are presented in Figure 4.35. The copolymers underwent decomposition after ~300 °C. Except p(PEA) all polymers underwent two step decomposition.

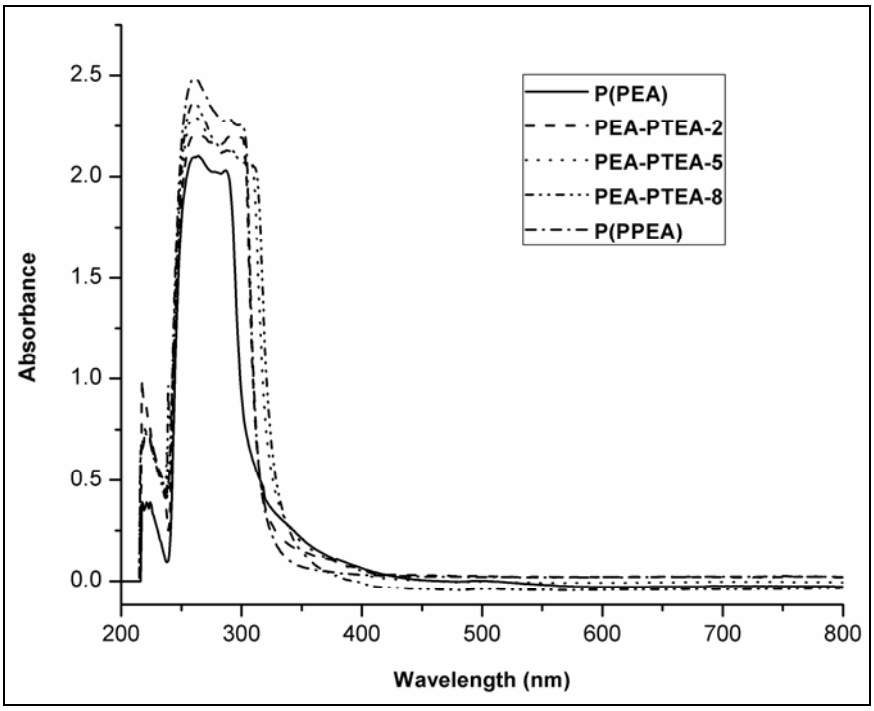

Figure 4.34: UV-visible spectra of poly(PEA), poly(PTEA) and poly(PEA-*co*-PTEA)

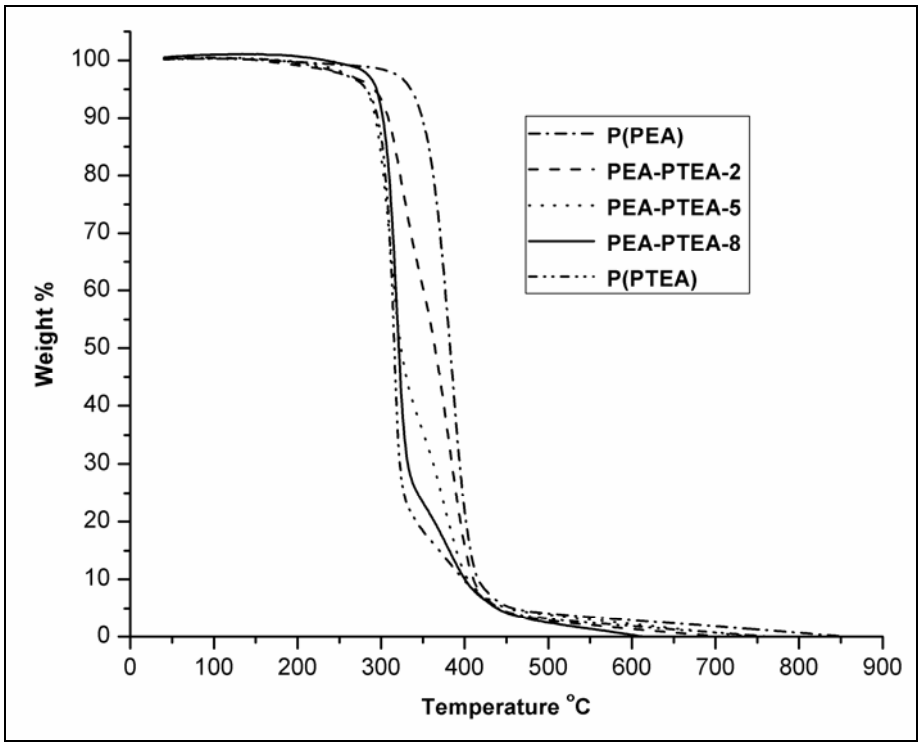

Figure 4.35: TGA thermograms of poly(PEA), poly(PTEA) and poly(PEA-*co*-PTEA)

4.9 Copolymerisation of 2-phenylethyl acrylate (PEA) and 2-phenyl-(2-phenylthio)ethyl methacrylate (PTEM)

4.9.1 Synthesis of poly(PEA-*co*-PTEM)

Copolymers of PEA with PTEM having different composition were synthesised in ethyl methyl ketone (EMK) solution using 2,2'-azobisisobutyronitrile (AIBN) as free radical initiator. The feed compositions of the monomers are presented in Tables 4.31. Appropriate quantities of the monomer, comonomer, EMK and AIBN (1 mol % of monomer) were taken in a polymerisation tubes and flushed with oxygen free nitrogen gas for 10 min. The tubes were tightly sealed and immersed in a thermostatic water bath at 70 °C. The reaction time was selected so as to yield moderate copolymer conversions in order to be within the realm of applicability of the differential copolymerisation equation. The conversions were controlled and determined by gravimetric measurements. After the reaction time, the copolymers were precipitated in methanol, filtered off, and purified by reprecipitations from chloroform solution into methanol and finally dried under reduced pressure for 24 h. Synthesis of the statistical copolymers, poly(PEA-*co*-PTEM), is depicted in Scheme 4.6.

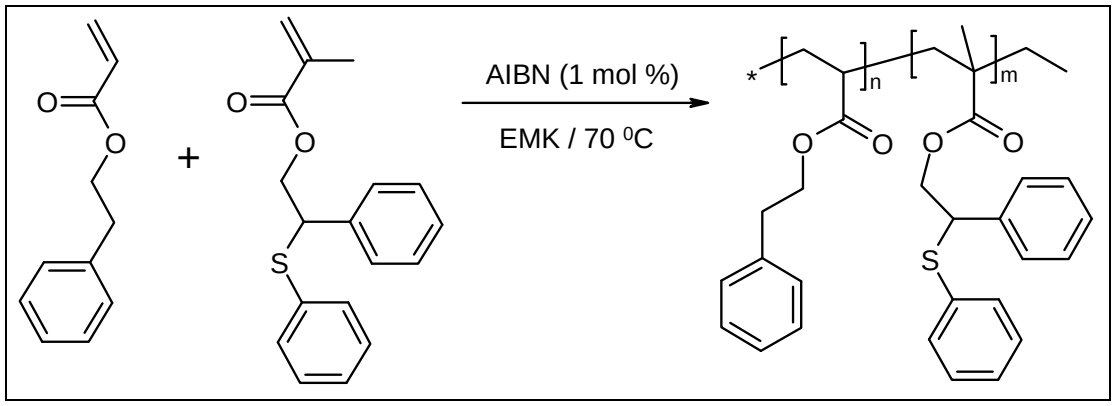

Scheme 4.6: Synthesis of poly(PEA-*co*-PTEM)

The copolymerisation of 2-phenylethyl acrylate with 2-phenyl-(2-phenylthio)ethyl methacrylate in EMK solution was studied in a composition interval with the mole fractions of PEA ranging from 0.1 to 0.9 in the feed.

The copolymers were soluble in solvents like tetrahydrofuran, dimethyl formamide, dimethyl sulphoxide, chloroform, methylene dichloride, toluene but were insoluble in hydrocarbons like n-hexane, petroleum ether and hydroxyl group containing solvents such as methanol, ethanol and 2-propanol.

Table 4.31: Composition data for copolymerisation of PEA with PTEM

Polymer Code	Mole fraction				Wight fraction conversion
	in feed		in polymer		
	M_1	M_2	m_1	m_2	
P(PEA)	1	0	1	0	-
PEA-PTEM-1	0.9002	0.0998	0.8287	0.1713	0.2745
PEA-PTEM -2	0.8005	0.1995	0.6897	0.3103	0.2503
PEA-PTEM -3	0.6996	0.3004	0.5639	0.4361	0.1131
PEA-PTEM -4	0.5975	0.4025	0.4438	0.5562	0.1660
PEA-PTEM -5	0.5103	0.4897	0.3916	0.6084	0.1529
PEA-PTEM -6	0.4274	0.5726	0.3148	0.6852	0.2031
PEA-PTEM -7	0.3187	0.6813	0.2347	0.7653	0.1188
PEA-PTEM -8	0.2089	0.7911	0.1446	0.8554	0.0982
PEA-PTEM -9	0.1378	0.8622	0.1051	0.8949	0.2337
P(PTEM)	0	1	0	1	-

The average compositions of copolymer samples were determined from the corresponding ^{1}H NMR spectra. The assignment of the resonance peaks in the ^{1}H-NMR spectra allows for the accurate evaluation of the content of both kinds of monomeric unit in the copolymer. The ^{1}H NMR spectra of the copolymers, poly(PEA-*co*-PTEM) are

shown in Figure 4.36. The mole fraction of PEA in the copolymer chains was calculated from the integrated intensities of aliphatic protons of both the monomeric units.

The peak at 2.8 ppm should be assigned to the methylene group (-CH_2-**CH_2**-Ph) of the PEA. The broad resonance observed at signal at 4.4 ppm is for the methylene proton (-CH-**CH_2**-O-) and methine protons (-S-**CH**(Ph)-CH_2-) of PTEM. Intensities of these well separated peaks were used to determine copolymer composition.

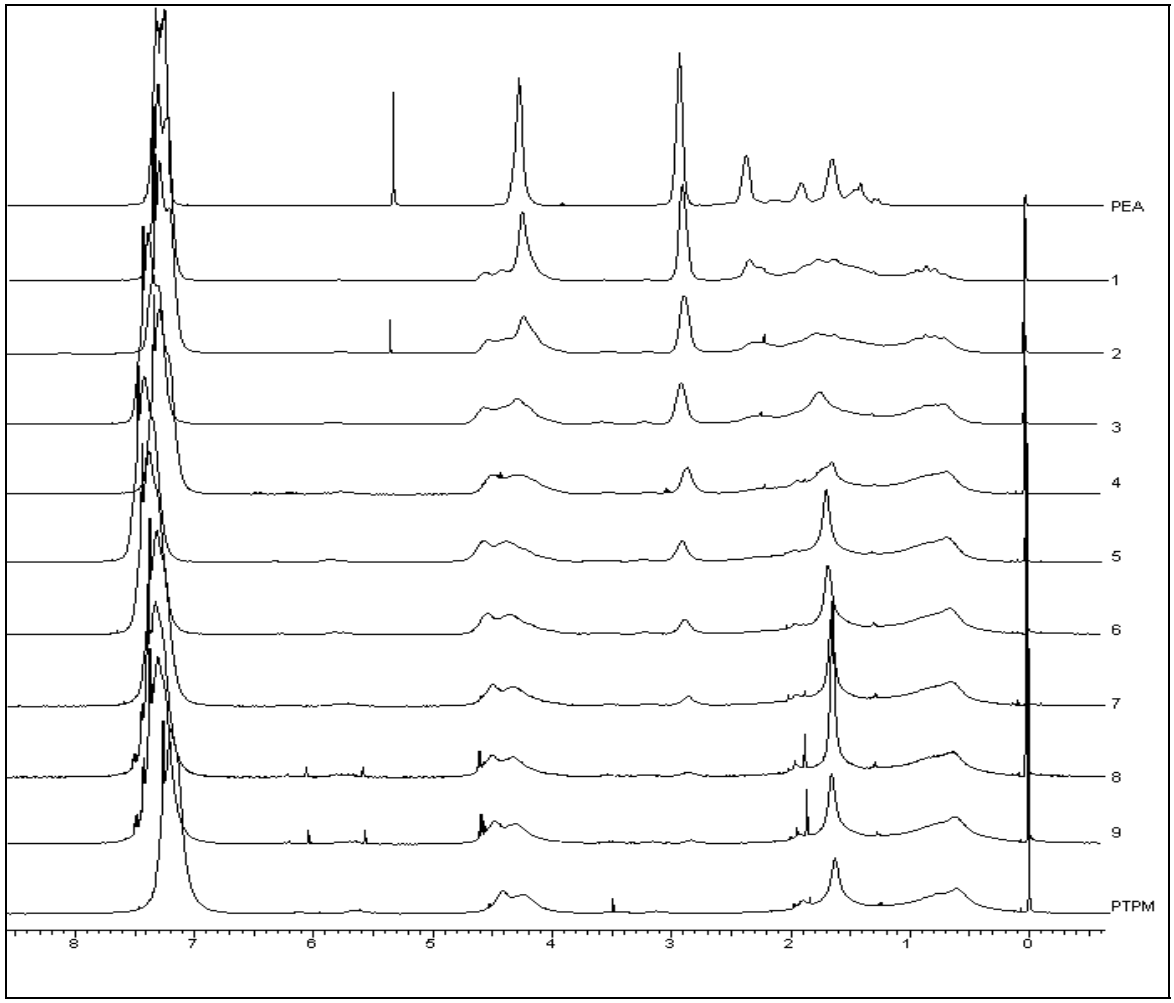

Figure 4.36: ^{1}H NMR spectra of poly(PEA), poly(PTEM) and poly(PEA-*co*-PTEM)

The following expression 4.46 is used to determine the composition of copolymers. Let F_1 be the mole fraction of PEA in copolymer.

$$F_1 = \frac{\int 2.8(-CH_2 - \underline{CH}_2 - Ph)/2}{\int 2.8(-CH_2 - \underline{CH}_2 - Ph)/2 \; + \; \int 4.4(\;)CH - \underline{CH}_2 - O-)/2} \qquad 4.46$$

The compositions of the poly(PEA-co-PTEM) copolymers assessed from ^{1}H NMR and gravimetrically determined weight fraction conversions are presented in Table 4.31.

4.9.2 Reactivity ratio determination for poly(PEA-*co*-PTEM) system

The knowledge of reactivity ratio is essential for the preparation of any copolymers having a definite composition. The reactivity ratios of PEA and PTEM were evaluated from the monomer feed ratios and the copolymer composition by the application of Finemann-Ross (FR), Kelen-Tudos (KT), extended Kelen-Tudos (Ex KT) and Mao-Huglin (MH) methods. The significance of the parameters of FR and KT for the copolymers is presented in Table 4.33 and that of extended KT is shown in Table 4.34. The reactivity ratios of PEA and PTEM are denoted as r_{PEA} (or r_1) and r_{PTEM} (or r_2) respectively and the values obtained from various methods are presented in Table 4.32.

Table 4.32: Reactivity ratios of PEA and PTEM computed by different models

Method	r_{PEA}	r_{PTEM}
Finemann-Ross	0.515	1.543
Kelen-Tudos	0.477	1.415
Extended Kelen-Tudos	0.419	1.428
Mao-Huglin	0.419	1.431
Average	0.458	1.454

The value of r_{PEA} is less than 1 and that of r_{PTEM} is greater than 1, which indicates presence of higher incorporation of PTEM units in the copolymer than feed. The product $r_{PEA} \times r_{PTEM}$ is less than 1, suggesting that there is a tendency for the formation of a random copolymer system.

Table 4.33: FR and KT parameters for the copolymerisation of PEA with PTEM

Polymer Code	$F=M_1/M_2$	$f=m_1/m_2$	$H=F^2/f$	$G=F(f-1)/f$	$\xi=H/(\alpha+H)$	$\eta=G/(\alpha+H)$
PEA-PTEM -1	9.0200	4.8387	16.8146	7.1559	0.8979	0.3821
PEA-PTEM -2	4.0125	2.2222	7.2452	2.2069	0.7912	0.2410
PEA-PTEM -3	2.3289	1.2931	4.1944	0.5279	0.6868	0.0864
PEA-PTEM -4	1.4845	0.7979	2.7619	-0.3761	0.5909	-0.0805
PEA-PTEM -5	1.0421	0.6438	1.6868	-0.5766	0.4687	-0.1602
PEA-PTEM -6	0.7464	0.4594	1.2127	-0.8783	0.3881	-0.2810
PEA-PTEM -7	0.4678	0.3067	0.7134	-1.0572	0.2717	-0.4026
PEA-PTEM -8	0.2641	0.1690	0.4126	-1.2983	0.1775	-0.5584
PEA-PTEM -9	0.1598	0.1174	0.2175	-1.2013	0.1021	-0.5640

Table 4.34: Extended Kelen-Tudos parameters for PEA-PTEM copolymer system

Polymer Code	ζ_1	ζ_2	Z	H	G	ξ	η
PEA-PTEM -1	0.4502	0.2415	0.4621	22.6617	8.3074	0.9076	0.3327
PEA-PTEM -2	0.3647	0.2020	0.4973	8.9847	2.4576	0.7957	0.2176
PEA-PTEM -3	0.1523	0.0846	0.5347	4.5222	0.5481	0.6621	0.0803
PEA-PTEM -4	0.2117	0.1138	0.5078	3.0942	-0.3980	0.5728	-0.0737
PEA-PTEM -5	0.1790	0.1106	0.5942	1.8235	-0.5995	0.4414	-0.1451
PEA-PTEM -6	0.2302	0.1417	0.5840	1.3471	-0.9257	0.3686	-0.2533
PEA-PTEM -7	0.1284	0.0842	0.6400	0.7488	-1.0832	0.2450	-0.3544
PEA-PTEM -8	0.1032	0.0661	0.6274	0.4294	-1.3245	0.1569	-0.4840
PEA-PTEM -9	0.2392	0.1757	0.7069	0.2350	-1.2485	0.0924	-0.4911

The graphical plots concerning the methods FR, KT and ex-KT are given in Figures 4.37 (a-c). The plots were linear in all cases and for all graphical methods, thus indicating that these copolymerisations follow conventional copolymerisation kinetics and that the reactivity of a polymer radical is determined only by the terminal monomer unit. As for some copolymers moderate yields were obtained, the extended KT and Mao-Huglin methods were employed as well. All methods provide similar data concerning the reactivity ratios for both monomers.

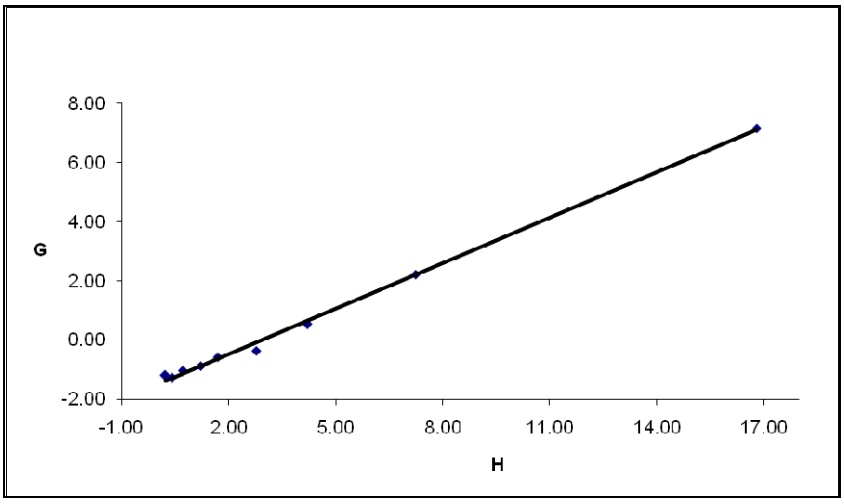

(a)

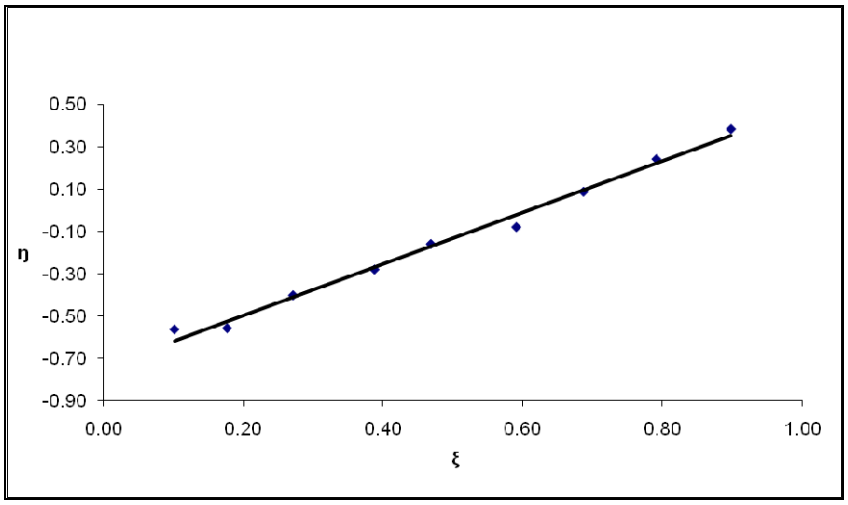

(b)

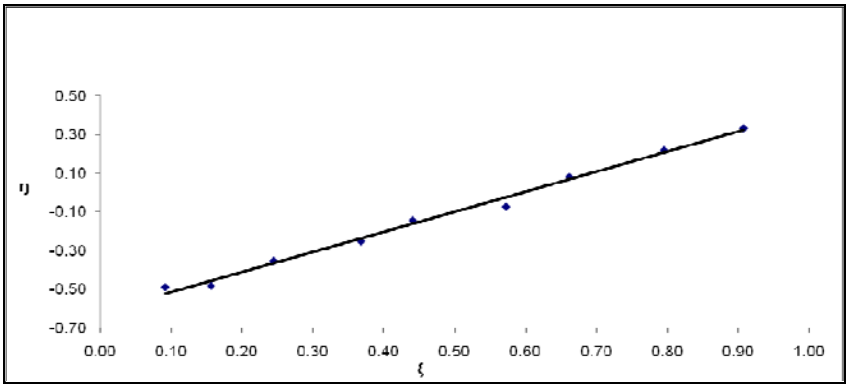

(c)

Figure 4.37: (a) FR, (b) KT and (c) Extended KT plots for the PEA and PTEM copolymer system

95 % joint confidence limit of the reactivity ratio values was calculated for Mao-Huglin method and has been plotted in Figure 4.38. Its equation is,

$$2.6328\ (r_1 - 0.4188)^2 - 1.3693\ (r_1 - 0.4188)\ (r_2 - 1.4305) + 0.5864\ (r_2 - 1.4305)^2 = 0.0060$$

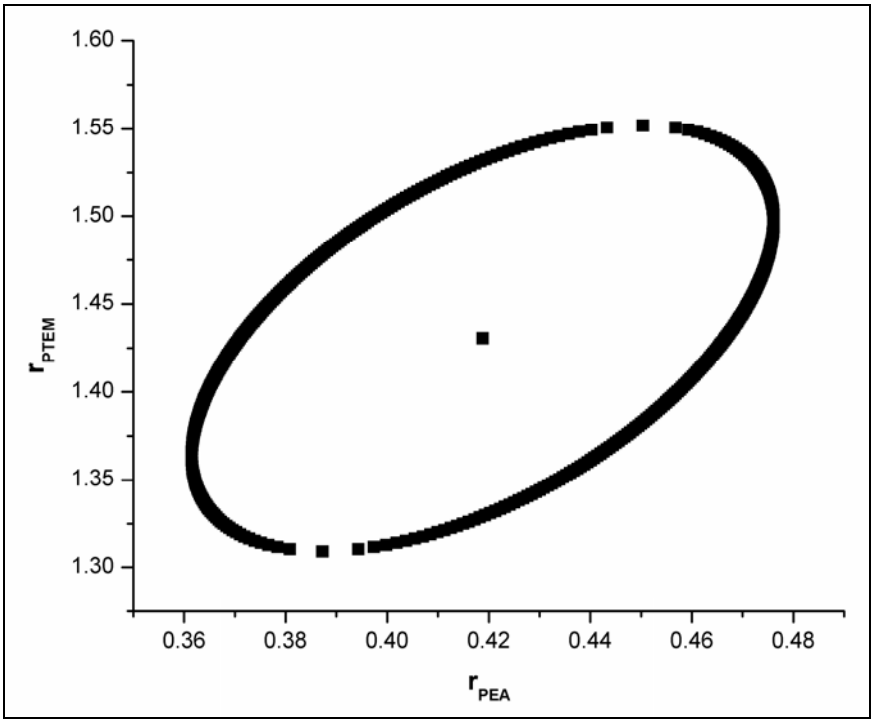

Figure 4.38: 95% Joint confidence interval of r_{PEA} and r_{PTEM} values by Mao-Huglin method for PEA-PTEM copolymer system

The statistical distribution of the dyad monomer sequences M_{PEA}-M_{PEA}, M_{PTEM}-M_{PTEM} and M_{PEA}-M_{PTEM} were calculated using the method proposed by Igarashi. Mean sequence lengths μ_{PEA} and μ_{PTEM} were also calculated. The data summarise in Table 4.35, and the variation of the dyad fractions with the PEA mole fraction in the copolymers is displayed in Figure 4.39.

Table 4.35: Structural data for poly(PEA-*co*-PTEM) system

Polymer Code	M_1-M_1	M_2-M_2	M_1-M_2	μ_{M1}	μ_{M2}
PEA-PTEM-1	0.6826	0.0251	0.2923	5.13	1.16
PEA-PTEM -2	0.4740	0.0947	0.4313	2.84	1.36
PEA-PTEM -3	0.3281	0.2002	0.4717	2.07	1.62
PEA-PTEM -4	0.2216	0.3341	0.4443	1.68	1.98
PEA-PTEM -5	0.1837	0.4004	0.4159	1.48	2.40
PEA-PTEM -6	0.1351	0.5055	0.3594	1.34	2.95
PEA-PTEM -7	0.0923	0.6229	0.2848	1.21	4.11
PEA-PTEM -8	0.0519	0.7627	0.1854	1.12	6.51
PEA-PTEM -9	0.0363	0.8261	0.1376	1.07	10.10

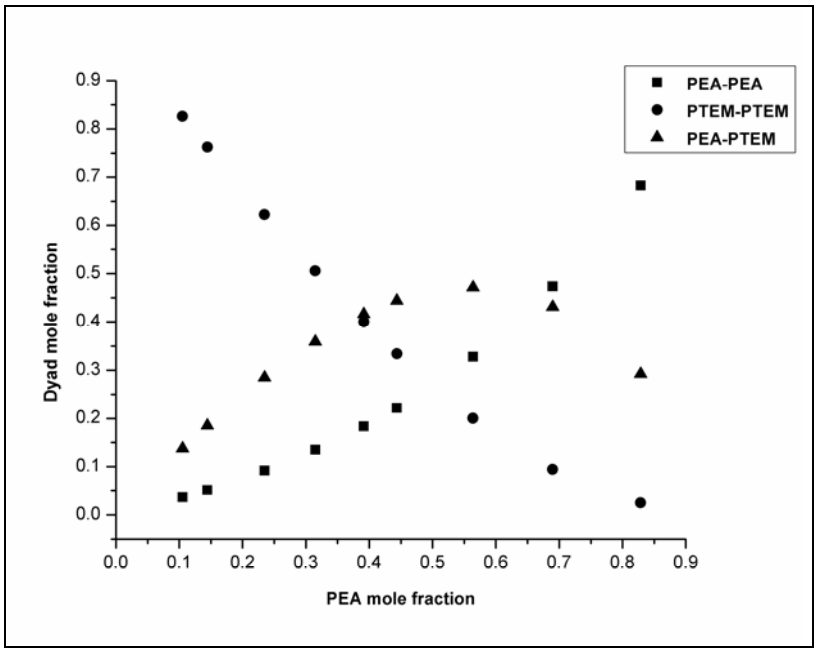

Figure 4.39: Dyad monomer sequence fractions versus PEA mole fraction for poly(PEA-*co*-PTEM)

4.9.3 Characterisation

All copolymers PEA and PTEM were analysed for refractive index, results are represented in Table 4.36. RI values are ranging from 1.550 to 1.668. The aromatic ring

and sulphur atom from PTEM contributed to increase the refractive index quite significantly.

Table 4.36: Refractive index, glass transition temperature and molecular weight data for poly(PEA), poly(PTEM) and poly(PEA-*co*-PTEM)

Polymer Code	R. I.	T_g (°C)	Molecular weight		P.D.I.
			M_n x 10^4	M_w x 10^4	
P(PEA)	1.550	-3.00	3.44	7.22	2.10
PEA-PTEM -1	1.565	15.63	2.744	6.01	2.19
PEA-PTEM -2	1.574	29.42	3.245	6.13	1.89
PEA-PTEM -3	1.586	38.85	4.579	8.10	1.77
PEA-PTEM -4	1.590	44.50	4.715	9.38	1.99
PEA-PTEM -5	1.589	52.54	3.672	7.27	1.98
PEA-PTEM -6	1.600	57.88	4.248	9.69	2.28
PEA-PTEM -7	1.612	61.21	5.894	10.90	1.85
PEA-PTEM -8	1.613	58.27	4.201	7.31	1.74
PEA-PTEM -9	1.617	57.62	4.514	9.21	2.04
P(PTEM)	1.618	68.55	5.106	9.24	1.81

Figure 4.40 shows the DSC traces obtained from homo and copolymers of PEA-PTEM. The results (Table 4.36) clearly indicate that T_g values of the copolymers mainly depend on the composition of comonomers and its value increases with increase in PTEM content in the copolymer.

The molecular weights [weight-average molecular weight (M_w) and number-average molecular weight (M_n)] and polydispersity indices for each synthesised copolymer are represented in Table 4.36. The values of number average and weight average molecular weights range from 27,440 to 58,940 and 60,100 to 1,09,000,

respectively. The polydispersity index of homo and copolymers varied in the range of 1.74 to 2.28.

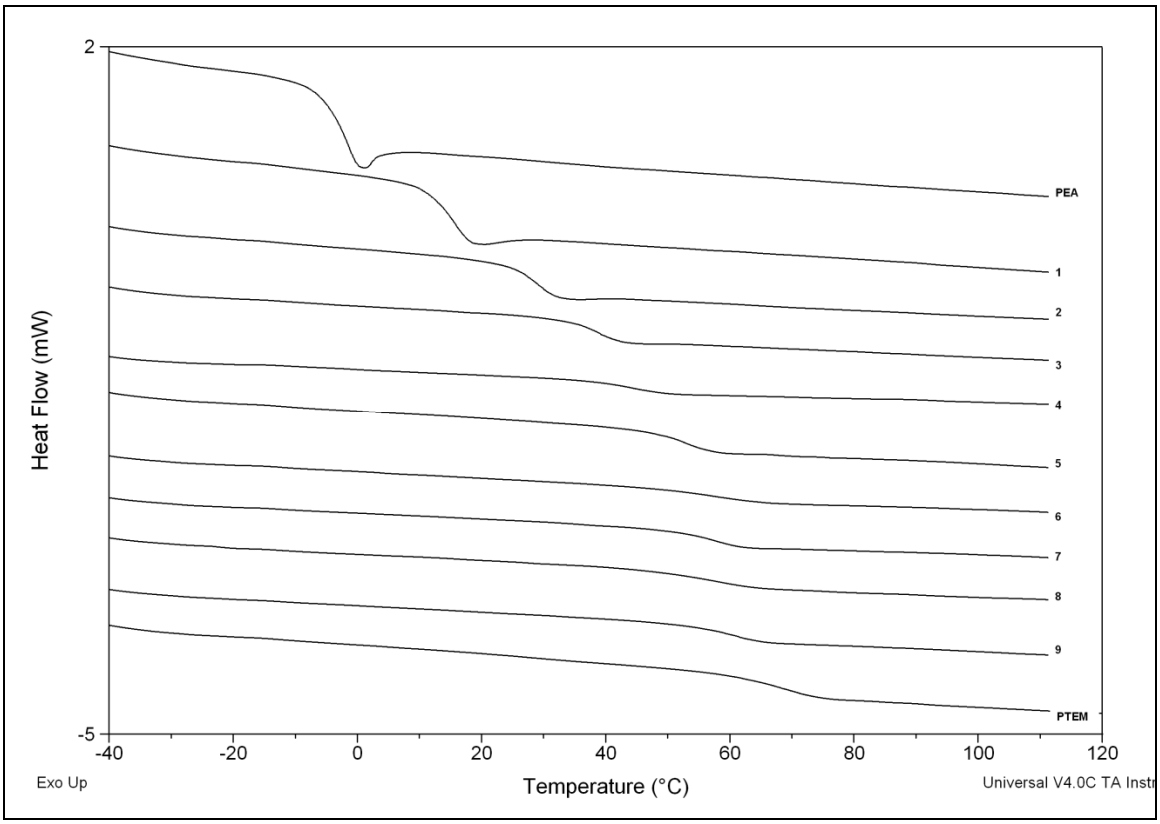

Figure 4.40: DSC thermograms of poly(PEA), poly(PTEM) and poly(PEA-*co*-PTEM)

Figure 4.41 shows UV-Visible absorption spectra of the homopolymers and representative copolymer solutions in chloroform. Clearly the polymers had no significant absorption in the visible region (in the wavelength range 200 - 800 nm).

The thermogravimetric curves for homopolymers and representative copolymers are shown in Figure 4.42. Results indicates that thermal stability of p(PEA) is higher than that of p(PTEM) and thermal degradation temperature of .copolymers shifted higher side as PTEM content increases in poly(PEA-*co*-PPEM)

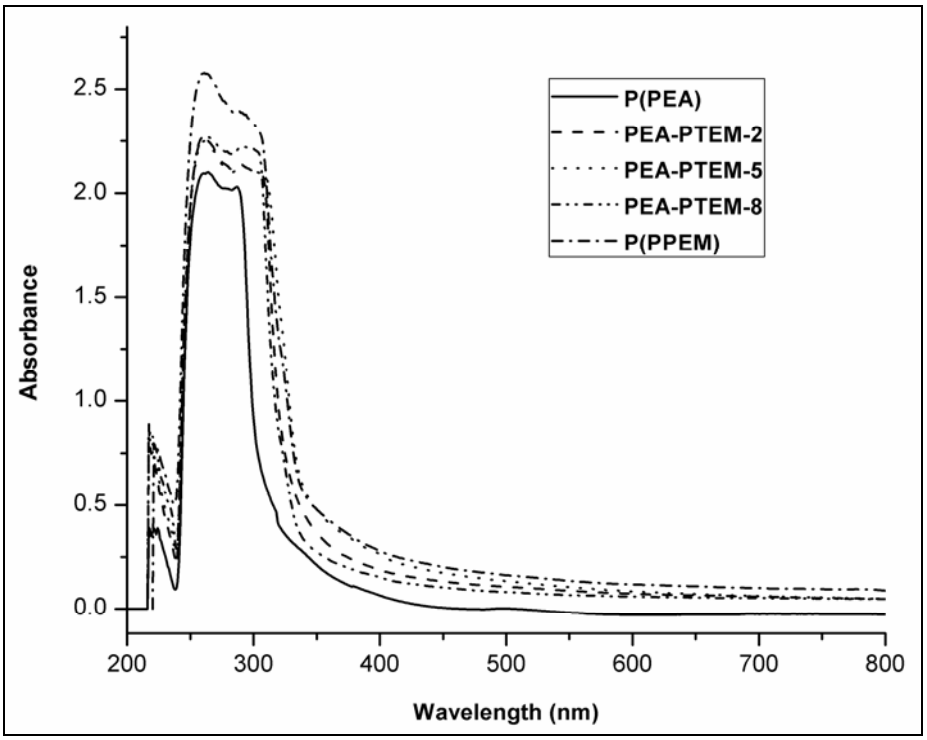

Figure 4.41: UV-visible spectra of poly(PEA), poly(PTEM) and poly(PEA-*co*-PTEM)

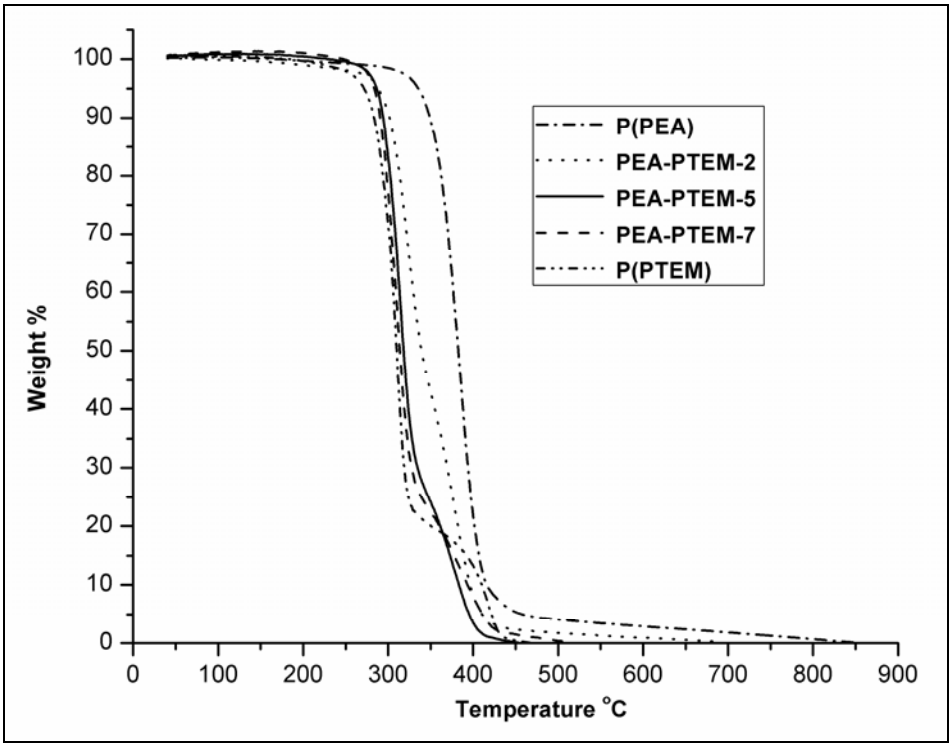

Figure 4.42: TGA thermograms of poly(PEA), poly(PTEM) and poly(PEA-*co*-PTEM)

4.10 References:

[1] D. A.Tirrell, *Copolymerization*. In *Encyclopedia of Polymer Science and Engineering;* H. F. Mark, N. M. Bikales, C. G. Overberger, G. Menges, Eds. Wiley-Interscience: New York, **1986**, 4, 192-233.

[2] C. L. McCormick, G. S. Chen, *Journal of Polymer Science: Polymer Chemistry Edition*, **1982**, 20,817-838.

[3] M. Hirooka, *Pure & Appl. Chem*., **1981**, 53, 681-690.

[4] Y. Shirota, M. Yoshimura, A. Matsumoto, H. Mikawa, *Macromolecules*, **1974**, 7, 1, 6.

[5] H. Hirai, *J. Macromolecular Sci.: Macromolecular Reviews*, **1976**, 11, 47-91.

[6] E. Tsuchida, T. Tomono, *Die Makromolekulare Chemie*., **1971**, 141, 265-298.

[7] M. Almgren, W. Brown, S. Hvidt, *Colloid. Polym. Sci*., **1995**, 273, 2-15.

[8] D. J. Meier, *J. Polymer Sci.: C*, **1969**, 26, 81-98.

[9] D. Cohn, H. Younes, *Journal of Biomedical Materials Research*, **1988**, 22, 993-1009.

[10] G. Moad, *Prog. Polym. Sci*., **1999**, 24, 81–142.

[11] R. Rengarajan, M. Vicic, S. Lee, *Journal of Applied Polymer Science*, **1990**, 39, 1783-1791.

[12] H. Staudinger, J. Schneiders, *J. Ann. Chim.* **1939,** *541*, 151.

[13] T. Alfrey, J. J. Bohrer, H. Mark, *Copolymerization*; Interscience: New York, **1952**.

[14] F. R. Mayo, F. M.Lewis, *J. Am. Chem. Soc.,* **1944,** *66*, 1594.

[15] C.Walling, *Free Radicals in Solution*, Wiley: New York, Chapter 4, **1957**.

[16] G. Odian, *Principles of Polymerization: 3rd Edition*; John Wiley and Sons Inc.: New York, **1991**.

[17] P. J. Flory, P. J. *Principles of Polymer Chemistry*; Cornell University Press: Ithaca, **1953**.

[18] Flory, P. J. *Principles of Polymer Chemistry*; Cornell University Press: Ithaca, **1953.**

[19] S. Ponrathnam, *Ph. D. Thesis,* **1976**.

[20] J. M. Gadgil, *Ph. D. Thesis,* **1993.**

[21] A. L. Polic, T. A. Duever, A. Penlidis, *J. Polym. Sci.: Part A,* **1998,** *36*, 813.

[22] G. B. Butier, J. T. Badgett and M. Sharabash, *J. Macromol. Sci. Chem.,* A **1970**, 4(1), 51-63.

[23] R. M. Joshi, S. G. Joshi, *J. Macromol. Sci. Chem*., **1971**, A5, 1329.

[24] R. M. Joshi, *J. Macromol. Sci. Chem*., **1973**, A7, 1231.

[25] M. Fineman, S. D. Ross, J. *Polym. Sci.,* **1950**, 5, 249.

[26] A. I. Yezrivlev, E. L. Brokhina, E. S. Roskin, *Vysokomol. Soedin*., **1969**, A11 (8), 1670-1679.

[27] T. Kelen, F. Tudos, B. Turcsanyi, *Polymer Bull.,* **1980,** *2*, 71-76.

[28] F. Tudos, T. Kelen, T. Foldes-Berezsnich, B. Turcsanyi, *J. Macromol. Sci.Part A* **1976,** *10*, 1513-1540.

[29] F. Tudos, T. Kelen, T. *J. Macromol. Sci.: Part A,* **1981,** *16*, 1283.

[30] T. Alfrey, Jr. J. J. Bohrer, H. Mark, *Copolymerization, Interscience, New York*, **1952.**

[31] P. W. Tidwell, G. A. Mortimer, *J. Polym. Sci.: Part A,* **1965,** *3*, 369.

[32] D. T. J. Hill, J. H. O'Donnell, *Makromol. Chem., Makromol. Symp.,* **1987,** *10/11*, 375.

[33] D. T. J. Hill, A. P. Lang, J. H. O'Donnell , P. W. O'Sullivan, *Eur. Polym. J.,* **1989,** *25*, 911.

[34] D. T. J. Hill, A. P. Lang, J. H. O'Donnell, *Eur. Polym. J.,* **1991,** *27*, 765.

[35] D. T. J. Hill, A. P. Lang, J. H. O'Donnell, *Eur. Polym. J.,* **1991,** *27*, 765-772.

[36] J. F. Kuo, C. Y. Chen, *J. Appl. Polym. Sci*., **1982**, 27, 2747-2750.

[37] R. Van Der Meer, H. N. Linssen, A. L. German, *J. polym. Sci. Polym. Chem*., **1978**, 16, 2915-2930.

[38] H. Patino leal, P. M. Rielly, *J. Polym. Sci. Polym. Lett. Ed*., **1980**, 18, 219-227.

[39] B. Yamada, M. Ytahashi, T. Otsu, *J. Polym. Sci. Polym. Chem. Ed*., **1978**, 16, 1719-1733.

[40] W. E. Wentworth, *J. Chem. Ed*., **1965**, 42, 96-103.

[41] D. R. Montgomery and C. R. Fry, *J. Polym. Sci.*, **1968**, C25, 59.

[42] T. Kelen, F. Tudos, *J. Macromol. Sci.-Chem.,* **1975**, A9, 1.

[43] J. P. Kennedy, T. Kelen, F. Tudos, *J. Macromol. Sci.-Chem*., **1975**, A13, 2277.

[44] R. Mao, M. B. Huglin, *Polymer,* **1993**, 34, 1709.

[45] F. Ziaee and M. Nekoomanesh, *Polymer,* **1998**, 39 (1), 203-207.

[46] S. Igarashi, *J. Polym. Sci. Polym. Lett. Ed.,* **1963**, 1, 359–363.

[47] H. G. Elias, *Macromolecules; Plenum Press: New York and London*, **1971**, 2, Chapter 22, 761.

[48] H. W. Melville, B. Noble, W. F. Watson *J. Polym. Sci.,* **1949**, 4, 629.

[49] J. P. Kennedy, T. Kelen, F. Tudos, *J. Polym. Sci.,* **1975**, A1, 2277.

[50] N. Jaacks, *Makromol. Chem.,* **1967**, 105, 289.

Chapter V

Bulk Polymer Networks

5.1 Introduction

In the eye, the crystalline lens provides the ability of focusing objects placed at different distances in a process referred as accommodation. The crystalline lens grows throughout life increasing in size and rigidity. Due to this growth, the accommodation capability decreases with age (presbyopia) and an external optical correction is often needed to focus at objects located at near distances. At the same time, the lens becomes gradually opacified causing what is known as cataracts. Cataract is the most common cause of visual loss in the world.[1] Aging or stress can change the morphology of the proteins, causing the natural lens to lose transparency. This loss in transparency is termed cataract formation. Cataract formation is irreversible and can eventually cause blindness. Cataract surgery is among the most common major surgical procedures performed on the elderly in developed countries. The technique consists of implanting an intraocular lens (IOL) after surgically removing the opacified or otherwise damaged natural crystalline lens.[2]

The natural crystalline lens is a precisely formed structure consisting of 65% water and 35% organic material (mostly structural proteins).[3] The proteins are structured in such a manner that there are negligible local variations in their density, resulting in a transparent material.[4] The natural lens has a refractive index of 1.42.

Intraocular lens (IOL) implantation is performed after cataract removal to replace the optical function of the natural lens. The first material used for IOL implantation was poly(methyl methacrylate) (PMMA). PMMA has good optical properties and is compatible with the tissues of the eye, but the glass transition temperature of PMMA makes it rigid at room temperature.

The incision to insert the optic is about 6-7 mm. The invention of phacoemulsification meant the natural lens could be liquefied and removed through a 1.5 mm incision.[22] Using a room temperature foldable material, the incision to implant the IOL could be made 3-4 mm in diameter, requiring no sutures. An increase of the refractive index is always desirable because it permits the manufacture of thinner IOL and the subsequent reduction in the size of the incision. As a result, various silicone, acrylate and hydrogel lenses have been developed for IOLs.

The goal of our studies was to synthesise hydrophobic, acrylic, foldable copolymers suitable for IOL applications. Acrylics were chosen as a starting point for foldable IOL materials. Because of its biocompatibility and good spectral transmittance, (meth)acrylate has been one of the most representative materials for ophthalmic devices, such as contact lens, intracorneal implants, and IOLs. To expand the medical application fields and improve their performances, it is very important to give these materials novel functional properties. The desired properties are low glass transition temperature (< 20 °C), high refractive index (1.55+), controlled unfolding rate (5 to 60 sec), and low equilibrium water content (< 1wt%).[6] Aromatic based (meth)acrylics were chosen because they exhibit the desired material properties.

Following points need to be considered in the development of polymers for intraocular lens material.

5.1.1 Monomer selection

A number of acrylic monomers are used for IOL fabrication.[5] Each monomer and its relative proportions affect the characteristics of the resulting polymer. A monomer is characterised by the presence of a polymeriasable functional group, C=C double bond.

Acrylate and methacrylate monomers are typically preferred over simple vinyl monomers for IOL fabrication because of their higher reactivity. Monomers possessing electron-rich aromatic moieties such as 2-phenylethyl acrylate exhibit greater refractive index values than non-aromatic monomer analogues.

5.1.2 Mechanical properties

The combinations of monomers with other constituents such as cross-linking entities determine the properties of the resultant copolymer. Depending on the combination, mechanical characteristics of the resulting material can affect ease of folding and subsequent unfolding time, stability of the lens after implantation, and sensitivity to changes in temperature. The mechanical parameters of hydrophobic IOL polymers are dependent on their glass transition temperature.[6-8] For poly(methyl methacrylate) (PMMA), T_g is higher than room temperature, but the T_g values of polymers used for hydrophobic acrylic IOLs are typically low (< 22 °C), thus ensuring easy manipulation such as flexing and rolling during the surgical procedure. At lower operating temperatures, some hydrophobic acrylic materials with higher T_g values can behave as rigid materials, in which case folding and compressing are more challenging. The structure of a particular monomer affects the magnitude of the polymer's T_g, whether it is composed of a single monomer, to form a homopolymer, or of combinations of monomers. For (meth)acrylate monomers, if the substituent 'R' group (Figure 5.1) has a chain structure, then its flexibility is approximately proportional to its length. This controls the T_g of the resulting polymer. For example, PMMA has a T_g of approximately 105 °C, but poly(ethyl methacrylate), with an extra carbon in the pendent chain, has a T_g of approximately 65 °C.[9] The use of monomers with different substituents is a

fundamental strategy employed by researchers to systematically control the T_g value while designing novel IOL materials.

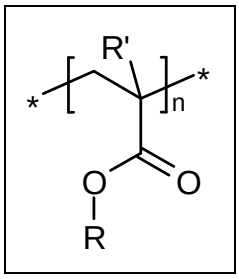

Figure 5.1: General structure of poly[(meth)acylate]

Acrylate monomers usually have lower T_g values than their methacrylate analogues,[9] due to the smaller hydrogen substituent on the reactive vinyl double bond. The consequence of using an acrylates monomer is that a polymer chain formed exclusively from the coupling of acrylate vinyl groups is minimally hindered from rotation, thus imparting a greater degree of chain flexibility. Through combination of otherwise structurally analogous methacrylate and acrylate monomers, the T_g of the resulting copolymer can be manipulated by adjusting the relative proportions of each component. The T_g for a methacrylate copolymer typically lies between that measured for the homopolymers of each component. The modulus or stiffness is also important in IOL materials design.

The modulus and its components such as elasticity and viscosity can be manipulated by selecting monomers that produce ease of folding of the material. The properties such as tensile strength and elongation affect the durability of the material, determining the degree of compression that can be achieved during injection. Despite the large role IOL design has on influencing incision size, it is ultimately the combination of the polymer's mechanical parameters that establishes the boundaries in which the lens

designer must work to minimise incision size. IOL polymer composition also influences how temperature changes affect mechanical behaviour.

Generally, materials become less pliable as temperature decreases; such is the case with hydrophobic acrylic polymers. The magnitude of the change in mechanical properties with variation in temperature is a function of the monomer and cross-linker composition.[6] Some polymers may show greater reduction in ease of folding and rate of unfolding than others at a particular temperature and this must be considered for surgical conditions. For example, it would be advantageous for the IOL polymer to be freely foldable at the likely temperature of the anterior chamber implantation.

5.1.3 Polymerisation techniques

Hydrophobic acrylic IOLs are manufactured by one of two methods: Either the lens optic is polymerised as a finished element (cast molding), or the lens is lathe cut to the required geometries from a larger polymer article (cryolathing). The latter process is performed at low temperatures to ensure that the material is kept below its T_g and therefore sufficiently rigid to accommodate precise machining. In either case, the polymer is formed through a free-radical polymerisation reaction. This reaction can lead to additional variations among the types of hydrophobic materials. Monomers play a crucial role in determining the structure of the polymer formed through any polymerisation process. All polymerisable components, including monomers and cross-linkers, have reactivity characteristics dependent on structural considerations. This reactivity is further influenced by the polymerisation condition and the presence of other components. Because more than one polymerisable component is always employed, the monomer constituents can be assembled into polymer chains exhibiting great

architectural diversity. In an ideal situation, the polymer units alternate consistently to create a regularly alternating copolymer. However, due to differences in the relative reactivity of the monomers at a set of polymerisation conditions, distribution of the monomer units tends to result in the formation of copolymer blocks that contain alternating segments composed of only one constituent monomer. When there is considerable disparity in the reactivity of the monomer components, these blocks may be large, affecting the properties of the polymer network.

The precise conditions of the polymerisation process, such as the amount of initiator and the delivery of activation energy (thermal or radiative: eg, ultraviolet light), contribute to the architecture, possibly leading to differences in the physical properties of the resultant polymer. Additionally, other differences in the nature of the monomers, such as polarity and solubility, can prevent the polymerised unimonomeric blocks from forming homogeneous blends. If blocks are formed from other monomer components, discrete immiscible phases may result, potentially affecting material properties, most notably optical clarity. The above considerations can also affect the degree of conversion of monomer units into the resulting polymer. The amount of residual monomer determines the viability of the resulting IOL.

5.1.4 Initiator

The free radical polymerisation is usually carried out in the presence of mono-functional initiator. The polymerisation rate is of first order with respect to the monomer concentration and half order with respect to the initiator concentration, while the degree of polymerisation is inversely proportional to the initiator concentration. It is the feature of traditional radical polymerisation that higher polymerisation rate and larger molecular

weight cannot be obtained simultaneously.[10,11] The initiator concentration and polymerisation temperature are primary factors regulating the polymerisation rate and molecular weight of the product. Increase in these factors will increase the polymerisation rate, but decrease the molecular weight. In the past few years, multifunctional initiators have provided a new route, as they allow higher polymerisation rate while increasing/ maintaining similar molecular weights in comparison to conventional mono-functional initiators.[12-15]

In the present study, a new bi-functional radical initiator, 2,5-dimethyl-2,5-di(2-ethylhexanoylperoxy)hexane (Luperox-256), has been used to initiate bulk free radical polymerisation. The decomposition route of Luperox-256 is shown in Scheme 5.1.

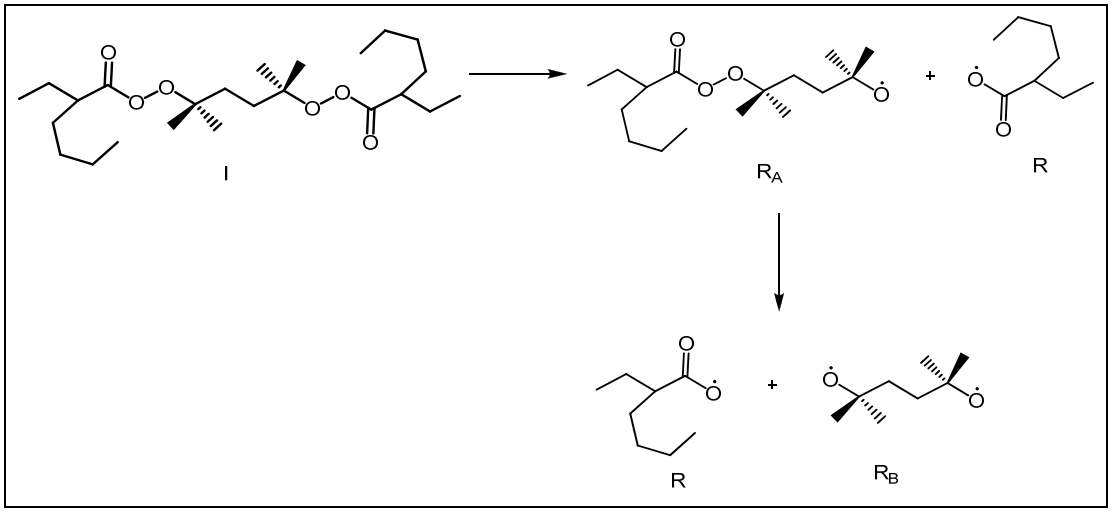

Scheme 5.1: Thermal decomposition route of Luperox-256

Luperox-256 decomposed thermally to generate two different primary radical species (R_A and R). The route of the peroxyester decomposition depends on the stability of each radical species produced by the above homolytic cleavage reaction. The radical species R_A containing undecomposed peroxide may decompose further to yield R and R_B. The primary radical species R and R_A may also undergo decarboxylation and β-scission

reaction, respectively. However, there will be no net change in the radical concentration as a result of such reactions. The peroxide groups are separated by a fairly long hydrocarbon segment so that the inductive effect may be negligible. The decomposition rate constant is unaffected by whether the neighbouring peroxide group has decomposed or not. The peroxide groups in the polymer chain ends have the same decomposition rate constant as the peroxide groups in the original bi-functional initiator, and may decompose to generate new radical species during the course of polymerisation.

5.2 Experimental

5.2.1 Materials

All new monomers were purified by column chromatography before use. Ethylene dimethacrylate (EGDMA) and hexanadiol dimethacrylate (HDDMA) were procured from Sigma Aldrich. 2,5-dimethyl-2,5-di(2-ethylhexanoylperoxy)hexane (Luperox-256), the thermal initiator, was procured from Arkema Inc. and used as received. 2-propanol (Merck) was used as received.

5.2.2 Polymerisation process

Polymer networks were prepared by radical copolymerisation of monomer combinations in the presence of cross-linker and bi-functional initiator. Monomer mixtures were weighed in centrifuge tubes and vortexed to allow the homogenisation. Nitrogen gas was bubbled through the mixture to remove most of the oxygen present. The mixtures were then syringed into glass moulds. Glass plates of the mould were separated by square shaped PTFE spacer of 0.5 mm thickness. The glass moulds were heated at 60 °C for 20 h followed by isothermally at 90 °C for 10 h to ensure complete polymerisation. Figure 5.2 illustrates the glass mould apparatus used for the bulk

polymerisation. After polymerisation, the cross-linked polymer networks were extracted using soxhlet extraction with 2-propanol to remove the unreacted monomers and oligomers until equilibrium was reached.

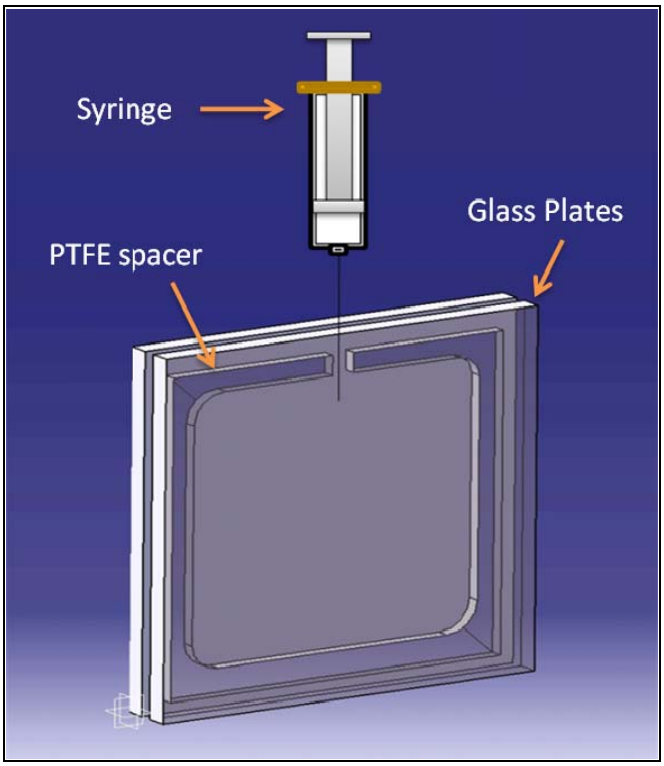

Figure 5.2: Bulk polymerisation mould

Block diagram describing the casting process for intraocular lens material is shown in Figure 5.3.

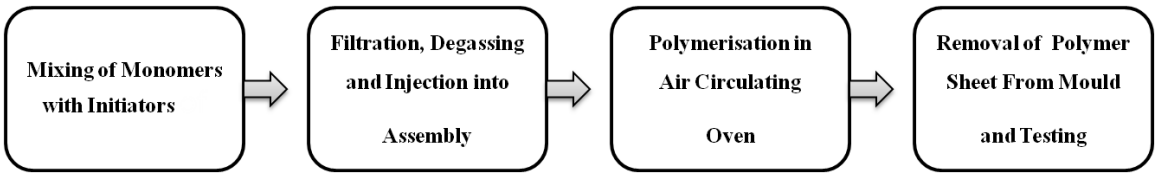

Figure 5.3: Block diagram describing the lens casting process

5.2.3 Characterisation techniques

5.2.3.1 IR spectroscopy

The IR spectra of monomers and the prepared samples were taken using a Fourier transform infrared (FT-IR) spectrophotometer (Perkin-Elmer) between 400 and 4000 cm^{-1}.

5.2.3.2 Differential scanning calorimetry (DSC)

Differential scanning calorimetry was performed on a TA Q100 DSC instrument to determine the glass transition temperatures (T_g) of the copolymers. All samples were run against an aluminium reference in crimped aluminium pans. A temperature range of -50 to 120 °C was used to determine the T_g. Two scans were performed on each sample at a heating rate of 10 °C/min. The second heating results were obtained in all cases.

5.2.3.3 Refractometry (R.I.)

Refractive index measurements were performed with an automatic refractometer, model PTR 46 X, from Index Instrument and calibrated with a standard. Each sample was allowed to equilibrate to 20 °C prior to the measurements. The measurements were done in triplicate and the average values recorded.

5.2.3.4 Transparency

The transparency of the polymer networks was measured with a Lambda-35 Perkin Elmer Ultraviolet-Visible spectrometer between 200 to 800 nm.

5.2.3.5 Monomer/Oligomer extraction

In bulk polymerisation, there will always be residual monomers at the end because a polymerisation reaction does not proceed to the point where exactly 100% of the monomer is converted. Residual monomers in the polymer film are a problem for two

reasons. First, any low molecular mass substances present in the polymer network, wherein the residual monomer, acts as a plasticiser. The rheological properties of the material will thus be different as compared to the same material without any residual monomers. Second, for medical applications like an IOL, a residual content of low molecular mass substances is potentially harmful because it will be released from the implanted IOL by diffusion. The residual monomer content of the cross-linked polymer networks made by chamber polymerisation was determined here.

Unreacted monomer and oligomer were removed by using soxhlet extraction. Each sample was placed between two cellulose extraction thimbles. The samples were weighed and the values recorded. The thimbles containing the sample were placed into a soxhlet extractor and the extractor placed on a 500 mL round bottom flask containing 250 mL 2-propanol. The 2-propanol was refluxed and the samples were extracted for 24 hours. Samples were then removed and dried in a vacuum oven at 65 °C for eight hours. Samples were weighed. This process was repeated until no further weight loss was evident; usually 24 hours.

5.2.3.6 Equilibrium water content (EWC)

Approximately 1g sample was cut from each polymer sheet and weighed dry. Samples were then placed in balanced salt solution (BSS) and allowed to hydrate for 24 hours. They were removed from the BSS, wiped dry, and the weights measured. The samples were rehydrated and measured again at five days. EWC was measured by the following equation 5.1:

$$EWC(wt\%) = \left[\frac{W_{wet} - W_{dry}}{W_{dry}} \right] \times 100 \qquad 5.1$$

where W_{wet} is the weight of wet specimen at equilibrium and W_{dry} is the initial weight of the dry specimen. In all the experiments a minimum of three samples were measured and averaged. The samples were allowed to hydrate until no further water uptake was observed.

Balanced salt solution (BSS) is a solution of sodium chloride (NaCl), potassium chloride (KCl), calcium chloride ($CaCl_2 \cdot 6H_2O$), magnesium chloride ($MgCl_2 \cdot 6H_2O$), sodium acetate ($C_2H_3NaO_2 \cdot 3H_2O$), and sodium citrate dihydrate ($C_6H_5Na_3O_7 \cdot 2H_2O$). BSS is isotonic to the tissues of the eyes.

5.2.3.7 Surface wettability (Water contact angle)

The contact angle measurement was performed to obtain the hydrophilicity/hydrophobicity of the lens materials. The basis of the contact angle measurement lies in the fact that the spreading of a drop on a surface is related to physical-chemical forces between the liquid and the material.[16] The sessile-drop method in air was used to quantify wetting ability, an indicator of hydrophilicity. The contact angle reading taken is the angle between the bordering surfaces, in this case formed between the IOL and the water surface. The wetting ability (and therefore hydrophilicity) is inversely proportional to the contact angle and to surface tension.

Water contact angles (CAs) of the copolymer networks were measured using the sessile drop technique in a contact angle measuring system Easy Drop (Kruss) using water as contact liquid at ambient humidity and temperature. Drops of deionised water ~1.0 μL in volume were applied to the sample surface. A minimum of 10 drops were applied on each sample.

5.2.3.8 Unfolding rate analysis

Three disk shaped samples of 10 mm in diameter and 0.5 mm thickness were cut from each polymer sheet. The sample was folded in half with a pair of forceps and placed on a horizontal surface to unfold at 37 °C. The amount of time for the polymer disc to return to its original shape was recorded. Each measurement was done three times and the average was taken.

5.2.3.9 Mechanical tensile testing

Mechanical tensile testing was performed on standard dumbbell-shaped specimens cut from the prepared 0.5 mm thick polymer sheets by a dumbbell-shaped cutting knife. A Linkam Tensile Stress Testing System – TST 350 was employed to measure the elastic modulus, failure strain, as well as the tensile strength of the networks with a constant extension rate of 1.0 mm/sec at 37 °C.

5.2.3.10 Thermogravimetric analysis (TGA)

The thermal stability of the copolymers was studied by thermogravimetric analysis (TGA) employing a STA 6000 TGA model from Perkin Elmer instruments. The samples were heated at a rate of 10 °C/min under nitrogen atmosphere.

5.2.3.11 Cytotoxicity

Biocompatibility is an important influencing factor for the application of copolymers in IOLs. Non-biocompatibility of IOLs could result in inflammatory response and posterior capsular opacification.[17] In order to test whether the prepared copolymers are cytocompatible or cytotoxic, cytocompatibility tests were performed with L929 mouse fibroblasts according to ISO protocol 10993-5.

The mouse connective tissue fibroblast cell line L929 (National Centre for Cell Science, Pune, India) was adopted and cultured in Dulbecco's modified Eagle's medium (DMEM) containing 10% fetal bovine serum (FBS), 100 U/mL penicillin, and 100 μg/mL streptomycin at 37 °C under a humidified atmosphere of 5% CO_2. For subculture, the cell monolayer was washed twice with phosphate-buffered saline (PBS) and incubated with trypsin-EDTA solution (0.05% trypsin, 0.25% EDTA) for 5 min at 37 °C to detach the cells. Cells were resuspended in culture medium and cocultured with the prepared copolymer networks in DMEM supplemented with 10% FBS for 7 days in a 24-well plate. The prepared disc of copolymer networks (10 mm diameter) were washed with ethanol in an ultrasonic cleaner and sterilised by autoclaving. The medium was changed every 2 to 3 days. Cultures were evaluated for cell viability/proliferation at days 1, 2, 3, 5 and 7 (MTT assay).[18] Cells were trypsinised, washed with phosphate-buffer saline, centrifuged at 5000 rpm, fixed on a glass slide and observed by Carl Zeiss Axio scope microscope to assess cell morphology. High density polyethylene (HDPE) and organo-tin poly(vinyl chloride) (PVC) films were used as negative and positive controls for cytotoxicity testing.

5.3 Synthesis of copolymer networks of 2-phenylethyl acrylate (PEA) and 2-phenoxy-2-phenylethyl acrylate (PPEA)

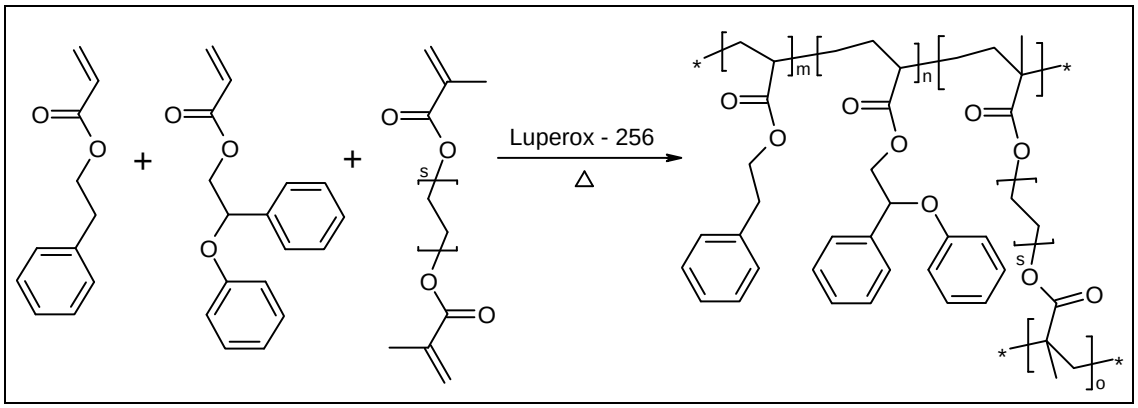

Scheme 5.2: Synthesis of poly(PEA-*co*-PPEA) bulk polymer networks

The synthetic method used to synthesise the poly(PEA-*co*-PPEA) copolymers is illustrated in Scheme 5.2. The poly(PEA-*co*-PPEA) networks were prepared by radical copolymerisation of 2-phenylethyl acrylate (PEA) and 2-phenoxy-2-phenylethyl acrylate (PPEA) in the presence of 2 mol % ethylene dimethacrylate (EGDMA) or hexanediol dimethacrylate (HDDMA) as a cross-linker and 0.2 mol% Luperox-256 as an initiator. The networks were prepared with varying molar ratios of PEA and PPEA. Monomers used and copolymerisation feed compositions are detailed in Table 5.1. Around 4 g monomer mixtures were weighed in centrifuge tubes and the appropriate amount of each component was added. Mixtures were vortexed for 60 seconds to allow the homogenisation. Nitrogen gas was bubbled through the mixtures to remove most of the oxygen present. Mixtures were then syringed into a glass molds. The glass molds were placed in an oven at 60 °C for 20 h followed by 90 °C for 10 h to ensure complete polymerisation. After polymerisation, the cross-linked poly(PEA-*co*-PPEA) networks were extracted using soxhlet extraction with 2-propanol to remove unreacted monomers and oligomers until equilibrium was reached.

5.3.1 IR spectroscopy

Comparison of spectra of the monomers with that of representative copolymer networks shows absorption peak of C=C double bond at 1637 cm^{-1} can be clearly observed in the monomers but disappears in the copolymer (Figure 5.4). This indicates that the C=C double bond was almost reacted during the polymerisation.

Table 5.1: Monomer compositions for PEA-PPEA bulk polymerisation system

Sr. No.	Code	PEA (mol %) A	PPEA (mol %) B	Cross-linker mol% (wrt. A+B)	% Wt. loss after solvent extraction
1	S1-EG-10	90	10	2 mol % EGDMA	1.2
2	S1-EG-15	85	15	2 mol % EGDMA	1.0
3	S1-EG-20	80	20	2 mol % EGDMA	0.9
4	S1-EG-25	75	25	2 mol % EGDMA	1.3
5	S1-EG-30	70	30	2 mol % EGDMA	1.1
6	S1-EG-35	65	35	2 mol % EGDMA	1.4
7	S1-EG-40	60	40	2 mol % EGDMA	1.2
8	S1-HD-20	80	20	2 mol % HDDMA	1.0
9	S1-HD-30	70	30	2 mol % HDDMA	0.9

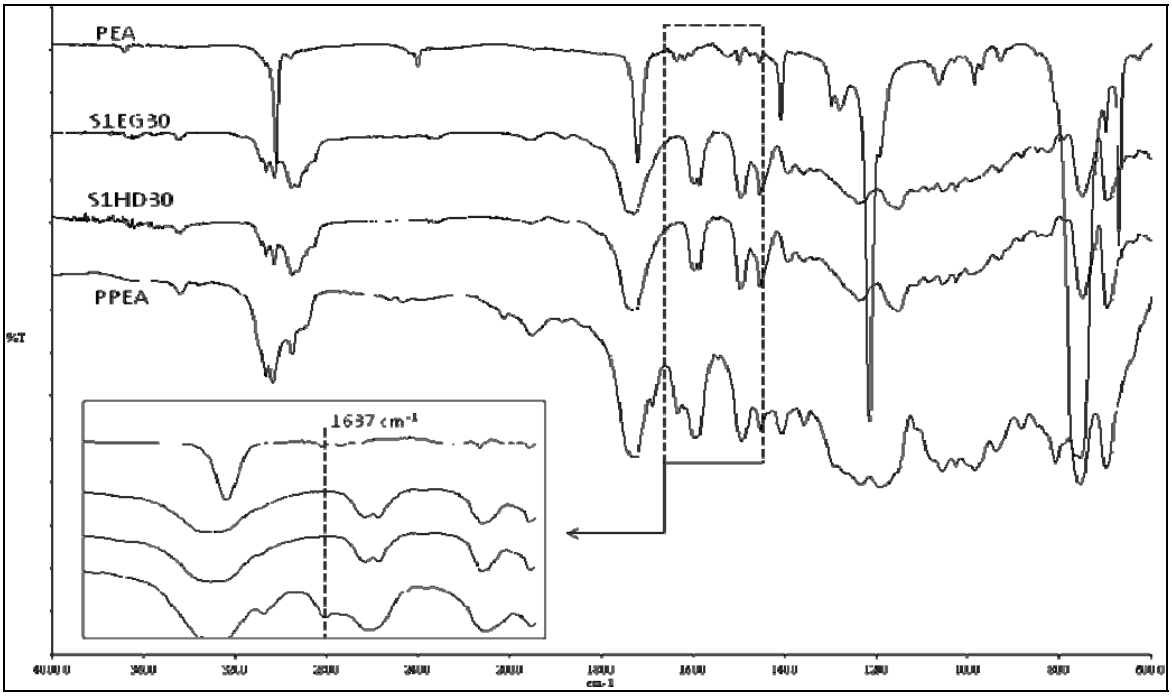

Figure 5.4: FT-IR spectra of PEA, PPEA and two poly(PEA-*co*-PPEA) networks

5.3.2 Differential scanning calorimetry (DSC)

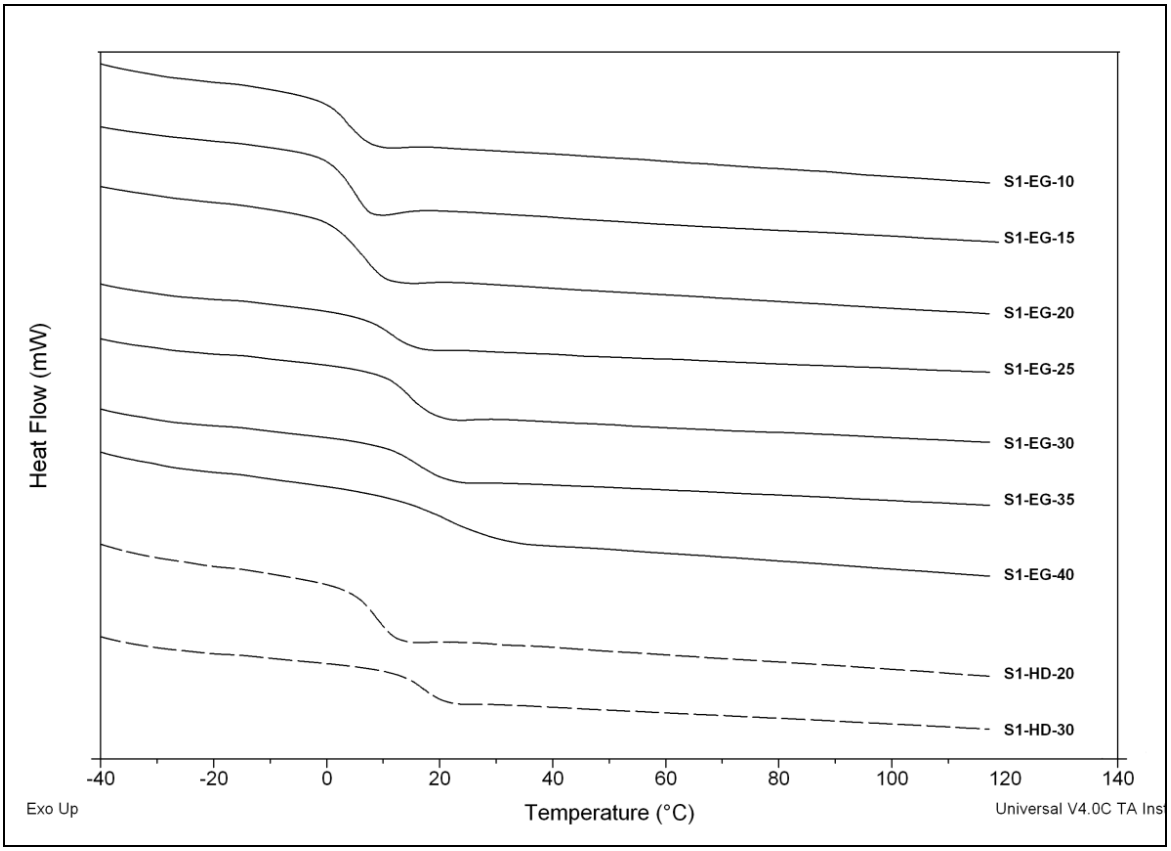

Figure 5.5: DSC thermograms of poly(PEA-*co*-PPEA) networks

Polymers based on (meth)acrylate monomers have potential for a broad range of thermo-mechanical properties, making them strong candidates for optical materials. As represented in Figure 5.5, with the increase of the concentration of PPEA monomer from 10 mol% to 40 mol%, the T_g of the copolymers increased from 5 to 18 °C. Copolymer networks with exorbitant T_g are not suitable for biomedical applications. In the subsequent study, to achieve an appropriate T_g of the prepared networks, the concentration of PPEA was determined to be 10 to 30 mol %.

Table 5.2: Refractive index, glass transition temperature, water contact angle and unfolding time of poly(PEA-*co*-PPEA) networks

Sr. No.	Code	R.I. (at 589 nm)	T_g (°C)	Contact Angle	Unfolding Time (sec)
1	S1-EG-10	1.560	3.53	76.01	4
2	S1-EG-15	1.562	5.03	78.01	4
3	S1-EG-20	1.564	6.84	79.80	6
4	S1-EG-25	1.566	11.45	80.90	8
5	S1-EG-30	1.568	14.79	81.31	11
6	S1-EG-35	1.570	15.75	81.87	16
7	S1-EG-40	1.572	21.49	82.16	-
8	S1-HD-20	1.563	8.73	79.28	7
9	S1-HD-30	1.566	16.89	82.91	14

5.3.3 Refractometry (R.I.)

Table 5.2 shows the values of the Refractive Indices of poly(PEA-*co*-PPEA) networks. RI of copolymers increases from 1.560 to 1.571 with the increase in the concentration of PPEA. The high RI of the copolymer networks are due to the high RI of PEA and PPEA because materials with aromatic ring structures always have higher RI.

5.3.4 Transmittance

The spectral transmittance of the poly(PEA-*co*-PPEA) networks is represented in Figure 5.6. Most of the copolymer networks have excellent optical transparency, and their spectral transmittance is higher than 85% in the visible wavelength region of 400-800 nm. Figure 5.7 shows the pictures of the prepared networks.

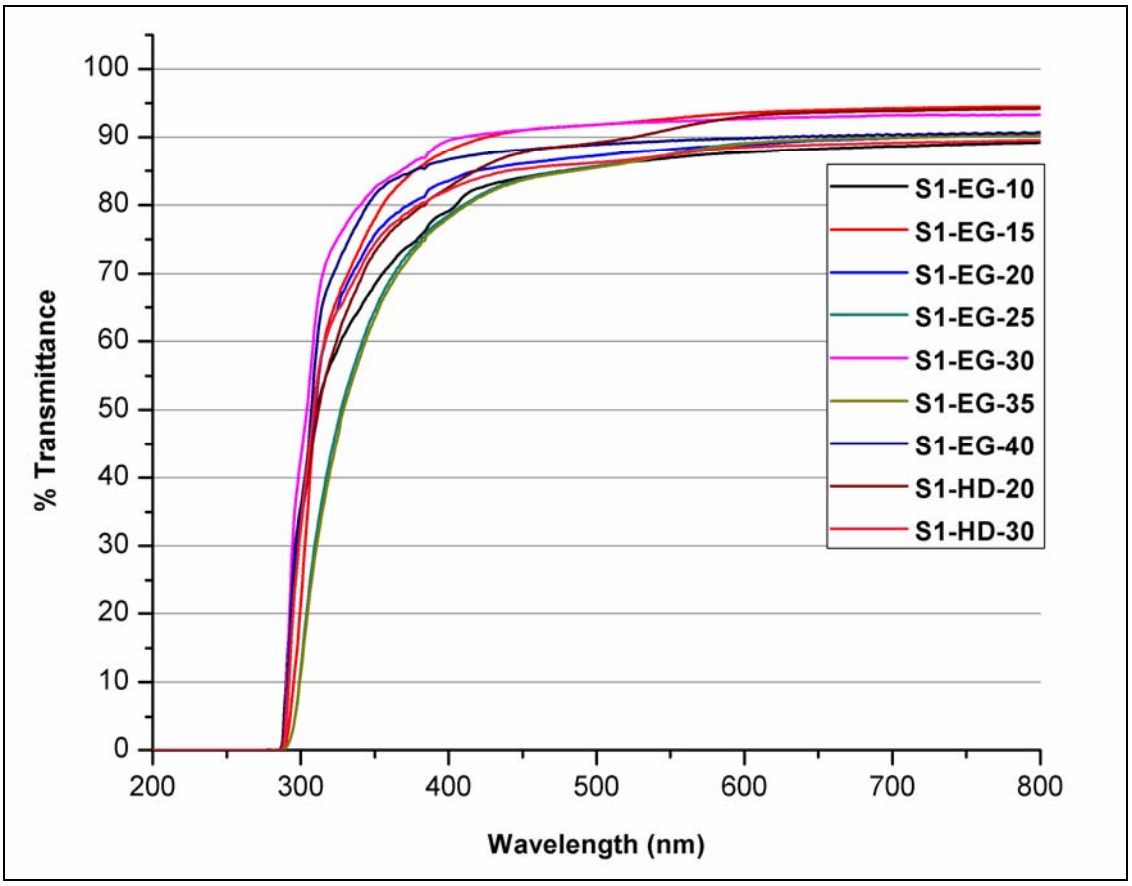

Figure 5.6: Spectral transmittance of poly(PEA-*co*-PPEA) networks

Figure 5.7: Pictures of prepared poly(PEA-*co*-PPEA) networks

5.3.5 Equilibrium water content (EWC)

The EWC of the all copolymers ranged from 0.1%-0.3% (Figure 5.8). These materials are hydrophobic in nature, so low EWC values were expected. The EWC values were measured on day 1 and day 5 after immersion into Balanced Salt Solution. No increase in EWC was seen after day 1.

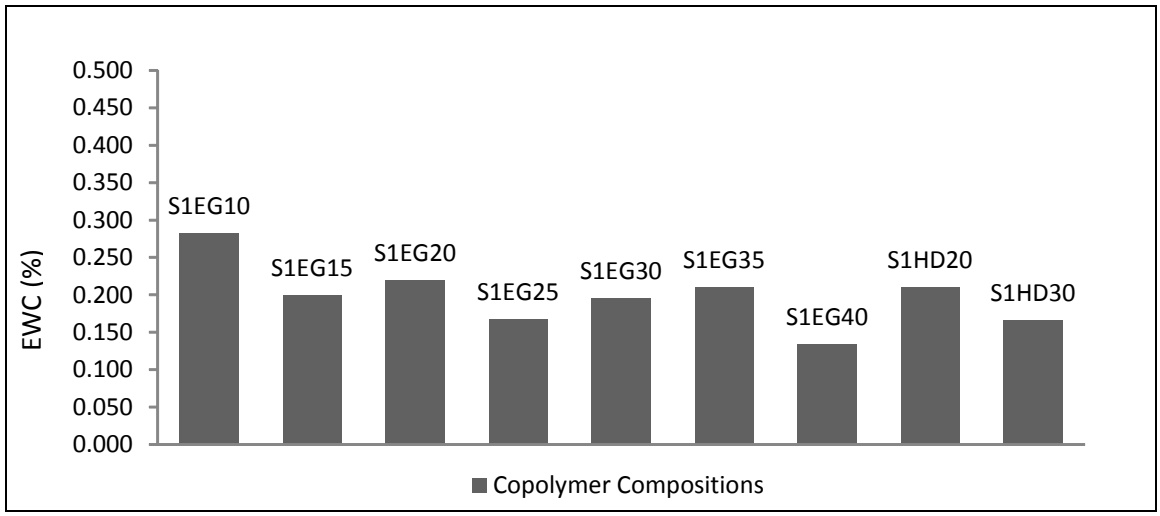

Figure 5.8: Equilibrium water content of poly(PEA-*co*-PPEA) networks

5.3.6 Water contact angle

S1-EG-10	S1-EG-20	S1-EG-30
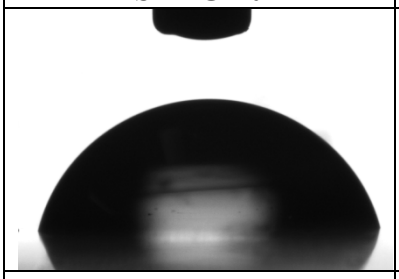	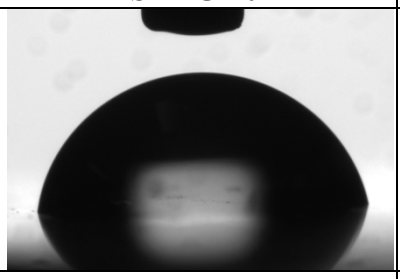	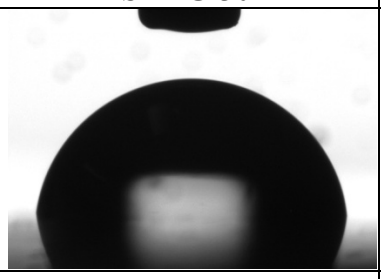
76.22°	79.60°	82.39°

Figure 5.9: Water drop profiles of representative poly(PEA-*co*-PPEA) networks

Water contact angles of the prepared copolymer networks, presented in Table 5.2, ranges from 76.01 to 82.91°. CA values indicated that hydrophobicity increased with the PPEA content in copolymer, due to higher aromatic character. Figure 5.9 shows the water

drop profiles on the three representative samples S1-EG-10, 20, and 30 with their CA values. These results are comparable to those marketed hydrophobic acrylic IOLs, whose CA generally ranges from 65 to 85°.[19,20]

5.3.7 Unfolding rate analysis

The acceptable values for IOL unfolding times are 5 to 60 sec. The main concern is the IOL optic will unfold too rapidly and rupture the posterior capsule, creating unnecessary complications. For this reason, extremely long and short unfolding times are not favourable. Unfolding time for synthesised bulk polymer networks are presented in Table 5.2. The times measured were within the acceptable range. The S1-EG-10 composition tended to adhere to itself for a brief moment before unfolding. Sample S1-EG-40 was brittle and difficult to fold.

5.3.8 Mechanical tensile testing

Figure 5.10 shows the stress plotted against its respective % strain determined from the mechanical tensile test. The tensile behaviour was measured at 37 °C, which is beyond the T_g of the networks. Table 5.3 represents values of Young's Modulus at 100% strain, strength at failure strain and % elongation of synthesised polymer networks. The failure strain decreases as the elastic modulus increases, whereas the tensile strength increases as the elastic modulus increases. In the ophthalmic application, high failure strain is more important than high tensile strength. This is because large deformation of the network is required to achieve a small incision size, whereas the stress generated from the eyeball is minimal. As a result, polymer networks with low elastic modulus and relatively high failure strain are very suitable for IOL.

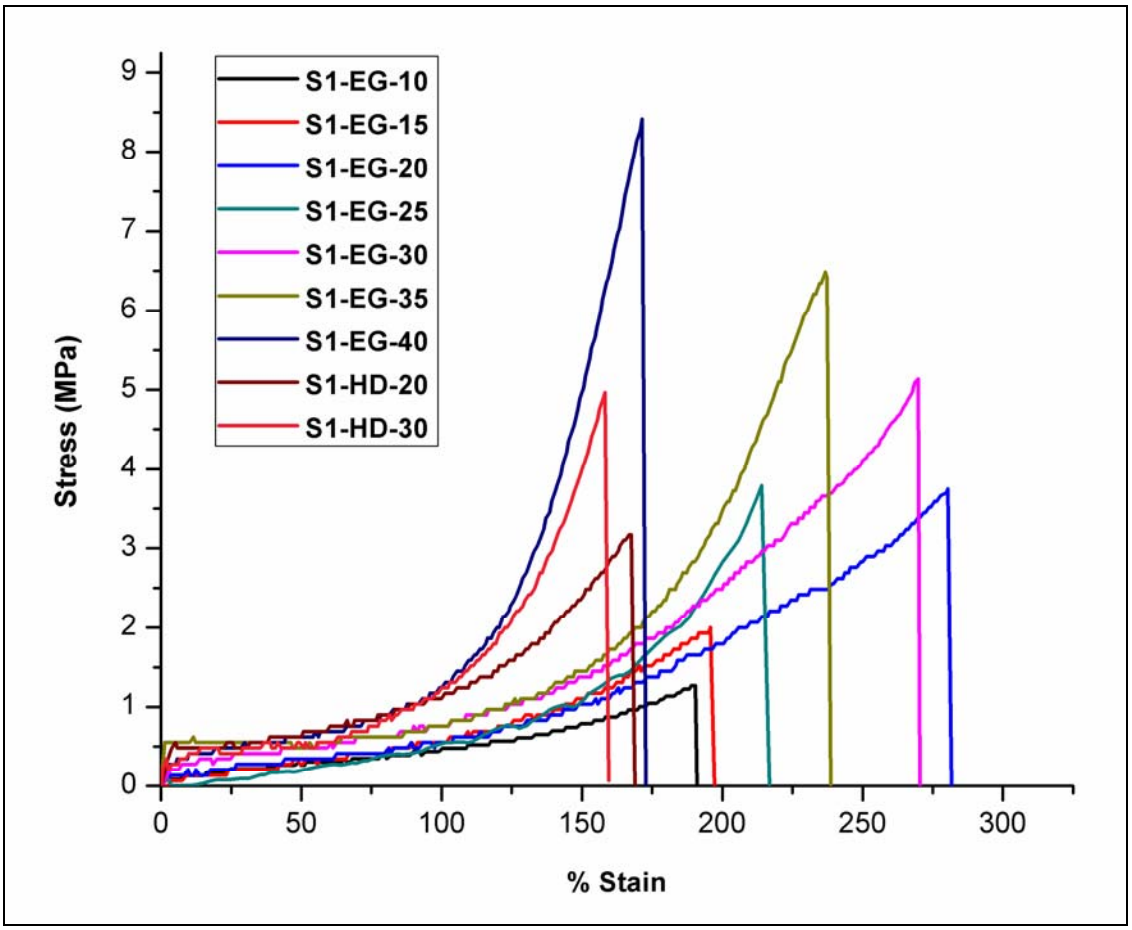

Figure 5.10: Stess vs strain curves for poly(PEA-*co*-PPEA) networks

Table 5.3: Mechanical tensile testing parameters for poly(PEA-*co*-PPEA) networks

Code	Young's Modulus at 100 % strain (MPa)	Strength at failure strain (MPa)	% Elongation
S1-EG-10	0.003	1.27	190
S1-EG-15	0.005	2.00	196
S1-EG-20	0.004	3.74	280
S1-EG-25	0.005	3.79	214
S1-EG-30	0.005	5.14	270
S1-EG-35	0.002	6.41	237
S1-EG-40	0.008	8.41	171
S1-HD-20	0.007	3.17	168
S1-HD-30	0.007	4.97	158

5.3.9 Cytotoxicity

Cytotoxicity of the prepared polymer networks to L929 mouse fibroblasts was tested. L929 mouse fibroblasts were cultured for 7 days in direct contact to the networks. The effects of the networks on cell morphology were investigated by Carl Zeiss Axio scope microscope. Figure 5.12 shows the microscopy images taken in bright field at 10X magnification obtained after incubation with polymer networks, in comparison with the negative control and positive controls. Live L929 mouse fibroblast adherent cells can propagate to a confluent monolayer with increase in the culture time, as can be seen from those of negative control. The death of the cell is observed using a positive control, the open area between cells indicates that cell lysis has occurred. In contrast, the fibroblast L929 cells incubated with polymer networks maintain their morphology typical of L929. No cell debris and no detachment from dish bottom is observed. Results regarding cell viability (MTT assay) of cultures are shown in Figure 5.11. L929 cells presented a high proliferation rate throughout the culture time. At early incubation times, that is, day 1, values of MTT reduction were similar in seeded networks and negative controls, suggesting an identical number of attached cells, whereas the cell viability of the positive control went down to ~19 % in one day and almost to 0 % in two days. On day 7, the cell viability was stable (almost 100 %) for the negative control, whereas for the networks, it was a bit lower than that of the negative control and much higher than that of the positive control. These results suggested a lack of Cytotoxicity of polymer networks developed in this study, which was critical for their biomedical application in the reduction of inflammatory response and PCO.

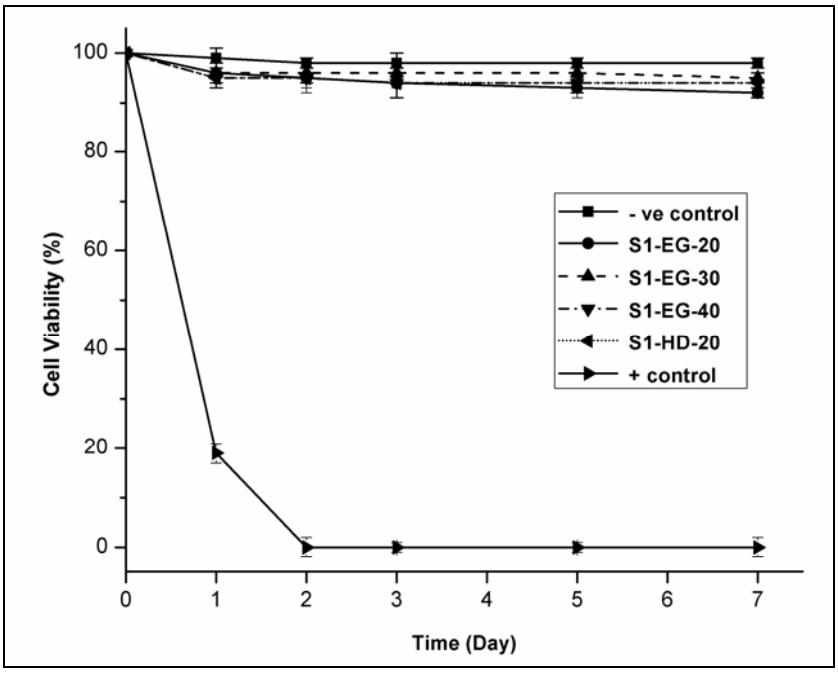

Figure 5.11: Cell viability of L929 mouse connective tissue fibroblasts as the result of MMT assay for representative poly(PEA-*co*-PPEA) networks with possitive and negative controls

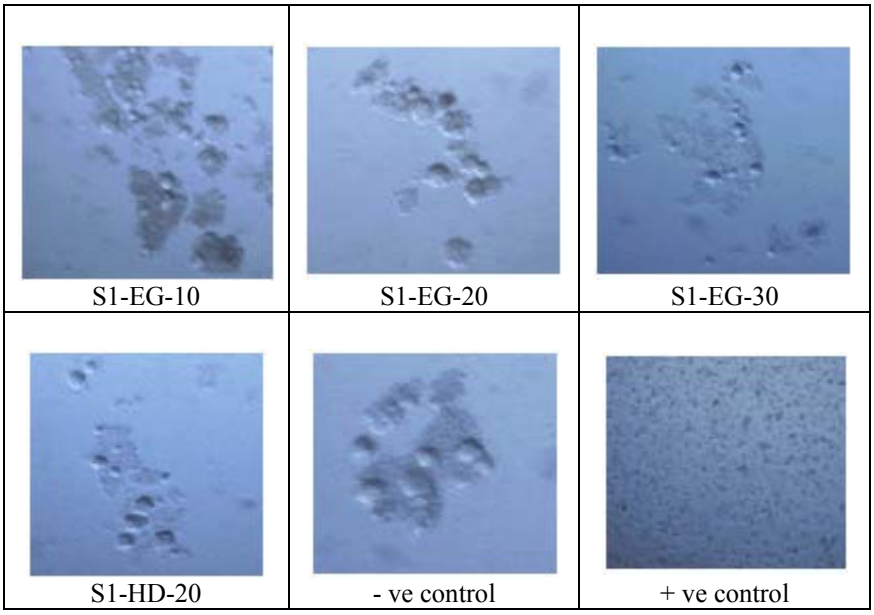

Figure 5.12: Carl Zeiss Axio scope microscopy images taken on day 7 showing the morphology of L929 mouse connective tissue fibroblast cocultured with four representative poly(PEA-*co*-PPEA) networks and controls.

5.3.10 Thermogravimetric analysis (TGA)

The thermal degradation of copolymers were characterised using TGA under nitrogen atmosphere. The TGA curves (Figure 5.13) clearly indicates that all polymers undergo single step degradation. In all polymers the weight loss was found to occur in a single step, starting at ~300 °C.

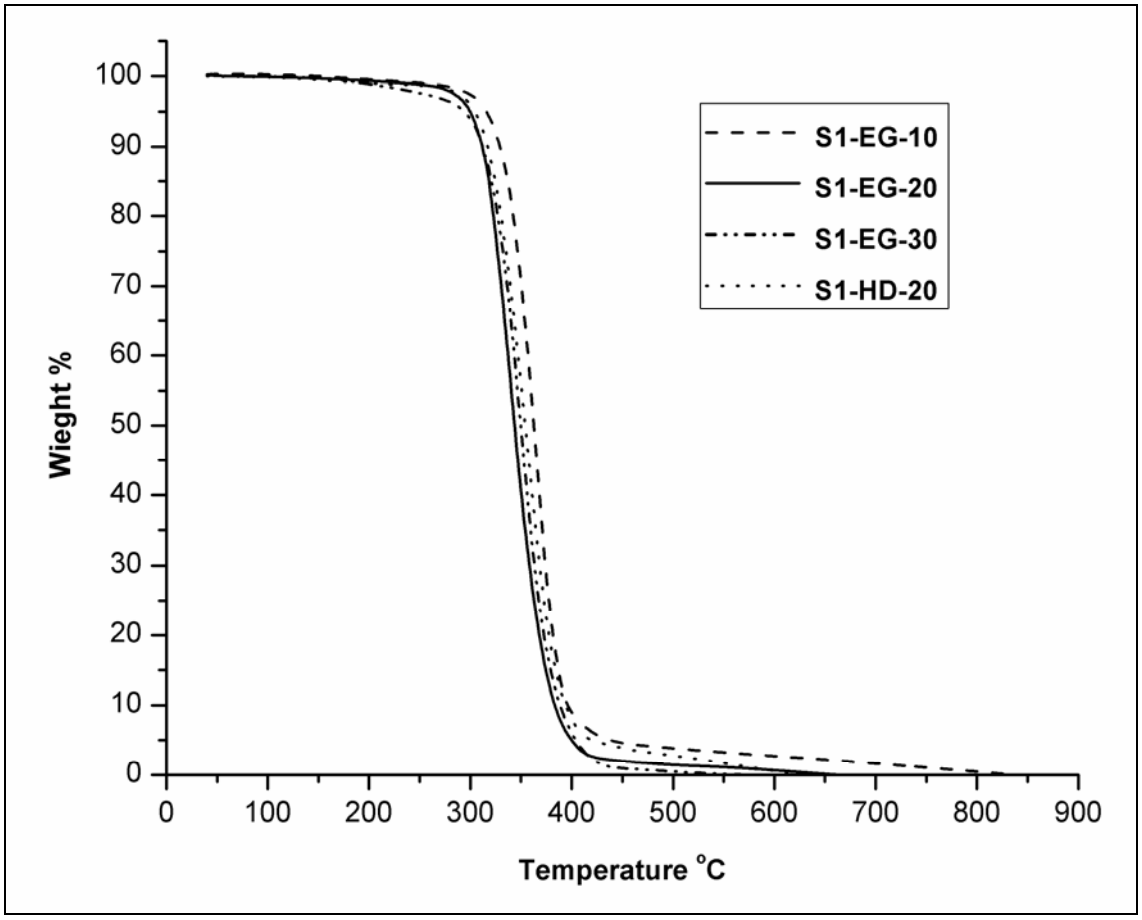

Figure 5.13: TGA thermograms for representative poly(PEA-*co*-PPEA) networks

5.4 Synthesis of copolymer networks of 2-phenylethyl acrylate (PEA) and 2-phenoxy-2-phenylethyl methacrylate (PPEM)

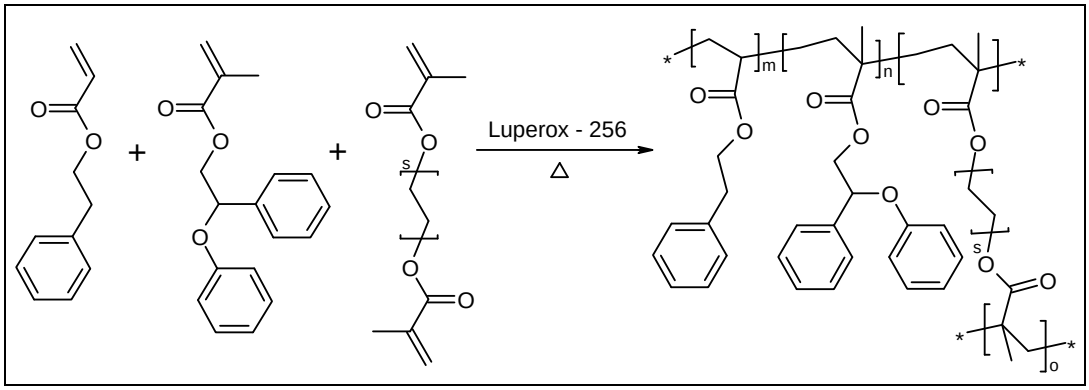

Scheme 5.3: Synthesis of poly(PEA-*co*-PPEM) bulk polymer networks

The synthetic method used to synthesise the poly(PEA-*co*-PPEM) copolymers is illustrated in Scheme 5.3. The poly(PEA-*co*-PPEM) networks were prepared by radical copolymerisation of 2-phenylethyl acrylate (PEA) and 2-phenoxy-2-phenylethyl methacrylate (PPEM) in the presence of 2 mol % ethylene dimethacrylate (EGDMA) or hexanediol dimethacrylate (HDDMA) as a cross-linker and 0.2 mol% Luperox-256 as an initiator. The networks were prepared with varying molar ratio of PEA and PPEM. Monomers used and copolymerisation feed compositions are detailed in Table 5.4. Around 5 g monomer mixtures were weighed in centrifuge tubes and the appropriate amount of each component was added. Mixtures were vortexed for 60 seconds to allow the homogenisation. Nitrogen gas was bubbled through the mixtures to remove most of the oxygen present. Mixtures were then syringed into glass molds. The glass molds were placed in an oven at 60 °C for 20 h followed by 90 °C for 10 h to ensure complete polymerisation. After polymerisation, the cross-linked poly(PEA-*co*-PPEM) networks were extracted using soxhlet extraction with 2-propanol to remove unreacted monomers and oligomers until equilibrium was reached.

5.4.1 IR spectroscopy

The FTIR spectra of two representative copolymers with different cross-linkers, as well as the corresponding monomers are represented in Figure 5.14. The absorption peak of C=C double bond at 1637 cm^{-1} can be observed clearly in the monomers, but disappears in the copolymers, which indicates that the C=C double bonds were almost exhausted during the polymerisation.

Table 5.4: Monomer compositions for PEA-PPEM bulk polymerisation system

Sr. No.	Code	PEA (mol %) A	PPEM (mol %) B	Cross-linker mol% (wrt. A+B)	% Wt. loss after solvent extraction
1	S2-EG-10	90	10	2 mol % EGDMA	1.1
2	S2-EG-15	85	15	2 mol % EGDMA	0.9
3	S2-EG-20	80	20	2 mol % EGDMA	1.1
4	S2-EG-25	75	25	2 mol % EGDMA	1.2
5	S2-EG-30	70	30	2 mol % EGDMA	1.0
6	S2-EG-40	60	40	2 mol % EGDMA	1.3
7	S2-HD-20	80	20	2 mol % HDDMA	0.8
8	S2-HD-30	70	30	2 mol % HDDMA	0.9

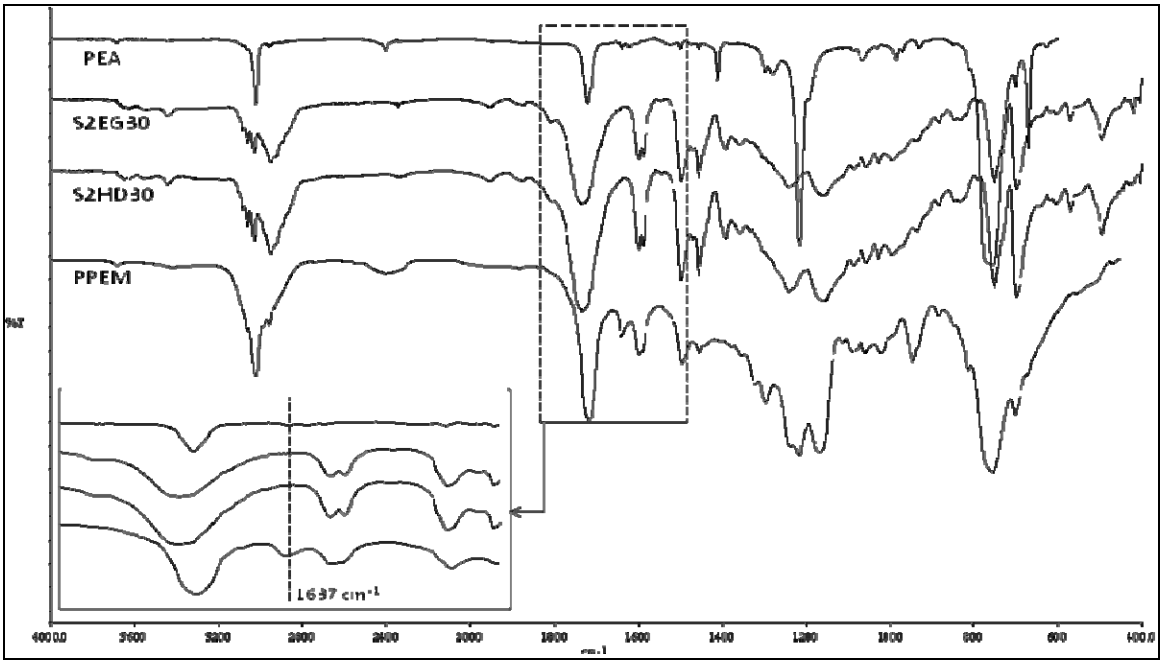

Figure 5.14: FT-IR spectra of PEA, PPEM and two poly(PEA-*co*-PPEM) networks

5.4.2 Differential scanning calorimetry (DSC)

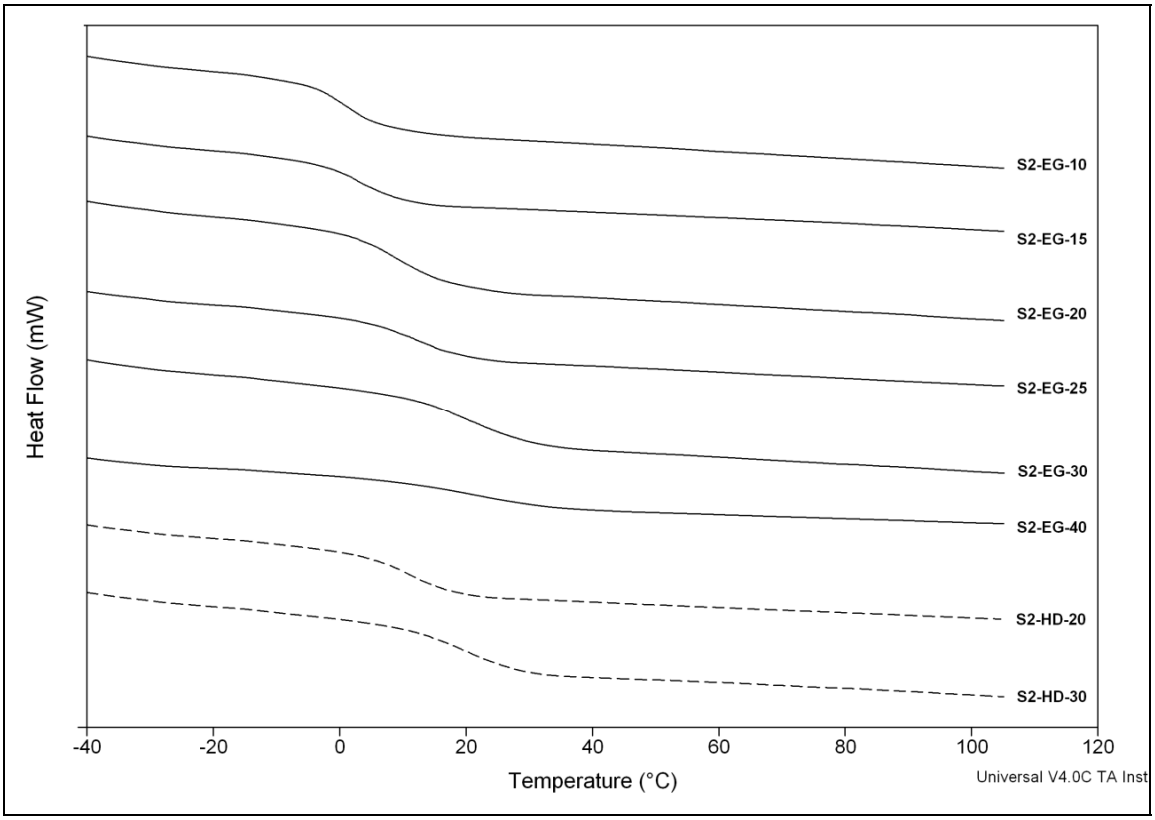

Figure 5.15: DSC thermograms of poly(PEA-*co*-PPEM) networks

Generally, the T_g increased as the rigidity in the molecule increased or by the addition of an α-methyl group. As shown in Figure 5.15 and Table 5.5, with the increase of the concentration of PPEA monomer from 10 mol% to 40 mol%, the T_g of the co-polymers increased from 1 to 21 °C. This is due to the fact that the asymmetrically substitution of the methyl group on the quaternary carbon in the main chain and aromatic rings in pendent group increases the steric hindrance and the internal rotation of the molecular chain is hindered. Copolymer networks with exorbitant T_g are not suitable for biomedical applications. In the subsequent study, to achieve an appropriate T_g (20 °C) of the prepared networks, the concentration of PPEM was determined to be 10 to 30 mol %.

Polymer T_g values higher than 20 ^oC are not suitable due to the rigid nature of the material at operating room temperatures.

Table 5.5: Refractive index, glass transition temperature, water contact angle and unfolding time of poly(PEA-*co*-PPEM) networks

Sr. No.	Code	R.I. (at 589 nm)	T_g (°C)	Contact Angle	Unfolding Time (sec)
1	S2-EG-10	1.558	1.53	76.86	3
2	S2-EG-15	1.561	2.82	78.26	5
3	S2-EG-20	1.563	8.42	81.74	8
4	S2-EG-25	1.566	13.52	82.53	10
5	S2-EG-30	1.567	18.70	83.03	16
6	S2-EG-40	1.572	21.21	85.01	-
7	S2-HD-20	1.562	11.18	79.32	7
8	S2-HD-30	1.566	19.59	83.65	17

5.4.3 Refractometry (R.I.)

Table 5.5 represents the values of the refractive indices of poly(PEA-*co*-PPEM) networks. RI of copolymers increases from 1.558 to 1.572 with the increase in the concentration of PPEM. The high RI of the copolymer networks are due to the high RI of PEA and PPEM because materials with aromatic ring structures always have higher RI.

5.4.4 Transmittance

After the polymerisation of PEA-PPEM systems, the transparent copolymers were obtained. The spectral transmittance of the poly(PEA-*co*-PPEM) networks is represented in Figure 5.16. The transmittances of copolymers are over 80 % in the visible light range. Figure 5.17 shows the pictures of transparent disc shaped prepared networks.

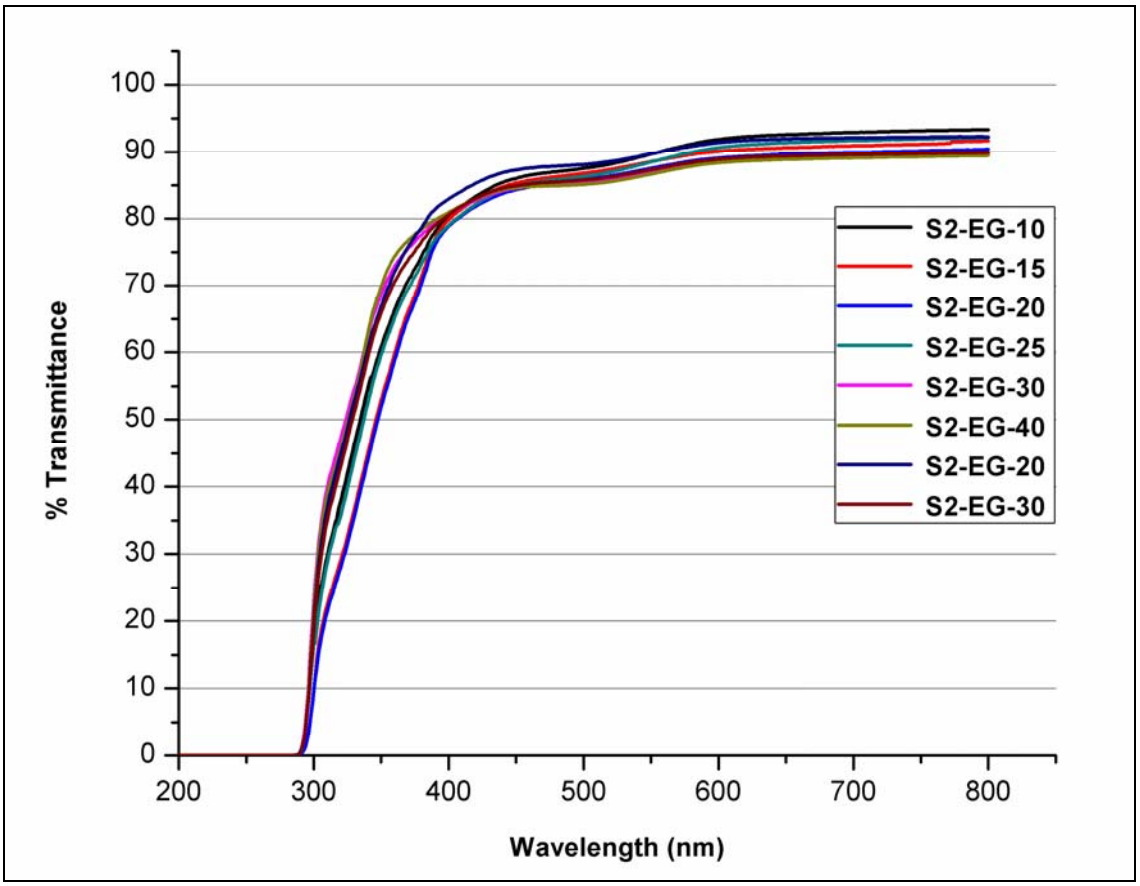

Figure 5.16: Spectral transmittance of poly(PEA-*co*-PPEM) networks

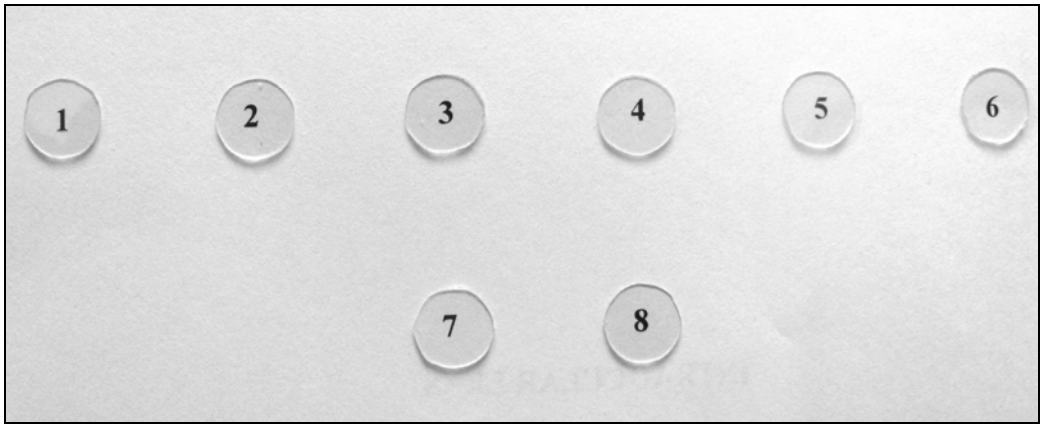

Figure 5.17: Pictures of prepared poly(PEA-*co*-PPEM) networks

5.4.5 Equilibrium water content (EWC)

The EWC of the selected copolymers ranged from 0.1% to 0.5% (Figure 5.18). These materials are hydrophobic in nature, so low EWC values were expected. The EWC values were measured on day 1 and day 5 after BSS immersion. No increase in EWC was seen after day 1.

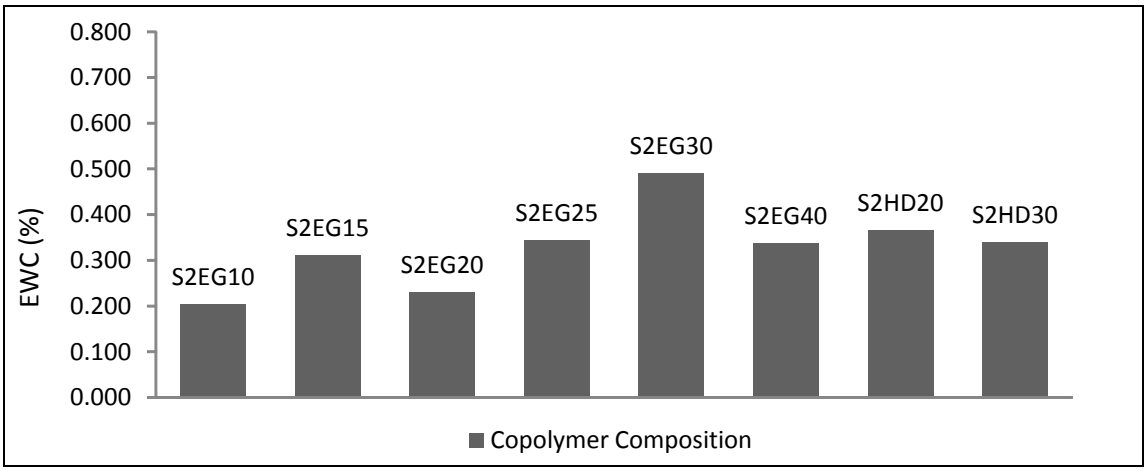

Figure 5.18: Equilibrium water content of poly(PEA-*co*-PPEM) networks

5.4.6 Water contact angle

Water contact angles of the prepared copolymer networks presented in Table 5.5, ranges from 76.86 to 85.01°. Figure 5.19 shows the water drop profiles on the three representative samples with S2-EG-10, S2-EG-20 and S2-EG-30. It should also be noted that the surface wettability of the networks could be adjusted by adding the monomer PPEM with methyl groups, the more PPEM, higher hydrophobic surface can be obtained.

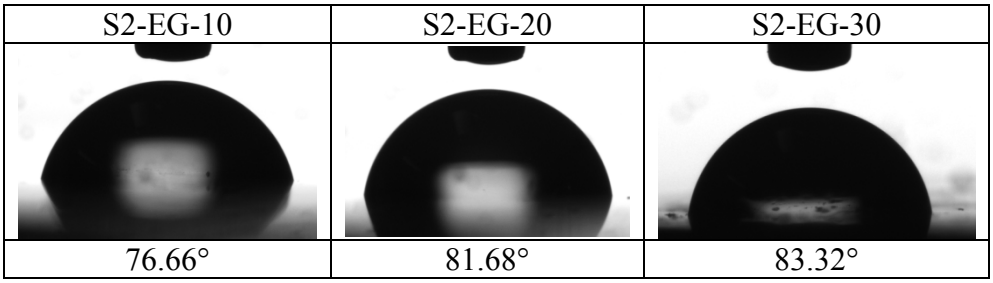

Figure 5.19: Water drop profiles of representative poly(PEA-*co*-PPEM) networks

5.4.7 Unfolding rate analysis

Polymer discs of 10 mm diameter and 0.5 mm thickness were folded in half and amount of time for the polymer discs to return to their original shape were recorded. Each measurement was done three times and the average was taken. Unfolding times represented in Table 5.5. For the S2-EG-10 copolymer network, the recovery time is 3 sec. As the concentration of PPEM increases to 30 mol%, the recovery time is prolonged to 16 sec. When the concentration of PPEM reaches to 40 mol%, the samples could not recover their shapes to the original ones at 37 °C.

5.4.8 Mechanical tensile testing

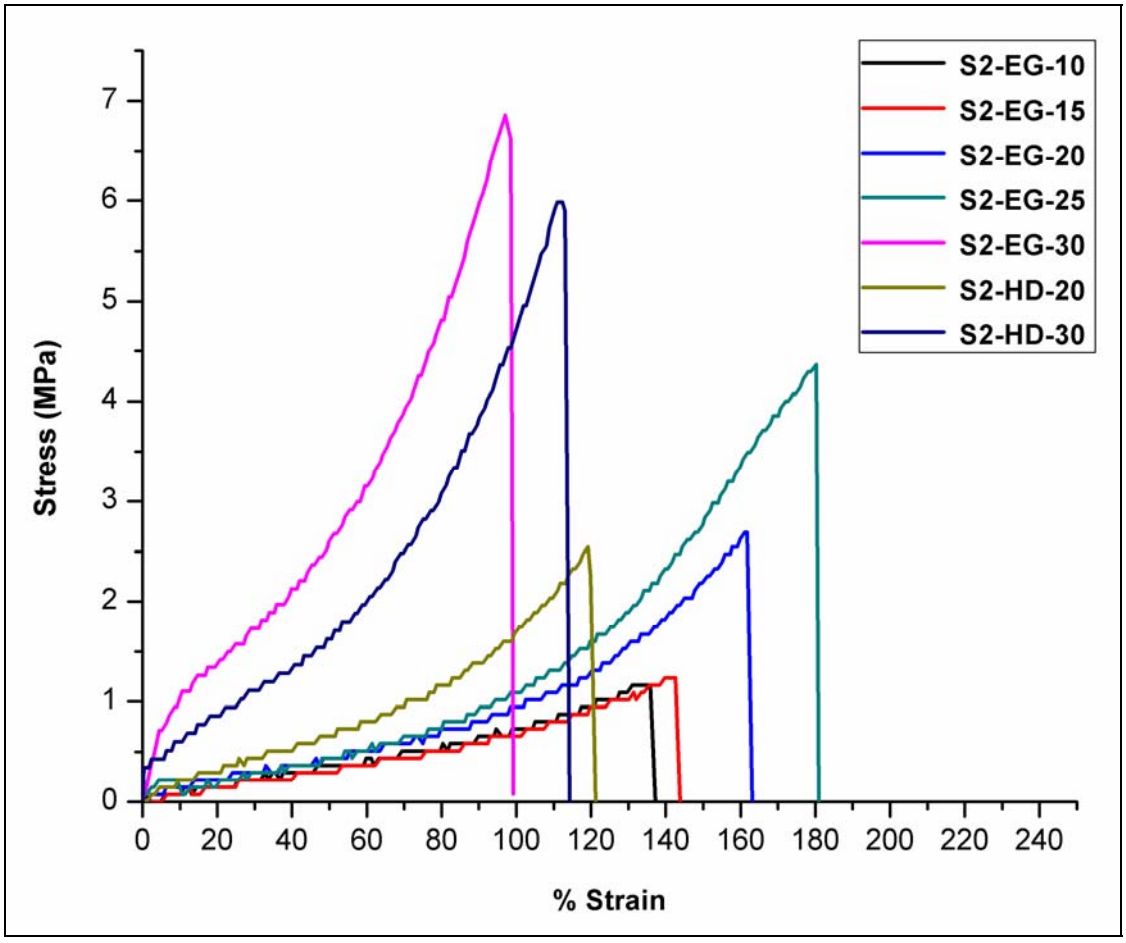

Figure 5.20: Stess vs strain curves for poly(PEA-*co*-PPEM) networks

Figure 5.20 shows the stress plotted against its respective % strain determined from the mechanical tensile tests. Polymers having PPEM concentration below 25 mol% exhibiting the *'J'* shaped stress-strain curve. The curve shows that initially, small increases in stress give large extensions, however, at larger extensions the material becomes stiffer, and more difficult to extend. Copolymers S2-EG-30 and S2-HD-30 gives *'S'* shaped stress-strain curves, which are particularly susceptible to elastic instabilities. The tensile behaviour was measured at 37 °C, which is beyond the T_g of the networks. Table 5.6 represents values of Young's Modulus at 100% strain, strength at failure strain and % elongation of synthesised polymer networks. From data it is observed that % elongation for poly(PEA-*co*-PPEM) networks is less than in comparison with poly(PEA-*co*-PPEM) networks, while stength at failure strain (stiffness) is more.

Table 5.6: Mechanical tensile testing parameters for poly(PEA-*co*-PPEM) networks

Code	Young's Modulus at 100 % strain (MPa)	Strength at failure strain (MPa)	% Elongation
S2-EG-10	0.006	1.236	142
S2-EG-15	0.006	1.164	135
S2-EG-20	0.008	2.690	161
S2-EG-25	0.009	4.363	180
S2-EG-30	0.060	6.856	100
S2-HD-20	0.015	2.545	119
S2-HD-30	0.040	5.899	113

5.4.9 Cytotoxicity

Figure 5.22 shows the microscopy images taken in bright field at 10X magnification obtained after incubation with polymer networks, in comparison with the negative control and positive controls. Live L929 mouse fibroblast adherent cells can

propagate to a confluent monolayer with the increase in the culture time, as can be seen from those of negative control. The death of the cell is observed using a positive control, the open area between cells indicates that cell lysis has occurred. In contrast, the fibroblast L929 cells incubated with polymer networks maintain their morphology typical of L929. No cell debris and no detachment from dish bottom is observed. Results regarding cell viability (MTT assay) of cultures are shown in Figure 5.21. L929 cells presented a high proliferation rate throughout the culture time. At early incubation times, that is, day 1, values of MTT reduction were similar in seeded networks and negative controls, suggesting an identical number of attached cells, whereas the cell viability of the positive control went down to ~19 % in one day and almost to 0 % in two days. At day 7, the cell viability was stable (almost 100 %) for the negative control, whereas for the networks, it was a bit lower than that of the negative control and much higher than that of the positive control.

These results suggested that copolymers developed in the study were cytocompatible. This slight toxicity, which turned out to be favorable, could prevent or reduce lens epithelial cell proliferation without any damage to other ocular tissues, because the IOL materials was confined within the capsule.[21]

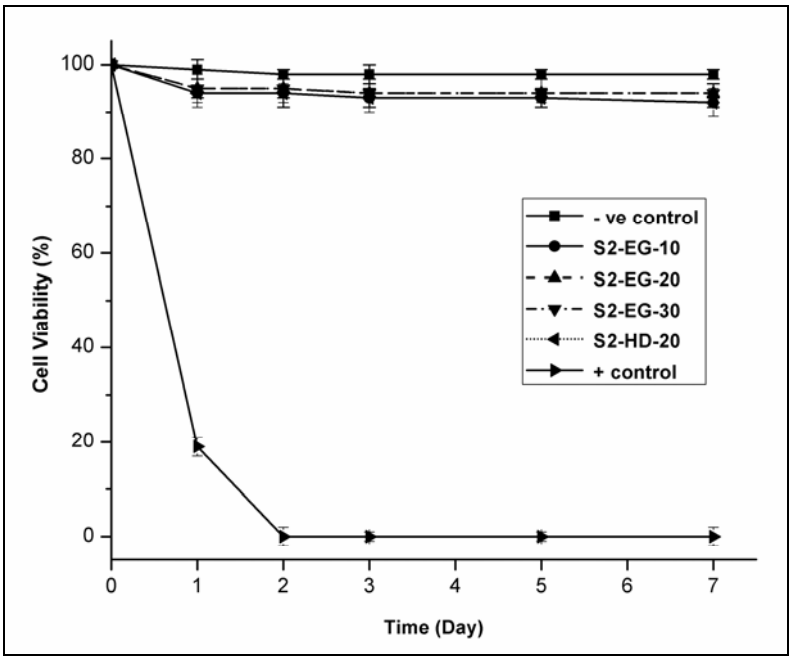

Figure 5.21: Cell viability of L929 mouse connective tissue fibroblasts as the result of MMT assay for representative poly(PEA-*co*-PPEM) networks with possitive and negative controls

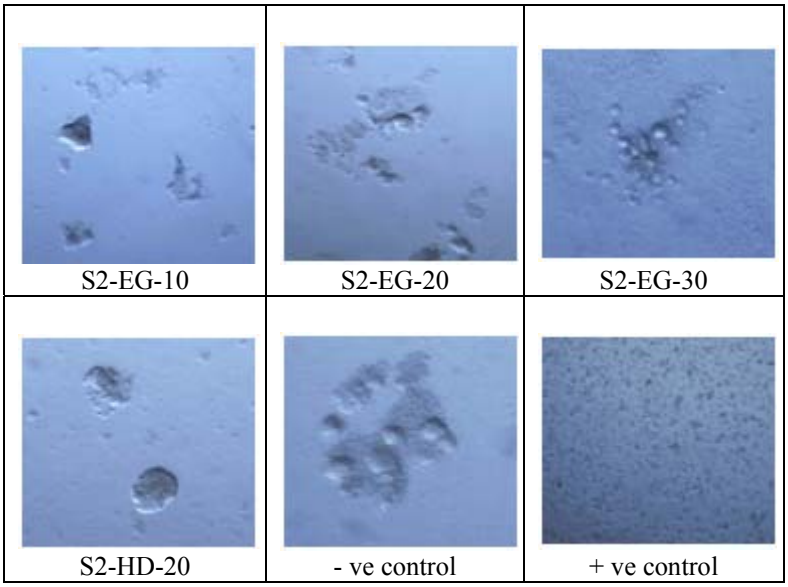

Figure 5.22: Carl Zeiss Axio scope microscopy images taken on day 7 showing the morphology of L929 mouse connective tissue fibroblast cocultured with four representative poly(PEA-*co*-PPEM) networks and controls.

5.4.10 Thermogravimetric analysis (TGA)

TGA curves for representative polymers represented in Figure 5.23. Thermograms indicate that polymer networks are thermally stable and decomposition of polymers starts at 310 °C. Single step degradation observed in all copolymers.

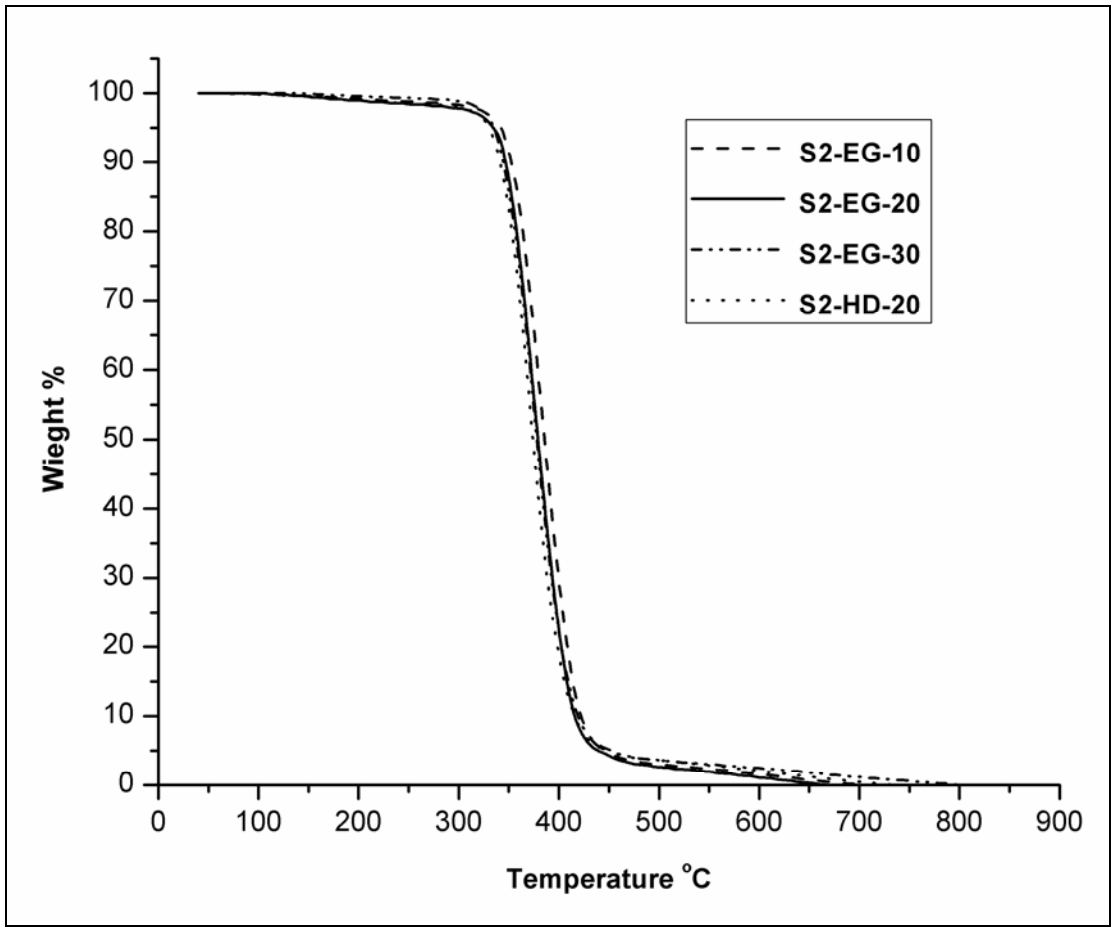

Figure 5.23: TGA thermograms for representative poly(PEA-*co*-PPEM) networks

5.5 Synthesis of copolymer networks of 2-phenylethyl acrylate (PEA) and 2-phenyl-(2-phenylthio)ethyl acrylate (PTEA)

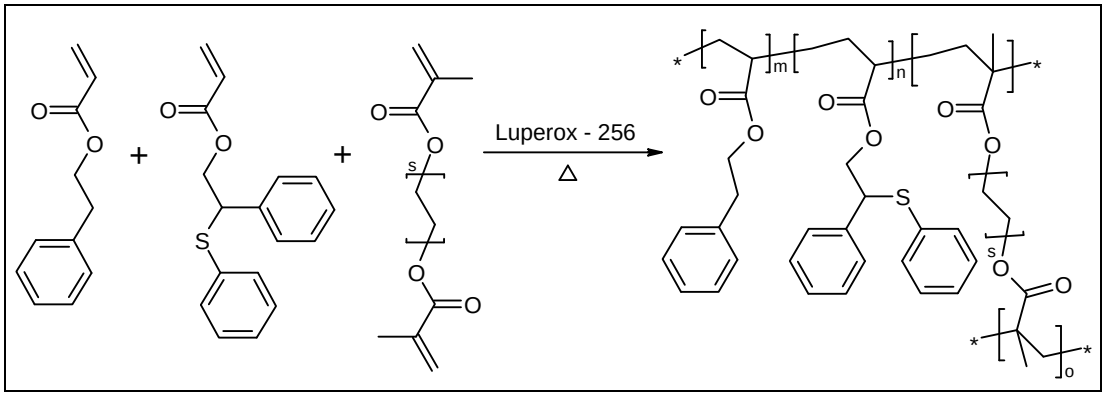

Scheme 5.4: Synthesis of poly(PEA-*co*-PTEA) bulk polymer networks

The synthetic method used to synthesise the poly(PEA-*co*-PTEA) copolymers is illustrated in Scheme 5.4. The poly(PEA-*co*-PTEA) networks were prepared by radical copolymerisation of 2-phenylethyl acrylate (PEA) and 2-phenyl-(2-phenylthio)ethyl acrylate (PTEA) in the presence of 2 mol % ethylene dimethacrylate (EGDMA) or hexanediol dimethacrylate (HDDMA) as a cross-linker and 0.2 mol% Luperox-256 as an initiator. The networks were prepared with varying molar ratio of PEA and PTEA. Monomers used and copolymerisation feed compositions are detailed in Table 5.7. Around 5 g monomer mixtures were weighed in centrifuge tubes and the appropriate amount of each component was added. Mixtures were vortexed for 60 seconds to allow the homogenisation. Nitrogen gas was bubbled through the mixtures to remove most of the oxygen present. Mixtures were then syringed into a glass molds. The glass molds were placed in an oven at 60 °C for 20 h followed by 90 °C for 10 h to ensure complete polymerisation. After polymerisation, the cross-linked poly(PEA-*co*-PTEA) networks were extracted using soxhlet extraction with 2-propanol to remove unreacted monomers and oligomers until equilibrium was reached.

5.5.1 IR Spectroscopy

Figure 5.24 shows IR spectra of representative copolymers. Comparison with monomer spectra indicates complete polymerisation as absorption peak of C=C double bond at 1636 cm^{-1} can be clearly observed in the monomers but disappears in the copolymer.

Table 5.7: Monomer compositions for PEA-PTEA bulk polymerisation system

Sr. No.	Code	PEA (mol %) A	PTEA (mol %) B	Cross-linker mol% (wrt. A+B)	% Wt. loss after solvent extraction
1	S3-EG-20	80	20	2 mol % EGDMA	1.4
2	S3-EG-30	70	30	2 mol % EGDMA	1.1
3	S3-EG-40	60	40	2 mol % EGDMA	1.0
4	S3-EG-50	50	50	2 mol % EGDMA	0.9
5	S3-EG-60	40	60	2 mol % EGDMA	0.9
6	S3-HD-40	60	40	2 mol % HDDMA	1.0
7	S3-HD-50	50	50	2 mol % HDDMA	1.1

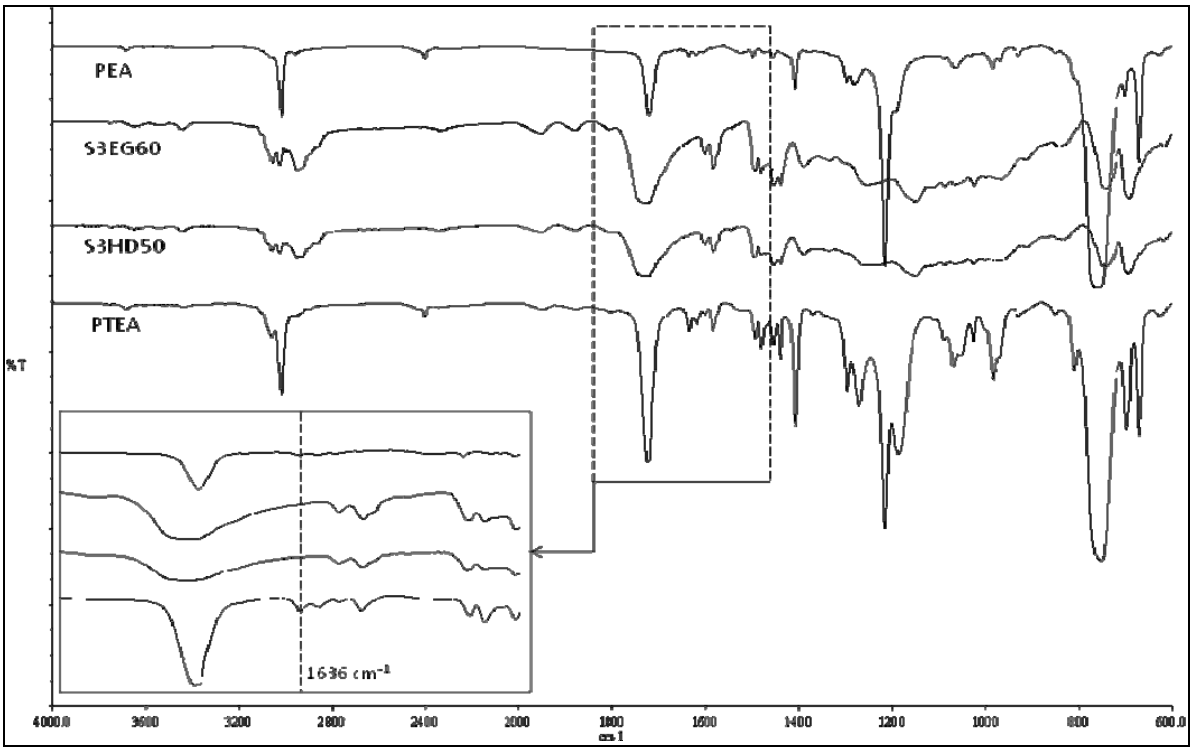

Figure 5.24: FT-IR spectra of PEA, PTEA and two poly(PEA-*co*-PTEA) networks

5.5.2 Differential scanning calorimetry (DSC)

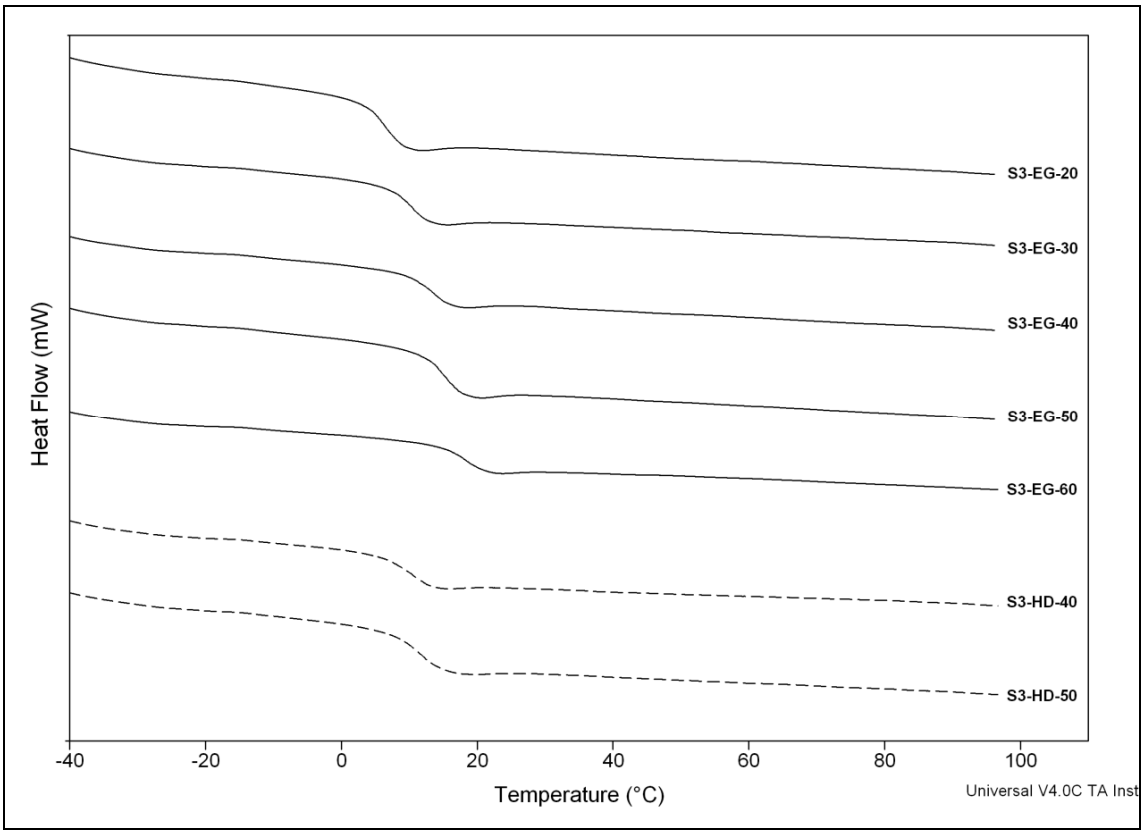

Figure 5.25: DSC thermograms of poly(PEA-*co*-PTEA) networks

The Glass transition temperatures (T_g) of the polymers represented in Figure 5.25. All of the cured acrylate resins show T_g's in the range of 6.10 to 18.26 °C measured by DSC. The increased concentration of PTEA containing two aromatic rings substantially reduces the mobility of polymer chains within the networks, as can be seen from the increase in the T_g represented in Table 5.8. Poly(PEA-*co*-PTEA) networks exhibiting lower T_g values than corresponding oxygen containing poly(PEA-*co*-PPEA) networks.

Table 5.8: Refractive index, glass transition temperature, water contact angle and unfolding time of poly(PEA-*co*-PTEA) networks

Sr. No.	Code	R.I. (at 589 nm)	T_g (°C)	Contact Angle	Unfolding Time (sec)
1	S3-EG-20	1.573	6.10	84.38	5
2	S3-EG-30	1.581	10.39	85.76	9
3	S3-EG-40	1.588	13.77	83.23	8
4	S3-EG-50	1.595	15.32	83.86	11
5	S3-EG-60	1.601	18.26	84.51	15
6	S3-HD-40	1.585	10.74	83.73	10
7	S3-HD-50	1.590	11.98	83.82	8

5.5.3 Refractometry (R.I.)

Values of refractive indices for all sulphur containing polymer networks listed in Table 5.8. All resulting polymers exhibit significantly high-refractive indices compared with corresponding oxygen containing bulk polymer networks. RI increases from 1.573 to 1.601 with the increase in the concentration of PTEA in polymer.

5.5.4 Transmittance

Copolymers are clear and colourless even at higher mol % of PTEA (60 mol %). This transparency of the polymer networks is considered to be a result of uniform distribution of PTEA resulting homogeneous medium, having an increased refractive index and PTEA does not scatter the visible light. As shown in Figure 5.26 all copolymers has a reasonable transmission (>85% ranging from 400 nm to 800 nm), which is comparable to the human lens and filters out most of the UV light. Figure 5.27 shows the pictures of the synthesised transparent networks.

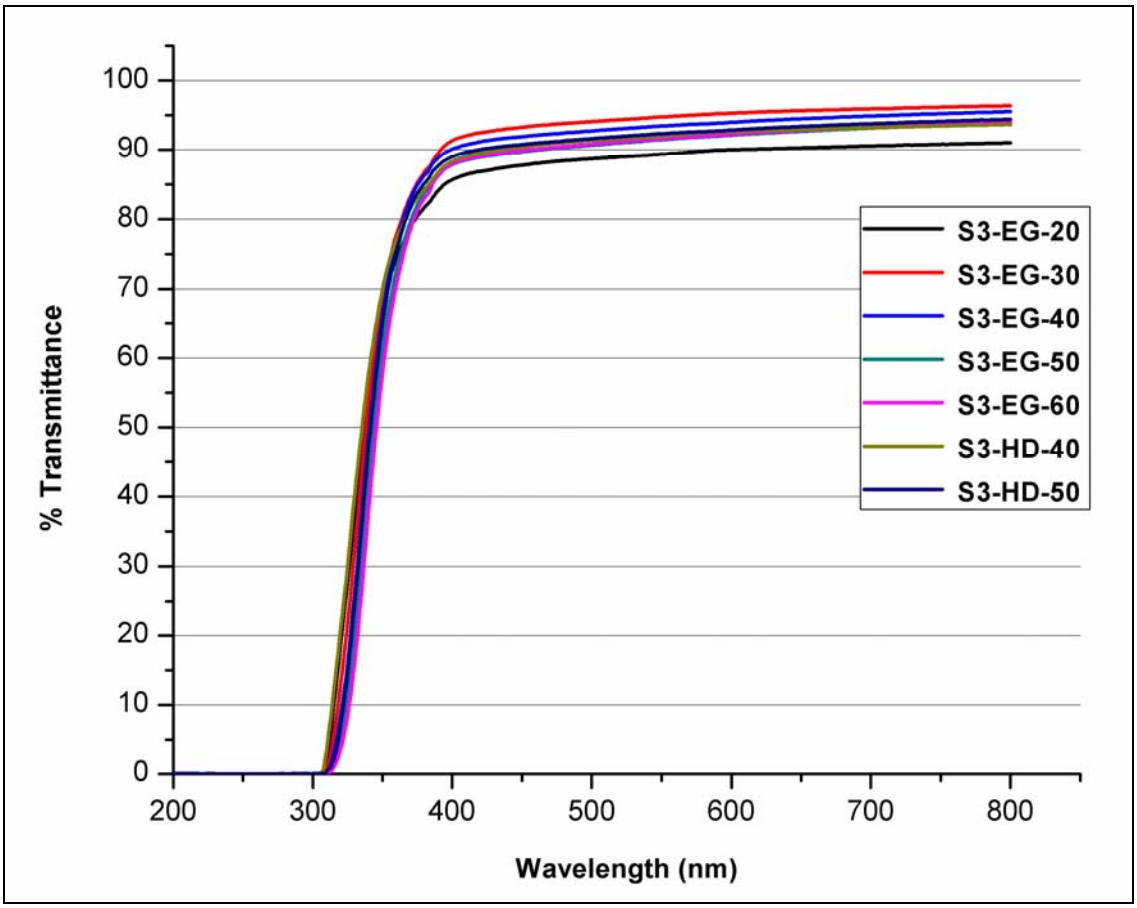

Figure 5.26: Spectral transmittance of poly(PEA-*co*-PTEA) networks

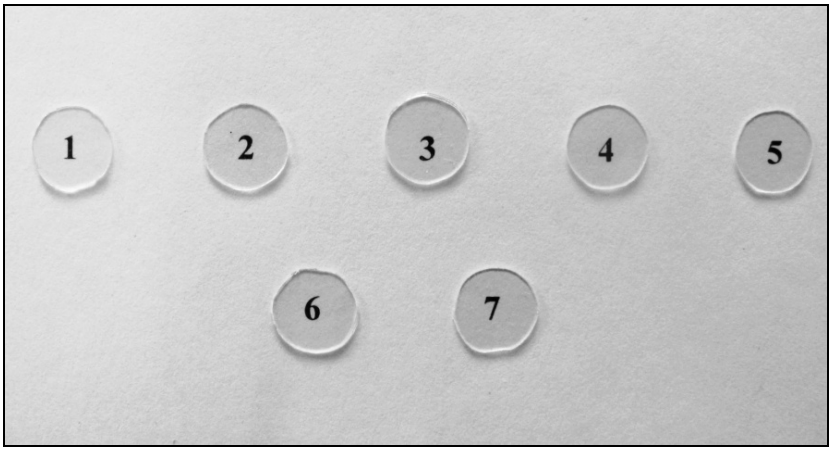

Figure 5.27: Pictures of prepared poly(PEA-*co*-PTEA) networks

5.5.5 Equilibrium water content (EWC)

The EWC of the selected copolymers ranged from 0.05% to 0.2% (Figure 5.28). These materials are hydrophobic in nature, so low EWC values were expected. The EWC values were measured on day 1 and day 5 after immersion into Balanced Salt Solution. No increase in EWC was seen after day 1.

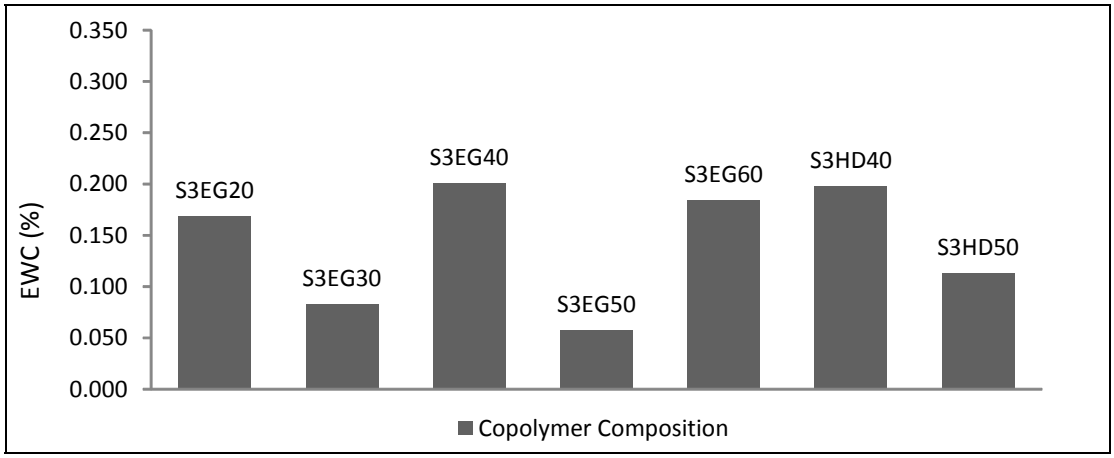

Figure 5.28: Equilibrium water content of poly(PEA-*co*-PTEA) networks

5.5.6 Water contact angle

Contact angle measurements for all the copolymers can be found in Table 5.8. Contact angle values for polymer networks slightly differ from each other and ranging from 83.23 to 85.76°. Figure 5.29 shows the water drop profiles on the three representative samples.

S3-EG-30	S3-EG-60	S3-HD-20
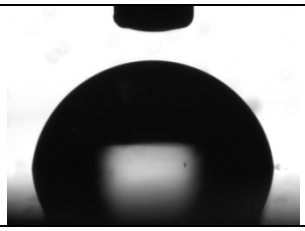	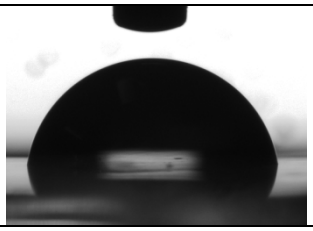	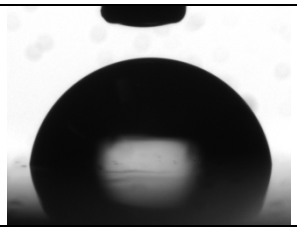
85.68°	84.62°	83.71°

Figure 5.29: Water drop profiles of representative poly(PEA-*co*-PTEA) networks

5.5.7 Unfolding rate analysis

Polymer discs of 10 mm diameter and 0.5 mm thickness were folded in half and amount of time for the polymer discs to return to their original shape were recorded. Each measurement was done three times and the average was taken. Unfolding times represented in Table 5.8. All the prepared copolymers could recover their original shape as time increased and the recovery ratios were 100% at the testing temperature. With the increasing concentrations of PTEA, the recovery time increased.

5.5.8 Mechanical tensile testing

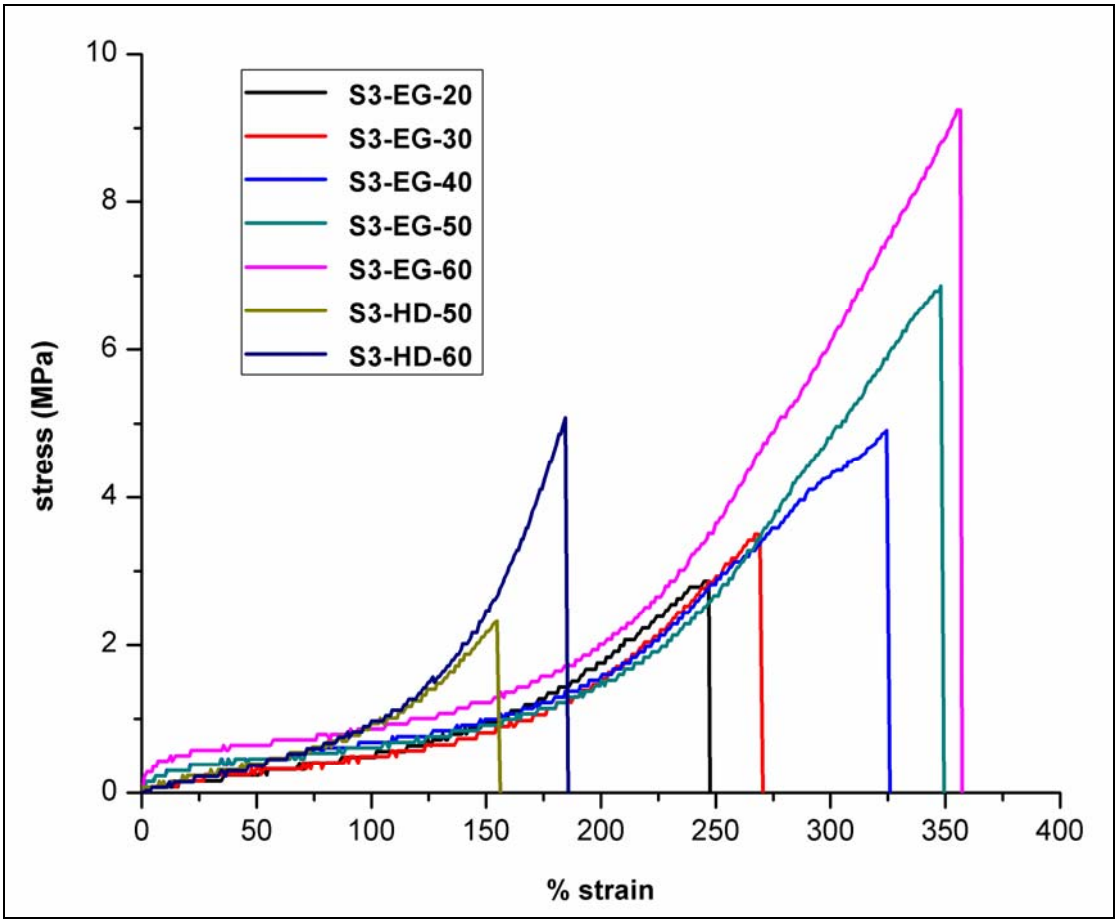

Figure 5.30: Stess vs strain curves for poly(PEA-*co*-PTEA) networks

Figure 5.30 displays representative stress–strain curves of the seven copolymer networks. Table 5.9 represents values of Young's Modulus at 100% strain, strength at failure strain and % elongation of synthesised polymer networks. Results indicate that as concentration of PTEA increases, the strength of material increases. All copolymer networks exhibit the '*J*-shaped' stress-strain curve, which is characteristic property of elastic rubbery polymers. The curve shows that initially, small increases in stress give large extensions, however, at larger extensions the material becomes stiffer, and more difficult to extend.

Table 5.9: Mechanical tensile testing parameters for poly(PEA-*co*-PTEA) networks

Code	Young's Modulus at 100 % strain (MPa)	Strength at failure strain (MPa)	% Elongation
S3-EG-20	0.004	2.867	247
S3-EG-30	0.004	3.421	269
S3-EG-40	0.004	4.908	324
S3-EG-50	0.004	6.863	348
S3-EG-60	0.005	9.247	357
S3-HD-40	0.007	2.320	154
S3-HD-50	0.008	5.078	184

5.5.9 Cytotoxicity

Cytotoxicity of the prepared polymer networks to L929 mouse fibroblasts was tested. L929 mouse fibroblasts were cultured for 7 days in direct contact to the networks. The effects of the networks on cell morphology were investigated by Carl Zeiss Axio scope microscope. Figure 5.32 shows the microscopy images taken in bright field at 10X magnification obtained after incubation with polymer networks, in comparison with the

negative control and positive controls. Live L929 mouse fibroblast adherent cells can propagate to a confluent monolayer with increase in the culture time, as can be seen from those of negative control. The death of the cell is observed using a positive control, the open area between cells indicates that cell lysis has occurred. In contrast, the fibroblast L929 cells incubated with polymer networks maintain their morphology typical of L929. No cell debris and no detachment from dish bottom is observed. Results regarding cell viability (MTT assay) of cultures are shown in Figure 5.31. L929 cells presented a high proliferation rate throughout the culture time. At early incubation times, that is, day 1, values of MTT reduction were similar in seeded networks and negative controls, suggesting an identical number of attached cells, whereas the cell viability of the positive control went down to ~19 % in one day and almost to 0 % in two days. On day 7, the cell viability was stable (almost 100 %) for the negative control, whereas for the networks, it was a bit lower than that of the negative control and much higher than that of the positive control. These results suggested a lack of Cytotoxicity of polymer networks developed in this study, which was critical for their biomedical application in the reduction of inflammatory response and PCO.

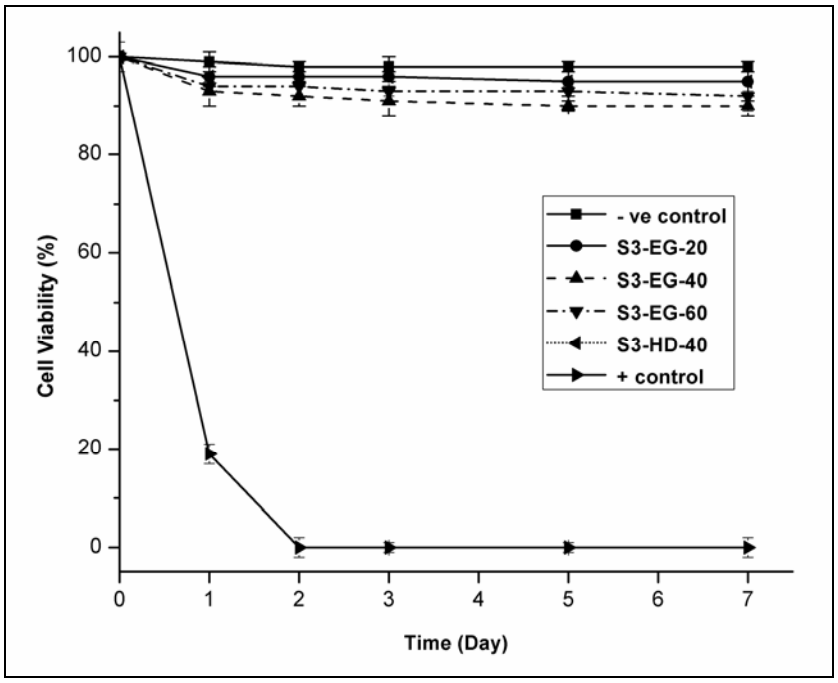

Figure 5.31: Cell viability of L929 mouse connective tissue fibroblasts as the result of MMT assay for representative poly(PEA-*co*-PTEA) networks with possitive and negative controls

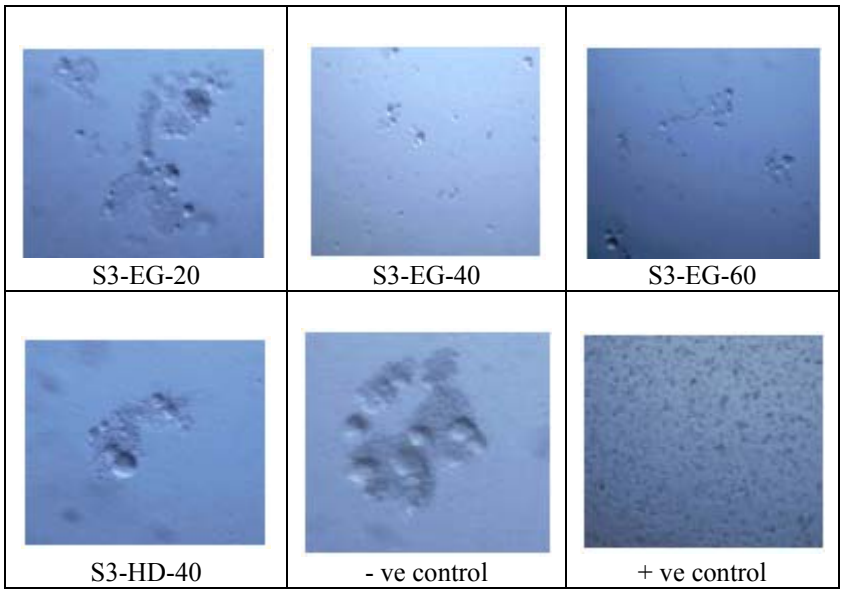

Figure 5.32: Carl Zeiss Axio scope microscopy images taken on day 7 showing the morphology of L929 mouse connective tissue fibroblast cocultured with four representative poly(PEA-*co*-PTEA) networks and controls.

5.5.10 Thermogravimetric analysis (TGA)

TGA curves for representative polymers represented in Figure 5.33. Thermograms clearly indicate that polymers undergo two-stage decomposition. The initial decomposition temperature of polymers is ~290 °C, while second decomposition temperature is ~ 340 °C.

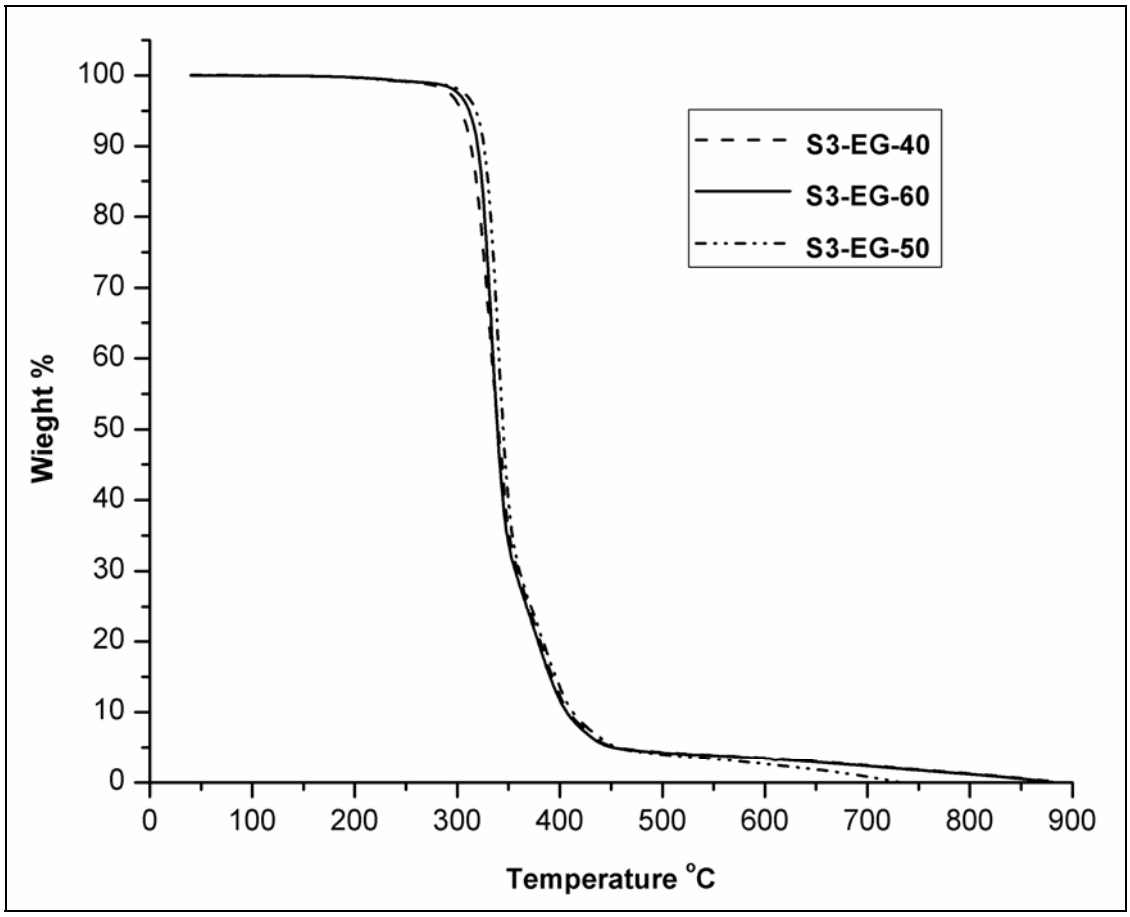

Figure 5.33: TGA thermograms for representative poly(PEA-*co*-PTEA) networks

5.6 Synthesis of copolymer networks of 2-phenylethyl acrylate (PEA) and 2-phenyl-(2-phenylthio)ethyl methacrylate (PTEM)

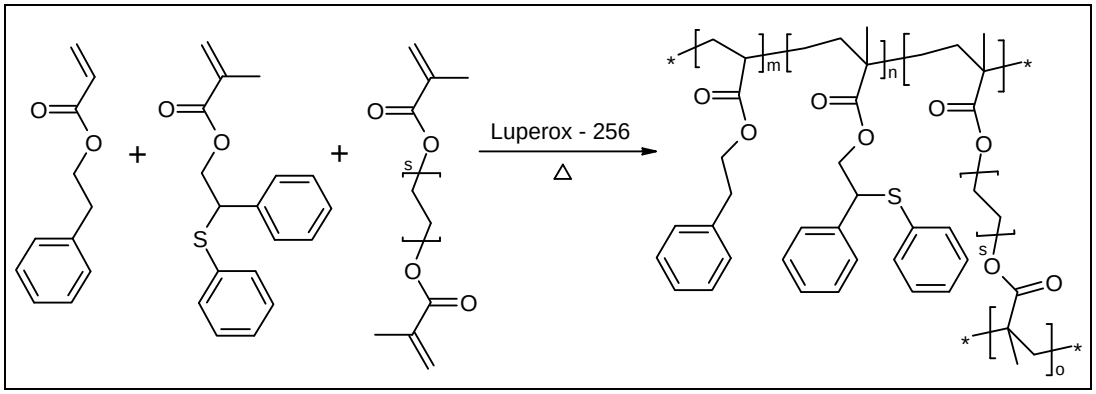

Scheme 5.5: Synthesis of poly(PEA-*co*-PTEM) bulk polymer networks

The synthetic method used to synthesise the poly(PEA-*co*-PTEM) copolymers is illustrated in Scheme 5.5. The poly(PEA-*co*-PTEM) networks were prepared by radical copolymerisation of 2-phenylethyl acrylate (PEA) and 2-phenyl-(2-phenylthio)ethyl methacrylate (PTEM) in the presence of 2 mol % ethylene dimethacrylate (EGDMA) or hexanediol dimethacrylate (HDDMA) as a cross-linker and 0.2 mol% Luperox-256 as an initiator. The networks were prepared with varying molar ratio of PEA and PTEM. Monomers used and copolymerisation feed compositions detailed in Table 5.10. Around 5 g monomer mixtures were weighed in centrifuge tubes and the appropriate amount of each component was added. Mixtures were vortexed for 60 seconds to allow the homogenisation. Nitrogen gas was bubbled through mixtures to remove most of the oxygen present. Mixtures were then syringed into a glass molds. The glass molds were placed in an oven at 60 °C for 20 h followed by 90 °C for 10 h to ensure complete polymerisation. After polymerisation, the cross-linked poly(PEA-*co*-PTEM) networks were extracted using soxhlet extraction with 2-propanol to remove unreacted monomers and oligomers until equilibrium was reached.

5.6.1 IR spectroscopy

The FTIR spectra of two representative copolymers and corresponding monomers are represented in Figure 5.34. Comparing the spectra of the monomers with those of the copolymers, the absorption peak of C=C double bond at 1637 cm^{-1} can be observed clearly in the monomers, but disappears in the copolymers, which indicates that the C=C double bonds were almost exhausted during the polymerisation.

Table 5.10: Monomer compositions for PEA-PTEM bulk polymerisation system

Sr. No.	Code	PEA (mol %) A	PTEM (mol %) B	Cross-linker mol% (wrt. A+B)	% Wt. loss after solvent extraction
1	S4-EG-10	90	10	2 mol % EGDMA	0.5
2	S4-EG-15	85	15	2 mol % EGDMA	1.3
3	S4-EG-20	80	20	2 mol % EGDMA	1.1
4	S4-EG-25	75	25	2 mol % EGDMA	1.1
5	S4-EG-30	70	30	2 mol % EGDMA	0.9
6	S4-HD-20	80	20	2 mol % HDDMA	1.4
7	S4-HD-30	70	30	2 mol % HDDMA	0.8

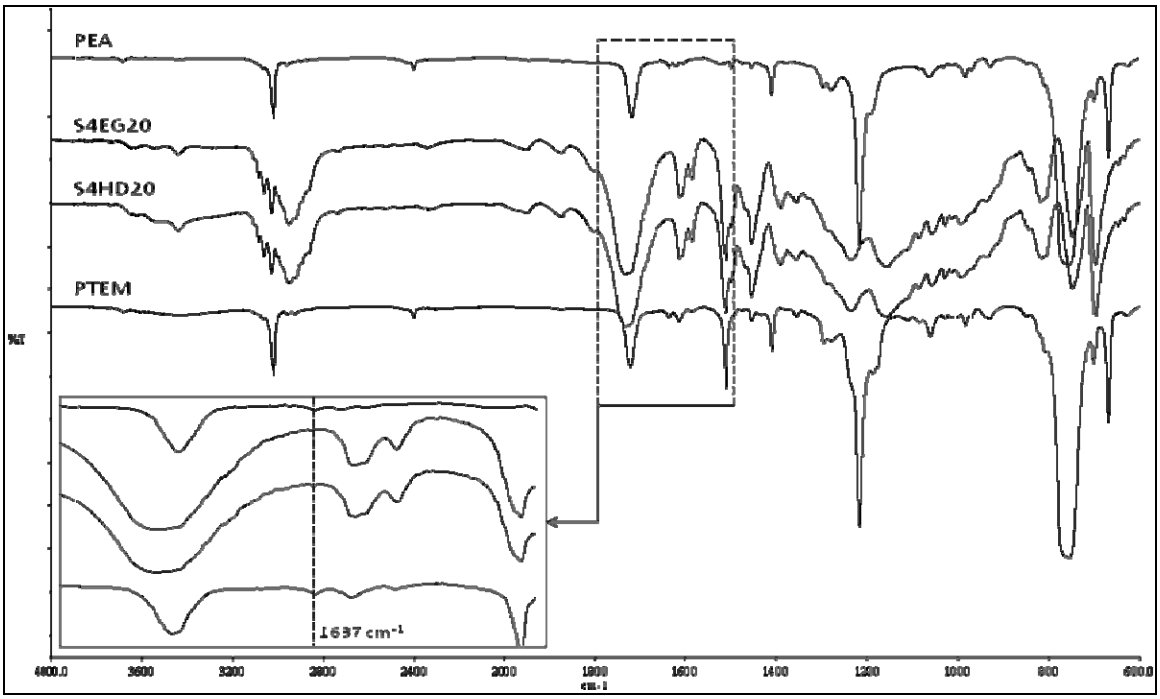

Figure 5.34: FT-IR spectra of PEA, PTEM and two poly(PEA-*co*-PTEM) networks

5.6.2 Differential scanning calorimetry (DSC)

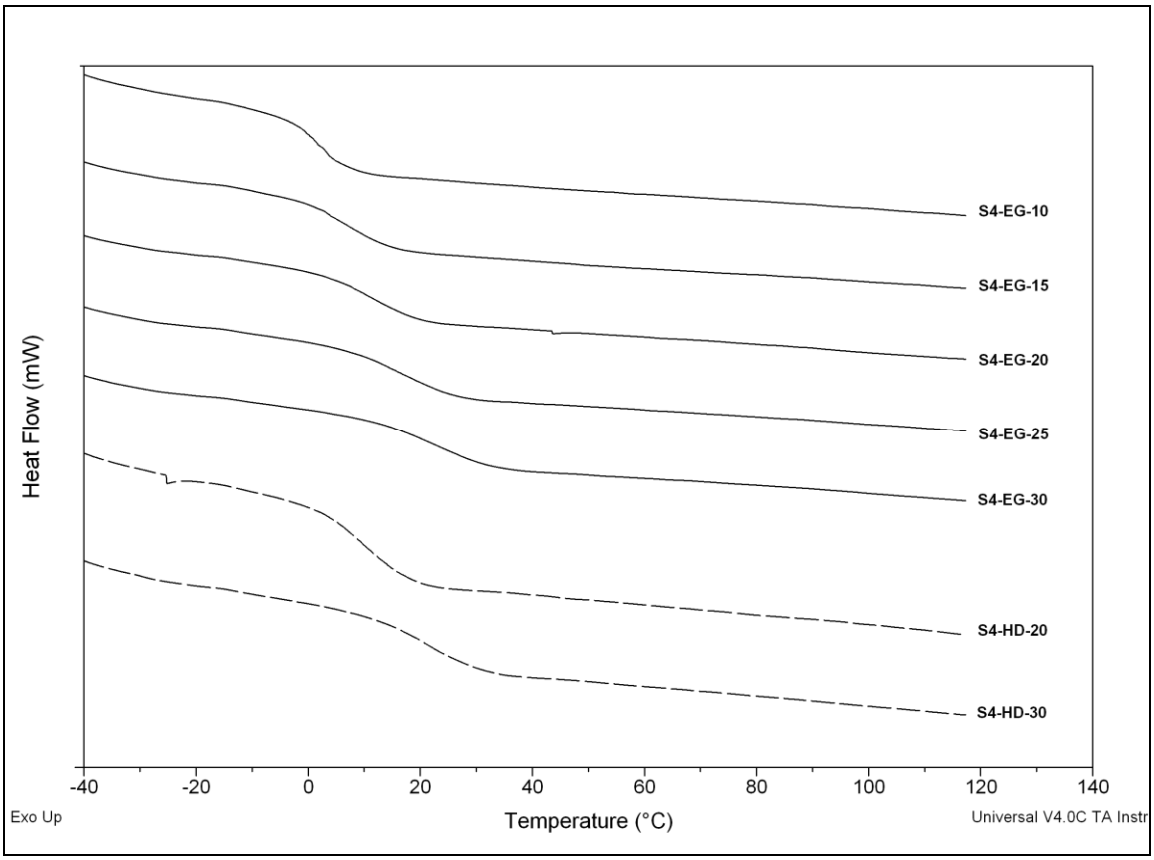

Figure 5.35: DSC thermograms of poly(PEA-*co*-PTEM) networks

The glass transition curves of the polymer networks derived from DSC represented in Figure 5.35. T_g for all five networks ranges between 2.84 and 21.67 °C. The glass transition temperatures of polymers are allowed to be optimised for intraocular lens application by adjusting the amounts of starting monomers without introducing any new monomers or additives into the system. The increased concentration of methacrylate substantially reduces the mobility of polymer chains within the networks, as can be seen from the increase in the T_g shown in Table 5.11.

Table 5.11: Refractive index, glass transition temperature, water contact angle and unfolding time of poly(PEA-*co*-PTEM) networks

Sr. No.	Code	R.I. (at 589 nm)	T_g (°C)	Contact Angle	Unfolding Time (sec)
1	S4-EG-10	1.559	2.84	81.74	4
2	S4-EG-15	1.563	4.45	83.21	4
3	S4-EG-20	1.567	11.22	84.80	6
4	S4-EG-25	1.573	15.00	85.35	10
5	S4-EG-30	1.578	21.67	87.35	19
6	S4-HD-20	1.567	9.89	83.86	7
7	S4-HD-30	1.577	21.45	86.46	18

5.6.3 Refractometry

RI of current acrylate foldable IOLs is approximately 1.51. Both the high RI and flexibility of the copolymers could be very helpful to reduce the implanted incision when they are used as IOLs. Table 5.11 shows the values of RI of copolymers with different concentrations and compositions of the monomers. With increasing the concentrations of PTEM from 10 to 30 mol%, the RI increased from 1.559 to 1.578. The high RI of the copolymers resulted from sulphur atom and aromatic rings of PTEM.

5.6.4 Transmittance

After the polymerisation of PEA-PTEM systems, the transparent copolymers were obtained. Figure 5.36 shows the UV–vis absorption spectra of the poly(PEA-*co*-PTEA) networks with a thickness of about 0.5 mm. All polymers show high transparency in the visible region (λ= 400–800 nm) with transmittance over 80% at 400 nm, indicating that the introduction of a thiophenol unit does not deteriorate the optical transparency of the

films. The thio-ether unit may suppress packing between the polymer chains, which is required for high transparency. Figure 5.37 shows the pictures of the prepared networks.

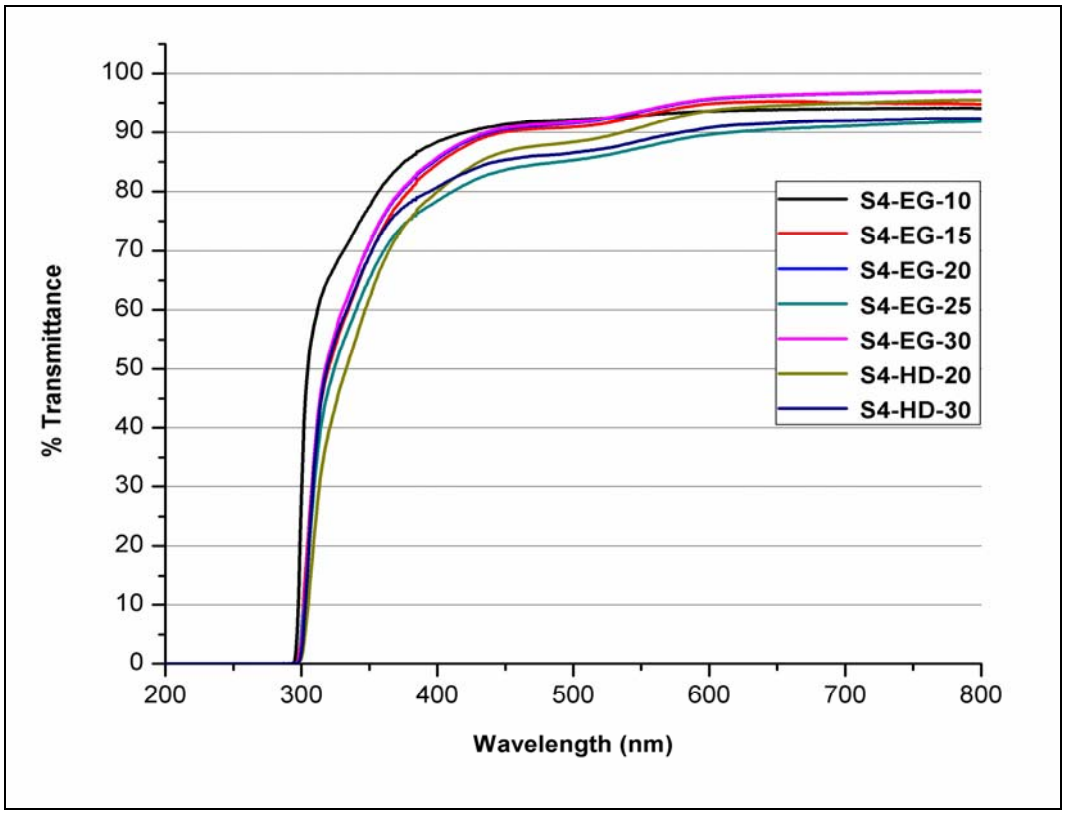

Figure 5.36: Spectral transmittance of poly(PEA-*co*-PTEM) networks

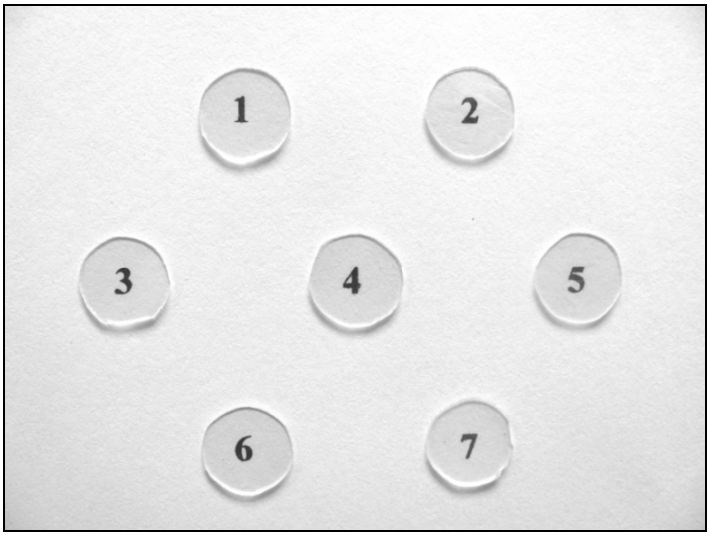

Figure 5.37: Pictures of prepared poly(PEA-*co*-PTEM) networks

5.6.5 Equilibrium water content (EWC)

The EWC of the selected copolymers ranged from 0.1%-0.4% (Figure 5.38). These materials are hydrophobic in nature, so low EWC values were expected. The EWC values were measured on day 1 and day 5 after immersion into Balanced Salt Solution. No increase in EWC was seen after day 1.

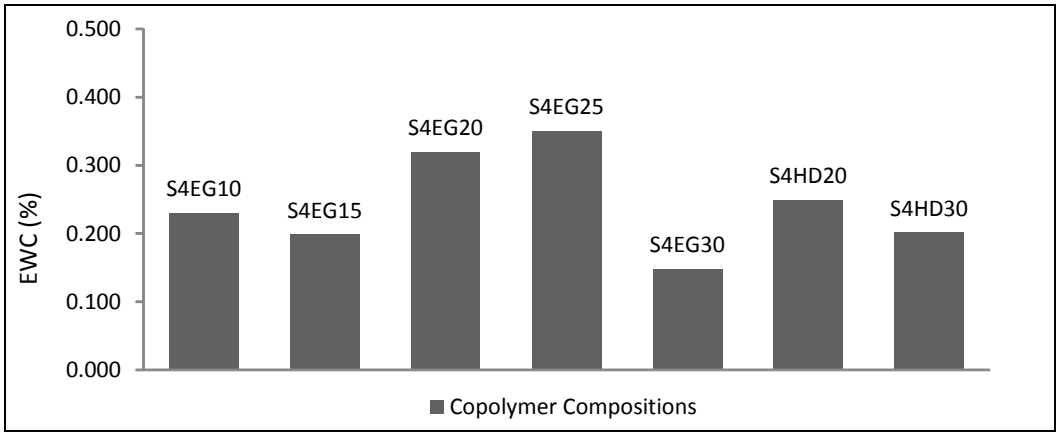

Figure 5.38: Equilibrium water content of poly(PEA-*co*-PTEM) networks

5.6.6 Water contact angle

Figure 5.39 shows the water drop profiles of representative copolymer networks. It should also be noted that the surface wettability of the networks could be adjusted by adding the monomer PTEM with methyl groups: the more the PTEM, the higher hydrophobic the surface could be obtained (Table 5.11).

S4-EG-10	S4-EG-20	S4-EG-30
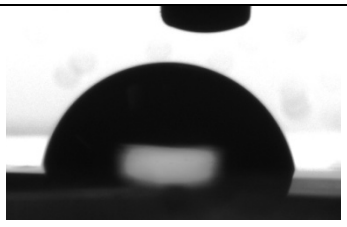	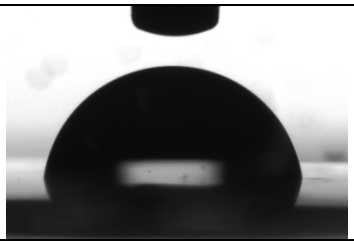	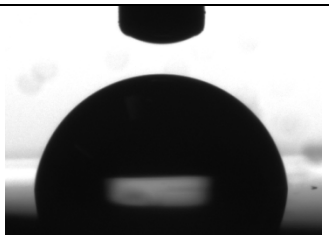
81.63°	84.81°	88.11°

Figure 5.39: Water drop profiles of representative poly(PEA-*co*-PTEM) networks

5.6.7 Unfolding rate analysis

Unfolding times for synthesised bulk polymer networks are represented in Table 5.11. Unfolding time is varying from 4 to 19 sec. The S4-EG-10 composition tended to adhere to itself for a brief moment before unfolding.

5.6.8 Mechanical tensile testing

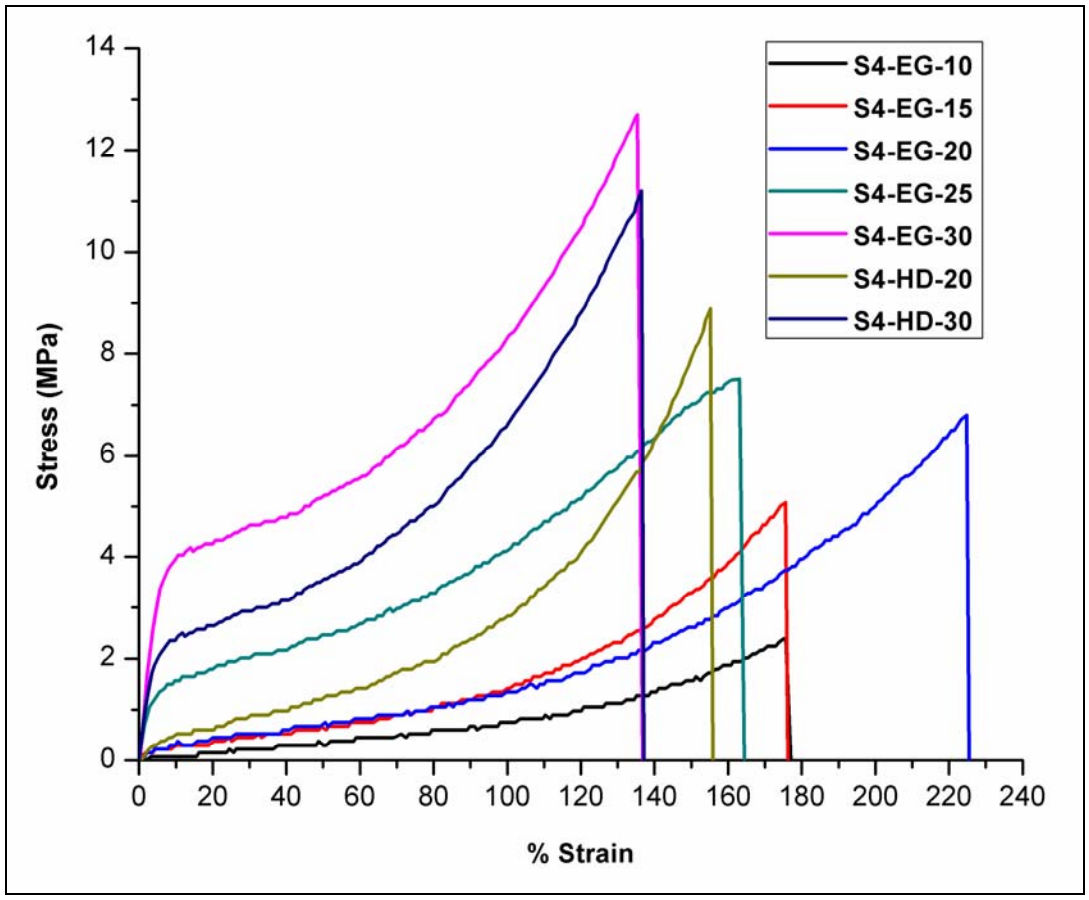

Figure 5.40: Stess vs strain curves for poly(PEA-*co*-PTEM) networks

Figure 5.40 shows the stress plotted against its respective % strain determined from the mechanical tensile test. Polymers having PTEM concentration below 25 mol% exhibiting the *'J'* shaped stress-strain curve. The curve shows that initially, small

increases in stress give large extensions, however, at larger extensions the material becomes stiffer, and more difficult to extend. Copolymers having PTEM content more than 25 mol% shows more stiffness and less elongation. The tensile behaviour was measured at 37 °C, which is beyond the T_g of the networks. Table 5.12 represents values of Young's Modulus at 100% strain, strength at failure strain and % elongation of synthesised polymer networks.

Table 5.12: Mechanical tensile testing parameters for poly(PEA-*co*-PTEM) networks

Code	Young's Modulus at 100 % strain (MPa)	Strength at failure strain (MPa)	% Elongation
S4-EG-10	0.007	2.390	176
S4-EG-15	0.011	5.078	176
S4-EG-20	0.011	6.795	225
S4-EG-25	0.028	7.507	163
S4-EG-30	0.051	12.696	135
S4-HD-20	0.024	8.886	155
S4-HD-30	0.045	11.193	136

5.6.9 Cytotoxicity

Cytotoxicity tests were performed with L929 mouse fibroblasts on the prepared networks. All the networks exhibit a favorable biocompatibility. Figure 5.42 shows the microscopy images taken in bright field at 10X magnification obtained after incubation with polymer networks, in comparison with the negative and positive controls. Live L929 mouse fibroblast adherent cells can propagate to a confluent monolayer with the increase in the culture time, as can be seen from those of negative control. The death of the cell is observed using a positive control, the open area between cells indicated cell lysis has occurred. In contrast, the fibroblast L929 cells incubated with polymer networks maintain

their morphology typical of L929. No cell debris and no detachment from dish bottom is observed. Results regarding cell viability (MTT assay) of cultures are shown in Figure 5.41. L929 cells presented a high proliferation rate throughout the culture time. At early incubation times, that is, day 1, values of MTT reduction were similar in seeded networks and negative controls, suggesting an identical number of attached cells, whereas the cell viability of the positive control went down to ~19 % in one day and almost to 0 % in two days. At day 7, the cell viability was stable (almost 100 %) for the negative control, whereas for the networks, it was a bit lower than that of the negative control and much higher than that of the positive control. The slight drop of cell viability in the prepared networks may be due to the inherent cytotoxicity of the (meth)acrylate polymers. These results suggest favorable cytocompatibility of polymer networks prepared in the study.

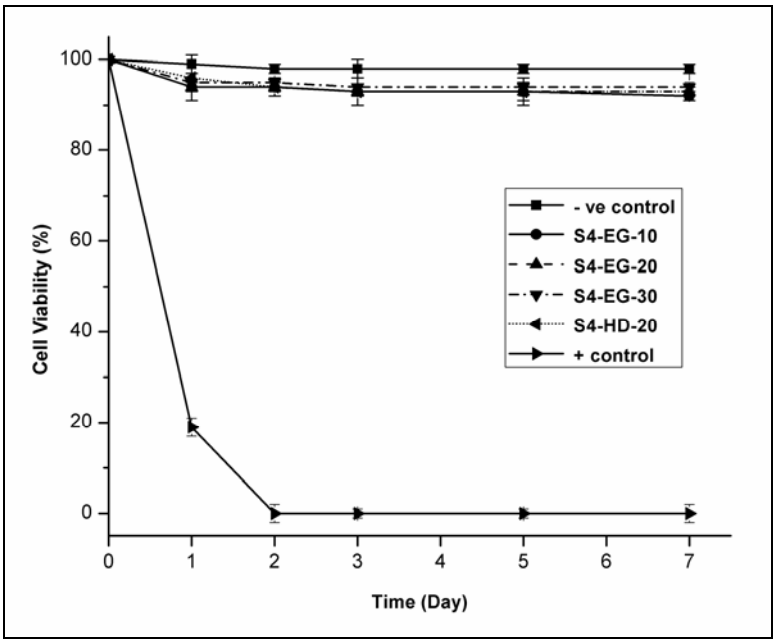

Figure 5.41: Cell viability of L929 mouse connective tissue fibroblasts as the result of MMT assay for representative poly(PEA-*co*-PTEM) networks with possitive and negative controls

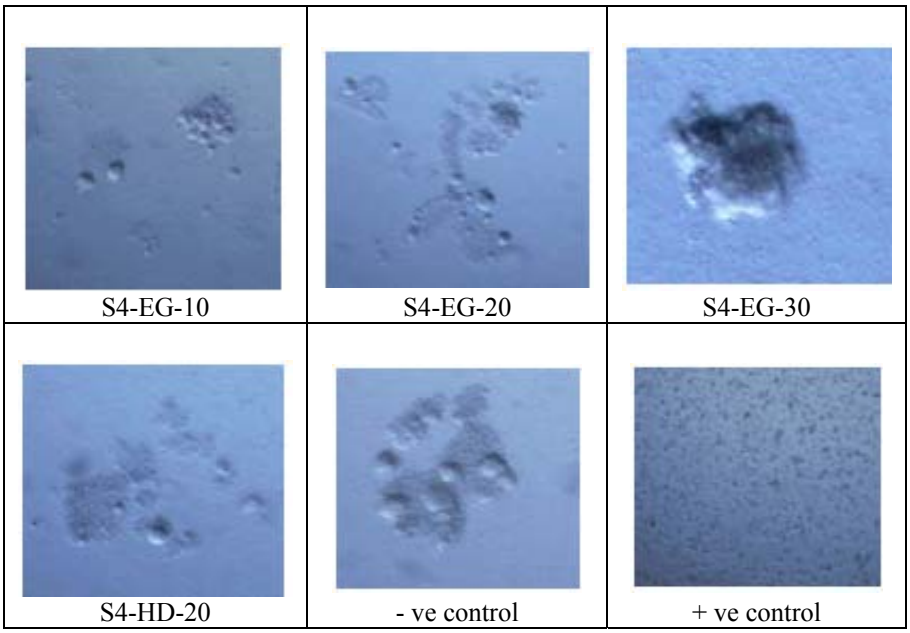

Figure 5.42: Carl Zeiss Axio scope microscopy images taken on day 7 showing the morphology of L929 mouse connective tissue fibroblast cocultured with four representative poly(PEA-*co*-PTEM) networks and controls.

5.6.10 Thermogravimetric analysis (TGA)

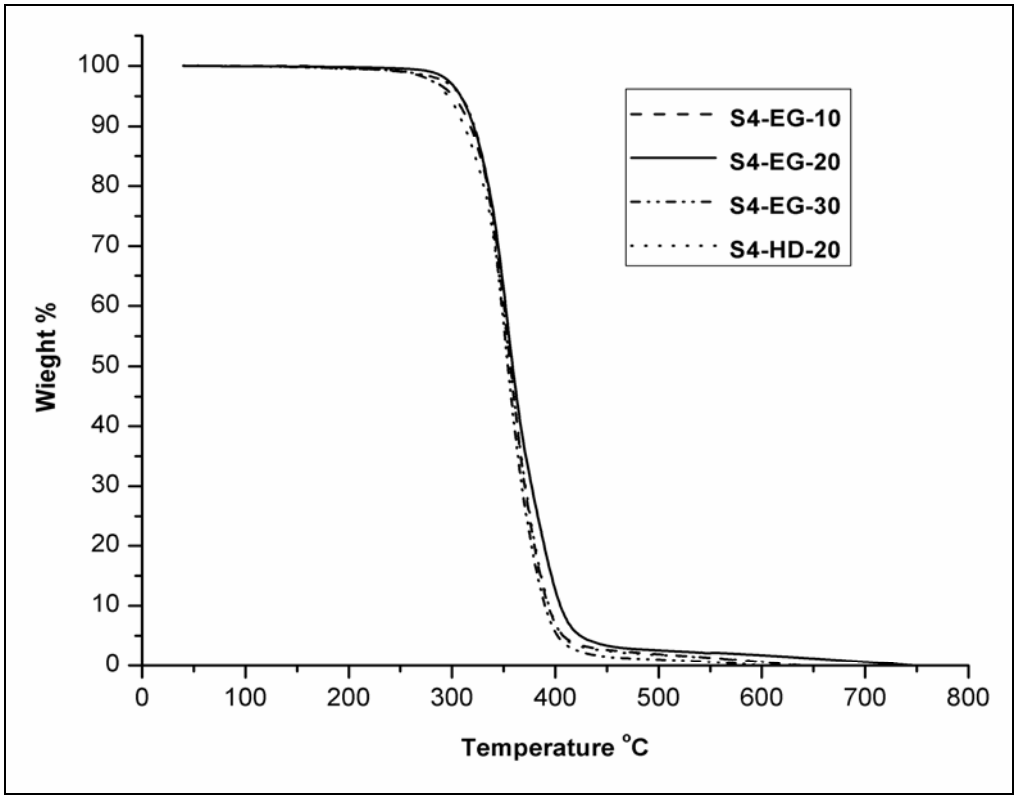

Figure 5.43: TGA thermograms for representative poly(PEA-*co*-PTEM) networks

The thermal stability of selected polymer networks was probed using thermogravimetric analysis (Figure 5.43). Polymers showed single step degradation with high thermal stability. All polymer networks are thermally stable up to 290 °C

5.7 References

[1] S. Neuss, I. Blomenkamp, R. Stainforth, D. Boltersdorf, M. Jansen, N. Butz, A. Perez-Bouza, R. Knuchel, *Biomaterials,* **2009***,* 30, 1697.

[2] WHO, Priority eye diseases, *www.who.int/blindness/causes/priority/en/index1.html,* cited on June, **2012.**

[3] J. H. D. Groot, F. J. Beijma, H. J. Haitjema, K. A. Dillingham, K. A. Hodd, S. A. Koopmans, S. Norrby, *Biomacromolecules*, **2001**, 2, 628-634.

[4] S. Lerman, *Radiant Energy in the Eye*, ed. S. Lerman, **1980**, New York, New York: Macmillan, 73-93.

[5] S. McIntyre, *Cataract & Refractive Surgery Today Europe*, **2011**, 39.

[6] L. Song, W. Hu, H. Zhang, G. Wang, H. Yang, S. Zhu, *J. Phys. Chem. B,* **2010**, *114,* 7172–7178.

[7] L. Song, W. Hu, H. Zhang, G. Wang, H. Yang, S. Zhu, *Journal of Biomaterials Science, Polymer Edition*, **2011**, 22, *1–17.*

[8] L. Song, W. Hu, H. Zhang, G. Wang, H. Yang, S. Zhu, *Macromol. Biosci*., **2010**, 10, 1194–1202.

[9] D. J. Plazek*, The Glass Temperature in Polymer Handbook*, 4th ed. (Brandrup, J., Immergut, E. H. & Grulke, E. A.) Vol. 1, 571 (Wiley, New York), **1999**.

[10] G. Odian, *Principles of polymerization*, 4th ed. New York: Wiley, **2004.**

[11] F. L. Marten, A. E. Hamielec, *J. Appl. Polym. Sci.,* **1982**, 27, 489–505.

[12] S. Suyama, T. Komai, *JP1242567*, **1989.**

[13] T. Fukumuru, *US 5254650*, **1993**.

[14] S. Fityani-Trimm, A. Penlidis, *Macromol. Chem. Phys.*, **2003**, 204(3), 436-42.

[15] M. J. Scorah, R. Dhib, A. Penlidis, *J. Polym. Sci., Part A: Polym. Chem.*, **2004**, 42, 5647–61.

[16] H. B. Dick, A. Frohn, A. Augustin, B. Wolters, T. Pakula, N. Pfeiffer, *Ophthalmic. Res.,* **2001**, 33, 303–309.

[17] S. Neuss, I. Blomenkamp, R. Stainforth, D. Boltersdorf, M. Jansen, N. Butz, A. Perez-Bouza, R. Knuchel, *Biomaterials,* **2009**, 30, 1697.

[18] T. F. Yang, C. N. Chen, M. C. Chen, C. H. Lai, H. F. Liang, H. W. Sung, *Biomaterials,* **2007**, *28*, 725–734.

[19] C. M. Cunanan, M. Ghazizadeh, S. Y. Buchen, P. M. Knight, *J. Cataract Refractive Surg.,* **1998**, *24*, 341–351.

[20] T. Tanaka, M. Shigeta, N. Yamakawa, M. Usui, *J. Cataract Refractive Surg.,* **2005**, *31*, 1648–1651.

[21] H. J. Hettlich, K. Lucke, C. F. Kreiner, *Ger. J. Opthalmol.,* **1992**, 1, 346.

[22] C. D. Kelman, *American Journal of Ophthalmology*, **1967**, 64, 23-25.

Chapter VI

Bulk Polymerisation Kinetics

PART-A: Photopolymerisation

6.1 Introduction

UV curable materials contain photo reactive monomers/oligomers and curing agents. Differential photo-calorimetry is one of the methods to study the radical and cationic photopolymerisations.[1] This method helps in optimising photopolymerisation. Formulations can have a mixture of di- or multifunctional additives with (meth)acrylate terminations to facilitate cross-linking. The photopolymerisation kinetics has been studied extensively for many systems.[2] It is observed that a high viscosity multifunctional acrylate is found to result in a lower conversion than a low viscosity mono or difunctional acrylate due to high initial viscosity of the system as well as due to the onset of earlier reaction diffusion.[3,4] The order of propagation is highly influenced by the diffusion controlled polymerisation which sets in after a certain limiting conversion has reached. The photopolymerisation kinetics in a photo DSC measurement can depend on many factors such as concentration of photo initiator, type of monomers used, reaction temperature, nature of purge gas, type of crosslinking agents, intensity and wavelength of irradiation.

It is known that photopolymerisation reactions have particular behaviours, such as autoacceleration[5], unequal functional group reactivity[6] and temporary free volume excess.[7] The temporary free volume increase during early stages of photopolymerisation before attaining maximum polymerisation rate will increase the radical diffusivity with an increase in rate of photopolymerisation (Trommsdorff effect). The polymerisation rate will however get reduced with time due to limitation in radical diffusion caused by an increase in viscosity of the system with conversion. The entire process is an outcome of

the time dependant influence of translational, segmental and reaction diffusion (diffusion of mobility restricted macroradical) processes.[2,8]

The major factors affecting the photopolymerisation of acrylate are the initial viscosity and the time of onset of reaction diffusion. Three termination models have been proposed for the process. As per the monomolecular model[9], all terminations occur by trapping of radicals. As per bimolecular termination model[10], the terminations follow a radical-radical bimolecular combination and in complex reaction model[11], both the monomolecular and bimolecular terminations occur in parallel. Photopolymerisation can be analysed by bimolecular termination model even though the complex reaction model may be more appropriate.

The rate of initiation (R_i) in photopolymerisation is found to depend on the molar extinction coefficient of the photoinitiator under monochromatic conditions. However the value of R_i is difficult to compute in the case of polychromatic radiation as the photoinitiator may have multiple excitation wavelengths. Hence stopping the irradiation at different conversions and monitoring the reaction in dark, one can compute the value of the ratio of rate constants (k_t^b / k_p) using bimolecular termination model.[12] As per the model, the rate of propagation (R_{prop}) and the rate of bimolecular termination (R_t^b) are respectively:

$$R_{prop} = \frac{-d[M]}{dt} = k_p[M][P\cdot] \qquad 6.1$$

$$R_t^b = \frac{-d[P\cdot]}{dt} = 2k_t^b[P\cdot]^2 \qquad 6.2$$

where *[M]* is the concentration of double bonds, *[P·]* is the concentration of radicals, k_p is the rate constant for propagation and k_t^b is the overall bimolecular termination rate constant.

If at a particular conversion, the photo irradiation is stopped, then the propagation reaction will still proceed as the initiation has already happened. Considering all terminations occurring during the dark reaction as exclusively bimolecular, the following linear equation can be obtained.[13]

$$\frac{[M]_t}{(R_p)_t} = \frac{2k_t^b}{k_p} + \frac{[M]_0}{(R_p)_0} \qquad 6.3$$

where $[M]_o$ and $[M]_t$ are the concentration of double bonds at the beginning of the dark period and at a later time *t* within the dark period. The value of ratio of rate constants can be thus obtained from the slope of $[M]_t/(R_p)_t$ vs *t*. The above expression represents partly integrated bimolecular termination model.

The variable autocatalytic model can also be applied to the autoaccelerating systems.[14,15] It has been observed that mono/diacrylate and dimethacrylate photopolymerisation follow the modified autocatalytic model even though photopolymerisation is an autoaccelerating process.[2] As per the model:[16,17]

$$\frac{d\alpha}{dt} = k\alpha^m(1-\alpha)^n \qquad 6.4$$

where, $d\alpha/dt$ is the time dependant rate of photopolymerisation and α is the corresponding conversion. The parameters *k, m* and *n* represent the rate constant, autocatalytic exponent and reaction order exponent respectively. A non linear regression analysis of the above equation can provide the individual values of kinetic parameters.[18]

The present work deals with the photopolymerisation of 2-phenylethyl (meth)acrylates and estimation of their kinetic parameters. Formulations were made by independently homogenising the monomers with photoinitiators of two different classes. Two different compositions of photoinitiators were used to study the effect of concentration of photoinitiator on cure kinetics. These compositions obtained were tested for photo curing performance using differential photocalorimetry (DPC) or photo DSC under polychromatic radiation. The heat flow against time was recorded for all formulations under isothermal conditions and the rates of polymerisation as well as the percentage conversions were estimated. It was observed that due to a longer timescale for reaction diffusion, the methacrylate formulations showed a higher conversion than acrylate formulations. Other parameters such as induction time, maximum rate and conversion attained as well as the time to attain peak maximum were noted. The photopolymerisation and kinetic estimations of the formulations including evaluation of kinetic models are discussed.

6.2 Experimental

6.2.1 Materials

IRGACURE 651 or 2,2-dimethoxy-2-phenyl acetophenone (Aldrich) and DAROCUR TPO or diphenyl-(2,4,6-trimethylbenzoyl) phosphine oxide (Aldrich) were used as received.

6.2.2 FT-IR studies

A Fourier transform infrared spectrometer (Model 68B – Perkin Elmer, USA) was used to identify the reactive functional groups before and after photopolymerisation

studies. The photopolymerisable formulations as well as the post polymerised films were studied.

6.2.3 Photopolymerisation studies

DSC Q 100 differential scanning calorimeter connected to Q Series PCA (TA Instruments, USA) was used for the online monitoring of the photopolymerisation processes. Two photoinitiators, one belonging to acetophenone type (IRGACURE 651) and the other belonging to phosphine oxide type (DAROCUR TPO) were used. Table 6.1 shows structures of photoinitiatores. The mixing of photoinitiators with the synthesised acrylate and methacrylate were done on glass vials in 0.5 g batch sizes. 0.25 and 1 wt% of each photoinitiator was homogenised with each monomer in a vibrating mill for 5 minutes to obtain 8 photopolymerisable formulations. The isothermal photocalorimetry was studied at 40 and 60 ^{o}C. The studies were carried out at 2.7 mW cm^{-2} using a 320-500 nm polychromatic radiation with standard aluminum pans.[21] Accurately weighed (about 3.5 mg) amount of sample was used for analyses under a nitrogen purge of 50 mL min^{-1}. The equilibration of each formulation was done for a period of 5 minutes prior to irradiation. The formulations were irradiated for a period of 8 minutes under a constant photo flux from the machine. The time dependant rate as well as conversion profiles of the *insitu* processes were noted. Kinetic parameters such as induction time (time taken for 1 % conversion), time to attain peak maximum, maximum polymerisation rate as well as maximum conversion reached were noted.

The dark reaction profiles of the (meth)acrylates containing 0.25 wt% of IRGACURE 651 were carried out at 5, 10, 15, 20, 30, 40, 50, 60, 70 and 80 percentage conversions at 40 °C. From the residual monomer concentration and corresponding rate

of polymerisation within the dark regime for the experiments carried out at the above mentioned conversions, the value of k_t^b/k_p was calculated for both the systems using bimolecular termination model.

Table 6.1: Structures Photoinitiators

Name of Photoinitiator	Structure
IRGACURE 651 (2,2-dimethoxy-2-phenyl acetophenone)	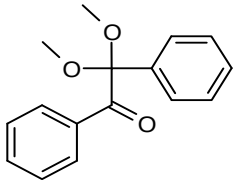
DAROCUR TPO (diphenyl-(2,4,6-trimethylbenzoyl) phosphine oxide)	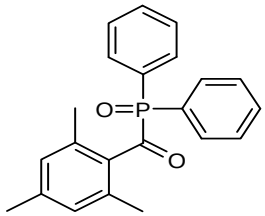

The variable autocatalytic kinetic model is applicable to cure curves with high rate of initiation.[15,22] As a result, the equation was applied to the photocuring profile of formulations containing 2-phenylethyl acrylate. Formulations involving 2-phenylethyl methacrylate were not considered for these analyses due to the presence of an initial shoulder in the cure curve (Figure 6.1b). Kinetic parameters such as *k, m* and *n* for the acrylate systems were noted using variable autocatalytic kinetic model. The values of pre-exponential factor and activation energy were calculated using classical Arrhenius equation.

6.3 Results and Discussion

6.3.1 Photopolymerisation – Total irradiation studies

The rates of photopolymerisations for all the studied formulations were calculated from the photo DSC heat flow measurements. If *dH/dt* represents the heat flow per unit time, then the rate of photopolymerisation *(R_p)* is given by:[23,24]

$$R_p = \frac{(dH/dt)}{\Delta H_{theor}} \qquad 6.5$$

where ΔH_{theor} is the total theoretical heat flow for complete polymerisation of the system. The ΔH_{theor} values were calculated based on the total heat released per mole for acrylate (20.6 kcal mol^{-1}) and methacrylate (13.1 kcal mol^{-1}) double bonds during polymerisation.[25,26] On integration of the above expression the corresponding conversion can be obtained. Hence the percentage conversion (*% C*) of the monomer was calculated using the expression:[23,24]

$$\%\ C = \frac{\Delta H_t}{\Delta H_{theor}} \times 100 \qquad 6.6$$

where ΔH_t denotes the heat flow up to a particular time *t* from the starting of the photopolymerisation process.

6.3.1.1 Analysis of heat flow

The rate profiles for the photopolymerisation of the formulations involving 2-phenylethyl acrylate and 2-phenylethyl methacrylate (Figure 6.1) are of expected nature as reported in literature.[2,10,27] The initial ascending nature of the rate curve is due to initiation followed by autoacceleration and diffusion controlled polymerisation processes while the later descending nature of the rate curve is the deceleration step where an increase in viscosity during photopolymerisation can impart restriction to the mobility of

polymerising moieties. Acrylate formulations showed a faster cure rate than that of the corresponding methacrylate formulations. The decrease in the rate of maximum polymerisation rate ($R_{p\ max}$) of acrylate at higher temperature accounts for the rapid attainment of limiting viscosity before $R_{p\ max}$ due to an enhancement in initial polymerisation rate with reduction in time for gelation.

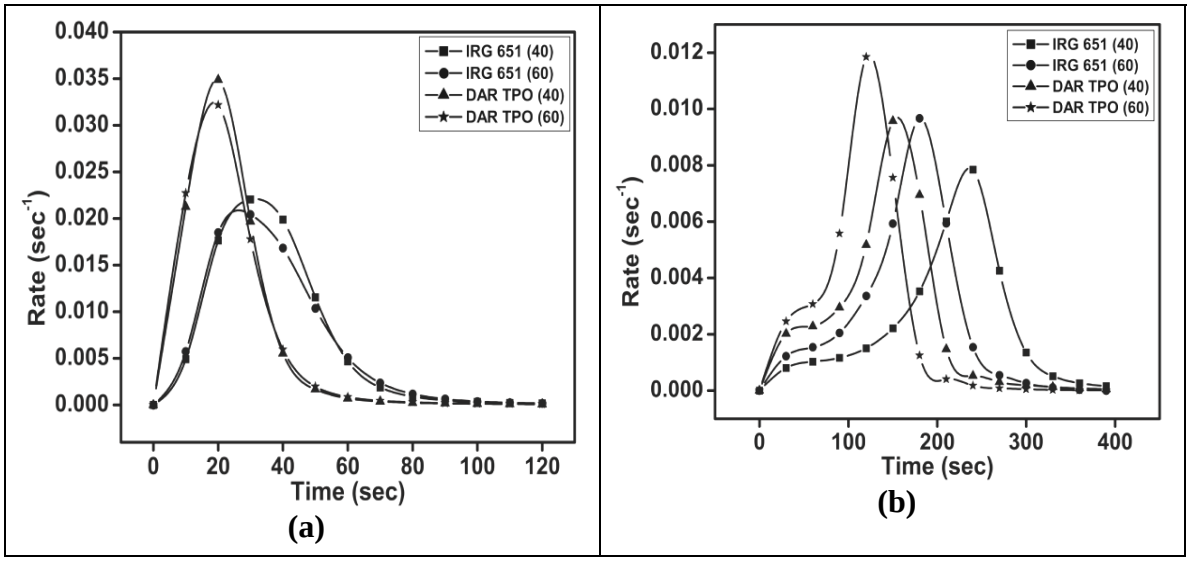

Figure 6.1: The time dependant rate of polymerisation for (a) 2-phenylethyl acrylate and (b) 2-phenylethyl methacrylate containing 0.25 wt% of IRGACURE 651 and DAROCUR TPO at 40 and 60 °C.

Due to a lower viscosity build up, the methacrylate showed a longer time scale for reaction diffusion than that of acrylate (Figure 6.1 and 6.2). This delay resulted in a higher conversion of methacrylate than the corresponding acrylate formulations. The fact that the reaction diffusion occurs for the methacrylate formulations over a longer time scale can also be explained by partial irradiation studies, which is discussed later.

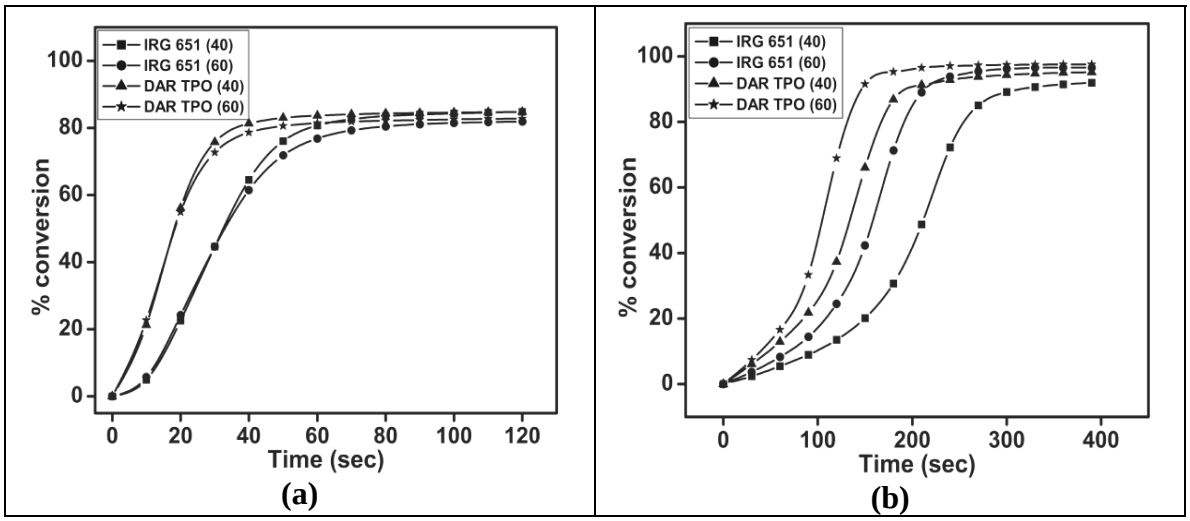

Figure 6.2: The time dependant monomer conversion for (a) 2-phenylethyl acrylate and (b) 2-phenylethyl methacrylate containing 0.25 wt% of IRGACURE 651 and DAROCUR TPO at 40 and 60 °C.

6.3.1.2 Estimation of kinetic parameters

The total number of effective free radicals involved in photopolymerisation is found to depend upon an optimum concentration. This concentration of effective radicals will vary for different systems due to many parameters such as autoacceleration, segmental and reaction diffusions, nature of the photopolymerisable system, purge gas used and irradiation conditions.

The Tables 6.2 and 6.3 show that for both acrylates and methacrylates, induction time decreases with an increase in concentration of photoinitiator and temperature. This is due to the enhancement of the rate of photopolymerisation at the beginning of the reaction resulting from an increase in number of propagating chains and mobility of the system.[28] The peak maximum time is also found to show the same behaviour due to the same effect. For formulations involving 2-phenylethyl methacrylate, the rate of maximum polymerisation was found to increase with increase in temperature as well as increase in concentration of photo initiator, showing low viscosity build up. The radicals produced

during initiation, which can effectively create new chains increases with increase in concentration of photo initiator and is further enhanced by higher mobility at higher temperatures during the initial stages which accounts for the above effect. In the case of acrylate formulations, the rate of maximum polymerisation was found to increase with increase in concentration of photo initiator. However an increase in temperature resulted in a decrease in $R_{p\ max}$. This behaviour of formulations involving acrylate is due to high initial rate of polymerisation than methacrylate.[27] With increase in temperature even though the radical mobility is enhanced, a faster autoacceleration will result in instantaneous viscosity build up which occur before $R_{p\ max}$ at higher temperature. This results in the reduction of $R_{p\ max}$ with increase in temperature for acrylates. During reaction diffusion, the rate of viscosity build up for acrylates is much higher than the methacrylates and the time of reaction diffusion gets reduced. This results in faster reaction of the acrylates than the corresponding methacrylates, resulting in a lower final conversion.

The kinetic estimations as per the variable autocatalytic model for formulations involving 2-phenylethyl acrylate (Table 6.2) show that the rate constant increases with temperature for a particular concentration of photoinitiator. The rate constant also shows an increase with increase in concentration of photo initiator at a particular temperature. On analyses, the variable autocatalytic model is a fit for the acrylate system as the values of *m* and *n* are nearly constant for all the studied formulations. Classical Arrhenius equation 6.6 was used to calculate the overall activation energy *(E_a)* and the pre-exponential factor (*A)* for the acrylate formulations.

$$k = Ae^{(-Ea/RT)} \qquad 6.6$$

where k is the temperature dependent rate constant and *T* is the absolute temperature in Kelvin. The overall activation energy is given by the expression:[29]

$$E_a = E_p + 0.5E_i - 0.5E_t \qquad 6.7$$

where E_i, E_p and E_t are the respective activation energies for initiation, propagation and termination reactions. The rate constant for photochemical initiation (k_i) involving bimolecular termination is expressed as:

$$k_i = \frac{k_p}{\phi\sqrt{k_t^b I_a}} \qquad 6.8$$

where ϕ is the quantum yield of initiation and I_a is the intensity of absorbed light. Since the value of k_t^b is much higher during initial stages, the value of the ratio $(k_p / (k_t^b)^{0.5}$ in the above expression is very low and hence lower will be the value of k_i. Hence the value of E_i for photochemical initiation is negligible and the equation reduces to:[29]

$$E_a = E_p - 0.5E_t \qquad 6.9$$

Table 6.3 shows an enhancement in pre-exponential factor as well as overall activation energy with an increase in concentration of photo initiator. With increase in concentration of photoinitiator the initial collisions are increased. Hence the initial speeds of reactions are increased and are observable from a decrease in induction and peak maximum times. This is reflected in the values of pre-exponential factor which is proportional to the frequency of collision. However, instead of an expected decrease in the value of overall E_a with increase in the concentration of photoinitiator, an increase was observed.[29] Even though collisions are higher at higher concentration of photo initiator at initial stages of the polymerisation, variations can occur in the effective

number of radicals which govern the kinetics of propagation reaction.[2] As a combined effect of drastic reduction in bimolecular termination along with an onset of viscosity build up are observable during the initial stages of polymerisation, an enhancement in the value of E_a as per the above reduced expression can be expected.

Table 6.2: The kinetic parameters obtained for the methacrylate formulations.

Photo Initiator	Temp (°C)	Conc. of PI (w/w)	Ind. Time (sec)	Peak max. time (sec)	$R_{p\,max}$ (x 10^{-3}) (sec^{-1})	C_{max} (%)	ΔH (J/g)
IRG 651	40	0.25	13.16	236.47	7.90	92.36	266.1
	60	0.25	8.59	180.79	9.67	96.56	278.2
	40	1.00	6.85	165.30	10.54	93.36	269.0
	60	1.00	4.50	121.71	14.55	99.75	287.4
DAR TPO	40	0.25	5.04	154.64	9.70	95.24	274.4
	60	0.25	4.31	123.25	11.94	97.60	281.2
	40	1.00	3.25	114.57	14.30	98.99	285.2
	60	1.00	2.21	88.040	18.50	99.02	285.3

Table 6.3: The kinetic parameters obtained for the acrylate formulations.

Photo Initiator	Temp (°C)	Conc. of PI (w/w)	Ind. Time (sec)	Peak max. time (sec)	$R_{p\,max}$ (x 10^{-2}) (sec^{-1})	C_{max} (%)	ΔH (J/g)	m	n	k (min^{-1})	ln A (min^{-1})	E_a (kJ/mol)
IRG 651	40	0.25	4.18	31.4	2.21	85.66	419	0.547	1.05	3.8	3.04	4.44
	60	0.25	3.48	26.2	2.09	82.76	404.8	0.566	1.4	4.21		
	40	1	0.81	20.9	3.4	84.74	414.5	0.458	0.97	5.1	3.77	5.57
	60	1	0.75	19.7	3.2	83.66	409.2	0.474	1.32	5.8		
DAR TPO	40	0.25	0.6	19.7	3.49	85.29	417.2	0.454	1.09	5.6	3.6	4.9
	60	0.25	0.52	18.7	3.24	83.66	409.2	0.457	1.43	6.27		
	40	1	0.61	13.9	4.24	86.11	421.2	0.481	1.43	8.9	4.46	5.91
	60	1	0.57	12.9	4.12	84.15	411.6	0.509	1.92	10.2		

6.3.2 Photopolymerisation – Partial irradiation studies

Since the final achieved conversions for the (meth)acrylate formulations are higher as observable from Table 6.2 and 6.3, the nature of terminations before attaining maximum achieved conversions can be considered to have a predominance of bimolecular rather than monomolecular terminations. Thus the ratio of rate constants to conversions lower than the maximum observed conversions were calculated using partially integrated bimolecular termination model.[12, 25] The values of k_t^b/k_p at different conversions using the bimolecular termination model for the dark reactions (Figure 6.3) are given in Figure 6.4. At very low conversions, the ratio of rate constant showed the highest value due to an enhancement in bimolecular terminations resulting from high segmental mobility and low system viscosity. With an increase in conversion, the rate of propagation reaction is accelerated coupled with reduced terminations. But with a further increase in conversion, the system viscosity is higher and the reaction diffusion sets in which drastically reduce the termination rate. The ratio thus represents a plateau due to a similar rate of termination as compared to propagation reaction. The plateau region was found more pronounced in the case of methacrylate than acrylate due to a longer timescale for reaction diffusion. The plateau region can be considered as the region where the reaction diffusion controls the photopolymerisation process.[25] However in the case of acrylate formulation, the ratio showed a slight increase after 70% conversion. The rate of decrease in propagation just before final achieved conversion is found to be marginally higher than that of termination which accounts for this effect.[2] Similar effect has been reported on different multiacrylates by Anseth et. al. using monochromatic condition.[25,26]

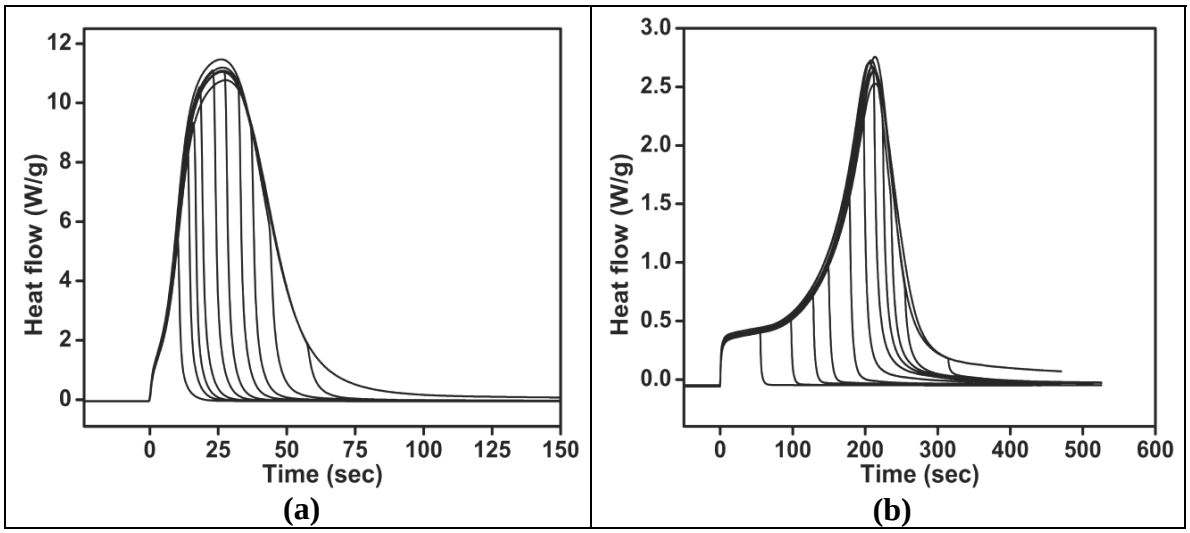

Figure 6.3: The time dependant heat flow profiles for the dark reaction studies at different conversions for (a) 2-phenylethyl acrylate and (b) 2-phenylethyl methacrylate containing 0.25% of IRGACURE 651 at 40 °C.

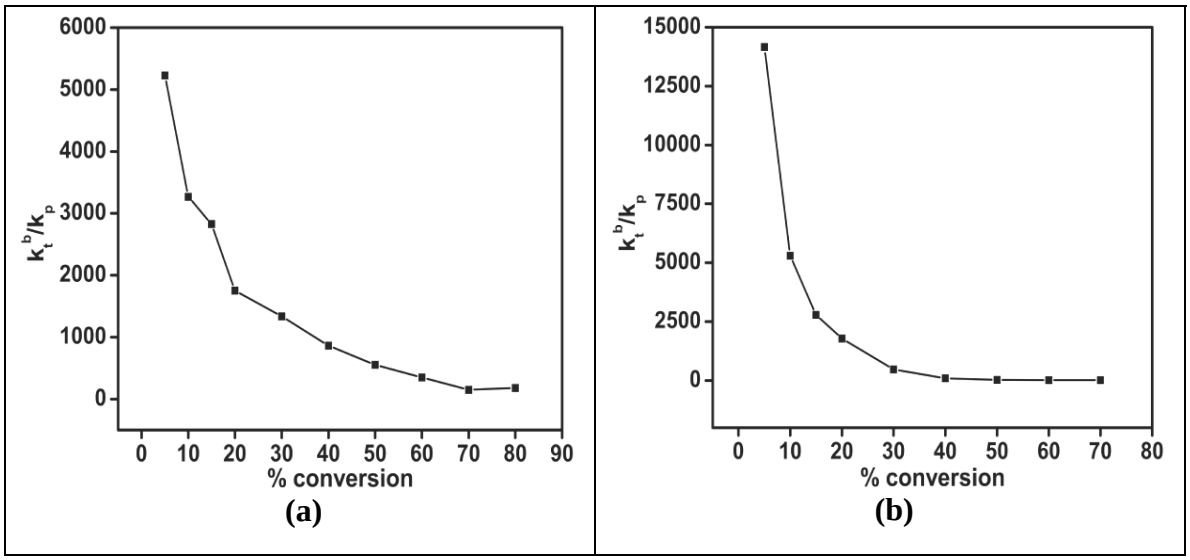

Figure 6.4: The ratio of rate constants as per bimolecular termination model under dark reaction conditions for (a) 2-phenylethyl acrylate and (b) 2-phenylethyl methacrylate containing 0.25% of IRGACURE 651 at 40 °C.

6.3.3 FT-IR analyses

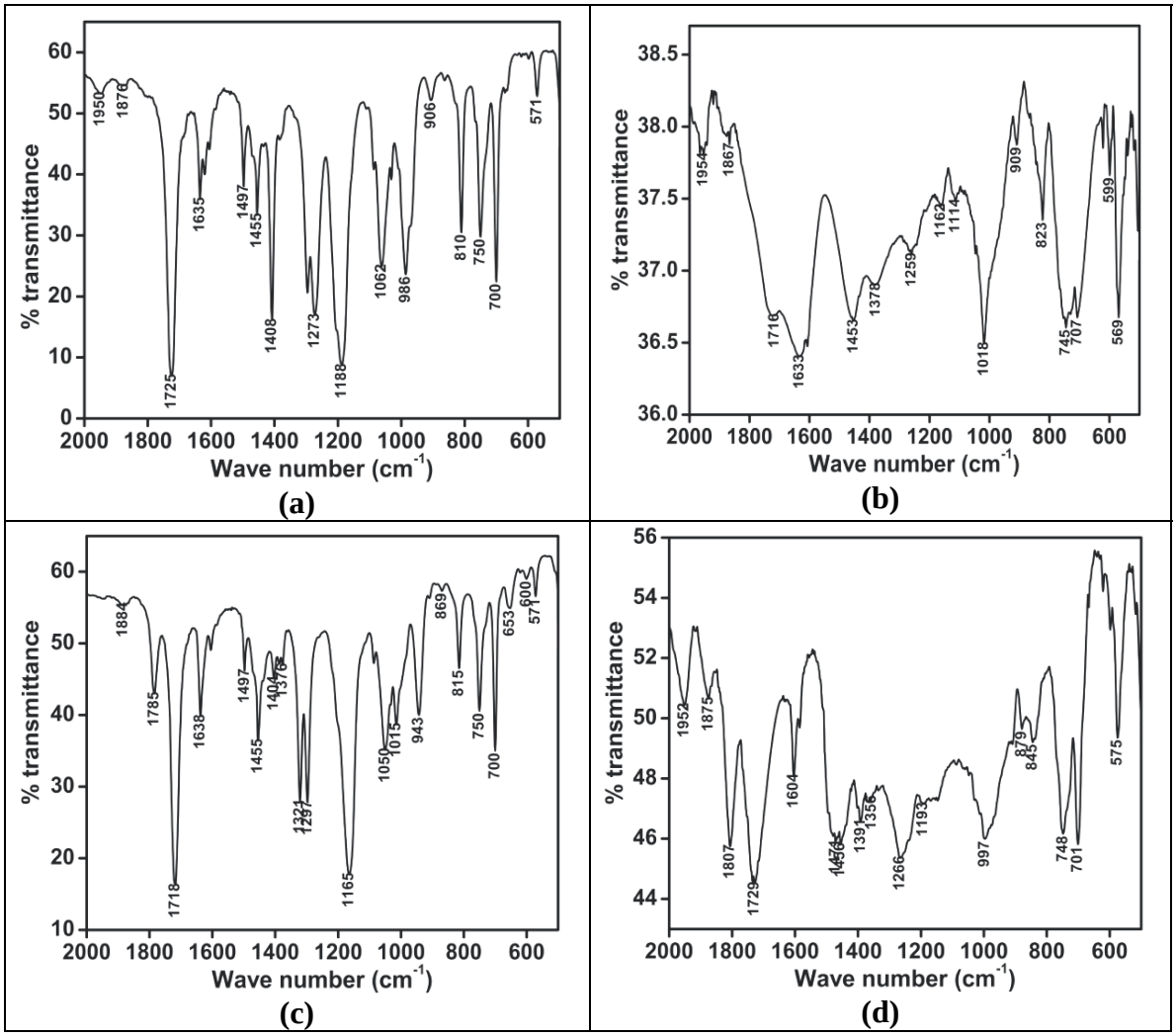

Figure 6.5: The infrared spectra of formulation involving 2-phenyl ethyl acrylate before (a) and after (b) polymerisation and 2-phenyl ethyl methacrylate before (c) and after (d) polymerisation.

The conversion profiles of C=C and =C-H groups of the meth(acrylates) can be monitored by IR spectra.[31] Infra red spectroscopy of the formulation based on 2-phenylethyl acrylate showed double bonds corresponding to acrylate functionality at 1635 and 810 cm^{-1}. On polymerisation, the peak at 810 cm^{-1} disappeared while the peak at 1633 cm^{-1} appeared much reduced. This shows reduction in the concentration of

acrylate functionality in the polymerised matrix (Figure 6.5 a-b). However the 2-phenylethyl methacrylate system showed total disappearance in the concentration of double bonds corresponding to methacrylate functionality at 1638 and 815 cm^{-1} showing that the residual methacrylate functionality in the photopolymerised matrix is negligible (Figure 6.5c-d). These observations also support the percentage conversion data of the formulations as given in Table 6.2 and 6.3.

PART-B: Thermal Polymerisation

6.4 Introduction

2-Phenylethyl acrylate and 2-phenylethyl methacrylate are widely used as specialty coatings, adhesives and various optical applications. Inspite of having such versatility in applications, not much literature is available about the thermodynamic properties of these (meth)acrylates, especially about their kinetic behaviour in case of bulk polymerisation. Due to their fast and highly exothermic nature of polymerisation, most methods of studying polymerisation kinetics (e.g., dilatometry or monitoring of unreacted monomer concentration) are not suitable for studying bulk polymerisation[32].

Various types of thermal analysis have been applied in almost all fields of material research. The thermoanalytical method, in which the properties of a sample heated at a constant rate of heating and observed continuously, is an effective method when the thermal response time is large. Compared with rate, considerable change occurs during the period of heating the sample up to the desired temperature in an isothermal measurement.

Thermal analysis techniques such as thermogravimetry (TG), differential thermal analysis (DTA) and differential scanning calorimetry (DSC) provide the kinetic parameters during not only physical but also chemical changes.[33-36] DSC provides both qualitative and quantitative information about material transitions. For some of these transitions, DSC can provide not only the temperature at which the transition (reaction) occurs and how much total heat is involved, but DSC can also provide valuable information about the rate (kinetics) of reaction.

Differential scanning calorimetry (DSC) is a powerful tool for evaluating miscibility of crystalline/amorphous polymer blends[44] and the direct measurement of the rate of an exothermic polymerisation. DSC has been used with success to follow the course of free-radical polymerisation with bulk monomer using either an isothermal or scanning method.[45-47]

DSC is used to measure the amount of energy to be supplied or removed to keep the temperature difference $\Delta T = 0$ between the sample and the reference with respect to time or temperature as the two specimen are heated at a controlled heating rate. The DSC technique has been widely employed to determine the physical transitions such as glass transition temperature (T_g), crystallization (T_c) and melting temperature (T_m) of the polymers and to study the varieties of reactions such as polymerisation, decomposition, oxidation, vulcanisation and curing reactions.[37-43]

DSC is a convenient tool to observe the reaction as endothermic or exothermic heat flow. The kinetics of chemical reaction can be evaluated from,[48,49] DSC exothermal peak obtained from either isothermal or non-isothermal measurements. Because of its advantages such as small sample size, handiness of manipulation, rapidity of performance and versatility, DSC seemed to be attractive for studying free radical polymerisation system. To induce the production of free radicals in the system, organic peroxides and diazo initiators are commonly used. Free radicals can be formed by thermal decomposition of initiators or by chemical decomposition in ambient temperature applications.[50-52] The free radical polymerisation of (meth)acrylates is a complex process in that several steps are involved. The polymerisation is highly exothermic and can be monitored by thermal analysis techniques such as differential scanning calorimetry.

The kinetic study of an exothermic reaction like the radical polymerisation allows us to determine how much, how fast and at what temperature range the heat is released. Any study of reaction kinetics requires the following fundamental data: reaction rate and degree of conversion of reactants.[53,54] In this technique it is assumed that the rate of exchanged heat is strictly proportional to the rate of the total chemical reactions at any instant as follows:

$$\frac{dH}{dt} = \Delta H \frac{d\alpha}{dt} \qquad 6.10$$

where dH/dt is the heat generated by time t unit or heat flow (DSC ordinate), $d\alpha/dt$ the rate of reaction and ΔH is the heat of reaction obtained as the area of DSC thermograrn. Therefore, it is possible to evaluate the reaction rate $d\alpha/dt$ at the time t and the degree of conversion α reached at time by means of the following expressions:

$$\frac{d\alpha}{dt} = \frac{1}{\Delta H}\frac{dH}{dt} \quad , \quad \alpha = \frac{\Delta H_t}{\Delta H} \qquad 6.11$$

where ΔH_t is the heat released up to time t and it can be obtained by integration of the calorimetric signal dH/dt up to time t.

Modelling the kinetics of material reactions provides the researcher and engineer with valuable information for process development and prediction of optimum reaction temperatures, process control by optimisation of reaction advancement or conversion, and estimation of material lifetimes. Several DSC approaches are available for obtaining this kinetic information.

6.4.1 Non-isothermal techniques

In theory, a non-isothermal DSC trace should contain all the kinetic information normally embodied in a series of isothermal experiments.[52] This makes the nonisothermal

approach highly attractive. This technique is fairly rapid and works reasonably well for simple reactions. On the other hand this technique is not applicable in any of the following cases,[55-58]

a. Overlapping reaction peaks

b. Decomposition occurs during reaction

6.4.2 Kinetic parameters

The kinetic analysis of free-radical polymerisation curves involves the search for the kinetic parameters the activation energy (E_a) and rates of reactions associated with the process. It was assumed that the dynamic heat obtained as the area between the DSC curve and the baseline was a good approximation for the total reaction heat of polymerisation.

6.4.2.1 Kissinger method

Murray and White[61] showed that the temperature of maximum deflection is defined by the kinetic constants of the material and the heating rate. The assumption that the peak temperature occurs when the reaction rate is a maximum is supported by the experimental work. It should then be possible to calculate the kinetic constants directly from DSC data by making a number of patterns at different heating rates.

For the first order thermal decomposition at constant temperature,

$$\left(\frac{\partial x}{\partial t}\right)_T = k_T(1-x) \qquad 6.12$$

where x is the fraction of material decomposed. The magnitude of the rate constant, k_T, is determined by the temperature and is given by the Arrhenius equation:

$$k_T = Ae^{-\frac{E_a}{RT}} \tag{6.13}$$

where R is the gas constant, T is the Kelvin temperature, and A and E_a are constants that are properties of the material. The constant E_a, called the activation energy, is often interpreted as the energy barrier opposing the reaction. The constant A, most often called the frequency factor, is a measure of the probability that a molecule having energy E_a will participate in a reaction. When the temperature is changing with time, the reaction rate is:

$$\frac{dx}{dt} = \left(\frac{\partial x}{\partial t}\right)_T + \left(\frac{\partial x}{\partial T}\right)_t \frac{dT}{dt} \tag{6.14}$$

The rate of change of x with temperature, with the time coordinate fixed, $(\partial x/\partial t)_t$ is zero, because fixing the time also fixes the number and position of the particles constituting the system. The only effect of an instantaneous change in temperature is in the velocity of thermal motion of the particles. The total rate of reaction may then be expressed as:

$$\frac{dx}{dt} = A(1-x) \quad e^{-\frac{E_a}{RT}} \tag{6.15}$$

The above expression 6.15 holds for any value of T, whether constant or variable, as long as x and T are measured at the same instant. When the reaction rate is a maximum, its derivative with respect to time is zero. Solving above equation for $(\partial/\partial t)(\partial x/\partial t)$:

$$\frac{d}{dt}\left(\frac{dx}{dt}\right) = \frac{dx}{dx}\left(\frac{E_a}{RT^2}\frac{dT}{dt} - Ae^{-\frac{E_a}{RT}}\right) \tag{6.16}$$

The maximum value of dx/dt occurs at temperature T_p, defined by:

$$Ae^{-\frac{E_a}{RT_p}} = \frac{E_a}{RT_p^2}\frac{dT}{dt} \qquad 6.17$$

Equation 6.17 derived by Murray and White[62]. From above equation it is shown that:

$$\frac{d\left(\ln\frac{\phi}{T_p^2}\right)}{d\left(\frac{1}{T_p}\right)} = -\frac{E_a}{R} \qquad 6.18$$

where T_p, ϕ, E_a and R is peak indicating temperature, heating rate, activation energy and the gas constant, respectively. According to equation 6.18 Kissinger[59,60] derived the following equation:

$$\ln\frac{\phi}{T_p^2} = -\frac{E_a}{RT_p} + C \qquad 6.19$$

The left term of the equation 6.19 was plotted *vs*. $1/T_p$, and then E_a can be evaluated from the slope.

6.4.2.2 Ozawa method

Ozawa method[63] allows determining the activation energy E_a for nth order reactions. It is based on the variation of peak temperature of exothermic DSC curve with heating rate. Assuming that the extent of reaction at the peak temperature is constant and independent of heating rate, Ozawa derived the following expression:

$$\ln\phi = const - 1.052\frac{E_a}{RT_p} \qquad 6.20$$

This expression shows a linear dependence of the reciprocal absolute peak temperature T_p on the logarithm of heating rate. The activation energy E_a is calculated from the slope of the straight line obtained by Ozawa plot.

6.5 Experimental

2-phenylethyl acrylate and 2-phenylethyl methacrylate are prepared by reacting 2-phenylethanol with acryloyl and methacryloyl chloride, respectively. Synthesised monomers were purified by distillation under reduced pressure. 2,2'-azobisisobutyronitrile (AIBN) was recrystallised twice from methanol. DSC Q 100 (TA Instruments, USA) was used for online monitoring of the bulk polymerisation process. Samples of mixture (monomer+initiator) were prepared in glass vials of 5 mL capacity and degassed by N_2 at 0 °C. The mol ratios of the compositions (monomer: initiator) were:

[PEA]: [AIBN] = 50.41:1, 76.34:1, 100.45:1, 124.45:1

[PEMA]: [AIBN] = 51.52:1, 76.01:1, 100.58:1, 126.71:1

The measurements were performed under nitrogen gas purge of 50 mL/min in aluminum pans filled with 10 mg of the sample for each polymerisation experiment. Heating rates of 2, 5, 7, 10, and 15 °C min^{-1} were used in case of 2-phenylethyl acrylate while 5, 7, 10, 15 and 18 °C min^{-1} were used in case of 2-phenylethyl methacrylate. Each sample was placed in the sample holder assembly of DSC at 40 °C and scanned up to 180 °C. Temperature calibration of the calorimeter was performed with pure indium metal.

6.6 Results and Discussion

Figure 6.6 (a-d) and Figure 6.7 (a-d) shows DSC thermograms for the PEA and PEMA polymerisation obtained at five different scan speeds for different concentrations.

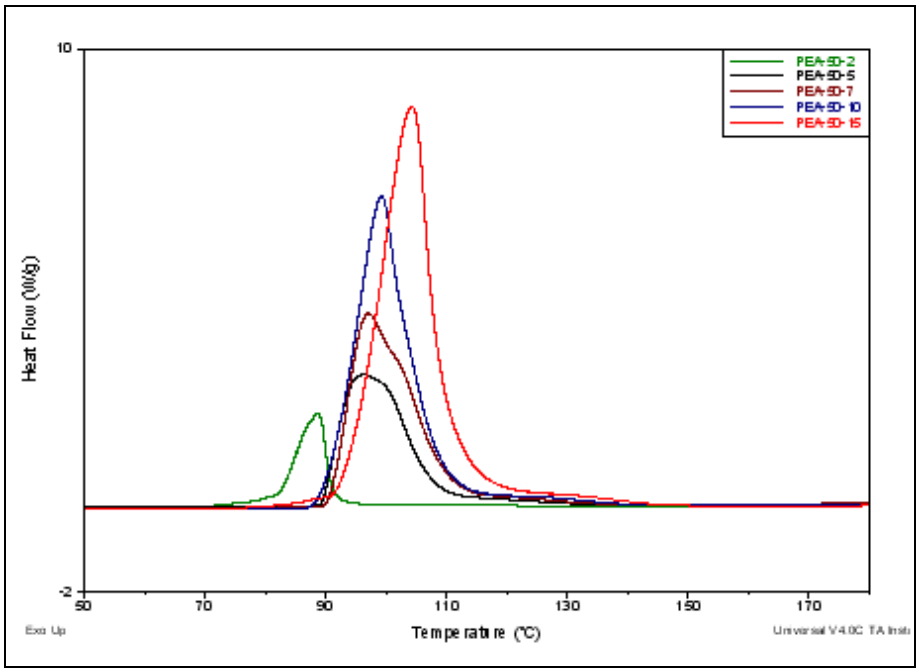

(a)

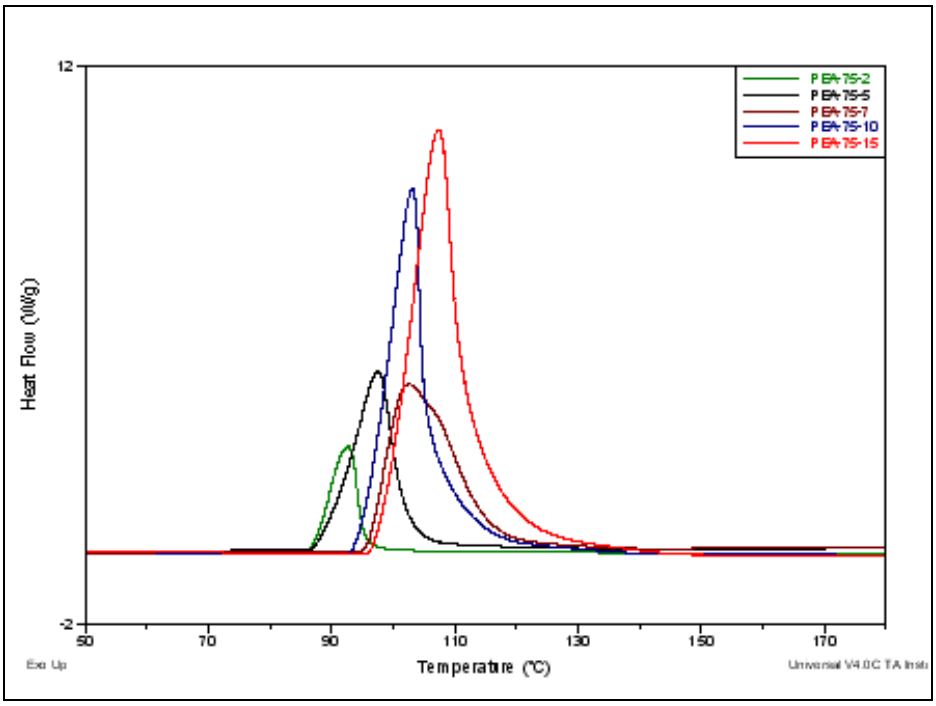

(b)

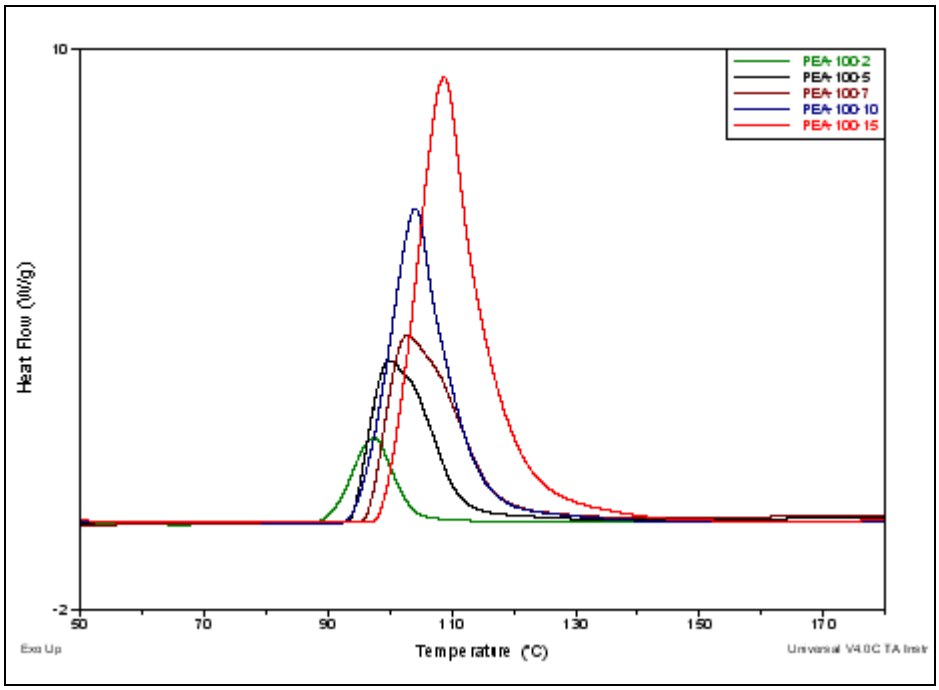

(c)

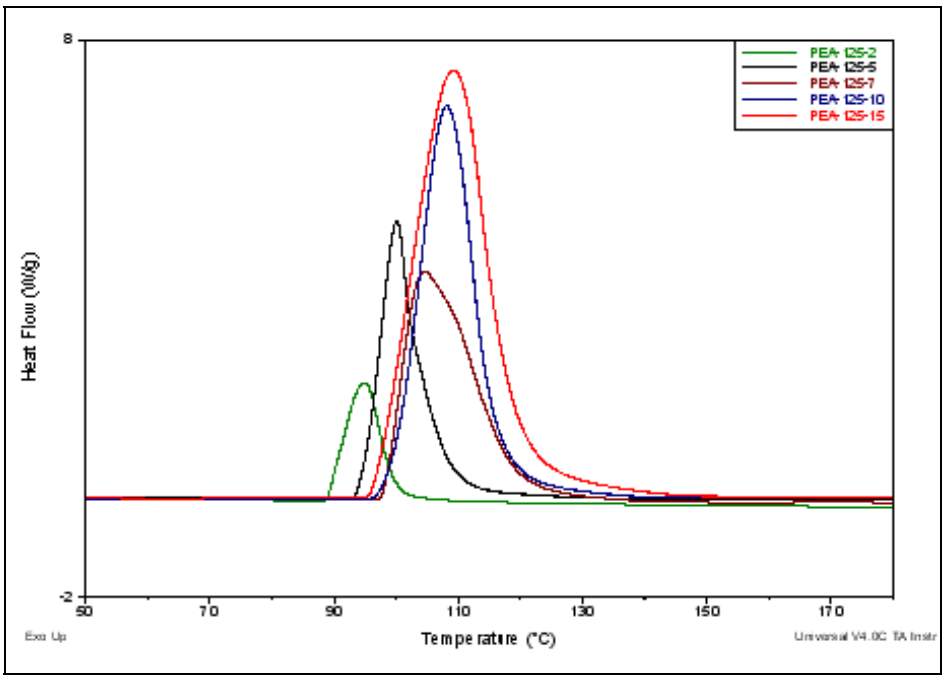

(d)

Figure 6.6: (a-d) DSC curves of the samples with concentration [PEA:AIBN] (a) 50.41:1, (b) 76.34:1, (c) 100.45:1 and (d) 124.45:1

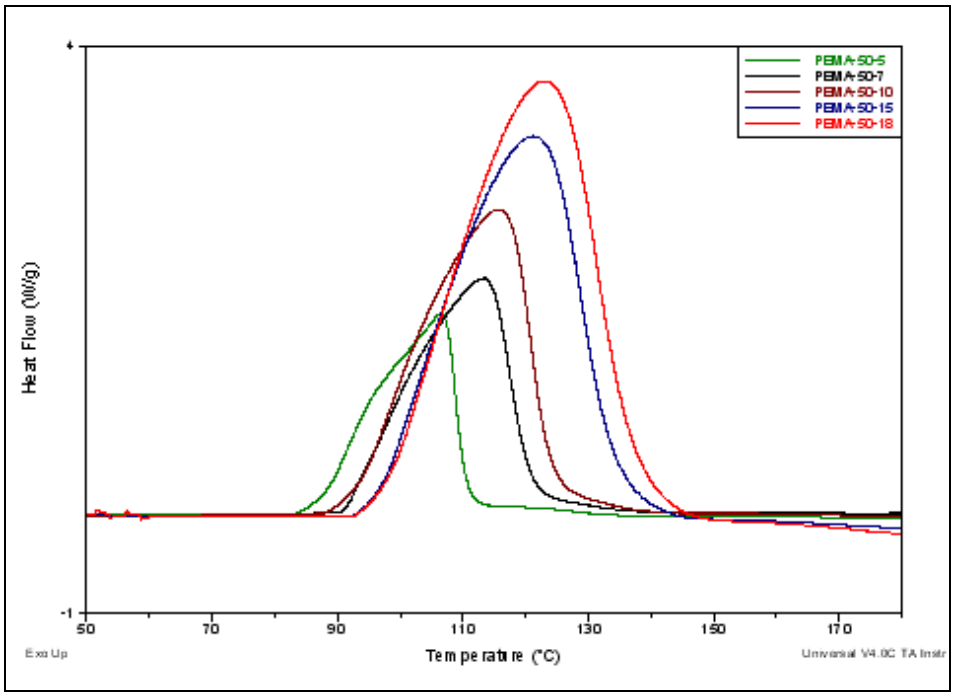
PBMA-50-5
PBMA-50-7
PBMA-50-10
PBMA-50-15
PBMA-50-18
Heat Flow (W/g)
Temperature (°C)
Exo Up
50
70
90
110
130
150
170
-1

(a)

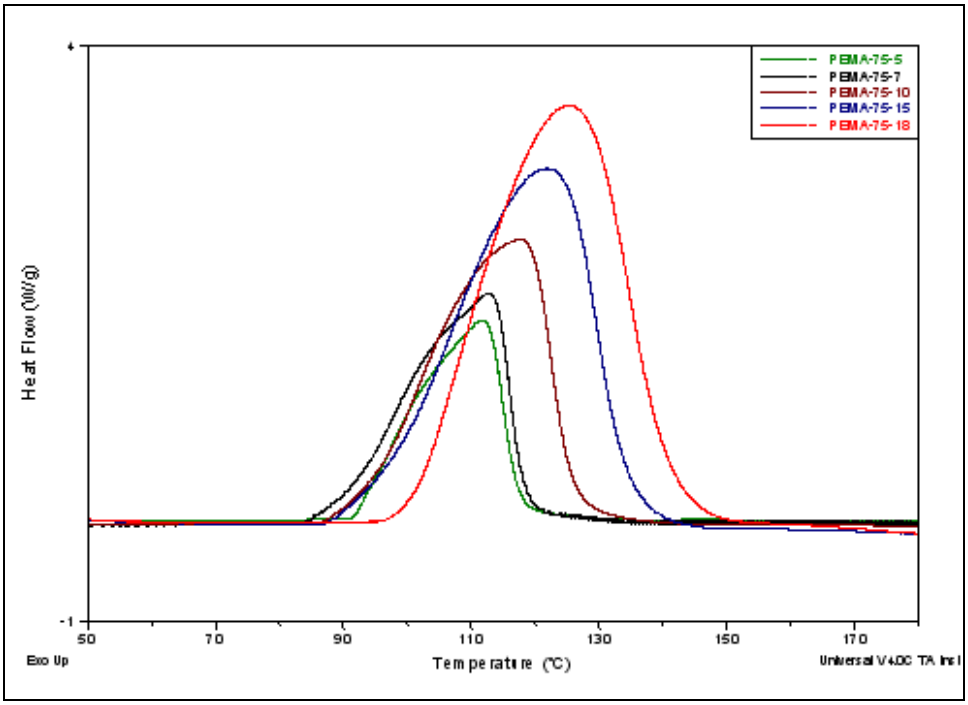
PBMA-75-5
PBMA-75-7
PBMA-75-10
PBMA-75-15
PBMA-75-18
Heat Flow (W/g)
Temperature (°C)
Exo Up
50
70
90
110
130
150
170
-1

(b)

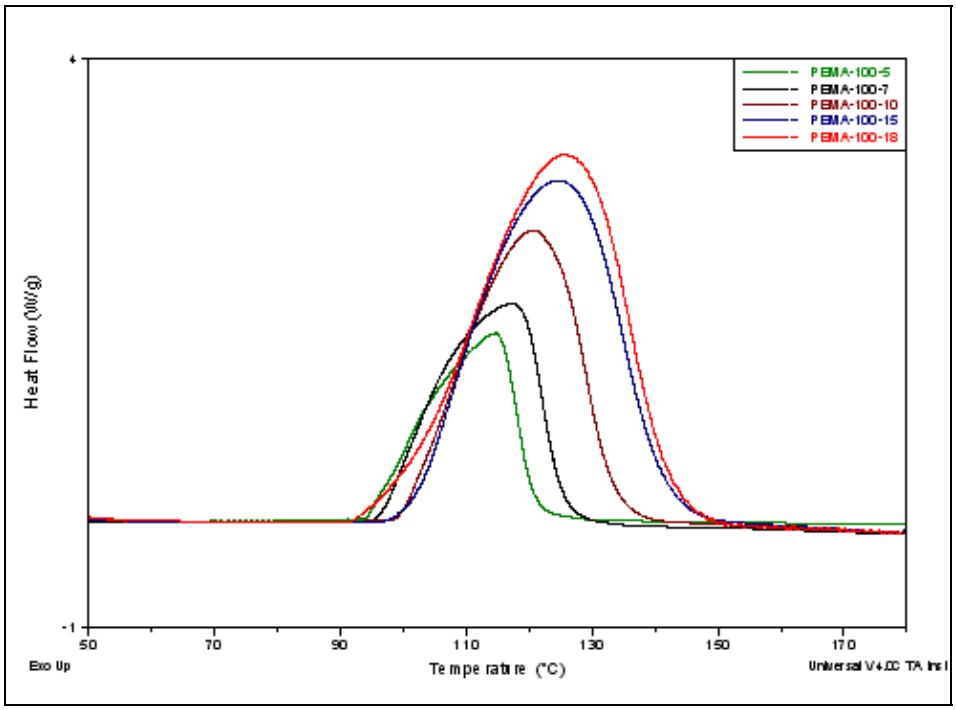

(c)

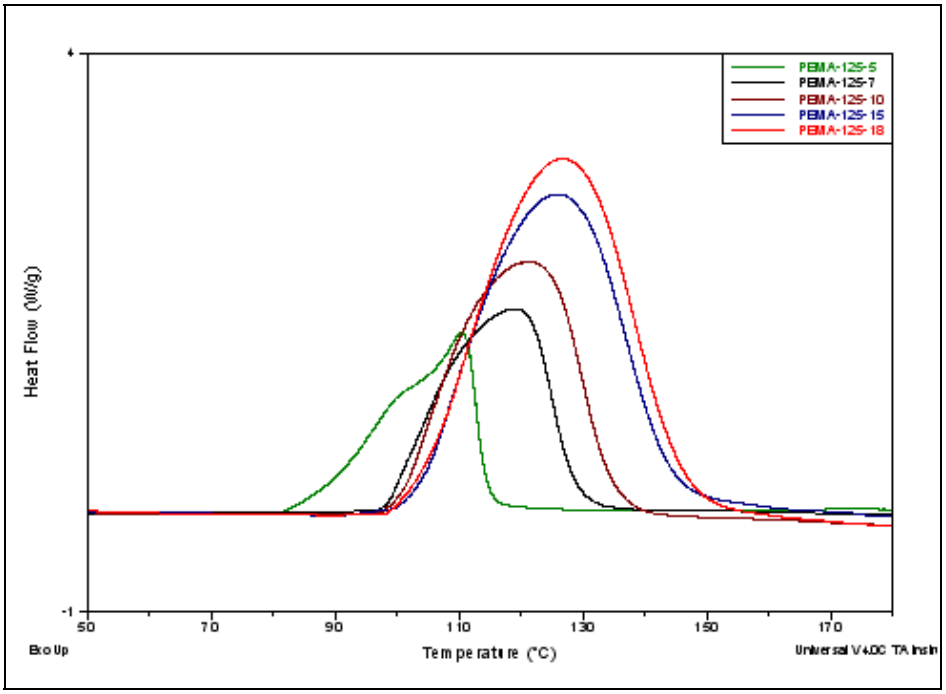

(d)

Figure 6.7: (a-d) DSC curves of the samples with concentration [PEMA:AIBN] (a) 51.52:1, (b) 76.01:1, (c) 100.58:1 and (d) 126.71:1

The kinetic analysis of free-radical polymerisation curves involves the search for E_a associated with the process. It was assumed that the dynamic heat obtained as the area between the DSC curve and the baseline was a good approximation for the total heat of polymerisation.

It is observed from these curves that peak maximum temperature of polymerisation exotherm increases with increase in heating rate and initiator concentration. Maximum of the curves shifted to higher temperature with increasing heating rate due to the dependence of monomer conversion on time and temperature. Similar results have been found in all samples with different molar ratios of [PEA]:[AIBN] and [PEMA]:[AIBN]. Table 6.4 and 6.5 gathers the exothermic DSC peak temperatures and heat of polymerisation of every sample at different heating rates for PEA and PEMA respectively. In case of PEA heat of polymerisation ranges from 71.82 to 85.67 kJ/mol whereas it ranges from 61.04 to 65.44 kJ/mol in case of PEMA.

Table 6.4: DSC peak temperature and Heat of polymerisation of for various concentrations of PEA:AIBN at different heating rates

ϕ (°C)	PEA:AIBN (mol:mol)							
	50.41:1		76.34:1		100.45:1		124.45:1	
	T_p (°C)	ΔH (kJ/mol)	T_p (°C)	ΔH (kJ/mol)	T_p (°C)	ΔH (kJ/mol)	T_p (°C)	ΔH (kJ/mol)
2	88.68	71.34	92.7	78.31	97.56	81.68	95.02	79.51
5	96.32	81.12	97.51	78.45	100.06	78.87	100.08	81.09
7	96.97	82.97	101.23	81.9	102.94	79.19	104.62	82.97
10	99.18	82.03	103.13	81.96	104.12	83.07	108.13	81.68
15	104.22	75.47	107.34	76.43	108.77	85.67	109.19	82.15

Table 6.5: DSC peak temperatures and Heat of polymerisation for four various concentrations of PEMA:AIBN at different heating rates

ϕ (°C)	PEMA:AIBN (mol:mol)							
	51.52:1		76.01:1		100.58:1		126.71:1	
	T_p (°C)	ΔH (kJ/mol)	T_p (°C)	ΔH (kJ/mol)	T_p (°C)	ΔH (kJ/mol)	T_p (°C)	ΔH (kJ/mol)
5	106.57	63.11	111.98	63.69	114.65	64.18	110.56	59.28
7	113.51	64.34	112.70	62.54	117.63	63.77	119.57	62.34
10	115.86	64.86	117.81	63.21	120.65	64.88	121.65	63.66
15	121.25	64.35	121.88	61.04	124.70	61.94	126.02	59.62
18	123.06	65.44	125.35	61.10	125.72	58.14	126.84	58.23

6.6.1 Kinetic parameters

Since the peak corresponding to polymerisation reaction is well resolved, non-isothermal methods are employed for kinetic analyses. Variable heating rates, which depend on peak maxima in DSC curve, are employed for the purpose, where the apparent variations in activation parameters caused by heating rates are taken care of. Moreover, the method does not invoke reaction order or fractional conversion in deriving the kinetic parameters. The Kissinger's and Ozawa's methods, based on variable heating rate were used for finding the activation parameters and their dependency on structure of the monomers.

According to Kissinger equation 6.9, $ln(\phi/T_p^2)$ was plotted *vs*. $1/T_p$ (Figure 6.8), and then E_a was evaluated from the slope. The obtained E_a values are listed in Table 6.4, mean E_a values for PEA and PEMA are 159.24 and 107.75 kJ/ mol, respectively. Also E_a values are determined applying Ozawa equation (6.10) by plotting $ln\ \phi$ *vs*. $1/T_p$ (Figure 6.9). According to Ozawa mean E_a values for PEA and PEMA are 174.16 and 120.19 kJ/ mol, respectively.

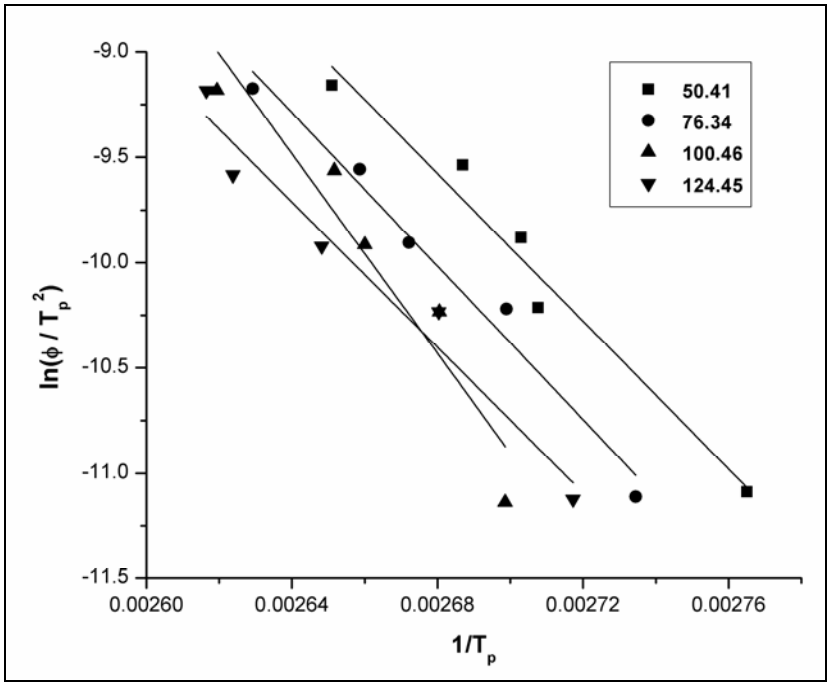

(a)

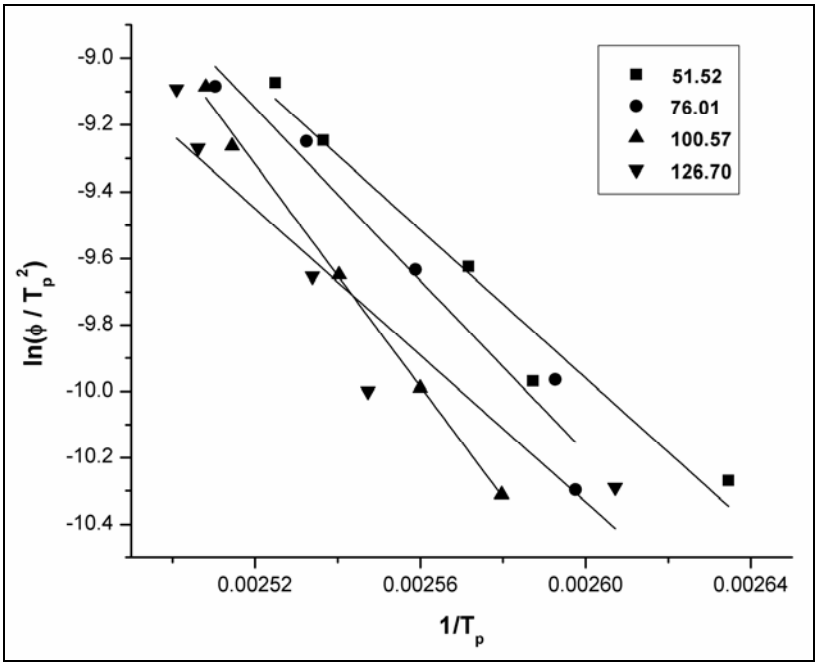

(b)

Figure 6.8 (a-b): Determination of activation parameters by Kissinger's method for polymerisation reaction of (a) PEA and (b) PEMA at various concentrations.

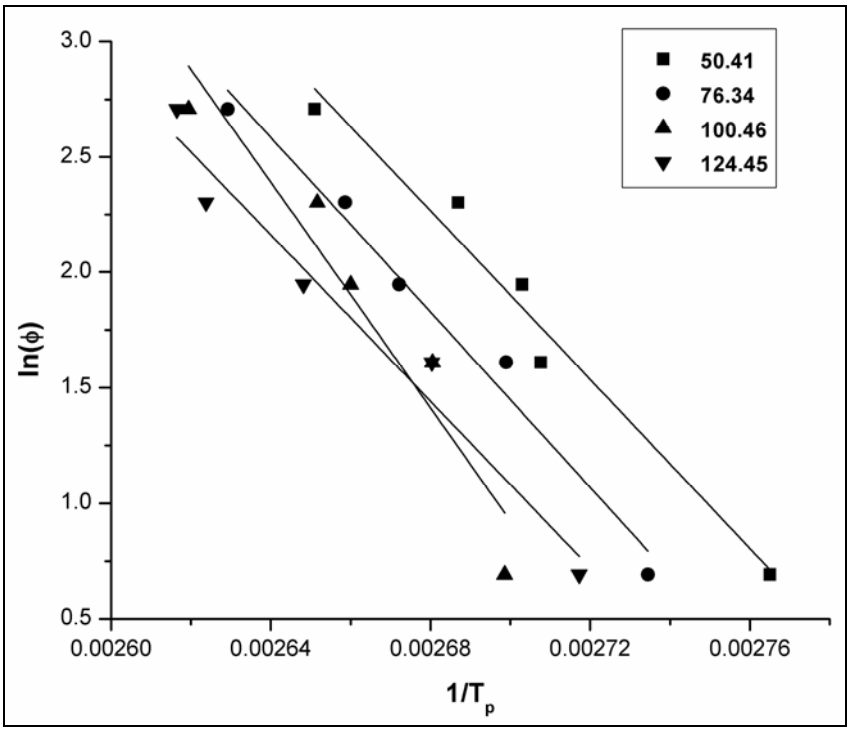

(a)

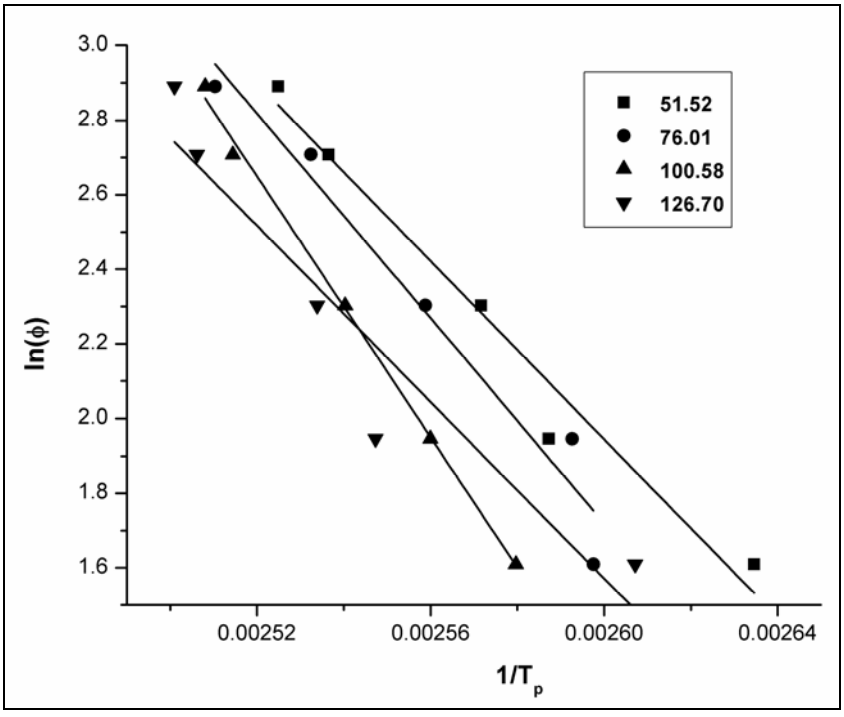

(b)

Figure 6.9 (a-b): Determination of activation parameters by Ozawa's method for polymerisation reaction of (a) PEA and (b) PEMA at various concentrations.

The polymerisation kinetics of (meth)acrylates ester initiated with AIBN is considered by a mechanism of free-radical polymerisation. This consists of a sequence of steps: initiation, propagation and termination. The mean E_a obtained by Kissinger method and Ozawa method is overall activation energy, which is the result of combining three separate Arrhenius-type equations for each process (initiation, propagation and termination).

Activation energies were calculated for the polymerisation reaction by Kissinger and Ozawa methods. The E_a values are compiled in Table 6.6. The lowest E_a value for the monomer implies a kinetically facile polymerisation reaction. It is found that the E_a value for PEMA is less than that of PEA.

Table 6.6: Activation energies for PEA and PEMA

PEA:AIBN (mol:mol)	Energy of Activation E_a (kJ/mol) for PEA		PEMA:AIBN (mol:mol)	Energy of Activation E_a (kJ/mol) for PEMA	
	Kissinger	Ozawa		Kissinger	Ozawa
50.41:1	145.69	159.72	51.52:1	92.74	104.35
76.34:1	151.34	165.75	76.01:1	107.64	120.09
100.45:1	196.52	213.74	100.58:1	138.85	152.95
124.45:1	143.40	157.42	126.71:1	91.76	103.38
Average	159.24	174.16	Average	107.75	120.19

6.6.2 Activation parameters

The pre-exponential factor A is the pre-exponential constant in Arrhenius equation, an empirical relationship between temperature and rate coefficient also A depends on probability *(P)* and number of collisions *(z)*. It is usually designated by A when determined from the experiment. A can be found from the relation 6.21,

$$A = \frac{\phi \ E_a e^{E_a/RT_p}}{RT_p^2} \qquad 6.21$$

The activation parameters are determined for concentration [monomer: initiator; 100:1] in case of both monomers and given in Table 6.7.

Table 6.7: Activation parameters determined by Kissinger and Ozawa methods

Conc. (mol/mol)	Kissinger	Ozawa
	A (s^{-1})	A (s^{-1})
PEA:AIBN; 100:1	$7.34 \cdot 10^{26}$	$2.15 \cdot 10^{29}$
PEMA:AIBN; 100:1	$2.07 \cdot 10^{16}$	$1.54 \cdot 10^{18}$

The lowest E_a value for the monomer implies a kinetically facile polymerisation reaction. Since rate constant depends on both A and E_a by the Arrhenius relationship,

$$k = Ae^{-E_a/RT} \qquad 6.22$$

The value of E_a alone does not give a correct idea about the facile nature of the reaction. Therefore, the rate constants were computed using E_a and A values for various temperatures and plotted in Figure 6.10.

It was found that the rate of reaction is less in case of PEMA than PEA. Under heating conditions, the acrylyl groups polymerise by free radical process. Acrylyl double bonds are sluggish in radical polymerisation for two reasons. The double bonds are not activated due to the initiator concentration. Secondly, the steric factor around the acrylyl double bonds retards the polymerisation. In the present case, the initiator concentration was the same for reaction mixtures. Hence, the difference in polymerisability came from the difference in steric hindrance around the acrylyl double bonds. For PEA, smaller steric hindrance was expected to be favorable for free radical polymerisation. However, in case of PEMA, α-methyl group on the double bond and 2-phenylethyl on ester group

have influenced the process of free-radical polymerisation. As the steric hindrance in PEMA is more than PEA, the polymerisability of the monomers was expected to be in the reverse order, viz. PEA> PEMA and the kinetic study confirmed this order of estimation.

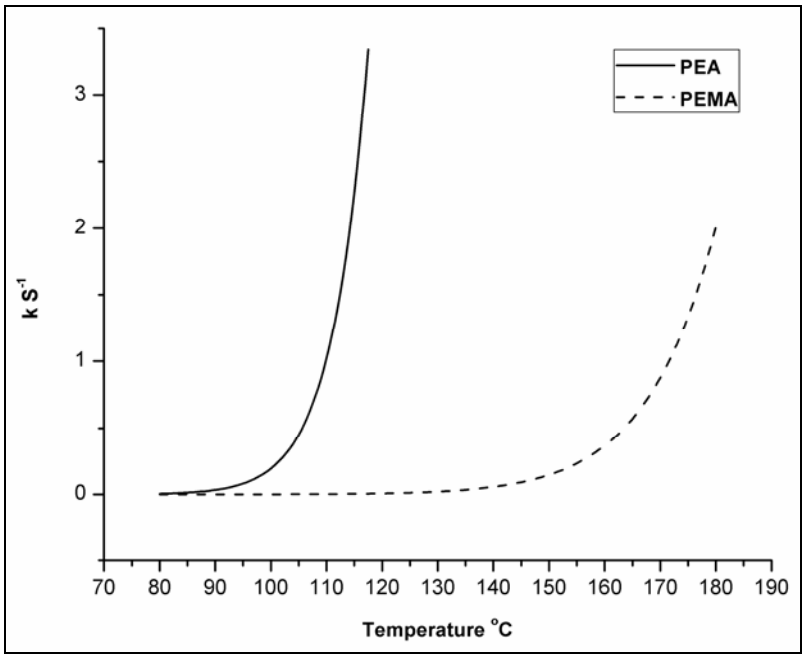

(a)

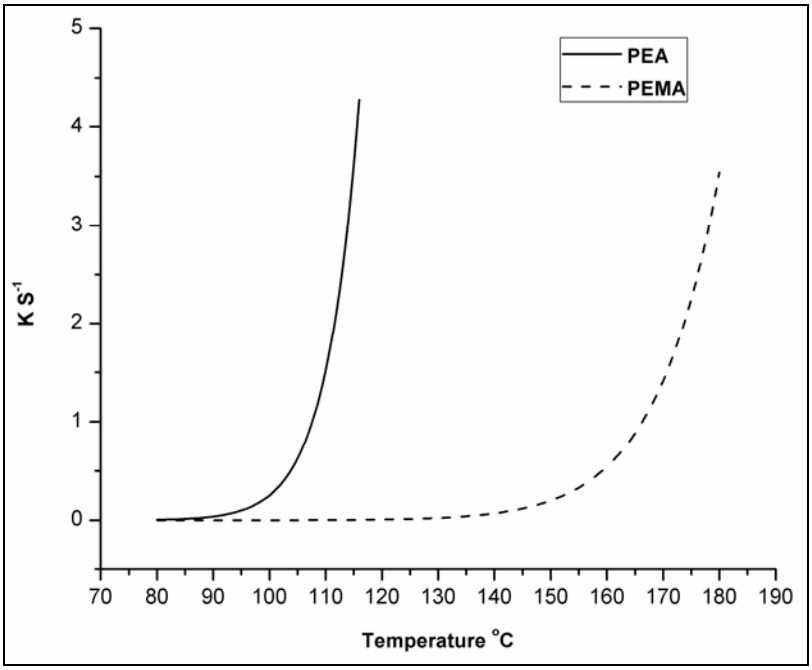

(b)

Figure 6.10: Temperature dependency of rate constants in case of (a) Kissinger and (b) Ozawa

6.7 References

[1] J. D. Cho, H. T. Ju, Y. S. Park, J. W. Hong, *Macromol. Mater. Eng.,* **2006**, 291, 1155-1163.

[2] E. Andrzejewska, *Prog. Polym. Sci*., **2001**, 26, 605-665.

[3] K.S. Anseth, C.N. Bowman, N. A. Peppas, *J. Polym. Sci. Polym. Chem.,* **1994**, 32, 139-147.

[4] J.S Young, C.N. Bowman, *Macromolecules,* **1999**, 32, 6073-6081.

[5] P. E. M. Allen, G. P. Simon, D. R. G. Williams, E. H. Williams, *Macromolecules*, **1989,** 22, 809-816.

[6] C. N. Bowman, N. A. Peppas, *Chem. Engg. Sci.,* **1992**, 47, 1411-1419.

[7] C. N. Bowman, N. A. Peppas, *Macromolecules*, **1991**, 24, 1914-1920.

[8] J. L. Mateo, M. Calvo, J. Serrano, P. Bosch, *Macromolecules*, **1999**, 32, 5243-5250.

[9] G. L. Batch, C. W. Macosko, *J. Appl. Polym. Sci.,* **1992**, 44, 1711-1729.

[10] G. R. Tryson, A. R. Shultz, *J. Polym. Sci. Polym. Phys*., **1979**, 17, 2059-2075.

[11] H. J Timpe, B. Strehmel, *Makromol. Chem.*, **1991**, 192, 779-791.

[12] E. Andrzejewska, D. Z. Tomkowiak, M. B. Bogacki, M. Andrzejewski, *Macromolecules*, **2004**, 37, 6346-6354.

[13] S. Khudyakov, W. S. Fox, Purvis, *Ind. Eng. Chem. Res*., **2001**, 40, 3092-3097.

[14] Sourour, M. R. Kamal, *Thermochim. Acta.*, **1976**, 14, 41-59.

[15] M. R. Keenan, *J. Appl. Polym. Sci*., **1987**, 33, 1725-1734.

[16] J. D. Cho, H. T. Ju, J. W. Hong *J. Polym. Sci. Polym. Chem*., **2005**, 43, 658-670.

[17] L. Macarie, A. Petrean, G. Ilia, S. Iliescu, A. Popa, M. J. M. Abadie, *J. Polym. Res*., **2005**, 12, 331-337.

[18] U. Khanna, M. Chanda, *J. Appl. Polym. Sci*., **1993**, 49, 319-329.

[19] G. H. Stempel, R. P. Cross, R. P. Mariella, *J. Am. Chem. Soc*., **1950**, 72, 2299.

[20] U. Senthilkumar, K. Ganesan, B. S. R. Reddy, *J. Polym. Res*., **2003**, 10, 21-29.

[21] S. Karatas, Z. Hosgor, N. K. Apohan, *J. Polym. Res*., **2010**, 17, 247-254.

[22] R. Chandra, R. K. Soni, *Polym. Inter.,* **1993**, 31, 239-245.

[23] L. Lecamp, B. Youssef, C. Bunel, P. Lebaudy, *Polymer*, **1997**, 38, 6089-6096.

[24] J. Wei, R. Lu, F. Liu, *J. Polym. Res*., **2011**, 18, 1001-1008.

[25] K. S. Anseth, C. M. Wang, C. N. Bowman, *Macromolecules*, **1994**, 27, 650 – 655.

[26] K. S. Anseth, C. M. Wang, C. N. Bowman, *Polymer*, **1994**, 35, 3243-3250.

[27] B. R. Nayak, L. J. Mathias, *J. Polym. Sci. Polym. Chem*., **2005**, 43, 5661-5670.

[28] M. J. M. Abadie, O. Novikova, V. Y. Voytekunas, V. G. Syromyatnikov, A. Y. Kolendo, *J. Appl. Polym. Sci*., **2003**, 90, 1096-1101.

[29] E. Andrzejewska, *Polymer,* **1996**, 37, 1039-1045.

[30] J. D. Cho, J. W. Hong, *Eur. Polym. J*., **2005**, 41, 367-374.

[31] C. Bai, X. Zhang, J. Dai, *J. Polym. Res*., **2008**, 15, 67-73.

[32] J. G. Kloosterboer, *Adu. Polym. Sci.,* **1981**, 84, 1.

[33] H. L. Friedman, *J. Polym. Sci.*, **1965**, C6, 183.

[34] T. Ozawa, *Bull. Chem. Soc. Jpn*., **1965**, 38, 1881.

[35] J. H. Flynn, L. A. Wall, *J. Polym. Sci*., **1966**, B4, 323.

[36] G. Z. Zhang, C. Q. Liu, H. Yoshida, *J. Therm. Anal. Cal*., **2006**, 85, 707.

[37] A. P. Gray, *Thermuchim Acta.,* **1970**, 1, 563.

[38] J. Chiu, In: *Anulytical Colorimetry,* S. Porter, J. F. Johnson, Eds. Plenum, New York, **1968,** 171.

[39] K. E. Barret, H. R. Thomas, *Brit. Poljm. J.,* **1970**, 2(1-2), 45.

[40] L. Rcich, D. W. Levi, *Macromol. Rev.,* **1968***,* 3, 49.

[41] A. Rudin, H. P. Schreiber, N. H. Weldman, *Ind. Engg. Chem*., **1961***,* 53, 137.

[42] M. L. Bhaumik, A. K. Sircus,D. J. Benerjee, *J. Appl.* Polym. *Sci.,* **1960,** 4**,** 366.

[43] J. Chiu, *Anal. Chem*., **1962***,* 34, 18141.

[44] G. Z. Zhang, C. Q. Liu, H. Yoshida, *J. Therm. Anal. Cal*., **2006**, 85, 707.

[45] P. K. Mahato, D. Chanda, A. Borthakur, *Thermochim. Acta.*, **1993**, 222-265.

[46] F. Severini, R. Gallo, G. Ricca, *Thermochim. Acta.*, **1988**, 132, 161.

[47] G. O. R. Alberda van Ekenstein, Y. Y. Tan, *Eur. Polym. J*. **1981**, 17, 839.

[48] J. L.Martin, A. Cadenato, J. M. Salla, *Thermochim. Acta*, **1997**, 306, 115.

[49] R. D. Radievi, D. M. Stoiljkovi, J. K. Budinski, *J. Therm. Anal. Cal*., **2007**, 90, 243.

[50] *J*. Sheppard, Peroxy Compunds in *Encyclopedia of Polym. Sci. Engg.,* Wiley New York, **1988**, 11, 1-21.

[51] J. Shelley, *Encyclopedia of Polym. Sci. Engg.,* Wiley New York, **1988**, 12, 257-290.

[52] R. B. Prime, E. A. Turi (Ed), *Thermal Characterization of Polymeric Materials*, Academic Press New York, **1981.**

[53] A. A. Duswalt, *Thermochim. Acta*. **1974**, 8, 57.

[54] M. E. Brown, *Introduction to Thermal Analysis,* Chapman, Hall, London, **1981.**

[55] R. B. Prime, *Polym. Eng. Sci.*, **1973**, 13, 365.

[56] R. B. Prime, E. Sacher, *Polymer*, **1972**, 12, 455.

[57] O. R. Abolafia, *Soc. Plast. Eng. [Tech. Pap.*], **1969**, 15, 610.

[58] H. E Kissinger, *Anal. Chem*., **1957**, 29, 1702.

[59] H. E Kissinger, *J. of Res. of Nat. Bur. Stand*., **1956**, 57(4), 217-221.

[60] L. J. Taylor, S. W. Watson, *Anal. Chem.*, **1970**, 42, 297.

[61] P. Murray, J. White, *Trans. Brit. Ceram. Soc*., **1949**, 48, 187-206.

[62] P. Murray, J. White, *Trans. Brit. Ceram. Soc*., **1955**, 54, 204-237.

[63] T. Ozawa, *J. Thermal Anal.,* **1970**, 2, 301.

Chapter VII

Summary and Conclusions

7.1 Summary and Conclusions

A family of novel, aromatic, sulphur containing aromatic acrylates and methacrylates were readily synthesised using a two step reaction scheme. Styrene oxide was precursor for all of the subsequent reactions. In the first step, the styrene oxide was reacted with a phenol and thiophenol. The oxygen and sulphur of the phenol and thiophenol were nucleophilically attacked, resulting in ring opening of the epoxy group, producing secondary alcohols. In the final step, intermediate alcohols were subjected to react with acryloyl chloride to produce corresponding acrylates. For methacrylate product, intermediate alcohols were reacted with methacryloyl chloride, to produce novel methacrylates. The newer synthesised monomers are represented in Table 7.1.

Table 7.1: Structures of new monomers

Sr. No.	Name of Monomer	Structure
1	2-Phenoxy-2-phenylethyl acrylate (PPEA)	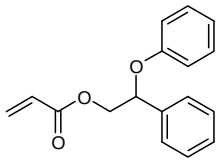
2	2-Phenoxy-2-phenylethyl methacrylate (PPEM)	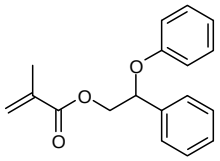
3	2-Phenyl-2-(phenylthio)ethyl acrylate (PTEA)	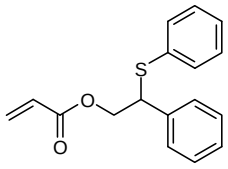
4	2-Phenyl-2-(phenylthio)ethyl methacrylate (PTEM)	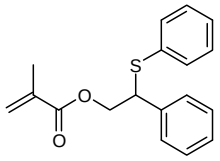

All newly synthesised intermediate alcohols and monomers were characterised by ^{1}H NMR, ^{13}C NMR, IR and mass spectroscopic techniques to confirm their structure. Homopolymers of newer monomers were synthesised by free radical solution polymerisation using 2,2'-azobisisobutyronitrile (AIBN). These new polymers were characterised for their thermal and optical properties. The refractive indices of the novel aromatic (meth)acrylate polymers were high (~1.58). Aromatic sulphur containing (meth)acrylate polymers had a refractive index of ~1.62, which was even higher than for the corresponding oxygen containing aromatic (meth)acrylate polymers. A higher refractive index was expected for new (meth)acrylates due to incorporation of polarisable constituents like sulphur atom and aromatic rings in their structures.

Chapter IV describes copolymerisation studies of new monomer combinations. Copolymerisation reactivity ratios enable the design of high conversion processes for the production of copolymers of well-defined properties for particular applications, such as the improvement of optical and thermomechanical properties of (meth)acrylates. The radical copolymerisation of 2-phenylethyl (meth)acrylate was conducted with the newly synthesised monomers in ethyl methyl ketone (EMK) at 70 °C. Copolymers were prepared by free radical solution polymerisation using 2,2'-azobisisobutyronitrile (AIBN). Compositions of copolymers were determined by ^{1}H NMR spectroscopy. The reactivity ratios were determined using Fineman-Ross (FR), Kelen-Tudos (KT), Extended Kelen-Tudos (Ex KT) and Mao-Huglin (MH) methods and the values were in good agreement. These results were confirmed by the calculation of the monomer dyad sequence fractions and mean sequence length. Six monomer pair combinations were studied. The data of their average reactivity ratio values are presented in Table 7.2.

Table 7.2: Reactivity ratios of new monomer combinations

Pair No.	Name of Monomer	RR Values
1	2-Phenylethyl acrylate (PEA)	r_{PEA} = 0.811
	2-Phenoxy-2-phenylethyl acrylate (PPEA)	r_{PPEA} = 0.704
2	2-Phenylethyl acrylate (PEA)	r_{PEA} = 0.234
	2-Phenoxy-2-phenylethyl methacrylate (PPEM)	r_{PPEM} = 1.842
3	2-Phenylethyl methacrylate (PEMA)	r_{PEMA} = 1.993
	2-Phenoxy-2-phenylethyl acrylate (PPEA)	r_{PPEA} = 0.508
4	2-Phenylethyl methacrylate (PEMA)	r_{PEMA} = 1.255
	2-Phenoxy-2-phenylethyl methacrylate (PPEM)	r_{PPEM} = 1.198
5	2-Phenylethyl acrylate (PEA)	r_{PEA} = 1.100
	2-Phenyl-2-(phenylthio)ethyl acrylate (PTEA)	r_{PTEA} = 1.009
6	2-Phenylethyl acrylate (PEA)	r_{PEA} = 0.458
	2-Phenyl-2-(phenylthio)ethyl methacrylate (PTEM)	r_{PTEM} = 0.666

Solubility of copolymers was tested in common solvents. The molecular weights [weight-average molecular weight (M_w) and number-average molecular weight (M_n)] and polydispersity indices (PDI) of the copolymers were determined with gel permeation chromatography (GPC). Refractive index was determined with Abbe refractometer. The refractive indices of copolymers increased with increase in concentration of aromatic and sulphur containing comonomer. Thermal data were obtained with a DSC and TGA instruments.

Copolymerisation of monomers was found to be extremely useful in the creation of controlled, high refractive index materials having desired RI values for optical end uses. Monomer selection affected other important properties of the copolymers including

refractive index, glass transition temperature, molecular weight and thermal stability. Properties of copolymers like refractive index and glass transition temperature were found to be linearly dependent on mol % of comonomers. In addition, all copolymers had good optical transparency in the visible region. Copolymers exhibited good thermal stability. The well-balanced properties of the copolymers make them good candidates for advanced optical applications.

The studies presented in Chapter V were aimed at the development of new and improved foldable, high refractive index acrylic polymers for intraocular lens application. Novel high refractive index copolymers were synthesised and characterised. Glass moulds were designed and fabricated for polymerisation process. Binary copolymer networks based on different compositions were synthesised by radical copolymerisation in bulk using Luperox–256 as radical initiator. Ethylene dimethacrylate and hexanediol dimethacrylate were used as cross-linkers.

In this work, we have reported the synthesis, optical, thermomechanical, and surface properties, as well as cytotoxicity of a series of novel (meth)acrylate copolymer networks intended to be used as ocular implants. The RI, T_g and hydrophobicity of the networks increased as the relative concentration of newly synthesised methacrylates in the copolymer was increased. Thus, these properties could be adjusted conveniently by changing the ratio of the monomers. Combined with the RI, transparency, cyatocompatibility and surface wettability of the prepared copolymer networks with comprehensive properties, hold great promise as materials for IOL applications (Figure 7.1).

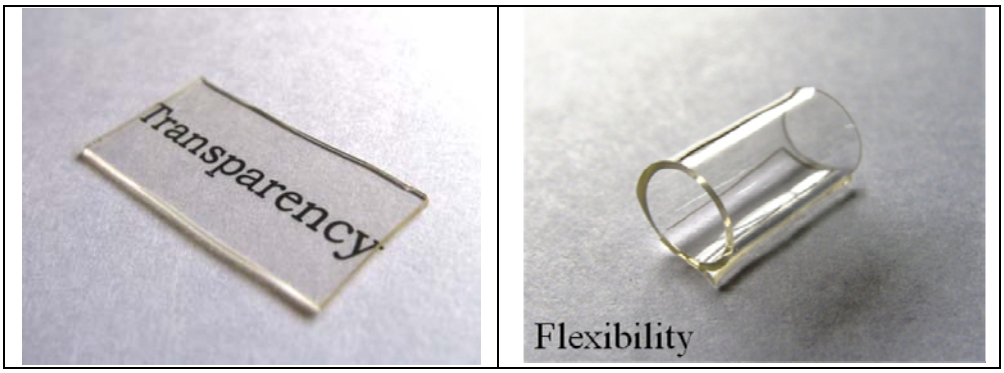

Figure 7.1: New, flexible, transparent bulk polymer networks

PEA/PPEA (Figure 7.2a) and PEA/PPEM (Figure 7.2b) copolymer compositions were successfully synthesised using bulk free radical polymerisation. Most compositions with PPEA content between 10 to 35 mol % and PPEM between 10 to 30 mol % were suitable for foldable IOL applications. The materials had low T_g (< 20 ^oC), were hydrophobic (<2 wt% EWC), had high refractive index (>1.56), good optical transparency in visible region (>80 %), rubbery nature and high thermal stability (> 290 ^oC), exhibited controllable unfolding and good cytocompatibility.

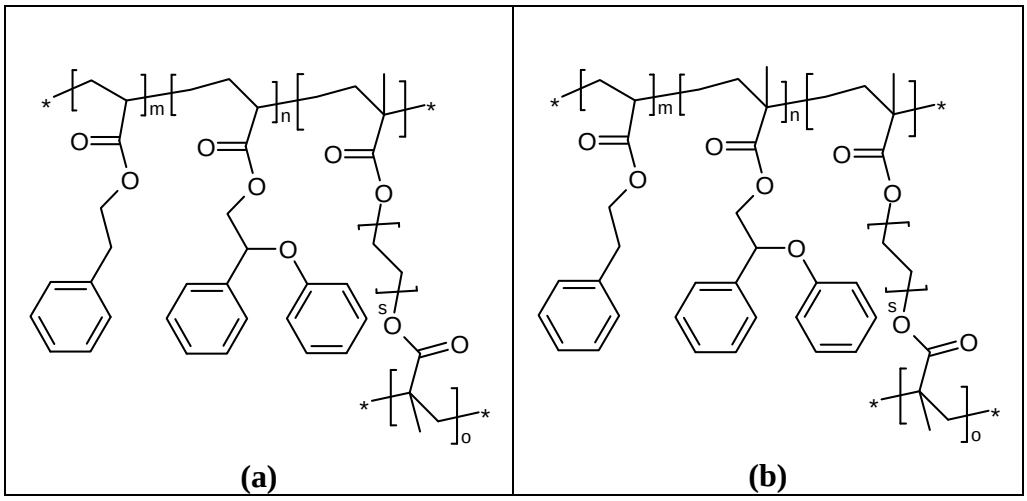

Figure 7.2: Structures of bulk polymer networks (a) poly(PEA-co-PPEA) and (b) poly(PEA-co-PPEM)

Newer sulphur containing monomers PTEA and PTEM were copolymerised with PEA using free radical bulk polymerisation. PEA/PTEA copolymers (Figure 7.3a) were a significant improvement over the PEA/PPEA, PEA/PPEM and PEA/PTEM (Figure 7.3b) copolymers. Compositions having PTEA content between 20 to 60 mol % and PTEM between 10 to 30 mol % were suitable for foldable IOL applications. These polymers were showing significant improvement in RI (1.57 to 1.59). The materials had low T_g (<20 ^oC), were hydrophobic (<2 wt % EWC), showed good optical transparency in visible region (>85 %), high thermal stability (>290 ^oC) and exhibited controllable unfolding. All polymers had high failure strain which is required for deformation of polymer networks to achieve a small incision size networks. Copolymers developed in the study were cytocompatibile.

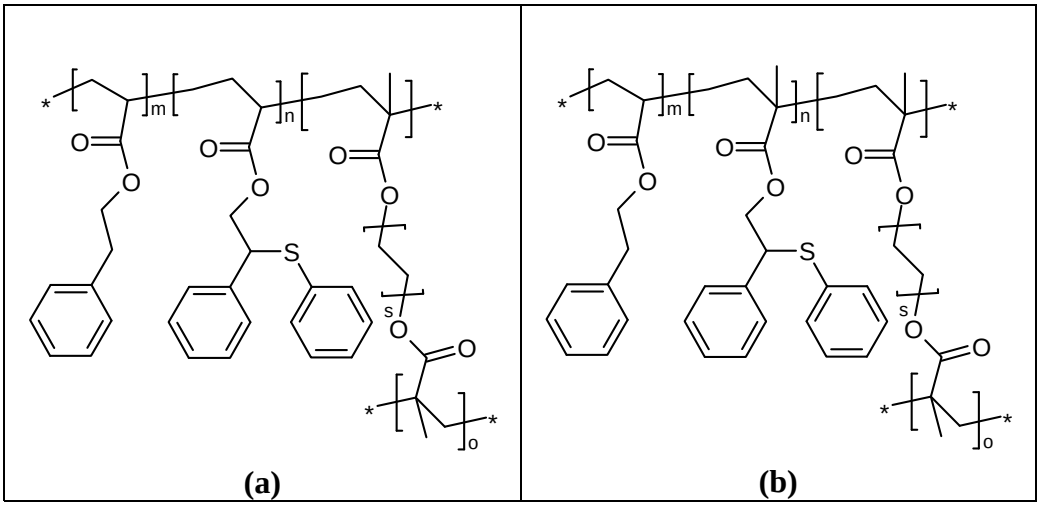

Figure 7.3: Structures of bulk polymer networks (a) poly(PEA-co-PTEA) and (b) poly(PEA-co-PTEM)

The results of this research demonstrated important technological advancements aimed at the development of improved hydrophobic, high refractive index, acrylic,

foldable IOLs. Further synthesis, characterisation, and process optimisation may be necessary for industrial scale applications.

Chapter VI (Part A) describes isothermal photopolymerisation studies of 2-phenylethyl acrylate and 2-phenylethyl methacrylate using differential photo-calorimetry. The photopolymerisation under similar irradiation conditions for formulations containing 2-phenylethyl (meth)acrylates showed that the conversions for methacrylate are much higher than that of acrylate. This is due to a reduced viscosity build up associated with gradual reaction diffusion process for the methacrylate formulations. For both the systems, the induction time as well as the time to attain peak maximum were found to decrease with increase in concentration of photo initiator as well as with an increase in temperature showing an enhancement in the speed and course of photopolymerisation from early stages up to $R_{p\ max}$. For both systems, the $R_{p\ max}$ was found to increase with an increase in concentration of photoinitiator. However an increase in temperature resulted in the decrease in $R_{p\ max}$ of acrylate formulations showing a comparatively higher rate of initiation (combined effect of *insitu* viscosity and time of onset of reaction diffusion) before $R_{p\ max}$ at higher isothermal conditions, which in turn leads to lesser final conversions than methacrylate formulations.

The studies done on acrylate formulations with variable autocatalytic kinetic model show an increase in rate constant with increase in temperature as well as increase in concentration of photo initiator. The pre-exponential factor and overall activation energy were found to increase with increase in concentration of photoinitiator due to enhancement in the frequency of collision and bimolecular termination at the initial stages of photopolymerisation process. From dark reaction studies we can infer that the

ratio of rate constants as per bimolecular termination model is found to decrease with increase in conversion for both the systems with methacrylate formulations showing a longer time scale for reaction diffusion.

In Chapter VI (Part II), free radical bulk polymerisation kinetics of 2-phenylethyl (meth)acrylate was determined by non-isothermal differential scanning calorimetry. Kinetics of free radical polymerisation of the monomers in the presence of 2,2'-azobisisobutyronitrile (AIBN) as initiator were investigated by differential scanning calorimetry in the non-isothermal mode. The polymerisation was investigated in temperature range 40 to 180 °C with varying ramp rates, at four different initiator concentrations**.** Kissinger and Ozawa methods were applied to determine the activation energy (E_a) of free-radical polymerisation. It was found that the rate of reaction is lower in case of PEMA than PEA. Under heating conditions, the acrylyl groups polymerise by free radical process. Acrylyl double bonds are sluggish in radical polymerisation for two reasons. The double bonds are not activated due to the initiator concentration. Secondly, the steric factor around the acrylyl double bonds retards the polymerisation. In the present case, the initiator concentration was the same for all reaction mixtures. Hence, the difference in polymerisability came from the difference in steric hindrance around the acrylyl double bonds. For PEA, smaller steric hindrance was expected to be favourable for free radical polymerisation. However, in case of PEMA, α-methyl group on the double bond and 2-phenylethyl ester group influenced the process of free-radical polymerisation. As the steric hindrance in PEMA is greater than that in PEA, the polymerisability of the monomers was expected to be in the reverse order, viz. PEA> PEMA, which was confirmed by kinetic studies.

7.2 Future Work

During the course of this research, many opportunities for further experimentation became evident. The following suggestions for future research highlight some of these potential directions.

- Synthesis of new UV-absorbing cross-linkers.
- Synthesis of different copolymer compositions by varying the cross-linker concentration.
- Incorporation of UV-absorbing molecules into the copolymer backbone to complete the foldable IOL composition.
- *In vivo* studies of synthesised polymer networks.
- Incorporation of surface modified high refractive index nanoparticles into the bulk polymer matrix and their detailed studies.
- Determination of kinetic parameters for polymerisation of newer monomers.